A Multi-Proxy Isotope Approach to Reconstruct Seawater Oxygenation

Thesis

A Multi-Proxy Isotope Approach to Reconstruct Seawater Oxygenation

Thesis presented for the degree of Doctor of Philosophy in Geochemistry

Felicity Sarah Amy Rhodes, MEarthSci (Oxon.)

June 2018

School of Environment, Earth and Ecosystems Science

The Open University, Walton Hall, Milton Keynes, MK7 6AA

Abstract

The isotopic composition of redox sensitive metals in marine sedimentary rocks have been used to provide insights into the degree and extent of oceanic anoxia during environmental changes such as oceanic anoxic events (OAEs). In this study a new method has been developed to determine the isotope composition ($\delta^{187}Re = [[(^{187}Re/^{185}Re)_{sample} / (^{187}Re/^{185}Re)_{SRM\ 3143}]-1]*1000$) of the redox sensitive element rhenium in sedimentary deposits. The method requires 1.5 – 6.0 ng Re per analysis and utilises a two-stage chromatographic separation and MC-ICP-MS analysis. The accuracy was tested using matrix test samples ($\delta^{187}Re = 0$) that have an average $\delta^{187}Re$ of -0.035 ± 0.112 ‰; and column processed aliquots of standard SRM 3143 of $\delta^{187}Re$ = -0.042 ± 0.108 ‰. The long-term reproducibility of standard analyses is 0.082 ‰ (2 SD). The reference sample SDO-1 had $\delta^{187}Re$ = -0.163 ± 0.113 ‰. The total measured range in $\delta^{187}Re$ was -1.087 ± 0.084 ‰ between a sediment sample from the Baltic Sea and SRM 3143.

The $\delta^{187}Re$ of marine mudrocks from the Toarcian OAE in Yorkshire, UK have a range of 0.699‰ from -0.019 ± 0.080 ‰ to -0.756 ± 0.085 ‰. During the OAE onset $\delta^{187}Re$ increases by 0.219 ‰. The main event is synchronous with a - 0.596 ‰ $\delta^{187}Re$ excursion. Minimum $\delta^{187}Re$ values correspond to the maximum global extent of anoxia indicated by other proxies. The $\delta^{187}Re$ decrease is interpreted to indicate a decrease in $\delta^{187}Re$ of contemporaneous seawater due to a progressive increase in the global extent of anoxia.

Recent sediments from the Gotland Deep, Baltic Sea have a $\delta^{187}Re$ range of 0.826 ‰ from -0.261 ± 0.084 to -1.087 ± 0.084 ‰. The cause of changes in $\delta^{187}Re$ is inconclusive and could include changes in local anoxia, the basin-wide extent of anoxia, anthropogenic Re, runoff variation and diagenesis.

Acknowledgements

I owe an enormous debt of gratitude to my supervisors, Angela Coe and Manuela Fehr; they have tirelessly supported me throughout the last five and more years, providing guidance with the laboratory work and writing. It is impossible to summarise here the impact they have had on my research. The thesis also benefited from early supervision by Anthony Cohen and I am grateful for his guidance during the first 3.5 years of my research. I would also like to thank Sam Hammond, Bruce Charlier and Marc Davies for support with the laboratory analyses. Particular thanks go to the members of the science faculty who have provided support during my studies: Sarah Sherlock, Pallavi Anand, James Bruce, and Tom Argles. Thanks to Clare Warren for always giving cheerful encouragement and helping me to stay positive. Thanks to Arlëne Hunter for all the words of encouragement along the way. Thank you to Caroline Slomp for providing the Baltic Sea samples and generous discussion about the Baltic Sea and choice of samples. Thanks also to Carolyn Bennett for tutoring support, and for keeping me calm in the months of writing.

There are a great many people to thank who have supported me along the way, and I would like to mention some of them here: Adele Cameron; colleagues from my year group, Sam, Tom and Bethan; Kate, Adele J, Kerry, Anouk, Simone, Hayley and Chris, Leanne and Peter, Matt, Chris, Alice, Catherine, Anne, Liz, John, Matt, Pete, Eleni, Stacy, Costanza. To the wonderful inhabitants of the Broughton House, I will always be grateful to you for housing me through my writing weeks in MK. My friends from Oxford, who have been constantly encouraging, Sam and Talia, Sian, Sarah K, Sarah J, Chandni, Marja, Tom, Anna, Manasi, Nabeelah, Erica and Cat. Thanks go to my wonderful dancing friends for providing a welcome distraction from the stresses of thesis writing.

Final and vitally important thanks go to my family for their love and support which has helped immensely in this undertaking. To Mum, Dad, and Tom, my eternal thanks. To George and June for the generous provision of horses to ride and excellent bacon sandwiches! To my grandparents, of whom sadly only one made it to the end of the thesis, but all of whom have contributed in a profound way to the person I strive to be. And finally, to Alice, without whose love and support none of this would have been possible. Thank you for your unwavering support in this colossal task, roll on the victory tour!

Table of Contents

Chapter 1: Introduction

Chapter 2: Introduction to rhenium

Chapter 3: Quantitative separation of rhenium from sedimentary rocks and high precision rhenium isotope ratio analysis by MC-ICP-MS

Chapter 4: Assessing δ^{187}Re in recent sediment samples of the Baltic Sea

---

Chapter 5: Introduction to the Toarcian Oceanic Anoxic Event

Chapter 6: The Toarcian Oceanic Anoxic Event: A rhenium isotope perspective

---

Chapter 7: Conclusions and future work

List of Figures

Chapter 1: Introduction

Chapter 2: Introduction to rhenium

Chapter 3: Quantitative separation of rhenium from sedimentary rocks and high precision rhenium isotope ratio analysis by MC-ICP-MS

Chapter 4: Assessing δ^{187}Re in recent sediment samples of the Baltic Sea

Chapter 5: Introduction to the Toarcian Oceanic Anoxic Event

Chapter 6: The Toarcian Oceanic Anoxic Event: A rhenium isotope perspective

Chapter 7: Conclusions and future work

List of Tables

Chapter 1: Introduction

Chapter 2: Introduction to rhenium

Chapter 3: Quantitative separation of rhenium from sedimentary rocks and high precision rhenium isotope ratio analysis by MC-ICP-MS

Chapter 4: Assessing δ^{187}Re in recent sediment samples of the Baltic Sea

Chapter 6: The Toarcian Oceanic Anoxic Event: A rhenium isotope perspective

Appendix: Standard data for SRM3143

Chapter 1

Introduction

This chapter presents the introduction and rationale for the thesis along with a summary of the thesis structure. The main scientific findings are presented in Chapters 3, 4 and 6, and more complete reviews of the literature on the three main topics are presented in Chapters 2, 4, and 5.

1.1 Introduction

Climate change caused by anthropogenic carbon dioxide emissions is one of the major issues facing society today (IPCC 2014). It has long been known that human activity is increasing pCO_2 in the atmosphere, with atmospheric pCO_2 increasing from 280 ppmv in pre-industrial times (Karl and Trenberth 2003) to >400 ppmv at present (Kennedy 2016). Currently on average, global CO_2 emission rates are 9.9 ± 0.5 GtC per year (Le Quéré *et al.* 2016). Elevated pCO_2 is a major cause of modern-day global warming (IPCC 2014), the impacts of which include decreased ocean productivity, altered food web dynamics, reduced abundance of habitat-forming species, shifting species distributions, and a greater incidence of disease (Hoegh-Guldberg and Bruno 2010, Rosenzweig *et al.* 2008). One of the underappreciated effects of global warming is ocean deoxygenation (Doney 2010, Shepherd *et al.* 2017).

Global warming causes ocean deoxygenation by (1) increasing seawater stratification, which reduces vertical mixing, and so limits the amount of oxygen brought into the ocean (Gruber 2011); and (2) decreasing oxygen solubility in warmer surface waters (Oschlies *et al.* 2017, Stramma *et al.* 2010). At the same time, elevated temperatures increase primary productivity, and increase the apparent utilisation of oxygen (Bopp *et al.* 2017), which acts as a positive feedback loop (Watson *et al.* 2017). Increased oxygen removal from the oceans together with lower levels

of dissolved oxygen increases areas of anoxia globally (Oschlies *et al.* 2017). Decreasing oxygen concentration has been observed in the North Atlantic between 1960 and 2009 (Stendardo and Gruber 2012), and also in the subpolar North Pacific, and in subtropical OMZs (Stramma *et al.* 2010, Whitney *et al.* 2007)

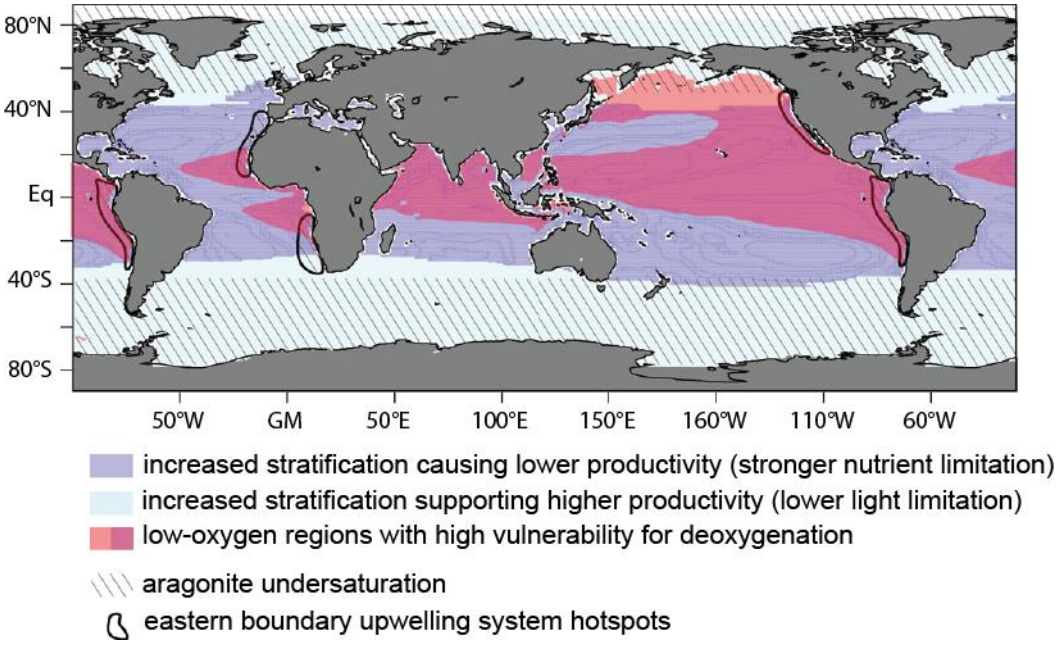

Figure 1.1: Map to show the regions of the ocean vulnerable to stressors (from Gruber (2011)). Highlighted in pink are the regions with particular vulnerability for deoxygenation.

Ocean deoxygenation has serious implications for ecosystem balance, causing localised extinctions and migration of species (Hoegh-Guldberg and Bruno 2010, McCormick and Levin 2017, Shepherd *et al.* 2017). Humans depend on the oceans for food from fisheries, and for leisure and tourism activities in coastal areas, and decreased ocean oxygen concentration has the potential to threaten the food supply and livelihoods of large population groups (IPCC 2014). Reef systems which are important for reducing coastal erosion may also be affected by ocean deoxygenation, the effects of which are likely to be irreversible on human timescales (Keeling *et al.* 2010). Current estimates indicate that there will be a decline in dissolved oxygen inventory of the global ocean of one to seven percent by 2100 (Schmidtko *et al.* 2017).

To better understand how the Earth system may respond to future increases in atmospheric pCO_2, we can look to past examples of major climate change, and the associated

redox changes in the ocean (Allen *et al.* 2000, Bopp *et al.* 2017, Dera and Donnadieu 2012, Rothman 2017). Models of how the ocean oxygen concentration may change in response to future climate change (Cao *et al.* 2014) rely on accurate records of present day changes in oxygen concentration in the ocean (Bopp *et al.* 2017).

1.2 Geochemical proxies of past ocean redox

1.2.1 Definitions of different redox conditions

The concentration of dissolved oxygen in seawater can be described using four categories representing a range of different redox conditions: oxic, suboxic, anoxic and euxinic. Table 1.1 defines the oxygen and hydrogen sulphide concentrations in these different conditions.

Table 1.1: Table to show the O_2 and H_2S concentrations of seawater in different redox conditions.

REDOX CONDITION	O_2 CONCENTRATION	H_2S CONCENTRATION
OXIC	>2 ml L^{-1}	None
SUBOXIC/HYPOXIC	<2 ml L^{-1}	None
ANOXIC	<0.2 ml L^{-1}	None
EUXINIC	None	Some free H_2S present

1.2.2 Elemental proxies for redox conditions

The concentration and isotope composition of redox sensitive metals can be used as a proxy for redox changes in the palaeo-oceans (Brumsack 2006, Calvert and Pedersen 2007, Lyons *et al.* 2009, Tribovillard *et al.* 2006). In reducing conditions, there is an authigenic enrichment of rhenium (Re), uranium (U), molybdenum (Mo), and iron (Fe) in sediment above the background detrital flux (e.g. Calvert and Pedersen 2007).

Uranium: The uptake of authigenic U into marine sediments begins at the redox boundary between Fe(II) and Fe(III) reduction, in suboxic conditions (Tribovillard *et al.* 2012). Anoxic

sediments are typically enriched in U due to the reduction of U below the sediment-water interface (Tribovillard *et al.* 2006). Uranium may be remobilised, and the U peak moved to a different depth in the sediment if oxygen penetration disrupts the accumulation of U (McManus *et al.* 2006).

Rhenium: Re is enriched under anoxic and euxinic conditions, with Re accumulation in the sediment being strongly influenced by the severity of reducing conditions (Morford *et al.* 2012). The behaviour of Re in seawater is discussed in more detail in Chapter 2 of this thesis.

Molybdenum: Mo is enriched in sediments deposited under a wide range of redox conditions, but is most enriched under euxinic conditions, where the relatively inert MoO_4^{2-} ion is reduced to reactive thiomolybdates ($MoO_xS_{4-x}^{2-}$) (Calvert and Pedersen 2007). Despite the importance of H_2S in the accumulation of Mo into sediment, pyrite is not the dominant host of Mo in sediments (Chappaz *et al.* 2014). Examples of the application of Mo concentration as a palaeoredox proxy include: Mo and Re/Mo ratio (Pearce *et al.* 2008); Mo/TOC (Algeo and Rowe 2012); Mo and U concentration variations and covariations from the Cariaco basin, the Black Sea, and the Eastern Tropical Pacific (Algeo and Tribovillard 2009), and in OAE 2, OAE 3, the Late Hauterivian, and the Toarcian (Tribovillard *et al.* 2012).

Re/Mo: The different redox sensitivities of Re and Mo can be used to differentiate between anoxic and euxinic conditions in sediment (Crusius *et al.* 1996). Rhenium is enriched in anoxic sediments; however, Mo is enriched in more reducing conditions in the presence of sulphidic conditions (Crusius *et al.* 1996). Re/Mo ratio above the seawater value of 0.4 mMol/Mol (0.78 ppb/ppm) with enrichment in Re and Mo concentration is indicative of anoxic conditions, however, under euxinic conditions the Re/Mo ratio is much closer to the seawater value (Calvert and Pedersen 2007, Crusius *et al.* 1996). Oxygen penetration depth, and the severity of reducing conditions alters the relative accumulation of Re and Mo in the sediment (Morford *et al.* 2005).

Changes in the Re/Mo ratio across the T-OAE indicate the persistence of bottom water euxinic conditions (Pearce *et al.* 2008).

Fe/Al: The normalisation of Fe concentration using Al is important due to the relatively high detrital flux of Fe into the ocean. Fe/Al values above the background oxic level indicates the transport of reactive Fe from the shelf into euxinic basins (e.g. Fehr *et al.* 2008). Changes in Fe/Al ratio above the background oxic level may indicate changing redox conditions, but could also indicate the changing ratio of the deep euxinic basin to shelf area over longer timescales (Lyons *et al.* 2009).

Manganese: Under oxic conditions, Mn(II) is oxidised to insoluble Mn oxyhydroxides (Calvert and Pedersen 2007). Manganese is involved in the transport of trace elements into sediments through the adsorption of these elements (such as Mo) to the surface of Mn oxihydroxide particles. Manganese is very mobile in reducing sediments, and is either released back into the water column, or is incorporated into authigenic Mn-carbonates (Tribovillard *et al.* 2006). It is therefore not a suitable redox proxy when one is focussing on reducing conditions (Tribovillard *et al.* 2006).

1.2.3 Metal isotope proxies of redox

Metal stable isotopes present a useful palaeoredox proxy because they can provide insights into temporal and spatial changes in metal cycling and ocean oxygenation (Anbar and Rouxel 2007), and therefore can provide insight into global redox changes as opposed to the local changes in redox conditions reflected in metal concentration data.

Mo isotopes as a redox proxy

Molybdenum has seven naturally occurring stable isotopes and is known as a redox sensitive metal. Its major source to seawater is from weathering, and the main sink of Mo from seawater is into deposits that accumulate in anoxic environments. The residence time of Mo in seawater is

~440 Kyr (Miller *et al.* 2011). Modern-day $\delta^{98/95}$Mo (defined as $\delta^{98/95}$Mo = $(((^{98}Mo/^{95}Mo)_{sample}/(^{98}Mo/^{95}Mo)_{standard})-1)*1000$) in seawater = 2.34 ‰ (Siebert *et al.* 2003), which reflects the balance between Mo removal to sulphidic and oxide rich sediments, and the isotope composition of Mo inputs to the ocean (Dickson *et al.* 2017). Under oxic conditions removal of Mo from seawater to Mn oxides causes isotope fractionation and leaves a relatively isotopically heavy seawater reservoir; euxinic conditions cause the quantitative removal of Mo and so the $\delta^{98/95}$Mo of sediments records that of contemporaneous seawater (Kendall *et al.* 2017), however it is important to identify which environments are most likely to have involved the quantitative draw down of Mo (Dickson 2017). Molybdenum isotope fractionation is mass dependent but appears to be more strongly associated with changing Mo speciation, rather than necessarily changing redox state (Anbar and Rouxel 2007). Analyses of Mo isotope composition are generally carried out using double spiking to correct for instrumental mass bias. Most recent publications record Mo isotope ratio relative to the reference standard NIST-SRM-3134 , which was first suggested as a reference standard by Goldberg *et al.* (2013). Changes in Mo isotope composition across the T-OAE have been used to infer changing areal extent of ocean redox during the T-OAE (Pearce *et al.* 2008). More recently, data from multiple euxinic sedimentary successions and from contrasting hydrographic regimes can be used to estimate the Mo isotope composition of open-ocean seawater, and hence the magnitude of deoxygenation during major climate change events (Dickson 2017). The Mo isotope system has been employed in many studies, some further examples of which are study of: the Great Oxidation Event (Duan *et al.* 2010), modern samples from the Peru margin (Scholz *et al.* 2017), the Late Permian Kupferschiefer Sea (Ruebsam *et al.* 2017), the Lower Cambrian euxinic mid-depth waters from South China (Cheng *et al.* 2016).

U isotopes as a palaeoredox proxy

There is natural variability in $^{238}U/^{235}U$ observed in various geological settings, with an overall variation of ~1.3 ‰ (Weyer *et al.* 2008). Also due to the differing half-lives of these two

isotopes, the absolute ratio has changed over the life span of the solar system (Andersen *et al.* 2017b). Uranium isotope composition responds across a range of oxic-anoxic-euxinic environments, and so may be useful in conjunction with other palaeo-redox proxies (Andersen *et al.* 2017b). Analysis of seawater and sediment samples from the Black Sea indicates that microbially mediated reduction is the primary mechanism controlling U fractionation in this area (Rolison *et al.* 2017). Fractionation of U isotopes during incorporation into $CaCO_3$ may affect the use of U isotopes as a palaeo redox proxy (Chen *et al.* 2016). The comparison between U isotope data for OAE 2 and sediments deposited in the Black Sea using mass balance calculations provides estimates of the areal extent of anoxic deposition during OAE 2 (Montoya-Pino *et al.* 2010). Comparisons between the U and Mo isotope composition of sediment and seawater from the Baltic Sea and the Kyllaren Fjord show values significantly isotopically lighter than those typical of organic-rich anoxic sediments (Noordmann *et al.* 2015).

Other isotope proxies

Several other isotope systems have been explored as redox proxies and this is an ever-growing field. Examples include: the chromium isotope system (e.g. Døssing *et al.* 2011, Ellis *et al.* 2002, Frei *et al.* 2011); the thallium isotope system (e.g. Nielsen *et al.* 2011, Owens *et al.* 2017, Them *et al.* 2018); and the Fe isotope system (e.g. Fehr *et al.* 2010, Fehr *et al.* 2008).

The Re isotope system shows potential as a redox proxy (Miller *et al.* 2015), but is as yet untested in geological examples of climate change events. Due to the differing redox sensitivities of various redox sensitive metals such as Mo, Re, and U (Calvert and Pedersen 1993, 2007, Crusius *et al.* 1996, Helz and Adelson 2013, Miller *et al.* 2011, Noordmann *et al.* 2015), the study of a range of different stable isotope redox proxies allows a better understanding of the magnitude and areal extent of redox changes in the ocean during palaeoclimate events. A more in-depth discussion of the potential for the Re isotope system to be used as a palaeo-redox proxy is presented in Section 1.4, and Chapter 2.

1.3 Rationale

The aim of this thesis is to develop $\delta^{187}Re$ defined as:

$$\delta^{187}Re = [[(^{187}Re/^{185}Re)_{sample} / (^{187}Re/^{185}Re)_{SRM3143}]-1]*1000$$

as a new proxy for past ocean redox conditions. To do this, three main areas of work were completed: firstly, method development building on the method established by Miller *et al.* (2009), to refine the precise determination of $\delta^{187}Re$ by MC-ICPMS (multi-collector inductively coupled plasma mass spectrometry); secondly, application of the method to samples from the Toarcian Oceanic Anoxic Event (T-OAE) to assess whether any variation in $\delta^{187}Re$ is observed across a period of major ocean redox change; and thirdly, analysis of recent sediment samples from the Baltic Sea (1950-2010) to establish how the Re isotope system is affected by known changes in bottom water oxygenation. Each of these areas of work, and the rationale for them is discussed in more detail in Sections 1.3 to 1.5.

The newly developed method was first applied to the study of a palaeo event, this was due to the ready availability of samples provided by Angela Coe; furthermore, since the T-OAE is already well studied, it provided an opportunity to assess whether $\delta^{187}Re$ did indeed reflect the redox changes interpreted to occur across the event. The order of the thesis chapters does not reflect the chronology of sample processing. The study of samples from the Baltic Sea is presented first to show a more logical flow of discussion from well constrained present-day environment to the study of a palaeo-environment.

1.4 Objectives

The key objectives of the thesis are:

1. To develop a method to determine the Re isotope composition of natural samples at high precision.

2. To determine $\delta^{187}Re$ for samples across the T-OAE, whether any variations correspond to changing redox conditions, and to assess whether this shows new features in the onset of the redox changes across the T-OAE.
3. To determine whether there are variations in $\delta^{187}Re$ corresponding with the modern hypoxic event of the Baltic Sea, and to understand the behaviour of Re isotopes in a modern-day anoxic environment where the bottom-water O_2 concentration is known.

1.5 Rhenium as a palaeoredox proxy

Rhenium has two naturally occurring stable isotopes (Gramlich *et al.* 1973). The analyses in this thesis aim to determine $\delta^{187}Re$. Chapter 2 summarises the limited knowledge of Re systematics, and the potential for Re isotopes to be developed as an isotope proxy for past ocean redox.

The Re isotope composition of marine sedimentary rocks could be a suitable palaeoredox proxy because:

- Re is geochemically similar to Mo (Morford *et al.* 2009), and the Mo isotope system has already been established as a palaeoredox proxy (Dickson *et al.* 2012, Pearce *et al.* 2008).
- Re is redox sensitive: it is authigenically enriched in sediments deposited in anoxic environments (Morford *et al.* 2012).
- Re is abiotic, it is not involved in any major biological reactions (Helz and Dolor 2012). However, Re has been shown to be incorporated into macroalgae (Racionero-Gómez *et al.* 2016).
- Re is conservative in seawater (Anbar *et al.* 1992).
- Re behaves slightly differently to Mo and U (Colodner *et al.* 1995); in particular, Re is enriched in sediment at less reducing conditions than Mo and U (Calvert and Pedersen 2007) and has a similar (or slightly shorter) residence time in the ocean to Mo (Re

residence time estimated to be 750,000 years by Colodner *et al.* (1993), and 130,000 years by Miller *et al.* (2011); Mo residence time is 440,000 years (Miller *et al.* 2011); residence time estimates for Re and Mo show significant overlap, see Table 2.1 for more details). Therefore, the Re isotope composition of sedimentary rocks might be able to show different features of redox history, particularly relating to the onset of redox events. Initial data from the work of Miller *et al.* (2009) show the potential of Re isotopes as a redox proxy. Modelling from Miller *et al.* (2015) show that the redox changes associated with deposition in anoxic environments could be associated with permil scale changes in δ^{187}Re.

Chapter 3 presents method development carried out to establish a method to determine δ^{187}Re for sedimentary rocks. This improves upon the method of Miller *et al.* (2009) in two ways. The method presented in Chapter 3 allows for the determination of δ^{187}Re for low concentration Re samples (requiring 1.6 - 6.0 ng Re compared to 10 ng required by Miller *et al.* (2009)), this is important because natural samples have very low Re concentration (Chapter 4 and Chapter 6). Secondly, the method of Miller *et al.* (2009) achieves incomplete separation of Re from matrix elements, which may compromise the determination of Re isotope composition. See section 3.4.2 for discussion of how the new method improves on this, and section 3.2 for discussion of why it is vital to achieve high purity Re separation.

This thesis expands the available Re isotope composition data for sediments and sedimentary rocks. A summary of δ^{187}Re data from this thesis (Figure 1.2) shows how the data presented here compares to previously available data, and is discussed further in Chapter 7.2.

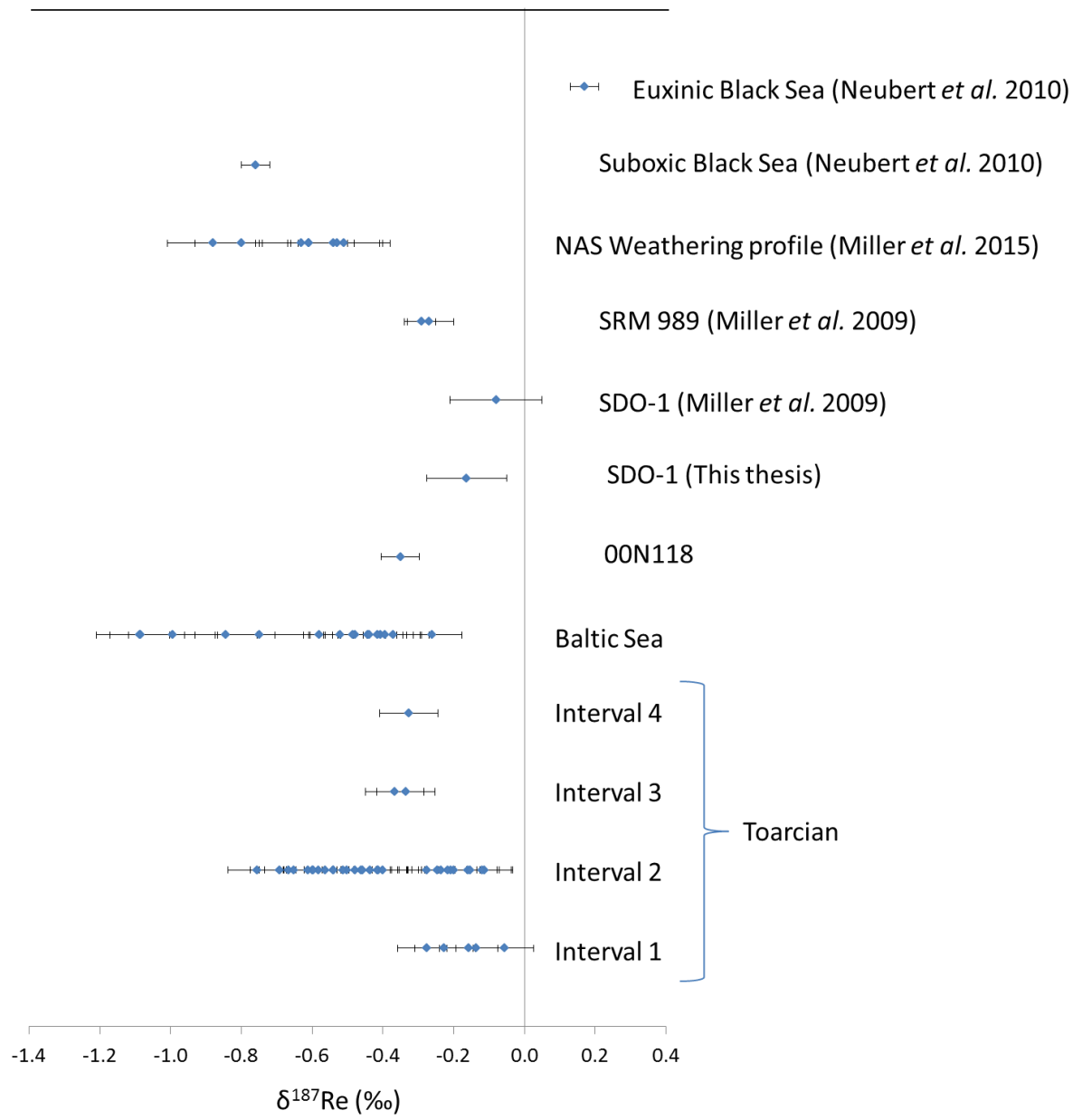

Figure 1.2: Summary of δ^{187}Re data of sediments and sedimentary rocks. Data for sedimentary rock samples from the Toarcian OAE from the Cleveland basin (Chapter 6), sediment samples from site BY15 in the Gotland Deep in the Baltic Sea (Chapter 4), 00N118 (an in-house reference sample created from organic rich mudrock from the Monterey Formation, Naples Beach, California, USA), and SDO-1 (a commercially available mudrock reference sample, Devonian Ohio Shale) are from this study. SDO-1 and SRM 989 (a single element Re standard) data from Miller *et al.* (2009), NAS weathering profile (sedimentary rock samples from the Devonian New Albany Shale near Clay City, Kentucky, USA) from Miller *et al.* (2015), and Black Sea sediment sample data from Neubert *et al.* (2010a) conference abstract. Data from other sources were analysed relative to SRM 989 and have been calibrated for comparability with δ^{187}Re determinations in this thesis, which were carried out relative to SRM 3143 (Chapter 3).

1.6 Oceanic anoxic events

Oceanic anoxic events (OAEs) are geological examples of major climatic change, characterised by widespread deposition of organic carbon (e.g. Jenkyns 1988). During an OAE, there are high atmospheric carbon dioxide concentrations (Jenkyns 2010b), elevated temperatures, high primary productivity, a decrease in oxygen concentration in the oceans (Pearce *et al.* 2008), and major biotic crises (Caswell and Coe 2012, 2013).

OAEs are likely to be caused by volcanic degassing from large igneous provinces (LIPs) (McElwain *et al.* 2005) and the destabilisation of methane hydrates (Hesselbo *et al.* 2000). Both processes increase global temperatures due to elevated carbon dioxide in the atmosphere, which increases primary productivity in the oceans, and in turn leads to lower oxygen inputs to the ocean and higher levels of oxygen utilisation due to aerobic respiration of organic matter on the seafloor (Figure 1.3). There have been eight OAEs during the Mesozoic period, the first of which was the T-OAE which occurred ~183 Ma (Pálfy and Smith 2000). All eight Mesozoic OAEs, and the PETM are correlated with flood basalt eruptions (Rampino and Caldeira 2017).

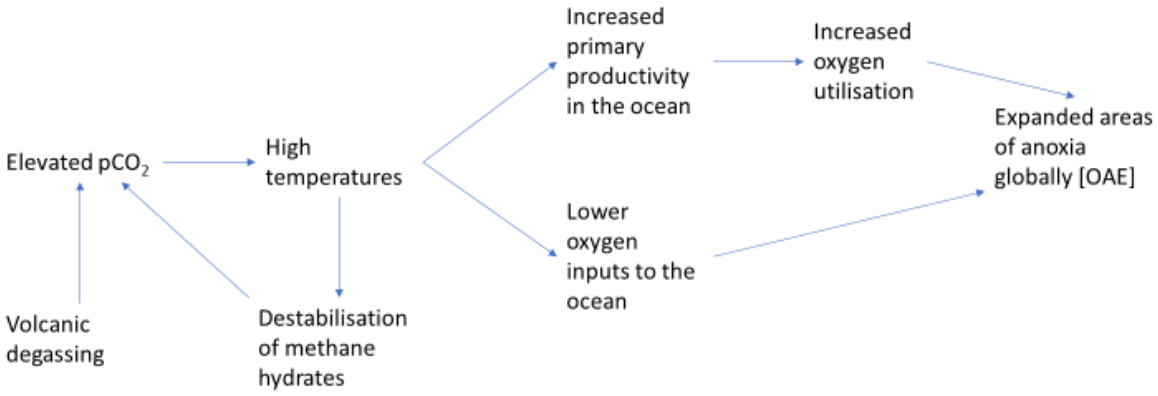

Figure 1.3: A simplified diagram to show the feedback mechanisms involved in the onset of OAEs.

Evidence for widespread anoxia during OAEs is provided by the widespread deposition of organic carbon globally (e.g. Jenkyns 1988), and changes in the geochemistry of sedimentary rocks across the events (e.g. Jenkyns 2010). Changing Mo concentration and $\delta^{98/95}$Mo during the

T-OAE and in comparison to other OAEs has been used to assess the areal extent of anoxic deposition (Dickson *et al.* 2012, Dickson *et al.* 2017, Pearce *et al.* 2010b, Pearce *et al.* 2008). Changing U isotope composition has been used to show evidence of two episodes of deoxygenation during OAE 2, the Cenomanian-Turonian boundary event (Clarkson *et al.* 2018).

The environmental changes which occur during an OAE are accelerated by positive feedbacks. For example, the re-mobilisation of phosphate minerals in anoxic depositional settings accelerates the enhanced productivity in the surface ocean and drives further anoxia (Mort *et al.* 2010, Watson *et al.* 2017). Once the environmental changes begin during the onset of an OAE, these feedbacks accelerate the progression to anoxic conditions. Basin geometry may also play a role in the development of anoxia, with shallow epicontinental seaways being the most vulnerable to its onset.

OAEs are geologically rapid, usually lasting around half a million years (Boulila and Hinnov 2017, Kemp *et al.* 2011). It is useful to understand the timescales over which OAEs occur, to make comparisons between OAEs and modern-day climate change. Estimates of pCO_2 and timescales over which OAEs occur allow us to compare these changes with the rate of carbon dioxide emissions in the modern day (Beerling and Brentnall 2007, Beerling 2002).

The T-OAE has been extensively studied at various sites from around the globe (see Chapter 5). Major redox changes are recorded across the T-OAE in $\delta^{13}C$ (defined as $\delta^{13}C = (((^{13}C/^{12}C)_{sample}/(^{13}C/^{12}C)_{Pee\ Dee\ Belemnite})-1) \times 1000$ ‰) data (Kemp *et al.* 2011), Re/Mo, element concentration data (Pearce *et al.* 2008), and biotic changes (Caswell and Coe 2014). The major redox changes observed suggests that this event might exhibit variation in $\delta^{187}Re$ if the proxy does indeed track redox variations.

The Yorkshire section has been characterised for a range of geochemical features, including high resolution $\delta^{13}C_{org}$ (Kemp *et al.* 2011) and $\delta^{98/95}Mo$ (Pearce *et al.* 2008), which present useful

comparison points for the δ^{187}Re data presented in Chapter 6. The samples chosen from the Yorkshire section were selected because they had been previously analysed for $\delta^{98/95}$Mo (Pearce *et al.* 2008), and these samples had been well correlated with high resolution δ^{13}C data from the same site (Kemp *et al.* 2011). The samples have reasonably high Re concentration (previously determined by Pearce *et al.* 2008), and so presented the possibility to test the Re isotope analysis method (Chapter 3) on samples using ~0.5 g of sample.

1.7 Determination of δ^{187}Re of recent sediment samples

The method for determining δ^{187}Re in marine sedimentary rocks was applied to recent marine sediment from the Baltic Sea. Samples were selected from a location with a well recorded redox history (site BY15 in the Gotland Deep, Figure 4.1), so that any variation in δ^{187}Re observed could be compared with known redox changes. The aim of this work was to better understand how the Re isotope system behaves in the ocean under a variety of redox conditions.

The requirements for samples were that they exhibited a change in redox conditions and included anoxic/euxinic deposition environments, that the bottom water dissolved O_2 concentration was known, and that they were geochemically and lithologically similar to the samples from the T-OAE. Options for sample sites include semi-restricted seaways, and equatorial upwelling zones, both of which are vulnerable to anoxia in the present-day ocean. The Baltic Sea was chosen due to continual records of bottom water oxygen concentration (Gustafsson and Medina 2011), and the availability of high resolution samples kindly provided by Caroline Slomp, University of Utrecht, The Netherlands. Site BY15 from the Gotland Deep in the Baltic Sea was chosen due to the high organic carbon concentration, elevated Mo concentration, and high-resolution Mo concentration available from the site (Jilbert and Slomp 2013b). Potential complications with the Baltic Sea sediment come from the close proximity to coastal cities, and thus the potential for anthropogenic Re to impact δ^{187}Re data at this site. This would be an issue for any anoxic sediment in the present day (except perhaps for remote areas with lower levels of

anthropogenic Re) since anthropogenically elevated Re concentration is observed in rivers (Miller *et al.* 2011, Rahaman *et al.* 2012), and in the surface waters of the Black Sea (Colodner *et al.* 1995). This is discussed further in Chapters 2 and 4.

1.8 Thesis structure

The main body of the thesis is structured into five chapters (summarised in Table 1.2). Chapters 3, 4 and 6 present the main findings of this study including the method developed and the application of this method to two examples. Chapters 2 and 5 present relevant parts of the critical literature review for this thesis. The chapters have been organized so that there is a logical scientific order. Chapter 2 is a literature review of Re in seawater, Re isotopes and the research to date on the development of Re isotopes as a palaeoredox proxy. Chapter 3 presents the method developed for use of Re isotopes as a palaeoredox proxy and used during this research project. Chapter 4 applies the method presented in Chapter 3 to modern day sediments in the Baltic Sea to attempt to constrain the behaviour of Re isotopes using modern sediments. Chapter 5 is a literature review of the Toarcian Oceanic Anoxic Event on which there is an extensive and ever-growing literature. As this presents the very wide context which is only relevant to Chapter 6, it has been placed immediately prior to Chapter 6. Chapter 6 applies the method presented in Chapter 3 to an example of past ocean anoxia, the T-OAE of Yorkshire. The thesis finishes with Chapter 7 which concludes the main findings of the thesis from both modern day and the Toarcian examples and proposes future work to further develop δ^{187}Re as a proxy for past ocean redox conditions.

Table 1.2: A summary of the aims of each of the chapters presented in the thesis.

Chapter	Summary	Aims
1	Introduction	To set up the rationale for the thesis.
2	Introduction to rhenium	To Introduce Re and its behaviour in seawater
3	Method development	To develop a method for the precise and accurate determination of δ^{187}Re in geological materials. To show that the method can produce reliable data.
4	The Baltic Sea	To assess how δ^{187}Re varies with known redox variations in organic rich sediment.
5	Introduction to the T-OAE	To introduce the current state of knowledge of the T-OAE, with specific reference to redox changes across the event.
6	Application of δ^{187}Re to the study of the T-OAE	To establish whether the redox changes across the T-OAE are recorded in δ^{187}Re. To assess whether the δ^{187}Re record can illuminate new features of the redox history of the T-OAE.
7	Conclusions and future work	To summarise the conclusions from the thesis, and to suggest future work which would be useful in developing δ^{187}Re as a proxy for past ocean redox conditions.

Chapter 2

Introduction to rhenium

This chapter provides a literature review of all the relevant published work on Re in seawater, Re isotopes and its use as a palaeoredox proxy which is the focus of this study. Rhenium has received relatively little attention to date; the chapter therefore also includes reference to conference abstracts.

2.1 Introduction

Rhenium was discovered in 1925, when it was detected spectroscopically in platinum ores and in the minerals columbite, gadolinite, and molybdenite (Noddack and Noddack 1929). Since then, Re has been observed in oxidation states ranging from -1 to +7 (I to VII) (Wedepohl 1976). Rhenium has two naturally occurring isotopes (Robinson and Thoennessen 2012): ^{185}Re, which has an abundance of 37.07%; and ^{187}Re, with an abundance of 62.93% (Gramlich *et al.* 1973). ^{187}Re is unstable and decays by β^- decay to ^{187}Os with a half-life of $4.3 \pm 0.5 \times 10^{10}$ years (Wedepohl 1976). This decay system is used in the dating of geological materials (Cohen *et al.* 1999, Dichiarante *et al.* 2016, Reisberg and Meisel 2002, Selby *et al.* 2007). The average concentration of Re in continental crust is 0.4 ng g^{-1} (McLennan 2001).

Rhenium occurs in seawater as ReO_4^- with Re in the (VII) oxidation state, but it may become enriched in sedimentary deposits by the reduction of Re to the (IV) form under reducing conditions (Morford *et al.* 2012). The measurement of Re concentration in a water depth profile in the Pacific Ocean has shown that Re is generally conservative in seawater (Anbar *et al.* 1992). The pattern of Re concentration observed within this water depth profile indicates that the main source of Re into the ocean is at the ocean surface or in shallow water, and that there is limited

scavenging of Re within the water column (Anbar *et al.* 1992). A lack of Re enrichment recorded in sediment trap samples from euxinic basins indicates that Re enrichment observed in anoxic sediment is likely to be caused by accumulation below the sediment water interface (Crusius *et al.* 1996).

2.2 Comparison with the Mo isotope system

The Mo isotope system has been relatively extensively studied compared to the Re isotope system (Anbar 2004, Anbar and Rouxel 2007, Kendall *et al.* 2017). The use of variations in Mo isotope composition as an ocean palaeoredox proxy was first proposed in the 1980s (Emerson and Huested 1991, Holland 1984). Since then, improved understanding of Mo cycling in the ocean (Crusius *et al.* 1996, Helz *et al.* 2011, Morford and Emerson 1999) has enabled the establishment of $\delta^{98/95}$Mo as a palaeoredox proxy (Barling *et al.* 2001, Siebert *et al.* 2003). This proxy has been applied in the study of modern ocean sediments from a range of redox environments (e.g. Morford *et al.* 2007, Neubert *et al.* 2008, Noordmann *et al.* 2015, Poulson *et al.* 2006, Siebert *et al.* 2006), and to a range of redox events in Earth's history (e.g. Dickson *et al.* 2012, Dickson *et al.* 2017, Dickson *et al.* 2016, Pearce *et al.* 2008, Siebert *et al.* 2005).

The dominant Mo species in oxygenated seawater is MoO_4^{2-} (Miller *et al.* 2011). Molybdenum has a much higher concentration in seawater than Re, of 104 nmol kg^{-1} compared to 40 pmol kg^{-1} (Collier 1985, Colodner *et al.* 1993, Miller *et al.* 2011, Morris 1975). The global seawater $\delta^{98/95}$Mo is 2.34 ± 0.10 ‰ (Barling *et al.* 2001, Nakagawa *et al.* 2012, Siebert *et al.* 2003), and is influenced by the balance between input fluxes, and removal to the ocean floor under euxinic and oxic conditions. The dominant source of both Re and Mo to the ocean is dissolved river flux (section 2.2), for which $\delta^{98/95}$Mo ranges between -0.1 and +2.3 ‰ (Neubert *et al.* 2011, Archer and Vance 2008). Low temperature hydrothermal systems make a minor contribution of Mo to seawater; high temperature hydrothermal fluids are not a source of Mo to the ocean, likewise for Re (Miller *et al*. 2011).

Molybdenum is authigenically removed from seawater under oxic and euxinic redox conditions, with differing effects on the $\delta^{98/95}$Mo of sediment depending on the severity of the redox conditions and the amount of exchange between the basin and the open ocean (Figure 2.1, Dickson 2017). Under euxinic conditions, Mo is taken into sediment by the reduction of MoO_4^{2-} to thiomolybdate species $MoO_{4-x}Sx^{2-}$, and then scavenging by adsorption onto Fe-Mn particles (Miller *et al.* 2011). In restricted basins with strongly euxinic conditions, *e.g.* the Black Sea, Mo is thought to be quantitatively removed from seawater and therefore sediment $\delta^{98/95}$Mo values reflect those of global seawater (Neubert *et al.* 2008, Noordmann *et al.* 2015, Dickson 2017). Where bottom waters are intermittently euxinic or have low H_2S, Mo is fractionated in its removal to sediment, and there is a range of $\delta^{98/95}$Mo in underlying sediment of -0.6 to +1.8 ‰ (Poulson *et al.* 2006, Siebert *et al.* 2006). Under oxic conditions, Mo is thought to be removed to sediment by adsorption to and/or co-precipitation with Mn oxide phases (Kendall *et al.* 2017). This process results in a fractionation of around 3 ‰ between seawater $\delta^{98/95}$Mo values and that of Fe-Mn nodules/crusts which have a $\delta^{98/95}$Mo = -0.7 ‰ (Barling and Anbar 2004, Siebert *et al.* 2003). The oxic sink of Mo covers ~80 % of the seafloor and removes between 30-50 % of riverine Mo supply; the comparatively rapid euxinic sink covers 0.3% of seafloor but removes ~6-15 % of Mo entering the ocean via rivers each year (Scott and Lyons 2012). By comparison to Mo, the sinks of Re to the ocean are relatively difficult to quantify (section 2.4). There is also a distinct lack of Re isotope composition data compared to the wealth of available data for $\delta^{98/95}$Mo (Figure 2.1, sections 2.6 and 2.7); in particular, δ^{187}Re of global seawater and of dissolved river flux is as yet unknown (section 7.3).

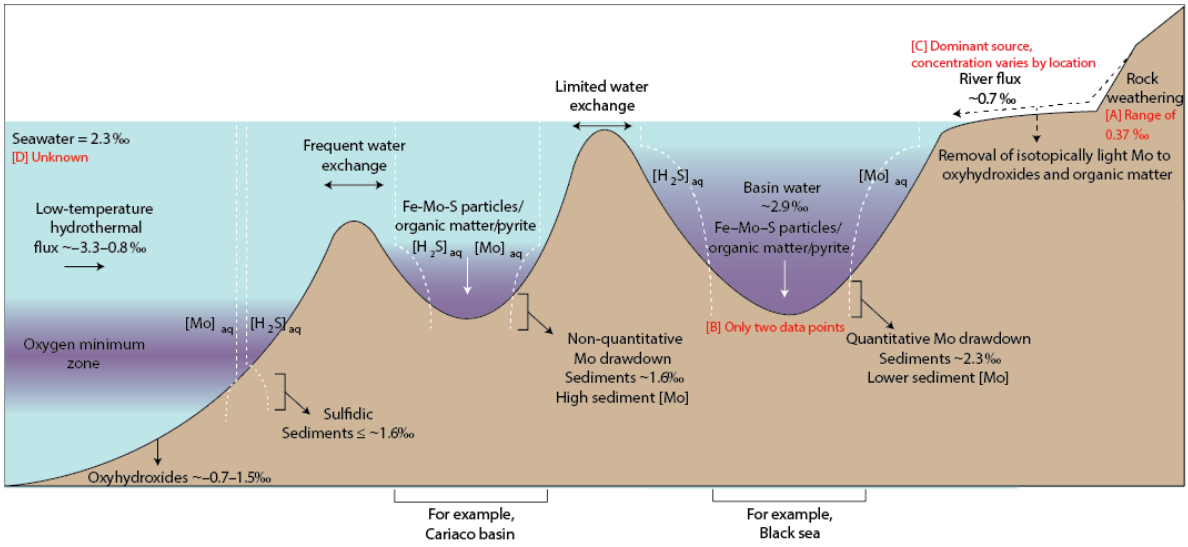

Figure 2.1: A summary of the Mo isotope system (edited from Dickson *et al.* (2017)), with comparisons to the Re isotope system. All writing in black relates to the Mo isotope system, and is taken from Dickson *et al.* (2017). The $\delta^{98/95}$Mo values of sediment and waters are from (Archer and Vance 2008, Arnold *et al.* 2004, Barling *et al.* 2001, McManus *et al.* 2002, Nägler *et al.* 2011, Nakagawa *et al.* 2012, Neubert *et al.* 2011, Neubert *et al.* 2008, Pearce *et al.* 2010a, Poulson Brucker *et al.* 2009, Poulson *et al.* 2006, Siebert *et al.* 2003, Siebert *et al.* 2015) and $Mo_{(aq)}$ and $H_2S_{(aq)}$ concentrations are schematic. Annotations added in red give information currently known about the Re isotope system: [A] the range in δ^{187}Re is from a weathering profile of New Albany Shale (Miller *et al.* 2015); [B] two data points for δ^{187}Re from suboxic and euxinic sediment from the Black Sea show a 1 ‰ variation in values (Neubert *et al.* 2010a, Figure 1.2); [C] dissolved river flux is the dominant source of Re to the ocean, though δ^{187}Re of these sources is unknown; [D] the δ^{187}Re value for global seawater is unknown.

2.3 Sources of Re to seawater

Weathering of continental crust (particularly sulphide minerals and organic rich sedimentary rocks) is the dominant source of Re to the ocean through dissolved riverine flux (Miller *et al.* 2011). Organic-rich sedimentary rocks contain high concentrations of Re, and contribute disproportionately to the upper continental crust Re inventory (Dubin and Peucker-Ehrenbrink 2015). The Re concentration of hydrothermal fluids is almost zero; high temperature hydrothermal fluids represent ~0.1 % of the magnitude of the flux of Re from riverine sources, and so are not a significant source or sink of Re to the ocean (Miller *et al.* 2011).

The global average concentration of Re in rivers (based on data from 38 rivers from five continents) has recently been estimated as 16.5 pmol kg^{-1}, which is corrected to 11.2 pmol kg^{-1}

after accounting for anthropogenic Re (Miller *et al.* 2011). However, estimates of Re concentration in the Himalaya and Peninsular India average 3 pmol kg^{-1} (Rahaman *et al.* 2012), a much lower concentration estimate than the world river average found by Miller *et al.* (2011). Rahaman *et al.* (2012) find large variation in the anthropogenic Re content of the rivers in their study, with up to 70% of the total Re supplied to the Bay of Bengal and the Arabian Sea originating from anthropogenic sources. This proportion is significantly higher than that estimated by Miller *et al.* (2011), who estimate that on average 32 % of Re in rivers worldwide is anthropogenic in origin. In Black Sea surface waters, Re concentration is anthropogenically enriched up to 80-fold (Colodner *et al.* 1995). There is clearly significant localised variation in both Re concentration, and the percentage of anthropogenic Re in rivers; the Re concentration is likely to be affected by the geology of the source area, and anthropogenic percent will be affected by local population density, and economy.

Current estimates of Re residence time in the ocean are calculated based on steady-state and flux-in estimates (Colodner *et al.* 1993, Miller *et al.* 2011; see section 2.5 below). Since anthropogenic Re sources are likely to compose an increasing proportion of present-day riverine Re budgets (Colodner *et al.* 1995), it is important that the anthropogenic inputs are well constrained to better estimate the residence time of Re in the ocean.

2.4 Rhenium sinks from seawater

Rhenium has a strong potential to become enriched in authigenic sediments due to its exceptionally high $[metal]_{seawater}/[metal]_{crust}$ ratio (Crusius *et al.* 1996). It has also been shown that Re is enriched in sedimentary deposits deposited in both anoxic and euxinic environments (Crusius *et al.* 1996). The sinks of Re in seawater are relatively difficult to quantify. Helz and Dolor (2012) conducted a study to assess how the accumulation of Re in anoxic sediments is initiated. They propose that the triggering mechanism is "neither reduction nor thiolation of ReO_4^-, but

instead saturation of sulphidic waters with a Fe-Mo-S phase". Rhenium sequestered into sediment is associated almost exclusively with sulphide minerals (Miller *et al.* 2011).

It is estimated that 43 % of the riverine input of Re to the ocean is removed annually into sediments covering ~0.3 % of the ocean floor, and therefore ocean Re budgets may be particularly sensitive to small changes in the areal extent of anoxic sedimentation (Colodner *et al.* 1993). As such, it may be possible to estimate the areal extent of anoxic sediment deposition if the reduction of Re shows measurable isotopic fractionation. The Mo isotopic system has been used to assess the areal extent of anoxic sediment deposition in a similar fashion (Dickson *et al.* 2012, Pearce *et al.* 2008).

Morford *et al.* (2009) present data and model the accumulation and removal of various redox sensitive elements from sediment, including Mo and Re. They found that the depth at which Re is removed to the sediment from pore waters extended throughout their depth of study (0 to 25 cm sediment depth). Their study also suggests that the lack of correlation between the Re concentration and the rate of remineralisation is indicative of an abiotic process of concentrating Re in sediments. Rhenium incorporation into sediment below the sediment water interface is generally considered to be abiotic (Colodner *et al.* 1995), however some evidence suggests that Re is preferentially incorporated into algae (Racionero-Gómez *et al.* 2016).

The analysis of modern-day sediments from the Atlantic Ocean has shown that the authigenic accumulation rates of Re mirrors the reduction potential of an environment (Morford *et al.* 2012). This was demonstrated using the analysis of pore water and solid phase depth profiles at three different sites on the Middle Atlantic Bight. The study also shows that whilst some re-mobilisation of Re from the sediment due to re-oxidation does occur, this process is limited to sites of shallow oxygen penetration depth (< 1 cm) and in most settings, is far outweighed by the effects of organic-carbon deposition and Re accumulation.

Helz and Adelson (2013) attempted to assess the relationship between changing redox conditions in Chesapeake Bay, USA, and changing Re concentration in sediment. They find only a modest (< 1 ng g^{-1}) elevation in Re concentration during the 20th century, despite a historic record of summertime O_2 depletion. Helz and Adelson (2013) suggest that the observed Re enrichment is therefore caused by anthropogenic input rather than changing redox conditions. In addition, seasonal variations in oxygenation of bottom water is likely to occur on too short a timescale to significantly affect the Re concentration of sediment.

Rhenium concentration in high temperature hydrothermal fluids is lower than seawater concentration, indicating that high temperature fluid circulation acts as a sink of Re from seawater (Miller *et al.* 2011). However, as discussed in section 2.3, the magnitude of this flux is very small, and is much smaller than the sink to anoxic sediments.

2.5 The residence time of Re in seawater

The sinks of Re in seawater are difficult to quantify and so the residence time is estimated by assuming a steady state system. Miller *et al.* (2011) estimate a river flux of 4.3 x 10^5 mol y^{-1}, this suggests a seawater residence time of 1.3 x 10^5 years (pre-anthropogenic), and 8.2 x 10^4 years when adjusted to account for the anthropogenically enhanced modern Re flux. However, Colodner *et al.* (1993) present a flux weighted average riverine flux of Re to the oceans of 2.3 pmol kg^{-1}, and hence a residence time of 7.5 x 10^5 years, which is significantly longer than that estimated by Miller *et al.* (2011). The reduced estimate of the residence time of Re in the ocean made by Miller *et al.* (2011) presents the possibility that the system has a higher sensitivity to changes in sources or sinks than previously thought. As this shorter residence time is longer than ocean mixing time of ~1500 – 2000 years, there is still the possibility that the Re isotopes recorded in sediments can be used to accurately represent the global average of seawater Re isotope composition.

Table 2.1 shows how the residence time of Re compares with Mo and U (two more established isotopic redox proxies). Since anoxic depositional environments are a major sink for redox sensitive elements, the area of anoxic deposition is likely to affect the ocean residence time of these elements; when the area of anoxic deposition increases, the residence time would be significantly reduced. It is possible that the residence time may differ in restricted basins compared to the open ocean, where the removal of these metals to sediments may occur at a much faster rate due to the effects of anoxia, or where changes to local inputs may have a proportionally larger effect relative to the size of the reservoir in the basin.

Table 2.1: Comparison of Re, U and Mo.

Element	**U**	**Re**	**Mo**
Residence time in seawater	400 Ky (Ku *et al.* 1977)	82 Ky in modern times (Miller *et al.* 2011) 130 Ky pre-anthropogenic (Miller *et al.* 2011) 750 Ky (Colodner *et al.* 1993)	440 Ky (Miller *et al.* 2011) 800 Ky (Morford and Emmerson 1999)
Reducing environment that the isotope proxy can be applied to	Suboxic (O_2 < 2 ml L^{-1} and no H_2S) (Andersen *et al.* 2014, Tribovillard *et al.* 2012)	Anoxic (O_2 < 0.2 ml L^{-1}, and no H_2S) (Crusius *et al.* 1996, Miller *et al.* 2009, Miller *et al.* 2011)	Euxinic (No O_2 with free H_2S present) (Dickson *et al.* 2017, Miller *et al.* 2011, Pearce *et al.* 2008)
‰ variation observed/expected	Isotope composition variation ~1.3 ‰ observed in various marine environments (Weyer *et al.* 2008)	Some natural variation observed, expected variation on the order of 1 ‰ based on theoretical calculations (Miller *et al.* 2009)	Isotope composition variation of a magnitude of ~3 ‰ observed in various natural environments (Kendall *et al.*2017)

2.6 Rhenium isotopes

The first attempts to analyse the Re isotope composition of geological samples centred around the accurate determination of Re concentration by isotope dilution for Re-Os dating (e.g. Cohen *et al.* 1999, Reisberg and Meisel 2002) although it is not possible to assess the naturally occurring Re isotope composition of samples using this method.

The range of Re isotope composition data available in published literature and conference abstracts (Table 2.2) indicates that high resolution Re isotope analyses are possible, and that there appears to be some small-scale variation in the Re isotope composition of Re standards. It is important to note that these sources employ a variety of methods, and employ different standards for standard-sample bracketing which is listed where available in Table 2.2.

Table 2.2: Re isotope composition data from published literature and conference abstracts.

Reference	Re isotope composition of various standards
Gramlich *et al.* (1973)	The expected $^{185}Re/^{187}Re$ ratio of bulk geological samples is 0.5974.
Zimmerman *et al.* (2011)	Reported $^{185}Re/^{187}Re$ of a standard after Carius tube digestion, found $^{185}Re/^{187}Re$ = 0.601608.
Zimmerman *et al.* (2013)	Analyses of $^{185}Re/^{187}Re$ of four molybdenite samples by N-TIMS, including NIST RM 8599, and AIRIE's Re standard solution (RR-4, prepared from potassium perrhenate), found mean $^{185}Re/^{187}Re$ = 0.5989 ± 0.0014 1 SD (n = 16).
Miller *et al.* (2009)	Analyses of SRM 989, SRM 3143, $HReO_4$, Alfa Aesar, and H. Cross ribbon Re single element standards by MC-ICP-MS, carried out using tungsten (W) external correction, and reported relative to SRM 989 exhibit a range in Re isotope composition of 0.29 ‰.
Liu *et al.* (2017)	Analyses of Re isotope compositions by MC-ICP-MS, using a W external correction, and reported relative to average values of BDS Aristar™ (lot: B2-RE-0168) show a range in Re isotope signatures of up to 0.30‰ between the standards: Alfa Aesar™, Alfa Aesar™ metal, BDH™, HPS™, and SRM 989.

During the precise determination of Re isotope composition by MC-ICP-MS mass bias is introduced by the instrument which must be corrected for (Poirier and Doucelance 2009). Since Re has only two stable isotopes, the double spiking method utilised for example in Mo isotope analyses is not suitable. Tungsten (W) spiking can be used to correct for instrumental mass bias in the determination of Re isotopic ratio by MC-ICP-MS (Poirier and Doucelance 2009). This method

is still possible when some matrix elements remain in the final Re solution (Poirier and Doucelance 2009). The use of Ir as a mass bias correction for Re isotope analyses by MC-ICP-MS was developed by Day *et al.* (2003) and Pearce *et al.* (2009) who were targeting the precise determination of Re concentration by isotope dilution in geological materials.

More recently, Liu *et al.* (2017) found variations in the Re isotope composition for different types of meteorites. Metal from IVB iron meteorites are systematically enriched in ^{187}Re relative to H chondrites by ~0.14 ‰, although the reason for this remains unexplained (Liu *et al.* 2017).

2.7 Rhenium isotopes as a palaeoredox proxy

Potential variations in the isotopic ratio of Re could provide insights into the redox conditions of past marine environments (Anbar and Gordon 2008, Miller 2009, Miller *et al.* 2015). Rhenium had been shown to accumulate below the sediment water interface (Crusius *et al.* 1996) and therefore its accumulation is more strongly influenced by authigenic rather than detrital processes. As such, the Re isotope composition of sediments is likely to be representative of contemporaneous seawater systems at the time of deposition.

There are currently limited Re isotope data available for sedimentary deposits in present-day oceanic settings (Neubert *et al.* 2010a, b). There is some evidence that Re isotope composition is altered by redox conditions, from a study of Black Sea sediment samples (Neubert *et al.* 2010a, b), and a weathering profile across Devonian New Albany Shale (Miller *et al.* 2015). There is a ~ 1 ‰ variation in the Re isotope signature between suboxic and euxinic sediment samples from the Black Sea with the euxinic sediment sample being enriched in ^{187}Re compared to the suboxic sample (Neubert *et al.* 2010a, Figure 1.2). There is a range of 0.37 ‰ in the Re isotope composition of samples across a weathering profile of Devonian Shale (Miller *et al.* 2015).

Theoretical calculations have been used to estimate the fractionation factors of Re isotopes from and to various Re species (Miller *et al.* 2015). Miller *et al.* (2015) compared the relative effects of mass dependent and nuclear volume fractionation factors on the net fractionation of $^{187}Re/^{185}Re$ relative to both Re^0 vapour and $Re^{VII}O_4^-$. The neutron-rich ^{187}Re tends to become more concentrated in more oxidised species due to mass dependent fractionation. However, nuclear volume fractionation tends to concentrate heavier nuclei species when the electron density of the nucleus is small, and therefore the more reduced Re^{IV} species tend to be ^{187}Re enriched. The theoretical models predict that nuclear volume effects are smaller than mass dependent ones, accounting for 25 to 50 % of the effect when evaluated relative to $Re^{VII}O_4^-$; therefore, Re isotope fractionation is expected to be dominated by the effects of mass dependent fractionation in which ^{187}Re is concentrated in the more oxidised species (Miller *et al.* 2015). $Re^{VII}O_4^-$ is the dominant aqueous species of Re in the ocean, and the total fractionation factor predicted for the removal of Re from seawater depends on the species that $Re^{VII}O_4^-$ is reduced to. The equilibrium fractionation of Re in seawater at surface temperatures is expected to result in ‰ level Re isotope composition variations (Miller *et al.* 2015).

2.8 Conclusions

Rhenium is a redox sensitive metal, which is preferentially enriched in sediments deposited in a reducing environment (Crusius *et al.* 1996, Miller *et al.* 2009, Morford *et al.* 2012). Recent studies have led to a better understanding of the geochemical cycling of Re in the oceans (Helz and Adelson 2013, Miller *et al.* 2011). There is evidence of naturally occurring variation of the Re isotope composition in geological samples (Liu *et al.* 2017, Miller 2009, Miller *et al.* 2015). Variations in the Re isotope composition in sediment and sedimentary rock samples appears to be influenced by redox changes (Miller *et al.* 2015, Neubert *et al.* 2010a). There are geochemical similarities between Re and Mo (Crusius *et al.* 1996), and the use of Mo isotopes as a past ocean redox proxy has already been established (e.g. Dickson *et al.* 2017, Duan *et al.* 2010, Kendall *et al.*

2017, Noordmann *et al.* 2015, Pearce 2007, Pearce *et al.* 2008, Ruebsam *et al.* 2017, Scholz *et al.* 2017, Siebert *et al.* 2003). Therefore, the determination of the Re isotope composition in marine sedimentary rocks has the potential to be developed as a new proxy for past ocean redox conditions. Rhenium and Mo exhibit differing redox sensitivities (Colodner *et al.* 1995, Crusius *et al.* 1996), and Re may have a shorter residence time in the ocean, although there are significant overlaps in the estimates of residence time for Re (84 ky to 750 ky) compared to Mo (440 ky to 800 ky), see Table 2.1 (Helz and Adelson 2013, Miller *et al.* 2011, Rahaman *et al.* 2012). The use of Re isotopes as a palaeoredox proxy therefore has the potential to illuminate new features of the redox history of sedimentary rocks.

Chapter 3

Quantitative separation of rhenium from sedimentary rocks and high precision rhenium isotope ratio analysis by MC-ICP-MS

This chapter of the thesis presents the development of a method to use Re isotopes as a seawater redox proxy. This method has then been applied in this research project to a modern-day example (Baltic Sea: Chapter 4) and an example from the geological record, the Toarcian Oceanic Anoxic Event (Chapter 6).

Note on contributions: All the method development and analytic work was carried out by FR, under the laboratory supervision of supervisor MF. The samples were identified and supplied by supervisor ALC. The results during the method development and further tests were discussed and developed by FR with the supervisor team. FR processed the results, wrote the chapter and prepared the figures and the supervisory team provided comments and suggested amends.

3.1 Summary

The rhenium (Re) isotope system provides a new proxy for past seawater redox conditions. This study presents a new technique for the precise and accurate determination of the Re isotope composition of geological samples (specifically marine mudrocks, see Chapter 6). The method involves the high purity extraction of Re and the use of Ir for mass bias correction. Rhenium was separated from the matrix using an improved two-stage anion exchange chromatographic procedure. Measurements of the Re isotope composition of standards and samples were carried out using a Thermo Neptune multiple-collector inductively coupled plasma mass spectrometer (MC-ICP-MS). We demonstrate the viability of this method using three

organic-rich mudrock samples of Toarcian (Early Jurassic) age from Yorkshire UK (Chapter 6 presents data from an expanded suite of samples), an in-house standard sample created from a mudrock from the Monterey Formation, USA (00N118), and a commercially available mudrock reference sample (SDO-1; Devonian Ohio Shale). The average Re isotope composition for the Toarcian samples are δ^{187}Re = -0.326 ± 0.146 ‰ (n = 4) for Tco 01-50, δ^{187}Re = -0.335 ± 0.197 ‰ (n = 6) for Tfa 01-25, and δ^{187}Re = -0.583 ‰ ± 0.071 ‰ (n = 6) for Tex 06-28. The average Re isotope composition for the standard samples are δ^{187}Re = -0.351 ‰ ± 0.053 ‰ (n = 3) for 00N118, and δ^{187}Re = -0.129 ‰ ± 0.109 ‰ (n = 3) for SDO-1. The maximum range in δ^{187}Re observed between geological samples analysed during this study is 0.454 ‰. The external reproducibility is 0.084 ‰ (2 SD) for standard solutions of 5 - 20 ng ml^{-1}, using 1.5 - 6 ng of Re for each analysis. The new method of measuring the natural variation in Re isotope composition in geological materials presented here provides a marginal improvement in reproducibility compared to previous studies and requires less Re (1.5 - 6 ng of Re compared to a minimum of 10 ng) making it possible to precisely determine the isotopic composition of samples with lower concentrations of Re.

3.2 Introduction

Rhenium occurs in trace quantities in the Earth's crust and seawater with average concentrations of 0.4 ng g^{-1} and 8.06 pg g^{-1}, respectively (Colodner *et al.* 1993, Miller *et al.* 2011). Rhenium has two naturally occurring isotopes, ^{185}Re (37.398 ± 0.016 %) and ^{187}Re (62.602 ± 0.016 %) (Gramlich *et al.* 1973). Until relatively recently, it had been assumed that the proportion of the two isotopes in nature was invariant (Gramlich *et al.* 1973). However, Miller *et al.* (2009) observed small variations in the Re isotope composition of some elemental and geological standards. The maximum variation observed by Miller *et al.* (2009) was 0.29 ± 0.07 ‰ between the single element standards SRM 989 and SRM 3143 (see Chapter 2 for a more complete discussion of the previous work on Re and its isotope variations). Other studies of Earth materials have shown

similar levels of variation in the isotopic composition of elements, such as Mo, Cr and U (e.g. Frei *et al.* 2011, Pearce *et al.* 2008, Weyer *et al.* 2008). These variations are thought to be related to redox and/or speciation processes operating in the Earth's crust and in seawater (e.g. Frei *et al.* 2011, Pearce *et al.* 2008, Weyer *et al.* 2008). A more complete discussion of isotopic variation in Earth materials due to these processes is presented in Chapter 1.

The potential for the rhenium isotope system to resolve changes in the areal extent of suboxic seafloor has been highlighted by Anbar and Gordon (2008) and Miller *et al.* (2015). The enrichment of redox sensitive elements below the sediment water interface occurs at different depths because the enrichment factor varies as the oxidation state of the ambient environment changes from anoxic, through suboxic to euxinic (Crusius *et al.* 1996). Morford *et al.* (2012) showed that the accumulation rate of rhenium in sediment is related to the extent of reducing conditions. Whilst it is possible to resolve features of the redox history of seawater from single proxies such as Mo (Pearce *et al.* 2008), using a range of proxies from elements of differing redox sensitivities (such as Re and Mo) has the potential to enable additional details about past redox conditions to be determined, for instance the relative proportions of anoxic and euxinic seafloor.

The analysis of natural variations in the Re-isotopic composition of sedimentary rocks is analytically challenging, due to the low concentration of Re and the small natural variations in Re isotope composition. Significant fractionation of Re isotopes can occur during its chemical separation and purification (Georgiev *et al.* 2018, Miller *et al.* 2009), therefore full recovery of Re from sample aliquots is essential in order to ensure that no isotopic fractionation is produced by the separation procedure; almost 100% recovery of Re is achieved both by the method presented in this chapter, and that of Miller *et al.* (2009). This requirement is particularly important since double-spiking techniques (similar to those used in Mo, U and Cr isotope analysis) are not available for Re analysis. Double spiking is not available because Re has only two isotopes and

lacks any artificial isotopes of sufficiently long half-life that could be used to correct for mass fractionation during sample preparation and analysis. Furthermore, matrix effects have the potential to cause biases in isotope ratio analysis when performed by MC-ICP-MS (Albarède *et al.* 2004). Some elemental and molecular species have the potential to cause isobaric interferences during Re isotope composition determination (Table 3.1). The Re fraction must therefore be of a very high purity to allow precise and accurate determination of the Re isotope composition. The abundance of Re in most geological samples is usually less than 100 ng g^{-1}, and consequently the absolute amount of Re available for mass spectrometric analysis is often no more than 10 ng. Miller *et al.* (2009) utilized a minimum of 10 ng Re for their isotope analysis of samples and noted that if the amount of sample was appreciably less than ~10 ng, analytical precision was likely to be impaired.

Several methods have been developed for the separation of Re from geological materials to determine accurate and precise Re abundance determinations; these are usually centred on isotope dilution approaches for Re-Os analysis (Georgiev *et al.* 2018). For example, Walker (1988) and Cohen and Waters (1996) used tribenzylamine to extract Re from acid digest solutions. More recently, methods based on ion exchange chromatography have been developed to circumvent the difficulty of ensuring complete Re recovery that often occurs during solvent extraction. For instance, Pearce *et al.* (2009) used Bio-Rad AG® 1-X8 anion exchange resin and a sequence of mobile phase reagents to first retain the Mo and Re and then to separate them sequentially from each other and the other elements in the sample. Miller *et al.* (2009) utilized a single column anion exchange chromatographic method to extract Re from geological materials for the determination of Re isotope composition. However, a drawback of the method used by Miller *et al.* (2009) is that it provides an incomplete separation of Re from other matrix elements (Georgiev *et al.* 2018); a feature which was improved upon with the new two-stage separation presented in this chapter, see section 3.4.2 for details. Complete separation is important because some

residual matrix elements have the potential to generate incorrect Re isotope data due to isobaric and molecular interferences (Table 3.1).

In this study, we present a new two-stage procedure based on anion exchange column chromatography for the extraction of Re from geological materials. This method provides a high purity Re fraction at ~ 100 % yield, with the separated and purified Re being suitable for high precision isotope composition analysis by MC-ICPMS. The determination of the Re isotope composition of samples of marine sedimentary rocks has the potential to define past marine redox conditions, and provide new insights into ocean chemistry during major changes in the Earth system such as oceanic anoxic events (see Chapter 6), particularly if the behaviour or Re isotope composition in differing marine redox conditions is better understood (Chapter 4).

Table 3.1 – Cup configuration for the determination of Re isotope composition, showing the relative abundance of isotopes measured, with isobaric and molecular interferences on the masses measured.

Measured mass (amu)		**185**	**186**	**187**	**188**	**189**	**191**	**193**
Cup		**L2**	**L1**	**C**	**H1**	**H2**	**H3**	**H4**
Relative abundance	**Re**	37.40		62.60				
	Os			1.96	13.24	16.15		
	Ir						37.30	62.70
Molecular interferences[1]		$^{171}Yb^{14}N$ (14.28) $^{169}Tm^{16}O$ (100.00) $^{157}Gd^{14}N_2$ (15.65) $^{153}Eu^{16}O_2$ (52.19) $^{145}Nd^{40}Ar$ (8.30) $^{105}Pd^{40}Ar$ (22.33)		$^{173}Yb^{14}N$ (16.30) $^{171}Yb^{16}O$ (14.28) $^{159}Tb^{14}N_2$ (100.00) $^{155}Gd^{16}O_2$ (14.80) $^{147}Sm^{40}Ar$ (14.99) $^{107}Ag^{40}Ar_2$ (51.84)	$^{174}Hf^{14}N$ (0.16) $^{174}Yb^{14}N$ (31.83) $^{173}Yb^{16}O$ (21.83) $^{160}Dy^{14}N_2$ (2.34) $^{156}Dy^{16}O_2$ (0.06) $^{160}Gd^{14}N_2$ (21.86) $^{156}Gd^{16}O_2$ (20.47) $^{149}Nd^{40}Ar$ (5.70) $^{149}Sm^{40}Ar$ (11.24) $^{108}Cd^{40}Ar_2$ (0.89) $^{108}Pd^{40}Ar_2$ (26.46)	$^{175}Lu^{14}N$ (97.41) $^{173}Yb^{16}O$ (16.13) $^{161}Dy^{14}N_2$ (18.91) $^{157}Gd^{16}O_2$ (15.65) $^{149}Sm^{40}Ar$ (13.82) $^{109}Ag^{40}Ar$ (48.16)	$^{177}Hf^{14}N$ (18.60) $^{175}Lu^{16}O$ (97.41) $^{163}Dy^{14}N_2$ (24.90) $^{159}Tb^{16}O$ (100.00) $^{151}Eu^{40}Ar$ (47.81) $^{111}Cd^{40}Ar_2$ (12.80)	$^{179}Hf^{14}N$ (13.62) $^{177}Hf^{16}O$ (18.60) $^{165}Ho^{14}N_2$ (100.00) $^{161}Dy^{16}O_2$ (18.91) $^{153}Eu^{40}Ar$ (52.19) $^{113}In^{40}Ar_2$ (4.29) $^{113}Cd^{40}Ar_2$ (12.22)

[1] Molecular interferences shown with relative abundances of metal isotopes in parentheses (%).

3.3 Experimental procedure

3.3.1 Samples

Experiments to develop the new method presented here were carried out using three unweathered organic-rich marine mudrock samples (Tco 01-50, Tfa 01-25, and Tex 06-28) of Toarcian age (~183 Ma ago) collected from the Yorkshire coast, UK (See Chapter 5 for background information on the Toarcian Oceanic Anoxic Event). Each of these samples was analysed 4 to 6 times. The total organic carbon (TOC) values of these samples are 3.41, 3.14, and 14.67 wt.% respectively (Harding 2004); their Re concentrations are 99.74, 90.15, and 23.75 ng g^{-1}; and they have Mo concentrations of 15.86, 23.10, and 7.53 µg g^{-1} respectively (Pearce *et al.* 2008). An organic-rich marine mudrock from the Monterey Formation, Naples Beach, California, USA (00N118) was used as an in-house reference sample. This sample has previously been used as an in-house reference sample for Mo isotope analyses (Dickson *et al.* 2012, Izon 2012, Pearce *et al.* 2008) and was processed twice and analysed three times during the course of this study. The Re isotope composition of the USGS reference sample, the Devonian Ohio Shale SDO-1 (Kane *et al.* 1990) was also analysed. The single element NIST standard SRM 3143 was processed three times, and analysed five times. Six "matrix test" synthetic samples, comprising natural sample matrix to which a known amount of SRM 3143 had been added, were processed through the chromatographic separation and analysed for their Re isotope composition.

3.3.2 Sample preparation

Sample preparation was carried out in a metal-free clean suite at The Open University, UK. All sample preparation utilised PFA (perfluoroalkoxy) Savillex® beakers and all acids were twice-distilled in sub-boiling PFA stills. All acids were diluted with 18 MΩ deionised water from a Millipore® ion exchange unit. Rhenium blank levels were determined for all reagents and column procedures; total procedural blanks were consistently <10 pg Re.

Aliquots of finely powdered rock samples (0.2–0.6 g) were accurately weighed into 90 ml Savillex® screw-top digestion vessels. A range of sample weights were used to allow for the varying Re concentration in the samples, aiming for ~10 ng Re to be present in each sample. Samples were digested overnight on a hotplate at ~ 150 ^{o}C in 12 ml inverse aqua regia and then evaporated to dryness on the hotplate before sealing with Teflon tape and placing in the oven at 120 ^{o}C in 6 ml inverse aqua regia for 5 days. The two-stage digestion allowed for the release of gasses in the initial hotplate step before the samples were sealed and placed in the oven. After digestion, samples were centrifuged for 20 minutes, then the supernatant liquid was removed, and the remaining solid was washed with 1 ml concentrated HNO_3 and centrifuged for another 20 minutes. The washing procedure was repeated and the resulting solutions combined for each sample. Solutions were then evaporated to dryness on a hotplate, and dried down a further 3 times with 1 ml concentrated HNO_3. Finally, samples were dissolved in 7 ml 4 mol l^{-1} HNO_3 and were diluted to 28 ml 1 mol l^{-1} HNO_3 with 18 MΩ deionised water.

Bio-Rad AG®1-X8 resin (1 ml, 200-400 mesh) loaded into pre-cleaned BioRad Poly Prep® chromatography columns was used for the separation of Re from matrix elements. The two-stage separation procedure is summarised in Table 3.2. The majority of matrix elements were either not retained on the column in the loading solution or were eluted during the initial wash with 0.5 mol l^{-1} HNO_3. Hafnium and Zr were subsequently eluted using a mixture of HCl and HF. Following this, the purified Re fraction was eluted using 4 mol l^{-1} HNO_3. When changing between HNO_3 and HCl – HF mix eluent, a 1 ml MQ H_2O wash step was introduced to ensure there was no mixing between the different acids. To obtain a high purity Re fraction, the separation process was then repeated using ion exchange columns containing 0.2 ml resin.

Table 3.2: Elution sequence of the anion exchange resin chromatographic separation procedure.

Eluent	Volume (ml)	Step
Column 1: 1 ml BioRad® AG1 X 8 anion-exchange resin (200-400 mesh)		
Sample loaded: Shale samples <0.6 g		
4 M HNO_3	10	Resin cleaning
1 M HNO_3	10.5	Resin conditioning
1 M HNO_3 (sample solution)	28	Load sample
0.5 M HNO_3	11.5	Rinse matrix
MQ H_2O	1	Rinse matrix
4 M HCl - 1 M HF	12	Rinse matrix
MQ H_2O	1	Rinse matrix
4 M HNO_3	14	Elute Re
4 M HNO_3	2	"check fraction"
Column 2: 200 µl BioRad® AG1 X 8 anion-exchange resin (200-400 mesh)		
Sample loaded: Re collected from previous column		
4 M HNO_3	2	Resin cleaning
1 M HNO_3	2.1	Resin conditioning
1 M HNO_3 (sample solution)	2	Load sample
0.5 M HNO_3	2.3	Rinse matrix
MQ H_2O	0.2	Rinse matrix
4 M HCl - 1 M HF	2.4	Rinse matrix
MQ H_2O	0.2	Rinse matrix
4 M HNO_3	4.2	Elute Re
4 M HNO_3	0.4	"check fraction"

3.3.3 Mass spectrometry

Determination of the Re isotope composition of the purified Re fraction was carried out using a ThermoFisher Scientific Neptune MC-ICP-MS at the Open University, UK. Aliquots of sample solutions were re-dissolved in 3% nitric acid to give Re concentrations in the range of 8–20 ng ml^{-1}, to which high-purity Ir solution was added to give an Ir concentration of 200 ng ml^{-1}. The sample aliquots were introduced to the MC-ICPMS using a quartz spray chamber and Teflon nebuliser (average flow rate of 62 µL min^{-1}). The MC-ICPMS was fitted with a standard sampler cone and an X-Skimmer cone. Each analysis consisted of 40 individual measurements with an integration time of 4.194 s.

Rhenium isotope ratios were corrected for potential isobaric interferences on ^{187}Re due to the potential presence of ^{187}Os, through the measurement of ^{188}Os and ^{189}Os. Corrections were usually insignificant (0.002 ‰ average relative change in the δ^{187}Re value between raw and Os interference corrected ratio) due to the low levels of Os present in all standards and samples. Correction for instrumental mass bias was carried out using the measured ^{193}Ir/^{191}Ir ratio using the exponential law.

Rhenium isotope ratios are reported as per mil deviations (δ^{187}Re) relative to NIST standard SRM 3143, calculated as δ^{187}Re (‰) = [[(^{187}Re/^{185}Re)$_{sample}$/(^{187}Re/^{185}Re)$_{SRM3143}$]-1] x 1000. The isotopic compositions of samples were determined using standard-sample bracketing. The uncertainty presented is given as the external reproducibility (2 standard deviations, 2 SD) of all bracketing standards run during an analysis session. Previous studies report sample data relative to the NIST SRM 989, a standard with a certified Re isotope ratio, however this standard is no longer commercially available and there is no certified replacement standard. Miller *et al.* (2009) report δ^{187}Re (‰) relative to SRM 989 and also report δ^{187}Re for NIST SRM 3143. A comparison of our data with those of Miller *et al.* (2009) is therefore possible by using NIST SRM 3143 as the common standard analysed to adjust the δ^{187}Re values reported. The offset in δ^{187}Re between NIST SRM 3143 and NIST SRM 989 is 0.29 ‰ (Miller *et al.* 2009).

3.4 Results and discussion

3.4.1 Ion exchange chromatographic procedure

The method presented in this study provides a means of complete separation of Re from the matrix elements of geological samples, resulting in a high purity Re fraction at very high (~ 100 %) yield. Achieving a very efficient recovery of Re (as close to 100% as possible) is necessary to avoid isotopic fractionation of Re that would occur during the chromatographic separation if Re yields were significantly lower than 100% (Miller *et al.* 2009). For each sample, following the

elution of the Re fraction, an additional 2 ml of 4 mol L^{-1} HNO_3 was passed through the column, and the Re concentration in that fraction was determined to check for any remainder in the Re elution and confirm that ~ 100% of the Re had been recovered in the main Re aliquot. The fractions collected after the main Re elution for both column passes together consistently contained <25 pg Re, equivalent to <0.5 % of the total Re (a minimum of ~ 5 ng) that was typically processed.

Procedural blanks were determined for each batch of samples processed and were consistently <10 pg Re, which is equivalent to <0.2% of the minimum amount of Re processed (>5 ng Re); the level of the Re procedural blank is therefore insignificant for these analyses.

3.4.2 The effect of Hf and Zr interferences

Rhenium was separated from most of the major matrix elements using a single column pass. However, small amounts of some elements, in particular Hf and Zr, are retained on the ion exchange resin and are released with the Re fraction when it is eluted (*e.g.* 0.67 ng Hf, 111 ng Zr and 3.3 ng Re; Figure 3.1). The presence of these elements in the Re fraction can produce isobaric and molecular interferences on the masses analysed. Due to natural variation in each sample, these interferences can cause matrix effects that can change the mass bias between each sample, thereby potentially compromising the quality of the Re isotope measurement.

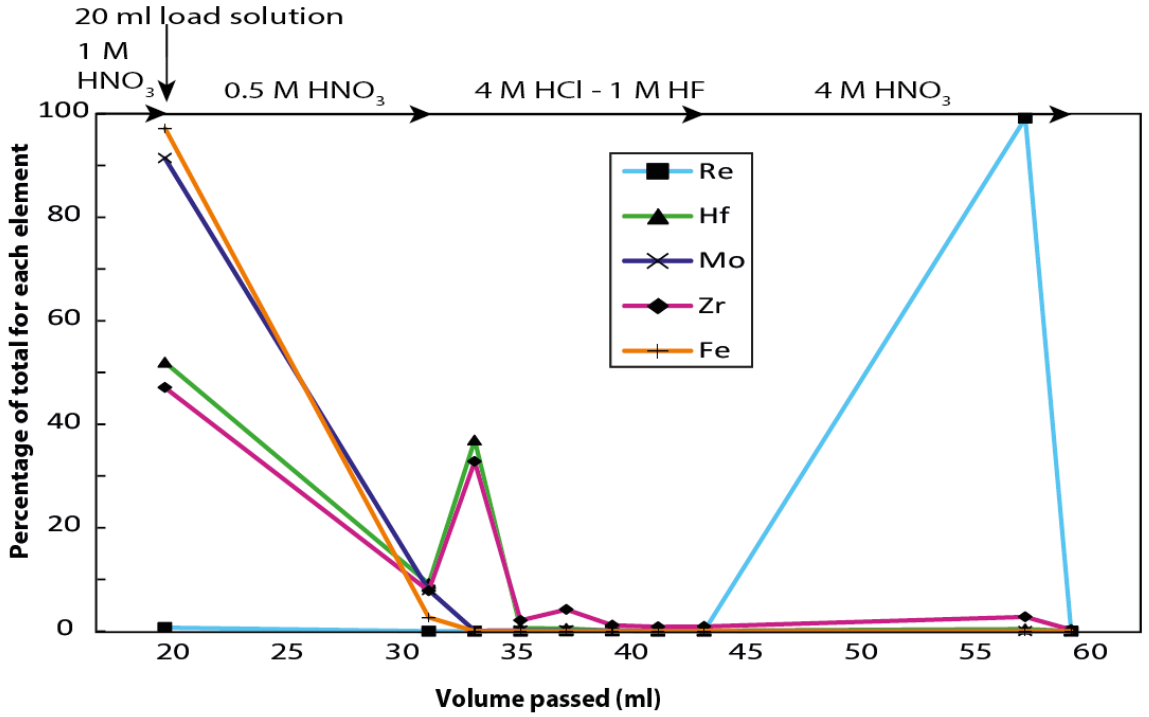

Figure 3.1: Elution curves for Re, Hf, Mo, Zr and Fe for an organic-rich mudrock sample (Tex 06-28) passed through a single column.

To assess whether residual Hf and Zr affected the measured Re isotope ratio, known amounts of Hf and Zr were added to the single element standard SRM 3143, and δ^{187}Re was determined for the range of solutions. A solution with Hf/Re weight ratio of 0.2 resulted in a measured δ^{187}Re of -0.813 ± 0.07‰ (Figure 3.2), which is significantly different from the pure SRM 3143 (δ^{187}Re = 0). When the Hf/Re weight ratio of the SRM 3143 with added Hf is 0.05 or less, the measured Re isotope composition (for instance, where: Hf/Re = 0.05, Zr/Re = 0, δ^{187}Re = -0.067 ± 0.079) is indistinguishable within analytical uncertainty from that of SRM 3143 (δ^{187}Re = 0) with no added Hf. In contrast, the presence of small amounts of Zr (with Zr/Re weight ratio in the measured aliquot in the range of 0 – 34) in the Re aliquot does not significantly alter the measured δ^{187}Re (Figure 3.2).

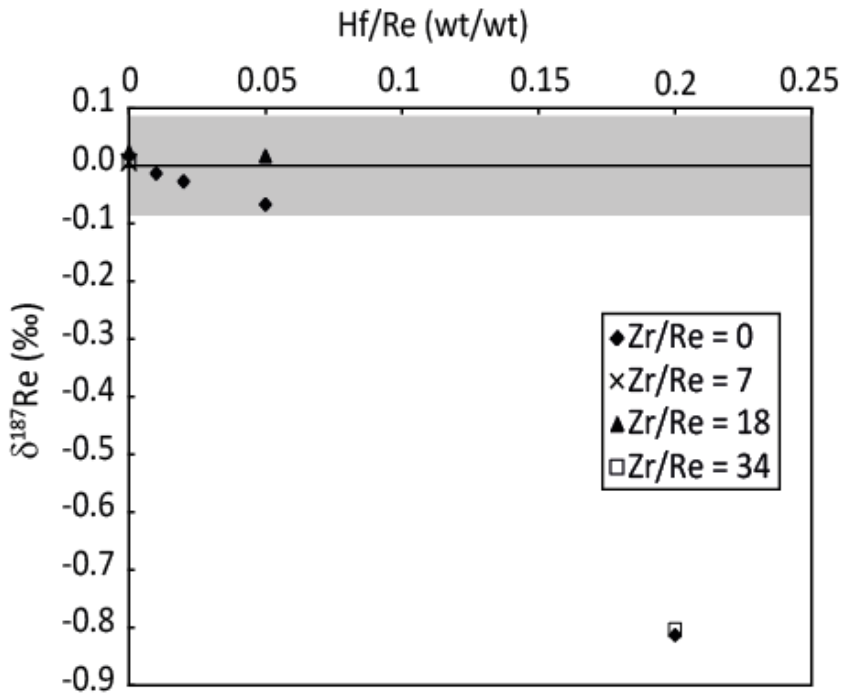

Figure 3.2: The effect of Hf and Zr contamination on the Re isotope results. The reference line at δ^{187}Re = 0 ‰ represents uncontaminated SRM 3143, and the grey band shows the reproducibility (2SD) of all SRM 3143 analyses obtained throughout the study (5 – 20 ng ml^{-1} Re).

A second, smaller clean-up column (Table 3.2) was therefore used to reduce the residual matrix elements Hf and Zr to insignificant levels. For each sample, the effectiveness of the chromatographic separations was assessed before the Re isotope determination by measuring the concentration of Hf and Zr in a 5% aliquot. For all samples, the second column separation reduced the levels of Zr and Hf in the Re fraction to very low levels; resulting Zr/Re and Hf/Re ratios ranged from 0 to 9 and 0 to 0.03, respectively. For the majority of samples, the Hf/Re ratio was <0.02 (Hf/Re, weight ratio) after two column passes; in practice, no measureable Hf remained in the majority of samples, and thus the potential isobaric interferences of molecular Hf species on masses 191 and 193 was insignificant.

Our analyses show that the presence of residual Hf in the purified Re fraction can cause a significant change in the measured Re isotopic composition (Figure 3.2). The bias in measured Re isotope composition is a consequence of inappropriate instrumental mass fractionation corrections when using Ir for this purpose, due to isobaric interferences on the ^{191}Ir and ^{193}Ir from

Hf oxides and nitrides (for example, $^{177}Hf^{14}N$ and $^{177}Hf^{16}O$). It is therefore essential to have a high purity Re fraction, specifically free from Hf, for reliable isotope ratio analysis. For all our determinations of the Re isotope composition of unknown samples, residual Hf levels were checked before each analysis (as discussed above) to ensure the Hf/Re weight ratio did not exceed 0.05.

3.4.3 Potential Os interferences

^{187}Os causes an isobaric interference on the ^{187}Re analysed during Re isotope ratio analysis, and it is therefore necessary to remove Os from samples prior to analyses. All volatile OsO_4 is lost during the chemical processing since all samples have been evaporated to dryness several times from highly oxidising solutions (inverse aqua regia and concentrated HNO_3). It is therefore not necessary to sparge (the removal of Os from oxidising solutions using Ar gas) the samples prior to analysis to further remove Os from the Re fractions as also noted by Miller *et al.* (2009). The consistently extremely low (almost below the limit of detection) levels of ^{188}Os and ^{189}Os present in the solutions analysed required very small corrections (0.002 ‰ average relative change in the $\delta^{187}Re$ value).

3.4.4 Accuracy of isotope ratio measurements

Single element standards and synthetic samples were used to evaluate the accuracy of the Re isotopic analyses. These experiments were designed to confirm that no fractionation is induced by the separation procedure and that matrix elements are successfully decreased to levels that do not compromise the accuracy of the Re isotope analyses of samples.

Three aliquots of SRM 3143 containing ~ 10 ng of Re were processed through the chromatographic separation procedure described above. The Re isotope compositions determined for these processed aliquots of SRM 3143 were identical within the stated analytical uncertainties to those of the unprocessed standard (average $\delta^{187}Re$ = -0.042 ± 0.108 ‰ for the

column-processed SRM 3143 (Figure 3.3a and Table 3.3), compared with δ^{187}Re = 0.000 ± 0.084 ‰ for the unprocessed standard). This result demonstrates that no detectable isotopic fractionation is induced by the chemical separation method presented here.

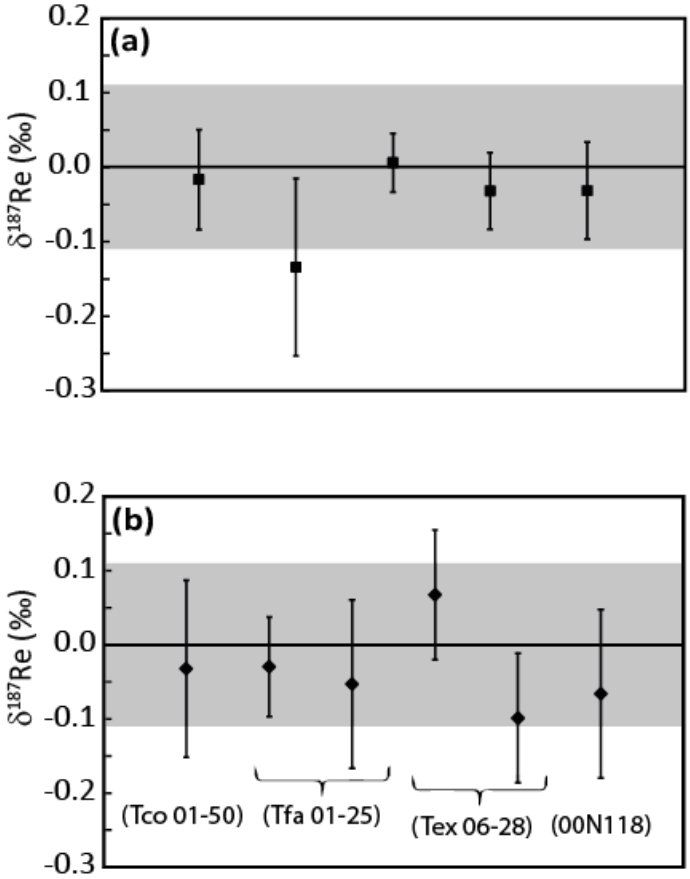

Figure 3.3: Rhenium isotope data for experiments to assess the accuracy of chemical processing. δ^{187}Re values for processed SRM 3143 (a), and for matrix test samples (b). The reference line at δ^{187}Re = 0 ‰ represents unprocessed SRM 3143 and the shaded grey band shows the reproducibility (2SD) of all processed SRM 3143, and of all matrix test samples in (a) and (b) respectively. Letters in brackets denote the samples from which the matrix elements were collected.

A further set of experiments was conducted in order to assess whether the new method provides accurate Re isotope composition data for samples with a range of chemical compositions. Six synthetic samples, comprising natural sample matrix to which a known amount of SRM 3143 had been added, were processed through the chromatographic separation and analysed for their Re isotope composition (Table 3.3). To produce these synthetic samples, the Re-

free matrix fractions were collected from four organic-rich mudrock samples (Tco 01-50, Tfa 01-25, Tex 06-28, and 00N118) during the anion-exchange separation procedure (Table 3.2). The samples from which these matrices were collected exhibit a range of Re isotope compositions from δ^{187}Re = -0.326 ± 0.146 ‰ to δ^{187}Re = -0.583 ± 0.071 ‰. The average δ^{187}Re of these synthetic "matrix test" samples was -0.035 ± 0.112 ‰, a result which is indistinguishable within the ascribed analytical uncertainty from the Re isotope composition of un-processed SRM 3143 (δ^{187}Re = 0; Figure 3.3b). These results confirm that our new chemical separation procedures provide accurate Re isotope composition data for samples with a range of chemical compositions. The Re isotope data are thus not biased by any facets of sample preparation or analysis, including fractionation during column processing, isobaric interferences and matrix effects arising from residual matrix elements.

Table 3.3: Matrix test samples and processed standard. For each sample, Ir concentration in aliquot analysed is 200 ng g^{-1}. For matrix test samples, all are individual digestion, chromatography and single analysis. Processed SRM 3143 standard is labelled as Processed SRM 3143_Na; where N = the digestion batch number, and a = the analysis number for a particular digestion batch.

Type of sample	Re concentration in aliquot analysed (ng g^{-1})	δ^{187}Re (‰)
Matrix test (matrix from Tco 01-50)	10	-0.032 ± 0.119
Matrix test (matrix from Tfa 01-25)	20	-0.029 ± 0.067
Matrix test (matrix from Tfa 01-25)	20	-0.053 ± 0.113
Matrix test (matrix from Tex 06-28)	20	0.067 ± 0.087
Matrix test (matrix from Tex 06-28)	20	-0.098 ± 0.087
Matrix test (matrix from 00N118)	20	-0.066 ± 0.113
Average matrix test		-0.035 ± 0.112
Processed SRM 3143_1a	10	-0.016 ± 0.067
Processed SRM 3143_1b	10	-0.134 ± 0.119
Processed SRM 3143_2	20	0.006 ± 0.039
Processed SRM 3143_3a	15	-0.032 ± 0.052
Processed SRM 3143_3b	9	-0.032 ± 0.065
Average Processed SRM 3143		-0.042 ±0.108

3.4.5 Reproducibility of Re isotope analysis of standard solutions

Analytical reproducibility, both short-term (daily) and long-term (11 months), was assessed by repeat analysis of SRM 3143. The overall reproducibility of 306 analyses of SRM 3143 performed during this study is 0.084 ‰ (2 SD), for Re concentrations of 5 – 20 ng ml^{-1} in the solution aspirated into the plasma. This concentration range matched that of the geological samples that were prepared for the determination of their Re isotope compositions. For a solution with Re concentration 20 ng ml^{-1} and Ir concentration 200 ng ml^{-1}, the beam size on ^{187}Re and ^{193}Ir was on average 1.2 V and 11.8 V, respectively. All analyses were carried out using 10^{11} Ω resistors on the faraday cups.

The Re concentration in the solution aspirated into the plasma affects the reproducibility that can be achieved for Re isotope composition analyses (Figure 3.4). The daily reproducibility

(2SD) of standard measurements using solutions of 5 to 20 ng ml^{-1} varied from 0.023 to 0.136 ‰ and was for most sessions below 0.1 ‰. However, the reproducibility for a 1 ng ml^{-1} standard was 0.458 ‰, significantly higher than for standards of higher concentration, indicating that there is a lower limit on the Re concentration at which high precision analyses can be achieved. When analysing natural samples, 0.1 ‰ has been taken as the maximum acceptable reproducibility. The reproducibility of the standard data, and its dependence on Re concentration, indicates that the minimum Re concentration in the solution aspirated into the plasma is ~ 5 ng ml^{-1}. Under the specific conditions detailed here, approximately 1.5 ng Re is required per analysis. The analytical reproducibility achieved using nanogram quantities of Re from natural samples has enabled this study to reliably characterise the small natural variations in $\delta^{187}Re$.

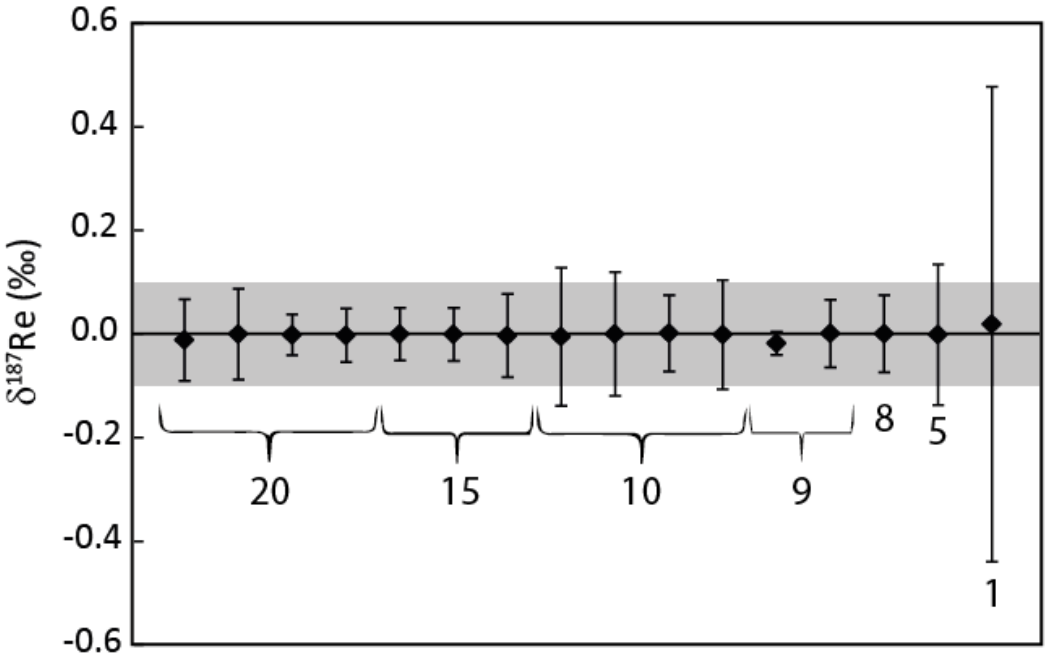

Figure 3.4: Daily averages of Re standard analyses of SRM 3141 measured at different Re concentrations. The numbers in the figure indicate the measured Re concentration in ng ml^{-1}**.** Measurements were obtained during 8 analytical sessions over a period of 11 months. Error bars are 2SD.

The Re isotope composition of an in-house Re standard (Specpure®) solution was determined at the start of each analytical session. These measurements are used to further

monitor the daily performance of the Neptune MC-ICP-MS. The average δ^{187}Re for the in-house standard over a 11-month period is -0.202 ± 0.097 ‰ (2SD) for 21 individual measurements obtained during 9 analytical sessions. The reproducibility of analyses of this standard solution is only marginally worse, compared to the long-term reproducibility of SRM 3143 (2SD = 0.084 ‰), which is used as a bracketing standard. The excellent long-term reproducibility of the in-house standard indicates that there is no daily bias affecting the determined Re isotope composition of samples.

3.4.6 Rhenium isotope analysis of geological materials

The mean δ^{187}Re of the in-house reference material 00N118 is -0.351 ± 0.053 ‰ (n = 3), and shows the high precision achieved by the method presented here. The rhenium isotope composition of SDO-1 has previously been determined by Miller *et al.* (2009) at -0.080 ± 0.130 ‰ for δ^{187}Re (re-normalised relative to SRM 3143). Our analyses of SDO-1 give a Re isotope composition of δ^{187}Re = -0.129 ± 0.109 ‰ (n = 3), which is, within the ascribed uncertainties, indistinguishable from the results reported by Miller *et al.* (2009). The maximum difference in δ^{187}Re between geological samples that we have observed is 0.454 ‰ between SDO-1 and Tex 06-28 (Table 3.4), which is significantly greater than the long-term reproducibility of bracketing standards (0.084 ‰).

Table 3.4: Rhenium isotope composition of geological samples. Ir concentration in aliquot analysed is 200 ng g^{-1} for each sample analysed in this study.

Sample[1]	Re concentration in aliquot analysed (ng g^{-1})	δ^{187}Re (‰)	
		Mean	2SD[3]
Tco 01-50 _1	10	-0.255	0.119
Tco 01-50 _2	10	-0.310	0.119
Tco 01-50 _3a	10	-0.428	0.119
Tco 01-50 _3b	10	-0.312	0.119
Average Tco 01-50		-0.326	0.146
Tfa 01-25_1	10	-0.530	0.119
Tfa 01-25_2a	10	-0.255	0.067
Tfa 01-25_2b	10	-0.299	0.119
Tfa 01-25_3a	10	-0.316	0.119
Tfa 01-25_3b	10	-0.291	0.067
Tfa 01-25_3	10	-0.317	0.119
Average Tfa 01-25		-0.335	0.197
Tex 06-28_1	9	-0.559	0.023
Tex 06-28_2a	10	-0.556	0.119
Tex 06-28_2b	10	-0.603	0.067
Tex 06-28_3	10	-0.586	0.119
Tex 06-28_4a	10	-0.643	0.119
Tex 06-28_4b	10	-0.551	0.119
Average Tex 06-28		-0.583	0.071
00N118_1a	10	-0.381	0.130
00N118_1b	10	-0.337	0.130
00N118_2	10	-0.335	0.119
Average 00N118		-0.351	0.053
SD0-1_1a	20	-0.162	0.067
SD0-1_1b	10	-0.066	0.067
SD0-1_2	20	-0.160	0.039
Average SDO-1		-0.129	0.109
SD0-1 (Miller *et al.* 2009)[2]		-0.080	0.130

[1] Samples are labelled as Sample name_Na; where N = the digestion batch number, and a = the analysis number for a particular digestion batch.

[2] Literature value of δ^{187}Re for SDO-1 is adjusted to show value relative to SRM 3143

[3] 2SD is given as 2 standard deviations for all δ^{187}Re values for bracketing standards (calculated by standard - sample bracketing) during the analysis session, at the particular concentration given.

The multiple analyses of the three organic-rich mudrock samples of Toarcian age (Tco 01-50, Tfa 01-25, and Tex 06-28), the organic-rich mudrock in-house reference sample (00N118), and the commercially available reference sample SDO-1 (Devonian Ohio shale) demonstrate good reproducibility of the analytical method. The overall range in δ^{187}Re of the Toarcian samples is 0.257 ‰ (Figure 3.5, Table 3.4). The Re isotope compositions of samples Tco 01-50 (δ^{187}Re = -0.326 ± 0.146 ‰, n = 4) and Tfa 01-25 (δ^{187}Re = -0.335 ± 0.197 ‰, n = 6) are indistinguishable from each other within analytical uncertainty. However, Tex 06-28 shows a significantly lower δ^{187}Re of -0.583 ‰ ± 0.071 ‰ (n = 6) compared with samples Tco 01-50 and Tfa 01-25. The analytical reproducibility for some mudrock samples is greater than the reproducibility from standard measurements generated throughout an analytical session. However, the two samples which exhibit the greatest analytical uncertainty (Tco 01-50 and Tfa 01-25) each contain an outlier from the range of individual analyses (Figure 3.5), and so this greater uncertainty is most likely to be caused by these extreme values. All other individual analyses of these two samples are highly reproducible; for Tco 01-50 δ^{187}Re = -0.292 ± 0.065 ‰, n = 3 and for Tfa 01-25 δ^{187}Re = -0.295 ± 0.050 ‰, n = 5. The overall range in δ^{187}Re of Toarcian samples of 0.257 ‰ indicates that there are natural variations in the δ^{187}Re of the Toarcian age mudrocks, and these small, naturally-occurring differences in the δ^{187}Re of geological samples can be identified and resolved using the procedures described in this study (a larger sample set is analysed and discussed in more detail in Chapter 6).

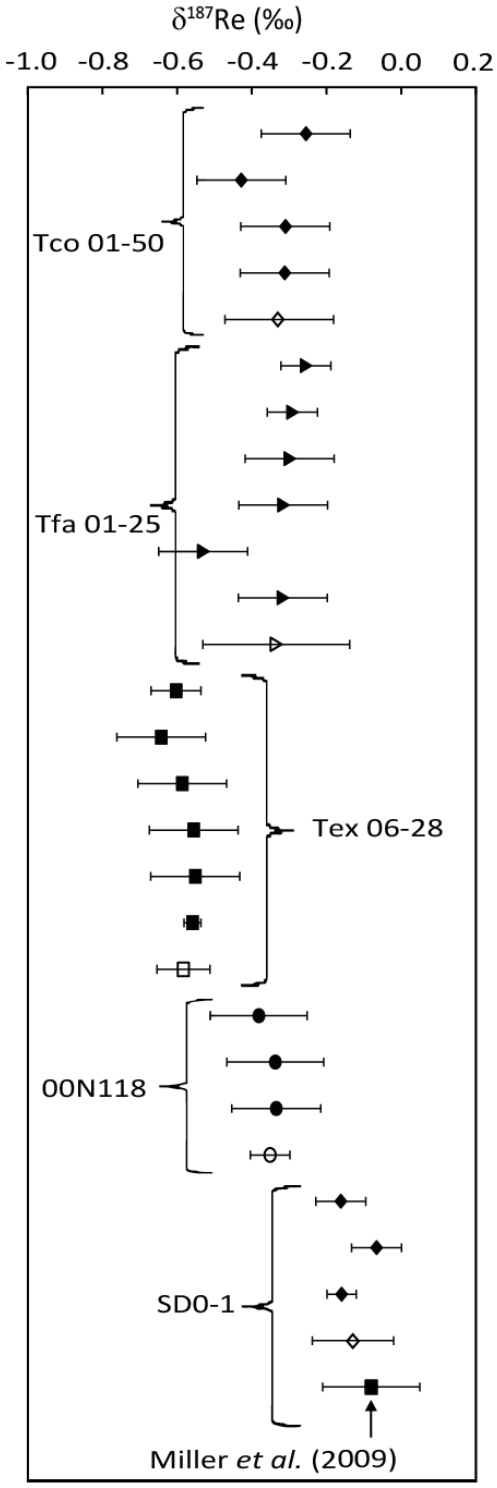

Figure 3.5: Rhenium isotope data for mudrock samples and USGS reference sample SDO-1. Closed symbols show individual analyses, open symbols display the average of all repeats; error bars represent the reproducibility (2SD). All data are reported relative to the SRM 3143 standard. The data of Miller *et al.* (2009) for SDO-1 have been recalculated relative to SRM 3143.

3.5 Conclusions

- This study provides an improved method for the extraction of Re at high purity and high yield from geological materials, enabling high precision determinations of the Re isotope composition to be made by MC-ICP-MS. The method requires 1.5 - 6 ng of Re (compared to a minimum of 10 ng required for previous methods) making it possible to precisely determine δ^{187}Re of samples with lower concentrations of Re.
- The determination of the Re isotope composition using Ir for mass bias correction is sensitive to bias by small residual levels of Hf in the Re fraction. The method developed here provides a pure Re fraction containing very low levels of Hf, such that the measured Re isotope data are free from bias.
- The observed range of δ^{187}Re of the three Toarcian mudrock samples used to develop this methodology is 0.257 ‰. The maximum difference in δ^{187}Re between geological samples analysed in this study is 0.454 ‰. Sample Tex 06-28 exhibits the greatest difference from the SRM 3143 standard with δ^{187}Re = -0.583 ± 0.071 ‰.
- The new method for Re isotope composition analysis presented here produces highly reproducible results for both Re standards and a range of geological samples. The reproducibility for all measurements of SRM 3143 during 9 analytical sessions over a period of 11 months is 0.084 ‰ (n = 277). We have shown that utilizing the presented method, the small but significant differences in δ^{187}Re between natural samples can be resolved beyond the analytical uncertainty.

Chapter 4

Assessing δ^{187}Re in recent sediment samples of the Baltic Sea

4.1 Introduction

This chapter of the thesis presents the application of the Re isotope seawater redox proxy developed during this project and outlined in Chapter 3 to a sediment core from the Baltic Sea. The aim is to evaluate the behaviour of Re isotopes in a modern-day anoxic deposition environment, where the redox conditions are well recorded.

Note on contributions: The samples and elemental (C_{org}, Mo, S, Fe, Mn, Zn, Ni, V, Al) concentration data were supplied by Caroline Slomp, Utrecht University, The Netherlands. FR completed the analyses, processed the results, wrote the chapter and prepared the figures and the supervisory team provided guidance, comments and suggested amends.

4.1.1 Introduction to the Baltic Sea

The Baltic Sea is a brackish water body of 415,266 km^2 located in Northern Europe (Figure 4.1) that experiences strong salinity stratification, leaving it vulnerable to hypoxia, defined as dissolved bottom water O_2 <2 mL L^{-1} (e.g. Gustafsson 2012). Seawater exchange between the Baltic Sea and the North Sea is restricted geographically by the small, shallow opening through the Danish Straights (eg. Conley *et al.* 2009). The Baltic Sea has an average depth of 55 m, however several deep basins (sometimes referred to as holes) reach greater depths. For instance the Gotland Deep in the East Gotland Basin (the location of site BY15, samples from this site are

investigated in this study) has a depth of up to 238 m, the Landsort Deep is up to 459 m deep and the Fårö Deep has a depth of ~200 m (Figure 4.1 B). A strong permanent halocline is formed at water depths between ca. 60 m – 80 m, which limits vertical mixing of the water column, and hence limits the vertical transfer of oxygen into the deep water (Conley *et al.* 2009). The Baltic Sea is the largest anthropogenically induced hypoxic area in the world (Carstensen *et al.* 2014a).

In recent decades, the environmental conditions in the Baltic Sea have been carefully monitored, and information recorded in the Baltic Environmental Database (www.balticnest.org). Continuous monitoring has been carried out since 1900, with the most detailed records collected since the 1960s (see e.g. Conley *et al.* 2009, Conley *et al.* 2002). Human activity has caused the accumulation of nutrients over the last 50-100 years, with intensified eutrophication in the central parts of the Baltic Sea becoming apparent after the 1950s (Andersen *et al.* 2017a). Since the 1980s there have been efforts to reduce eutrophication by reducing the nutrient loading from the surrounding areas, which have had limited success (Andersen *et al.* 2017a).

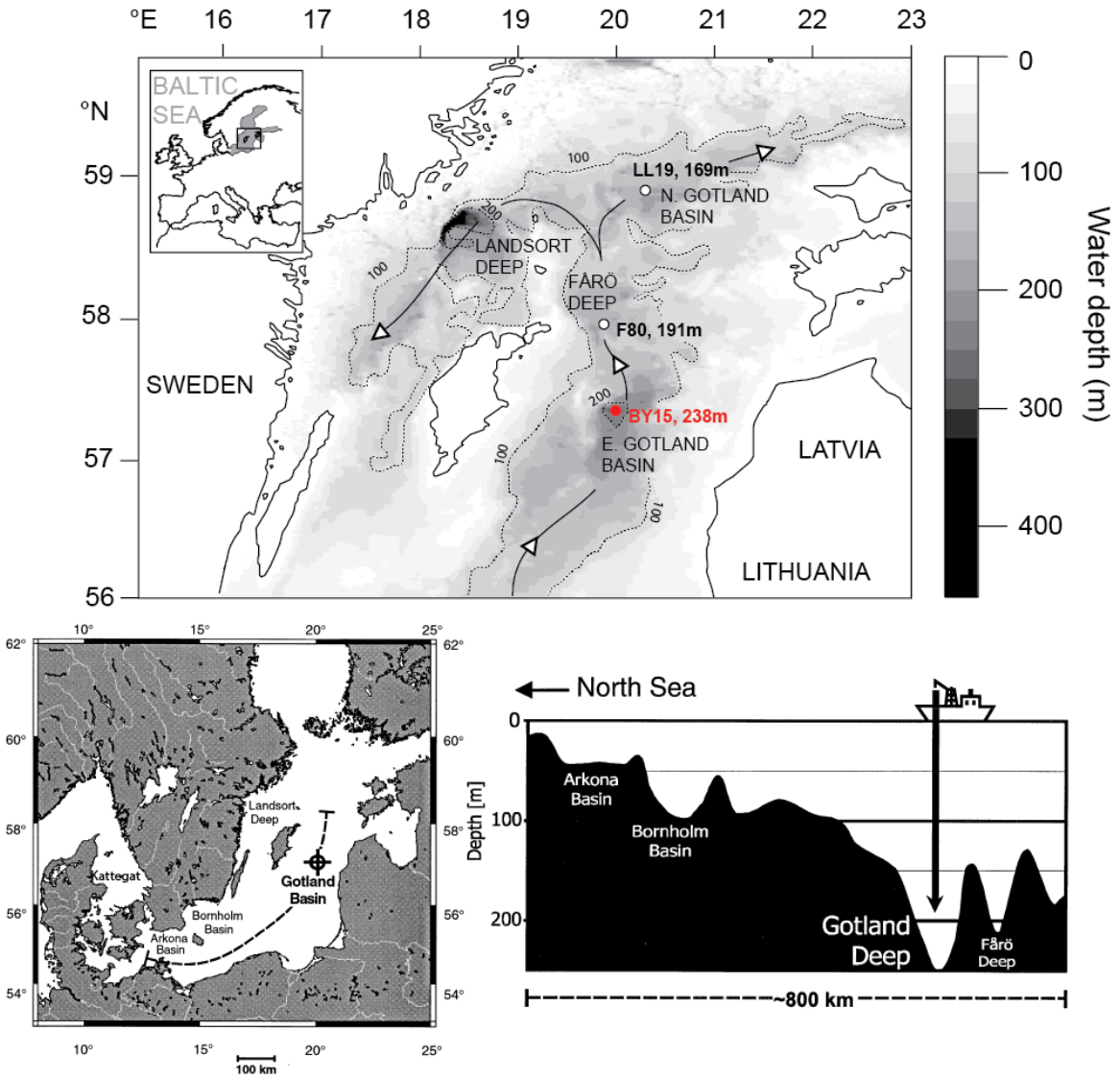

Figure 4.1: Top: The location of the Baltic Sea and study sites, figure from Jilbert and Slomp (2013b). Circles indicate coring sites LL19, F80, and BY15 of the HYPER/Combine cruise of R/V Aranda (May-June 2009). Arrows indicate the direction of inflowing North Sea seawater at depth. Samples studied in this chapter were collected at site BY15, which is highlighted in red. Left: the location of the Baltic Sea in Northern Europe. Right: Bathymetric cross section of the Baltic Sea through the line shown in the map on the left, figure from Neumann *et al.* (2002).

4.1.2 Redox conditions in the Baltic Sea

Intense salinity stratification and restricted water exchange with the North Sea leaves the Baltic Sea vulnerable to hypoxia regardless of the additional effects of anthropogenic eutrophication (Gustafsson 2012). Areas with a water depth of greater than 250 m (such as the Landsort Deep) appear to have been predominantly hypoxic since ~8500 yr BP (Zillén *et al.* 2008).

Laminated sediments, indicative of anoxic or euxinic deposition conditions (see Chapter 1.2.1 for a definition), were deposited in areas with a water depth between 74 m and 250 m during three major periods: 8,000 – 4,000 cal. yr BP, 2,000 – 800 cal. yr BP, and after 1800 AD. These hypoxic intervals overlap the Holocene Thermal Maximum (c. 9,000 – 5,000 cal. yr BP), the Medieval Warm Period (c. 750 – 1200 AD) and the modern historical period (1800 AD to present) (Kabel *et al.* 2012, Zillén *et al.* 2008).

The present-day reducing conditions observed in the Baltic Sea are thought to be unprecedented since 1500 (Hansson and Gustafsson 2011), and are the result of background susceptibility to anoxia and anthropogenic causes. Since ~1850, the industrial revolution in Northern Europe saw human population growth, intensified cutting of drainage ditches, and the expansion of agricultural and forest industry, which increased anthropogenic nutrient loading into the Baltic Sea (Zillén and Conley 2010, Zillén *et al.* 2008). Eutrophication caused by increased human inputs of phosphorus to the Baltic Sea is considered to have driven hypoxia (Carstensen *et al.* 2014a, Carstensen *et al.* 2014b, Conley *et al.* 2009). During this time, anthropogenic CO_2 emissions causing increased global temperatures have also contributed to the development of hypoxia in the Baltic Sea (Zillén *et al.* 2008).

Between 1905 and 2002 the Baltic Sea experienced a thirteen-fold increase in the areal extent of hypoxia (Savchuk *et al.* 2008), a significant period of hypoxia known as the "modern hypoxic event" (Jilbert and Slomp 2013b). Since 1950, the areal extent of hypoxic bottom water in the Baltic Sea expanded from less than 10,000 km^2 to greater than 60,000 km^2 in 2000 (Carstensen *et al.* 2014b). This expansion in hypoxic area is likely to have been caused by anthropogenic nutrient discharges (Carstensen *et al.* 2014a, Carstensen *et al.* 2014b), compounding the effects of global warming. However, between 1972 and 1993 the hypoxic area contracted from 70,000 km^2 to 12,000 km^2 (Figure 4.2, Conley *et al.* 2009, Conley *et al.* 2002). This decrease in hypoxic area coincides with a "stagnation period" (1980 – 1993) in which very few Major Baltic Inflows (MBIs)

occurred (Figure 4.3; MBIs are inflows of relatively oxygenated and salty seawater from the North Sea into the Baltic Sea through the Danish Straights, described in more detail in section 4.1.3). The lack of MBIs during the "stagnation period" are likely to have caused the severity of salinity stratification to diminish, therefore reducing the areal extent of hypoxic bottom waters (Mohrholz *et al.* 2015). This indicates that physical forcing can in some cases reduce the impact of eutrophication in the Baltic Sea (Carstensen *et al.* 2014a). Since 1993, the area of hypoxic bottom waters increased rapidly again to the pre 1972 extent of 60,000 km^2 (Figure 4.2, Conley *et al.* 2009, Conley *et al.* 2002) this is likely to be due to intensified salinity stratification following the 1993 MBI.

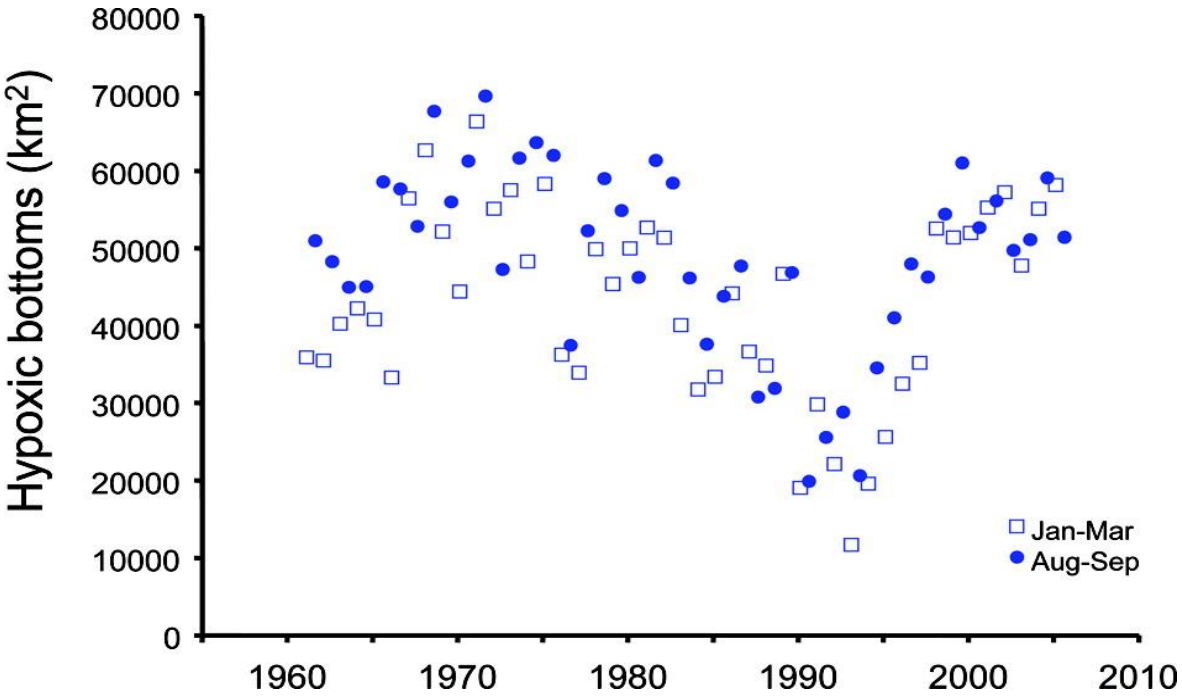

Figure 4.2: Variations in the extent of the bottom area of the Baltic Sea covered by hypoxic waters containing less than 2 ml L^{-1} dissolved oxygen 1960 - 2009 from Conley *et al.* (2009). Oxygen data are averaged over August–September (filled circles) and January–March (open squares) for each year.

The feedback loop between increased hypoxia, the enhanced regeneration of P, and increased primary productivity is thought to accelerate the onset of hypoxic events in the Baltic Sea, and increase the severity of reducing conditions (Carstensen *et al.* 2014b). During seasonal hypoxia, Fe-bound P in surface sediments acts as a major internal source of P (Mort *et al.* 2010).

There are indications of an accelerated P cycle during periods of maximum hypoxic area in the Baltic Sea (Jilbert *et al.* 2011); this is thought to be because P re-mineralisation intensifies with increasing anoxia, as does burial of organic P below the redoxcline (Jilbert *et al.* 2011). The onset of hypoxic events is likely to be accelerated by positive feedbacks in the P cycle during these transitions (Jilbert and Slomp 2013a). The total burial of P in euxinic basins (such as the deeper waters of the Baltic Sea) is expected to be influenced by the distribution (ratio of source to sinks) of submarine Fe and Mn oxide particle shuttles (Jilbert and Slomp 2013a, Jilbert *et al.* 2011). Climate, anthropogenic pressures, and internal feedback mechanisms are therefore all thought to have played a role as drivers of hypoxia through time in the Baltic Sea (Zillén *et al.* 2008).

The most extreme reducing conditions in the Baltic Sea are observed in the deepest basins. These areas experience intermittently anoxic and euxinic conditions (e.g. Conley *et al.* 2009, Conley *et al.* 2002, Jilbert and Slomp 2013b, Zillén *et al.* 2008), as directly recorded in bottom water oxygen, and H_2S concentration data. Bottom water oxygen, and H_2S data (with H_2S plotted as negative O_2 concentration; bottom water data from Gustafsson and Medina 2011) and high-resolution Mo/Al data from site BY15 (Figure 4.6) indicate that the most recent period of euxinic conditions developed in the Gotland Deep between 1980 and 1993 and has persisted to present day (discussed further in section 4.1.4), with the exception of brief episodes of oxygenation following the 1993 and 2003 MBIs (e.g. Jilbert and Slomp 2013b). The increased severity of reducing conditions at site BY15 between 1980 and 1993 coincided with the period of reduced areal extent of hypoxic deposition in the Baltic Sea as a whole (Figure 4.2); this apparent contradiction may be explained by anthropogenic nutrient loading (Conley *et al.* 2009), and/or increased temperature (Zillén *et al.* 2008), and/or biogeochemical feedbacks (Andersen *et al.* 2017a, Carstensen *et al.* 2014b, Jilbert and Slomp 2013a) that encouraged the worsening of euxinic conditions in deep basins of the Baltic Sea, whilst a lack of MBIs between 1983 and 1993 is

expected to have reduced the severity of salinity stratification and thus reducing the overall areal extent of hypoxia (Conley *et al.* 2009, Mohrholz *et al.* 2015).

4.1.3 The nature and frequency of Major Baltic Inflows (MBIs)

As briefly mentioned in Section 4.1.2, major Baltic Inflows are periodic rapid inflows of salty seawater from the North Sea into the deep water of the Baltic Sea, through the Danish Straits between Kattegat and the Arkona Sea (Figures 4.1B, 4.3; Matthäus and Franck 1992, Mohrholz *et al.* 2015). The volume of highly saline waters entering the Baltic Sea during MBIs is generally > 100 km^3 (Matthäus and Franck 1992). The brackish waters of the Baltic Sea are characterised by freshwater at the surface and in the north east from riverine inputs, and salty seawater from the North Sea in the south west and in the deeper waters. During MBIs, the low saline Baltic Sea water flows outward, separated from the saline inflowing bottom water. The transport is regulated by water level differences between the northern Kattegat and the Arkona Sea (Bendtsen *et al.* 2009). All MBIs occur in the "inflow season" between the end of August and the end of April, and are preceded by small positive sea level rise in the Kattegat compared to the Baltic Sea (Matthäus and Franck 1992).

The frequency of MBIs is not uniform through time (Figure 4.3). There have been fewer MBIs over the last 30 years, with major MBIs only occurring every ~10 years (Mohrholz *et al.* 2015). The largest MBIs in the last 30 years were in 1993, 2003, and 2014 which was the third largest on record (Figure 4.3, Mohrholz *et al.* 2015). A lack of MBIs during the stagnation period is thought to be caused by increased precipitation and runoff into the Baltic Sea during the 1980s (Schinke and Matthäus 1998).

The MBIs ventilate the deep basin by introducing more oxygenated water into the deep basins (Matthäus and Franck 1992), but also are expected to facilitate intensified stratification of the Baltic Sea, by increasing the strength of the salinity gradient through the water column

(Conley *et al.* 2009). This intensified stratification is likely to enhance the areal extent of hypoxic bottom water conditions in the basin (Conley *et al.* 2009, Conley *et al.* 2002). The bottom water area with $O_2 < 2$ ml L^{-1} was at a minimum at the end of the longest stagnation period (during which there were no MBIs for ten years) in 1993, but after the 1993 inflow the extent of the hypoxic area expanded again (Conley *et al.* 2002).

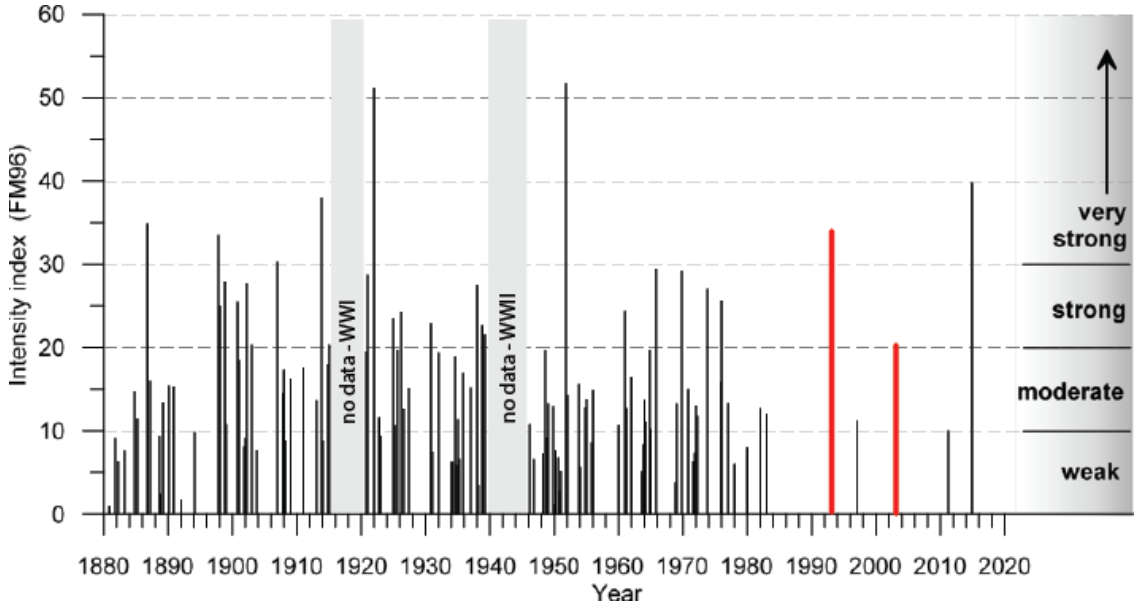

Figure 4.3: The timing and intensity of Major Baltic Inflows (MBIs) modified from Mohrholz *et al.* (2015). The stagnation period when there were fewer MBIs between 1983 and 1993 is clearly visible, the 1993 and 2003 MBIs are highlighted in red.

4.1.4 Geochemical studies of redox changes in the Baltic Sea

The redox history of Baltic Sea sediments has been investigated using the variation in concentrations and stable isotope compositions of redox-sensitive elements including Mn, Fe, Mo, U, and Re (e.g. Fehr *et al.* 2010, Fehr *et al.* 2008, Jilbert and Slomp 2013b, Noordmann *et al.* 2015). High resolution Mo/Al data for sediments from the Gotland Deep at site BY15 suggest that in 1980 there is a rapid onset of euxinic deposition conditions (Figures 4.6, 4.7; Jilbert and Slomp 2013b). Elevated Mo/Al values since 1980 are interrupted by two rapid decreases associated with the 1993 and 2003 MBIs. The minima in Mo/Al observed in 1993 and 2003, that are likely to have

been caused by ventilation of bottom waters due to the 1993 and 2003 MBIs, nonetheless display a higher Mo/Al ratio than the 1950 background (Figure 4.5). This is can be explained by the presence of H_2S in the porewater of the sediment which partly buffers the upper sediment from the ventilation induced changes in H_2S in the overlying bottom waters (Jilbert and Slomp 2013b). This suggests that conditions in the porewater and sediment remain more reducing than the overlying bottom water during MBIs (Jilbert and Slomp 2013b).

Small but significant variations in the Fe isotopic composition were observed in Holocene sediments from the Gotland Deep due to the shift from a limnic environment with oxygenated bottom water, to brackish water with periodically euxinic conditions (Fehr *et al.* 2008). Surface sediments of the Gotland Deep are enriched in isotopically light Fe, and have high Fe/Al values, likely due to the shuttling of Fe from the shelf to the euxinic basin (Fehr *et al.* 2010). Uranium and Mo stable isotope data of a sediment core from the Landsort Deep in the Baltic Sea have compositions that are isotopically significantly lighter than those of typical organic-rich sediments from anoxic basins (Noordmann *et al.* 2015). Noordmann *et al.* (2015) conclude that this could be due to major overturning events that could modify the Mo and U isotopic signatures of the sediments by re-mobilisation of Mo that was previously bonded to ferromanganese oxides.

Sediment depth profiles of a core from the Landsort Deep (Baltic Sea) show increasing Re concentration from 1.9 ng g^{-1} at 14.5 cm to a maximum of 4.0 ng g^{-1} at 4.5 cm depth, and decreasing Re/Mo ratio from 0.4 at 14 cm depth, to consistently < 0.1 above 6 cm depth (Noordmann *et al.* 2015). The Re concentration data from the Landsort Deep are consistent with anoxic deposition conditions in the upper part of the sediment core. Rhenium concentration data show low (< 0.3 ng g^{-1}) values in the surface sediments of a non-euxinic part of the Baltic Sea in the Bothnian Bay (Ingri *et al.* 2014); these authors find decreasing Re concentration with increased oxygenation of the sedimentation site (6 m to surface). Rhenium concentration (and U/Al) data from several sites in the Baltic Sea are available (Slomp 2016, unpublished,

pers.comm.) and these data are shown as Re/Al ratios in Figure 4.4. All sites, except the shallowest site (the Arkona Basin BY2) show increased Re concentration in the topmost sediment layers. This indicates that Re concentrations were enriched in several locations in the Baltic Sea in recent years, and that there is likely to be increased drawdown of Re in the Baltic Sea, particularly in the deep basins.

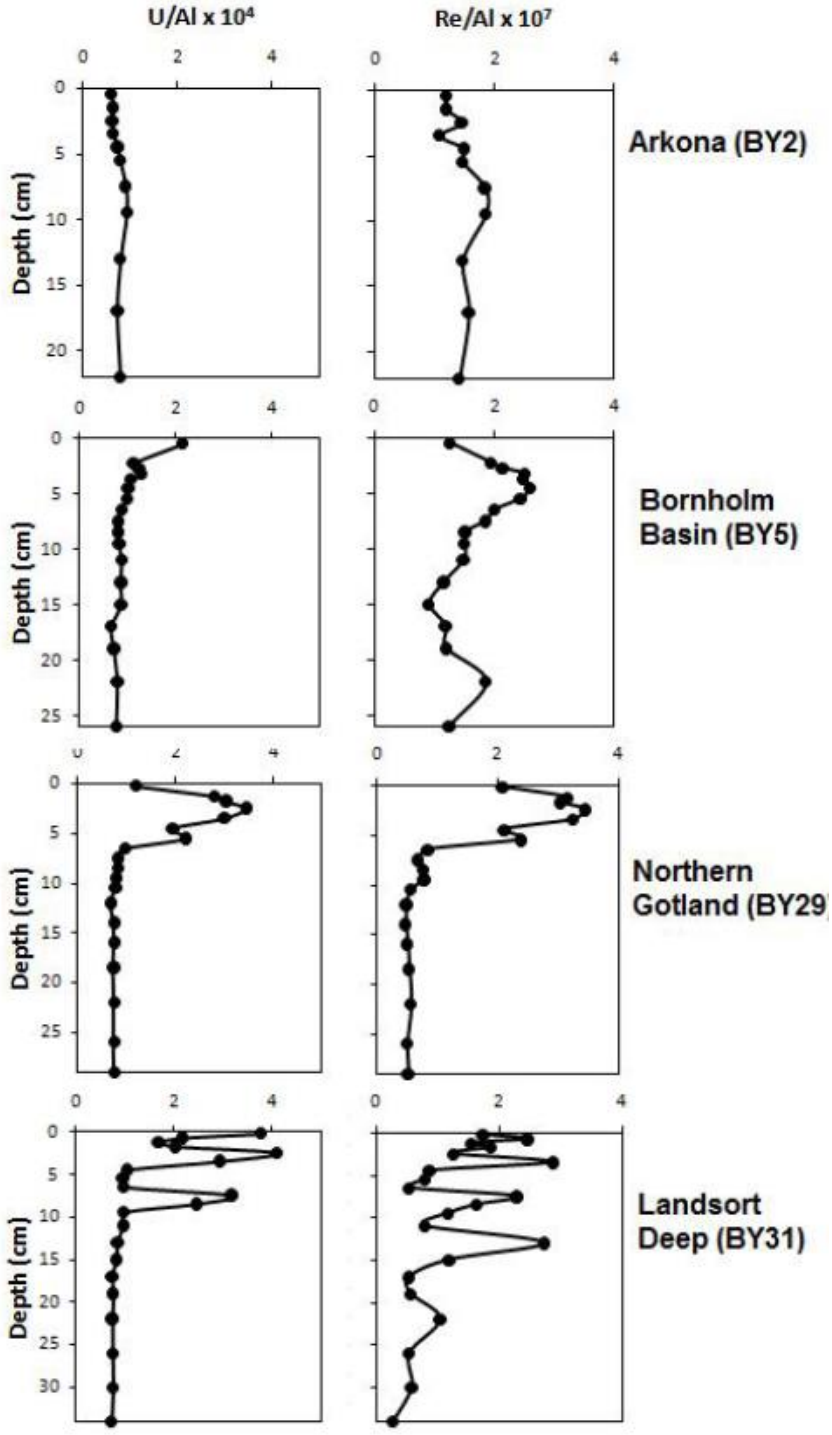

Figure 4.4: Rhenium/Al and U/Al ratios of sediments from various sites in the Baltic Sea; figure from Slomp (2016, unpublished, pers.comm.)

4.1.5 Using Baltic Sea sediment samples to constrain the behaviour of Re isotopes

The Re isotope composition of marine sediment is expected to show per mil level variations due to changing redox conditions, based on theoretical modelling of equilibrium mass dependent fractionation, and nuclear volume effects among a variety of Re^{VII} and Re^{IV} species (Miller *et al.* 2015), discussed in more detail in Chapter 2. Rhenium is incorporated into anoxic sediment below the sediment-water interface (Colodner *et al.* 1993), and is generally considered to be abiotic, although some evidence suggests that it is preferentially incorporated into algae (Racionero-Gómez *et al.* 2016). Rhenium is associated predominantly with the organic matter component of sedimentary rocks, but there is likely a small silicate component (Miller *et al.* 2015, Selby and Creaser 2003). Changes in $\delta^{187}Re$ (defined in section 1.3) have been measured in sedimentary rocks spanning the T-OAE during this study (Chapters 3 and 6).

Sediments from the Baltic Sea at site BY15 were chosen to study how $\delta^{187}Re$ may vary with changing bottom water redox conditions. This site was chosen because well constrained data are available for other redox sensitive elements, such as Mo concentration data (Jilbert and Slomp 2013b); there is a continuous bottom water oxygenation record (Gustafsson and Medina 2011); and the sediment has high organic-carbon concentration (Lenz *et al.* 2015b) and high Mo concentration (Jilbert and Slomp 2013b), which makes it geochemically similar to the Toarcian sedimentary rock samples studied in Chapter 6, and used in Chapter 3 to develop the method. The selected samples were deposited between ~1960 to 2009 (Jilbert and Slomp 2013b) and therefore include the change from hypoxic to euxinic conditions observed around 1980, and the two increases in bottom water oxygenation caused by the 1993 and 2003 MBIs. The aim of this chapter is to understand the behaviour of Re isotopes in a modern ocean setting by the study of $\delta^{187}Re$ in a shallow sediment core across a range of different redox conditions.

4.2 Methods and samples

Determination of δ^{187}Re was carried out for a set of 16 sediment samples from site BY15 in the Gotland Deep of the Baltic Sea (57.3200°N, 20.0500°E, 238 m water depth). Samples were collected by Caroline Slomp by multicore (~0-50 cm) during the HYPER/Combine cruise of the R/V *Aranda* in May-June 2009 (Jilbert and Slomp 2013b). The core was sliced under nitrogen at 0.5 – 2 cm resolution, and has previously been analysed for TOC %, Mo, P and Al contents (Jilbert and Slomp 2013b, Lenz *et al.* 2015b). All samples were freeze-dried and finely ground, and provided in powdered form by Caroline Slomp, Utrecht University, Netherlands.

All sample processing and δ^{187}Re determinations were carried out at the Open University using the clean lab suite, and Thermo Neptune multiple-collector-ICP-MS. Following sample digestion, Re was separated from the samples using a two stage anion exchange chromatographic separation procedure to provide a high purity high (~100 %) yield Re fraction. The δ^{187}Re values were calculated by standard sample bracketing. Further details of analytical methods are presented in Chapter 3. The sixteen samples were each analysed only once; the reference sample SDO-1 and aliquots of the Re single element standard SRM 3143, which had been processed by the separation procedure were analysed once or twice (Table 4.1). Iridium was used to correct for instrumental mass bias; the Re concentration in the analysed sample aliquots of Re (after separation from bulk samples) range from 7 ppb to 20 ppb, and the Ir concentration in all aliquots analysed is 200 ppb. The Re concentration in the original sample was determined by analysis of a small aliquot of 5% of the final purified Re fraction by MC-ICPMS relative to Re standards of known concentrations.

To plot the δ^{187}Re data alongside the bottom water O_2 concentration data, hypoxic bottom water area data, and timing of the MBIs, it is necessary to correlate depth in sediment with age. The age model applied to the sediment samples is from Jilbert and Slomp (2013b); the core was initially dated by ^{210}Pb chronometry using a 'Constant Rate of Supply' algorithm, then

the age model was tuned by matching four peaks in the LA-ICP-MS derived Mo/Al profile to minima in the bottom water O_2 concentration data from site BY15. This age model is subject to the errors on the ^{210}Pb chronometry, and the assumptions made in the Mo/Al tuning process, most importantly that the Mo/Al maxima always correspond to O_2 minima. Uncertainty in the exact age of discrete sediment samples increases with depth: the two possible supported background ^{210}Pb energies of 113 mBq/g and 137 mBq/g have a range in age estimates of ~30 years at 11cm depth, but the range is < 5 years at < 4cm depth. The difference between the ^{210}Pb age and the Mo/Al tuned age is around 10 years deeper in the core, but closer to one year in the shallower samples (Jilbert and Slomp 2013b). The uncertainties in the age model causes potential difficulties when matching $\delta^{187}Re$ data with the redox changes observed throughout the period of study, particularly when correlating the shifts in $\delta^{187}Re$ with the timing of the MBIs. The potential implications of the use of this age model on the interpretation of the $\delta^{187}Re$ data are discussed in section 4.4.3 below.

Table 4.1: Rhenium isotope composition data and Re concentration data for samples from site BY15 of the Gotland Deep in the Baltic Sea.

Sample	Depth in sediment (cm)	Year[a]	[Re][b] (ppb)	[Re][c] (ppb)	$\delta^{187}Re$ (‰)	± 2 SD[d]
HY222	0.25	2008.7		5.27		
HY223	0.75	2007.2		6.04		
HY222 + HY223 combined	0.5	2008.0	7		-1.084	0.125
HY225	1.25	2005.6	7	5.19	-0.993	0.125
HY226	1.75	2004.1	20	14.52	-0.844	0.088
HY227	2.25	2002.2	7	6.60	-0.580	0.125
HY228	2.75	1999.3	10	6.02	-1.087	0.084
HY229	3.25	1996.3	7	3.41	-0.749	0.125
HY230	3.75	1991.3	20	9.13	-0.479	0.088
HY231	4.25	1988.6	10	7.94	-0.522	0.084
HY232	5	1985.2		9.19		
HY233	6	1982.0	15	7.35	-0.370	0.075
HY234	7	1978.2	15	3.19	-0.408	0.075
HY235	8	1973.4	10	2.61	-0.261	0.084
HY236	9	1968.6	7	2.34	-0.486	0.125
HY237	10.5	1961.6	10	2.53	-0.443	0.084
HY238	12.5		7	1.78	-0.438	0.125
HY239	14.5		7	1.70	-0.416	0.125
HY240	16.5		7	1.55	-0.394	0.125

[a] Age model calculated by Jilbert and Slomp (2013b), using ^{210}Pb chronometry, and further tuned using peaks in the Mo/Al and bottom water O_2 record.
[b] Concentration of Re in sample solution aliquot analysed for $\delta^{187}Re$.
[c] Concentration of Re in original sample.
[d] ± 2 SD is the daily reproducibility of bracketing standards at the concentration analysed.

Table 4.2: δ^{187}Re data for column processed SRM 3143 and SDO-1.

Sample	Processing No.	Analysis	[Re][a] (ppb)	δ^{187}Re (‰)	± 2 SD[b]
Single element standard					
processed SRM 3143	1	a	20	0.029	0.088
processed SRM 3143	2	a	10	-0.004	0.084
processed SRM 3143	2	b	15	-0.004	0.075
Average processed SRM 3143				0.007	**0.038**
Reference sample					
SD0-1	1	a	20	-0.180	0.088
SD0-1	1	b	10	-0.227	0.084
SD0-1	2	a	15	-0.124	0.081
SD0-1	3	a	15	-0.264	0.075
Average SD0-1 (this chapter)				-0.199	**0.121**
Average SD0-1 (Chapter 3)				-0.129	**0.109**
SDO-1 (Miller *et al.* 2009)[c]				-0.080	**0.130**

[a] Concentration of Re in sample solution aliquot analysed for δ^{187}Re.
[b] For single analyses, ± 2 SD is the daily reproducibility of bracketing standards standards at the concentration analysed. For the averages of repeat analyses, ± 2 SD is the reproducibility of the individual values.
[c] Literature value of δ^{187}Re for SDO-1 is adjusted to show value relative to SRM 3143.

4.3 Results

4.3.1 Changes in δ^{187}Re with sediment depth

The Re isotope composition remains relatively consistent between 18 and 6 cm sediment depth in the core from site BY15, within analytical uncertainties, with an average δ^{187}Re = -0.402 ± 0.133 ‰ (Figure 4.5, Table 4.1). There is a slight gradual decrease in δ^{187}Re from -0.394 ± 0.125 ‰ to -0.486 ± 0.125 ‰ between 16.5 cm and 9 cm depth, though this is not resolvable within the uncertainties. There is then a brief positive excursion at 8 cm depth (δ^{187}Re = -0.261 ± 0.084 ‰). This is followed by a gradual decrease of 0.261 ‰ between 8 cm and 4.24 cm to a minimum of -0.522 ± 0.084 ‰. Above 3.75 cm sediment depth, δ^{187}Re remains consistently below -0.500 ‰. There are two rapid decreases to minimum values in the upper part of the core: from 4.25 cm to 2.75 cm, δ^{187}Re shifts from -0.522 ± 0.084 ‰ to -1.087 ± 0.085 ‰, and from 2.25 cm to 0.5 cm δ^{187}Re shifts from -0.580 ± 1.25 ‰ to -1.084 ± 0.125 ‰. These two rapid decreases in the Re

isotope composition define a shift towards more positive δ^{187}Re values between 2.75 and 2.25 cm depth (Figure 4.5). The changes in δ^{187}Re with depth can be directly compared to Re concentration data (this study), and elemental ratio data C_{org}% (organic carbon), S, Mo, Al, Fe, Mn, Zn, Ni, and V concentration data from Jilbert and Slomp (2013b), Lenz *et al.* (2015b).

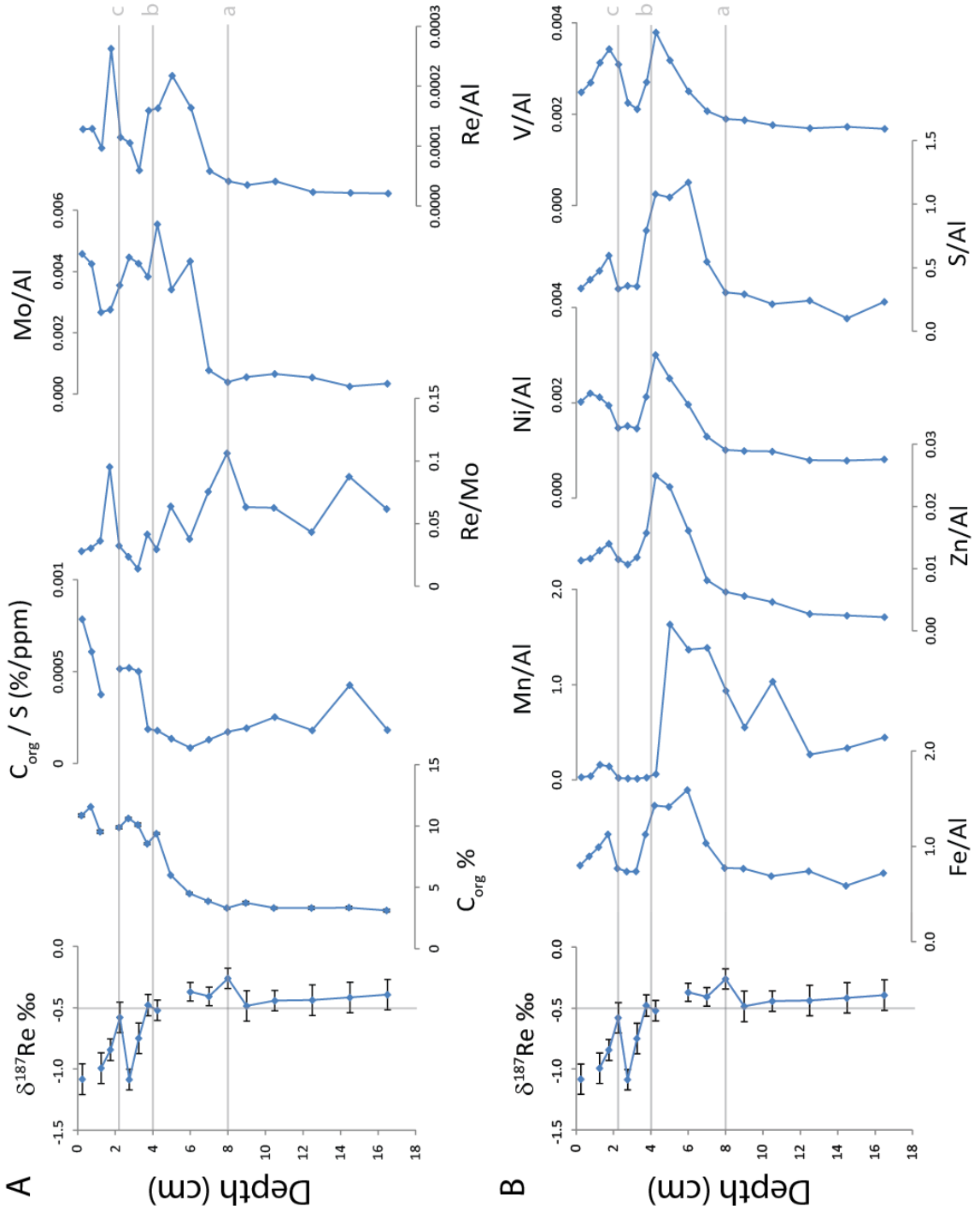

Figure 4.5: Rhenium isotope (δ^{187}Re) and element/Al data plotted relative to depth in sediments from the Gotland Deep in the Baltic Sea. Rhenium concentration, and δ^{187}Re data, this study; C_{org} % (organic carbon), S, Mo, Al, Fe, Mn, Zn, Ni, and V concentration data from Jilbert and Slomp (2013b), Lenz *et al.* (2015b). The horizontal grey lines b and c show the two maxima in δ^{187}Re values before each of the negative shifts, the horizontal grey line a shows the base of the increases in element/Al, and C_{org} values. The vertical grey line shows the division in δ^{187}Re values between the lower and upper sediment depths as discussed in section 4.4.2.

4.3.2 Reproducibility of data

The reproducibility of δ^{187}Re values for BY15 samples, all of which were analysed only once, has been estimated from the reproducibility of bracketing standards during analysis at each concentration on a particular day. For the Baltic Sea samples in this study, the daily ± 2 SD reproducibility of standards ranges from 0.075 ‰ to 0.125 ‰, with an average of 0.104 ‰ for δ^{187}Re. An additional estimate of reproducibility is provided by repeat analysis of column processed aliquots of the Re single element standard SRM 3143 (δ^{187}Re = 0), with three repeats yielding δ^{187}Re = 0.007 ± 0.038 ‰. Additionally, four analyses of the reference sample SDO-1 have δ^{187}Re = -0.199 ± 0.121 ‰, which is within analytical uncertainty of the literature value (Miller *et al.* 2009), and the data from this reference sample collected in Chapters 3 and 6 (Table 4.2). The Re isotope composition of an in-house Re standard (Specpure®) solution was determined at the start of each analytical session. These measurements are used to further monitor the daily performance of the Neptune MC-ICP-MS. The average δ^{187}Re for the in-house standard over a 7-month period is -0.203 ± 0.065 ‰ (2 SD) for 21 individual measurements obtained during 3 analytical sessions.

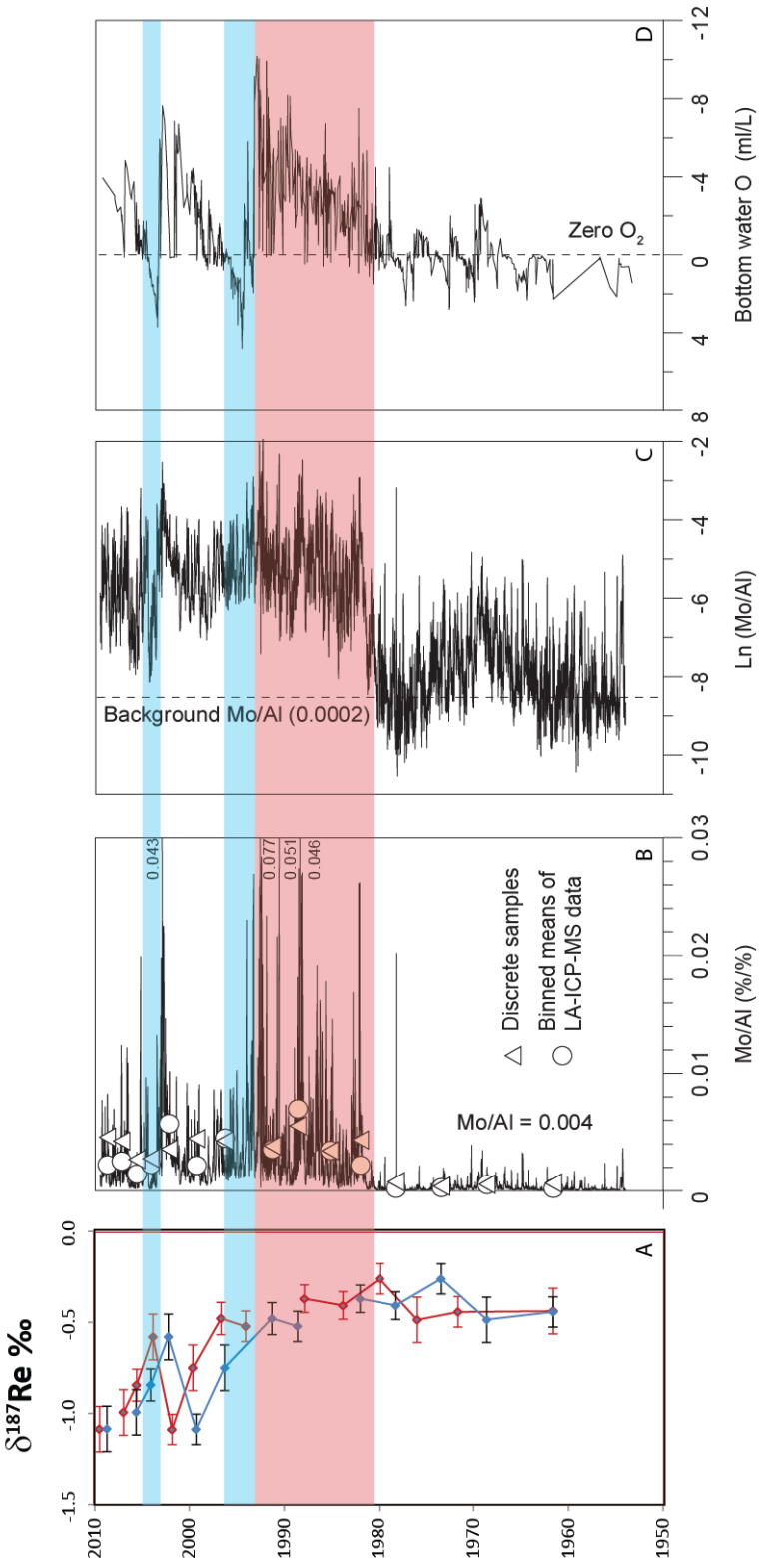

Figure 4.6: Rhenium isotope (δ^{187}Re) data plotted against year for sediments from the Gotland Deep in the Baltic Sea (this study, panel A). Panels B, C and D are: Mo/Al, Ln (Mo/Al), and bottom water O_2 concentration (figure from Jilbert and Slomp 2013b), respectively. Solid lines from high resolution LA-ICPMS, discrete samples indicated by triangles (Jilbert and Slomp 2013b). Age of

discrete samples was reconstructed by Jilbert and Slomp (2013b) using Mo concentration data from high resolution LA-ICPMS scanning (Jilbert and Slomp 2013b). For the $\delta^{187}Re$ data, the red data points show the age of samples using ^{210}Pb dating, the blue data points show the age of samples using the Mo-tuned age model. Bottom water oxygen concentrations at site BY15 (right; data assimilated from Baltic Environmental Database by Gustafsson and Medina (2011), and presented by Jilbert and Slomp (2013b)). Positive values indicate presence of O_2 and negative values indicate presence of H_2S, assuming stoichiometry 1 mol H_2S = 2 mol O_2 (Jilbert and Slomp 2013b). Red shading indicates the onset of the modern hypoxic event from 1980 to 1993 as shown by the data in Figure 4.2, and the two blue shaded bands show the two MBIs of the modern hypoxic event from 1993, and 2003 until the return to euxinic conditions for each MBI.

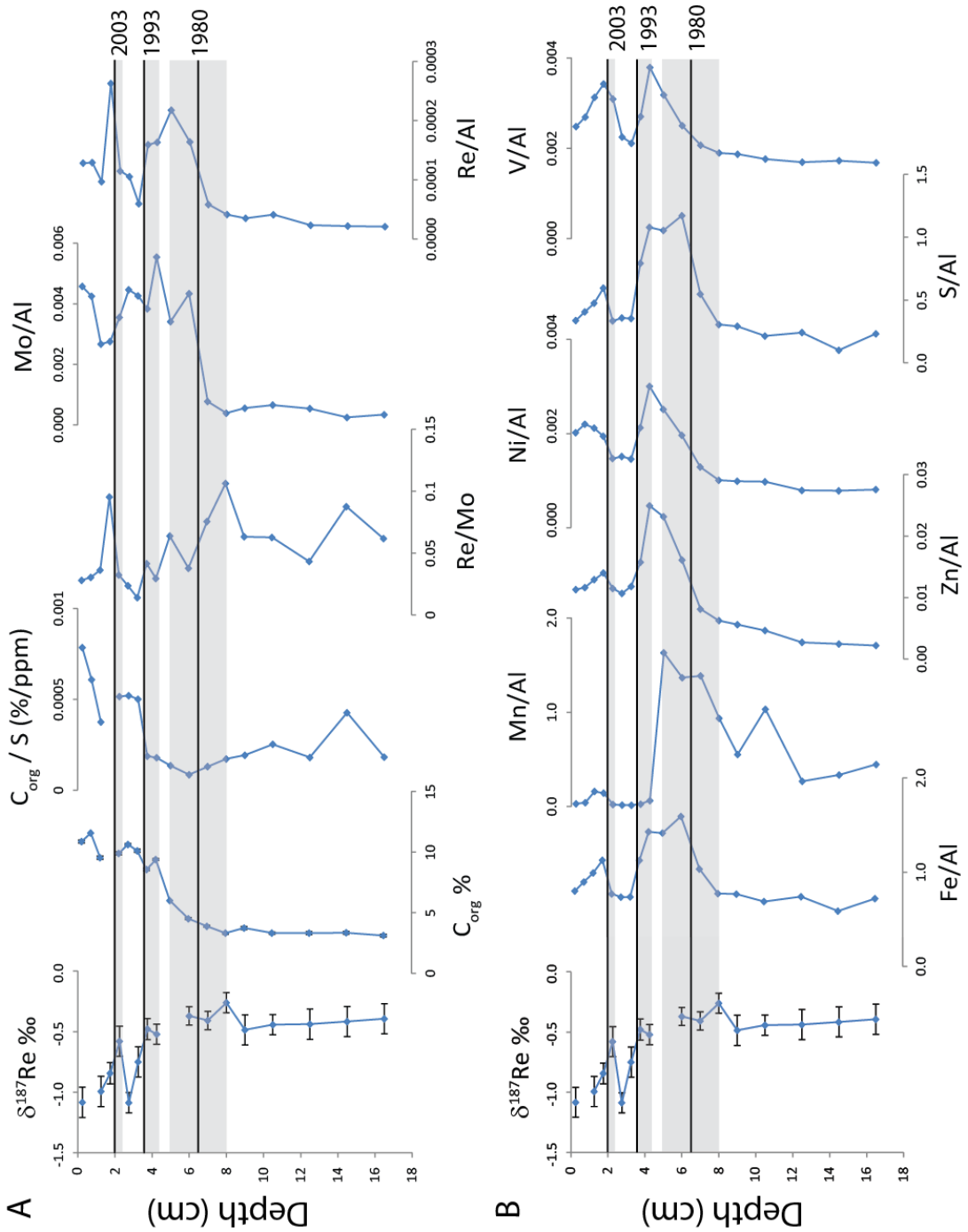

Figure 4.7: Rhenium isotope data (δ^{187}Re) plotted against sediment depth from the Gotland Deep in the Baltic Sea. Organic carbon %, Fe/Al, Zn/Al, Ni/Al, V/Al, S/Al, Mo/Al, and Mn/Al data from Jilbert and Slomp (2013b). Rhenium concentration and δ^{187}Re data, this study. The grey horizontal bands show the depth estimated of 1980, 1993, and 2003 as labelled, with the upper and lower limits showing the two possible supported background ^{210}Pb energies of 113 mBq/g and 137 mBq/g respectively (Jilbert and Slomp 2013b). The horizontal black lines show the depth of those three ages as calculated by the Mo/Al tuned age model (Jilbert and Slomp 2013b).

4.4 Discussion

4.4.1 Chemical processes involved in recording δ^{187}Re in sediment

Interpreting the causes of changes in δ^{187}Re in sediment samples from the Baltic Sea requires consideration of the chemical mechanism by which Re is incorporated into sediment, and any fractionation of Re isotopes which may occur during this process. The exact chemical mechanism affecting the authigenic enrichment of Re in sediments under reducing conditions, and its effect on δ^{187}Re, remains poorly understood (Miller *et al.* 2015). It is possible that Re is quantitatively removed from the water column under anoxic conditions, which is assumed to be the case for Mo under euxinic conditions (Dickson *et al.* 2012, Dickson *et al.* 2017, Kendall *et al.* 2017, Pearce *et al.* 2008). If this is the case, then the δ^{187}Re values of sediment deposited under anoxic/euxinic conditions would reflect the δ^{187}Re of seawater. In this case we would expect to see δ^{187}Re of sediment samples trending towards seawater values under the anoxic /euxinic conditions of the deep basins in the Baltic Sea. Alternatively, it is possible that fractionation of Re isotopes occurs during the process by which Re is authigenically accumulated in sediment, which would imply that the δ^{187}Re of sediment reflects fractionation of Re as it is incorporated into sediment, rather than recording seawater δ^{187}Re values. Given that the δ^{187}Re of seawater is not known, it is unclear whether quantitative removal of Re to the sediment occurs, and hence whether changes in δ^{187}Re in the sediment directly reflect changes in the δ^{187}Re of Baltic seawater. Further to this, it is not yet known whether Baltic seawater has the same δ^{187}Re as that of global seawater, given the limited exchange between the Baltic Sea and the North Sea, and also the possibility that the brackish conditions in the Baltic Sea may have some effect on the δ^{187}Re of Baltic seawater.

Nonetheless we can use δ^{187}Re data and Re/Al data to test two hypotheses which may in turn shed light on whether Re is quantitatively removed from seawater or not. These hypotheses are: (1) that the δ^{187}Re recorded in sediment reflects changing local redox conditions, which can

be tested by comparing δ^{187}Re with elemental ratios and bottom water O_2 concentration data at site BY15; and (2) that δ^{187}Re recorded in sediment reflects regional variation in the areal extent of hypoxia, which can be tested by comparing δ^{187}Re in the sediment with data on the changing hypoxic area in the Baltic Sea. Sections 4.4.2 to 4.4.4 discuss whether the δ^{187}Re data supports these hypotheses, and sections 4.4.5 to 4.4.7 explore other factors including anthropogenic input and diagenesis which may influence the recording of δ^{187}Re in sediment.

4.4.2 The relationship between δ^{187}Re and elemental ratio changes in sediment samples from the Gotland Deep

In this section, the δ^{187}Re and Re concentration data (plotted as Re/Al) from this study are discussed in comparison to the elemental data of Jilbert and Slomp (2013b), Lenz *et al.* (2015a).

16.5 cm to 8 cm

The very small-scale changes in δ^{187}Re between 16.5 and 8 cm sediment depth (Figure 4.5: below line a) in the sediment samples from Gotland Deep BY 15 display and very little change in redox sensitive metal composition (metal/Al), and C_{org} indicate no change in ocean chemistry. However, despite the lack of change across this interval, the Mo/Al, Re/Al, Zn/Al, Ni/Al, S/Al, and V/Al values remain above the levels observed in average shales (Brumsack 2006), indicating that local redox conditions are generally hypoxic. The Fe/Al values (apart from one datum point), are higher than the suggested composition of the detrital background in the Baltic Sea of Fe/Al = 0.63 (Fehr *et al.* 2008) and hence maybe indicative of euxinic conditions; however, there are other factors which may influence the absolute Fe/Al value recorded in sediment, such as changes in the rate of Fe shuttling to the deep basins, and potentially re-mobilisation of Fe within the sediment.

8 cm to 4 cm.

The increases in Mo/Al, Re/Al, Fe/Al, Zn/Al, Ni/Al, S/Al, and V/Al between 8 and 4 cm (Figure 4.5: between lines a and b) are interpreted to indicate intensified reducing conditions at site BY15, but are associated with very little change in δ^{187}Re (a 0.261 ‰ change between 8 cm and 4 cm depth). The changes in each of these elements do not occur at the same rate as each other. The rapid increase in Mo/Al values at 6 cm to 7 cm depth is interpreted to indicates rapid onset of euxinic conditions (Jilbert and Slomp 2013b), whereas accumulations of Zn, Ni, S, and V occur more gradually. The sudden and marked increase in Re/Al ratio, between 7 cm and 5 cm depth indicates the intensification of anoxic conditions causing enhanced authigenic accumulation of Re in the sediment. There is a gradual increase in C_{org} values indicating more reducing conditions, and possible elevated productivity leading to a higher flux of organic carbon to the sediment. Despite conditions already being hypoxic below 8 cm, there is clear evidence for intensification in reducing conditions in this interval, but very little change in δ^{187}Re values. Therefore changing local redox conditions in this depth interval do not appear to drive changes in δ^{187}Re recorded in the sediment.

At 4.25 cm there is a sudden and marked decrease in Mn/Al, despite not being a suitable proxy for redox on its own, the sudden decrease in Mn/Al may be caused by euxinic conditions causing the re-mobilisation of Mn from sediment. There may also be changes in the distribution of Fe-Mn shuttles to the deep basins in the Baltic Sea (Lenz *et al.* 2015a, Lenz *et al.* 2015b).

4 cm to surface

The significant decrease in δ^{187}Re values from -0.479 ± 0.088 ‰ to -1.087 ± 0.084 ‰ between 3.75 cm and 2.75 cm sediment depth is coincident with the high C_{org} ~10 % indicating the persistence of locally anoxic conditions. As Re/Mo remains low over the same interval the conditions are interpreted as locally euxinic. The decrease in Mo/Al between 4.25 cm and 1.25 cm

spans both the sudden decreases in $\delta^{187}Re$ above lines b and c (Figure 4.5); the decreasing Mo/Al ratio indicates a decrease in the severity of anoxia at site BY15, however the values do not decrease as low as the background values observed below 8 cm as has been previously discussed by Jilbert and Slomp (2013b). The decrease in Re/Al values between 5 cm and 3.25 cm is interpreted to indicate that conditions are perhaps less severely anoxic, that the budget of Re in the Baltic Sea is depleted, or that the intermittently oxic conditions associated with the MBI disrupt the enrichment of Re in the sediment. Decreases in Zn/Al, Ni/Al, S/Al, and V/Al correlate more closely with the first negative shift in $\delta^{187}Re$ and indicate that there are less severely reducing conditions, or that these elements are more strongly affected by the MBIs causing intermittently oxic conditions. These values also remain above the background values observed below line a, indicating that conditions are still more severely reducing than those lower down in the core.

The sharp decrease in $\delta^{187}Re$, from -0.580 ± 0.125 ‰ to -1.084 ± 0.125 ‰ between 2.25 cm and 0.5 cm depth (Figure 4.5: above line c) and the associated brief increase in Zn/Al, Ni/Al, and V/Al is interpreted to indicate intensified hypoxia. As C_{org} remains high, persistently hypoxic conditions are indicated and the Mo/Al increases between 2 cm depth and the surface are interpreted to indicate increased euxinic conditions. The brief increase in Re/Al after the maximum in $\delta^{187}Re$ at 2.25 cm could indicate either intensified anoxia, or a renewed supply of Re to the deep waters of the Gotland Deep which may have had a depleted budget of Re due to the earlier expansion of hypoxic deposition. Persistently euxinic conditions in the topmost 2.25 cm of the studied sediment core (Figure 4.5: above line c) are indicated by high C_{org}, low Re/Mo ratio, and elevated Mo/Al values, however in the same interval there is significant variation in $\delta^{187}Re$, and so the $\delta^{187}Re$ of sediment may not be directly affected by changing redox conditions.

Above 4 cm (Figure 4.5: line b) there are 2 sharp decreases in $\delta^{187}Re$ punctuated by an increase at 2.25 cm (Figure 4.5: line c), the largest variation in $\delta^{187}Re$ values in the core (a 0.608 ‰ range), and the lowest $\delta^{187}Re$ values in the core are observed, with all values remaining below -0.5 ‰. The Re/Al and Mo/Al ratios show the most variation, but remain elevated above values seen below 4 cm, and in the case of Re/Al above the values seen below 8 cm, indicating varying severity of reducing conditions but still generally persistent anoxia or euxinia. The decreased in the Re/Al, and Mo/Al ratios may be associated with a return to more oxygenated conditions, however, the Re/Mo ratio remains low indicating that conditions remain persistently euxinic. An alternative explanation of the decrease in Re/Al ratio above 4 cm could be increased basin-wide drawdown of Re as anoxic conditions expand to larger areas in the Baltic Sea.

Above 4 cm, the $\delta^{187}Re$ remains below - 0.5 ‰ (Figure 4.5). The interval of euxinic deposition above 4 cm at site BY15 is associated with the most dramatic changes in $\delta^{187}Re$ in the core, however the rapid shifts in $\delta^{187}Re$ do not correlate stratigraphically with any coherent trends in redox conditions indicated by the Re/Mo, Mo/Al, Re/Al, and Fe/Al ratios, or the $C_{org.}$ This suggests that the $\delta^{187}Re$ recorded in sediment is not solely controlled by changes in local redox conditions.

4.4.3 Changes in $\delta^{187}Re$ relative to bottom-water oxygen concentration at site BY15

During the onset of euxinic conditions between 1980 and 1993, the change in bottom water oxygen concentration to negative values is accompanied by only a small (-0.218 ‰) shift in $\delta^{187}Re$ (Figure 4.6). The small shift in $\delta^{187}Re$ over this time interval could imply that any local changes in bottom water oxygen concentration do not have much impact on $\delta^{187}Re$ recorded in sediment. However, in contrast to the relatively small changes in $\delta^{187}Re$ observed before 1993, there are two distinct shifts in $\delta^{187}Re$ to negative values after this date which broadly correlate with the sudden changes in bottom water redox conditions at site BY15, associated with the 1993

and 2003 MBIs (Figure 4.6). Depending on which age model is applied to the data (section 4.2), a slightly different pattern of δ^{187}Re changes is observed with each of the MBIs (Figures 4.6 and 4.7). Both of the negative shifts in δ^{187}Re with minima at 2.75 cm and 0.5 cm occur following the 1993, and 2003 MBIs regardless of which age model is applied to the data (Figure 4.6). However, the oxic bottom water conditions of the 2003 MBI at site BY15 either correlate with the brief increase in δ^{187}Re at 2.25 cm (^{210}Pb age model), or the oxic conditions occur just after the maximum in δ^{187}Re (Mo-tuned age model). Despite the Mo-tuned age model being interpreted by previous authors to give better correlation of the sediment age particularly lower in the core (Jilbert and Slomp 2013b), the ^{210}Pb age model gives a more consistent pattern of δ^{187}Re changes relative to the two MBIs at 1993 and 2003 (Figure 4.6, 4.7, 4.8). During the oxic bottom water conditions (blue bands in Figure 4.6), δ^{187}Re values peak at close to - 0.5 ‰, but during the return to euxinic conditions following the MBIs, δ^{187}Re reach minimum values of - 1.087 ‰ and - 1.084 ‰.

The decrease in δ^{187}Re following the 1993 and 2003 MBIs could suggest that the lowest δ^{187}Re are caused by incoming salty oxygenated water. If this is the case, the low δ^{187}Re values could reflect either more oxic local bottom water conditions, or incoming seawater which may be isotopically distinct from the prevailing Baltic Sea water with respect to δ^{187}Re. Alternatively, the shift towards high δ^{187}Re at the start of the 2003 MBI, and the comparatively higher δ^{187}Re values during the oxic conditions of the 1993 MBI, could instead suggest that salty oxygenated waters cause higher δ^{187}Re values to be recorded in the sediment, and that the two negative shifts in δ^{187}Re instead reflect the prevailing euxinic conditions in the bottom water. However, given such low δ^{187}Re values (~ - 1 ‰) are not observed during the onset of euxinic conditions between 1980 and 1993 (Figure 4.6), this explanation relies on features of the Re budget in the bottom water (discussed in more detail in section 4.4.8 below). In this case the prevailing euxinic conditions cause quantitative removal of Re and hence the recording of seawater δ^{187}Re in the sediment.

Elevated Re/Al ratios are present in several locations in the Baltic Sea in shallow sediment samples (Figure 4.4). Above the first maximum in Re/Al at BY15 at 5cm (Figure 4.5), Re/Al decreases (above line b) potentially due to reduced availability of Re from the overlying seawater caused by increased areal spread of Re deposition into sediment. The elevated Re/Al values immediately after the 2003 MBI (above line c) could indicate that the MBI brings in seawater with a higher Re concentration than is present in the now depleted bottom water of the Baltic Sea. The interpretation of a depleted Re budget in the bottom water of the Baltic Sea supports the idea of quantitative removal of Re from seawater. The potential effect of the changing areal extent of hypoxic deposition on $\delta^{187}Re$ is discussed in more detail in section 4.4.4 below.

The lack of major change in $\delta^{187}Re$ during the onset of euxinic conditions at site BY15 between 1980 and 1993 could indicate that there is a lag time of approximately 10 years between the onset of locally euxinic conditions and the most noticeable changes in $\delta^{187}Re$. In this case, the initial shift to lowest $\delta^{187}Re$ (3.75 cm depth to 2.75 cm depth) would correspond with the onset of euxinic conditions between 1980-1993, and the second negative shift in $\delta^{187}Re$ (2.25 cm depth to 0.5 cm depth) would reflect the second development of euxinic conditions following the 1993 MBI, between 1993-2003. However, this interpretation is not supported by the correlation between Re/Al data and bottom water oxygenation data between 1980 and 1984 which would suggest that the Re in the bottom water is rapidly affected by changing oxygen conditions (Figure 4.7). Alternatively, it is possible that the onset of euxinic conditions between 1980 and 1993 at site BY15 do cause changes in the $\delta^{187}Re$ of seawater, but that these changes are not significant relative to the overall Re budget in the bottom water, and therefore are not resolvable in the sediment record. Comparison of sediment $\delta^{187}Re$ data and bottom water oxygen concentration data from site BY15 recorded between 1960 and 2010 reinforces the interpretation that $\delta^{187}Re$ in sediment is not directly controlled by changing local redox conditions (Figure 4.6).

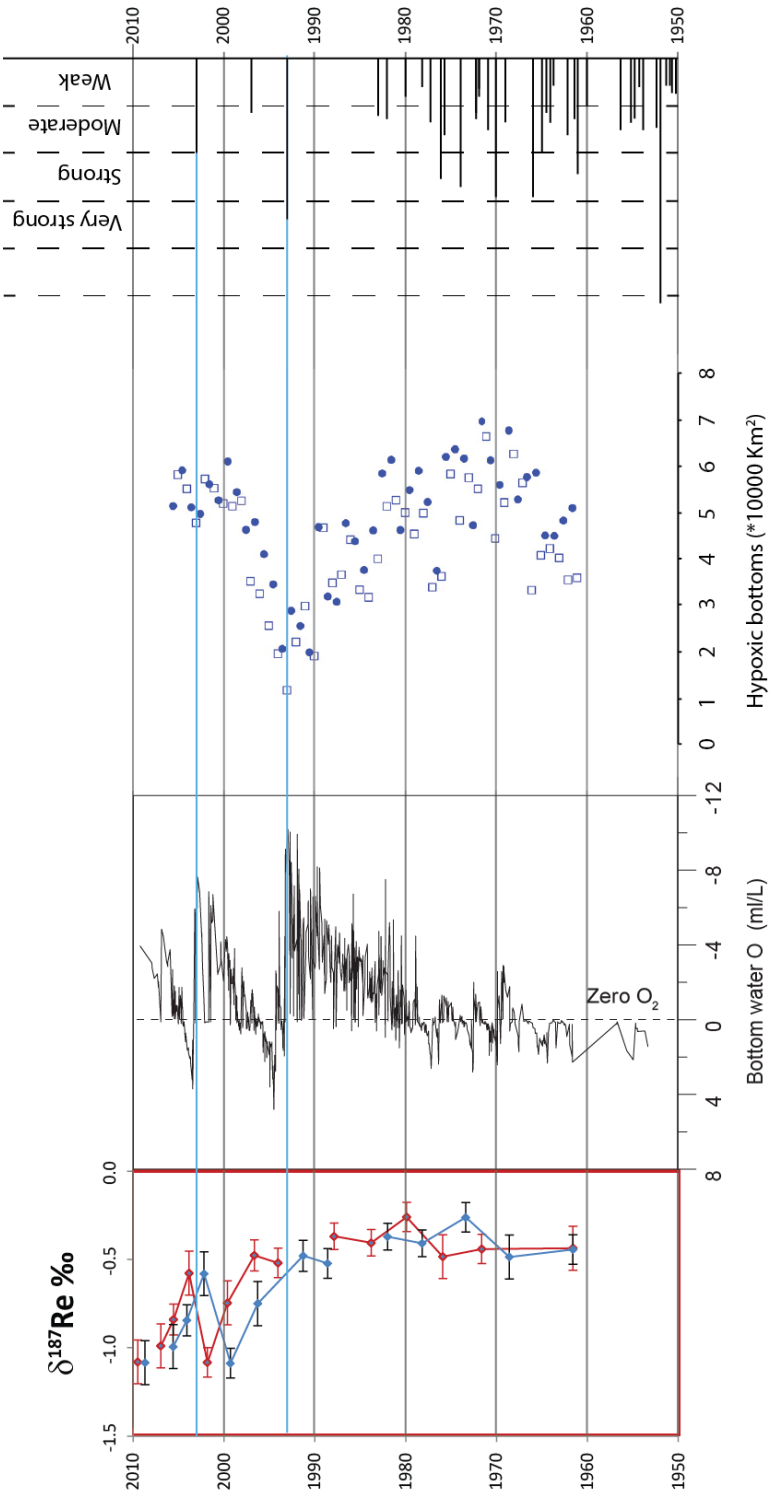

Figure 4.8: Panels from left to right: δ^{187}Re data for sediment samples from site BY15 (this study), the red data points show the age of samples using ^{210}Pb dating, the blue data points show the age of samples using the Mo-tuned age model, the age model is from Jilbert and Slomp (2013b); bottom water O_2 data from the same site (figure from Jilbert and Slomp (2013b); data assimilated from Baltic Environmental Database by Gustafsson and Medina (2011)); changing areal extent of hypoxic deposition for the whole Baltic Sea (figure from Conley *et al.* (2009)); and the timing and intensity of MBIs (figure from Mohrholz *et al.* (2015)).

4.4.4 Changes in δ^{187}Re relative to changes in the areal extent of hypoxic deposition in the Baltic Sea

In this section, the changes in δ^{187}Re at site BY15 are compared to the regional changes in redox conditions, as recorded by the areal extent of hypoxic deposition in the Baltic Sea (Figure 4.8), to assess whether regional redox changes influence the δ^{187}Re recorded in sediment.

The contraction in hypoxic area in the Baltic Sea between 1970 and 1993 is associated with negligible change in δ^{187}Re and could indicate that decreasing hypoxic area has little or no effect on the δ^{187}Re recorded in the sediments of the Gotland Deep (Figure 4.8). In contrast, the marked expansion in hypoxic area between 1993 and 2009 corresponds with the most significant changes in δ^{187}Re (a decrease of ~ 0.5 ‰) in the studied section. During this period, the lowest δ^{187}Re values are associated with the most extensive hypoxic area, which suggests that the increase in hypoxic area in the Baltic Sea may have caused an excursion to negative δ^{187}Re values. However, the second shift in δ^{187}Re at 2.25 cm to 0.5 cm (after 2003) is not associated with a large change in the areal extent of hypoxia (Figure 4.8), indicating that changes in δ^{187}Re are not exclusively associated with changing hypoxic area. The correlation between the hypoxic area extent and δ^{187}Re from 1993 to 2000, but not before this period, suggests that there may have been a change in the behaviour of δ^{187}Re around 1993, or that the areal extent of hypoxic deposition in the Baltic Sea is not the most significant driver of changes in δ^{187}Re in the sediment.

It may be possible to explain the differing behaviour of δ^{187}Re before and after 1993 by considering the effects of the budget of Re in the Baltic Sea bottom waters. After 1993, there was likely a depleted budget of Re in the Baltic Sea bottom waters (see section 4.4.3 above) caused by enhanced drawdown of Re into the sediment at the onset of euxinic conditions since ~1980 (Figure 4.7). Following this sustained period of depletion to the Re budget in Baltic seawater, it is possible that small changes in isotopic composition had a proportionally larger effect on the δ^{187}Re recorded in the sediment. This could explain why the expanded hypoxic area after 1993 has

a larger effect on δ^{187}Re than the similar magnitude contraction of hypoxic area prior to 1993 (Figure 4.8).

The change in areal extent of hypoxia associated with the 2003 MBI is small in magnitude (< 10,000 km^2) and not clearly resolved due to the large spread of data during this time period (Figure 4.2; Conley *et al.* 2009). However, this relatively small change corresponds with the second negative shift in δ^{187}Re recorded in the sediment at site BY15. This further suggests that either hypoxic bottom water area in the Baltic Sea does not drive δ^{187}Re changes; or that there is an increased sensitivity in δ^{187}Re after 1993 when the Re budget is sufficiently depleted.

4.4.5 The impact of anthropogenic Re on the Re isotope composition of the sediment

Anthropogenic Re sources include mining, processing and use of coal, petroleum, metal ores, the disposal of industrial waste, and high temperature catalysis (Chappaz *et al.* 2008, Chen *et al.* 2009, Colodner *et al.* 1995, Miller *et al.* 2011, Rahaman *et al.* 2012). Anthropogenic Re is estimated to account for at least 30 % of riverine Re concentration globally (Miller *et al.* 2011), and up to 70 % in some rivers in the Indian sub-continent (Rahaman *et al.* 2012). The amount of anthropogenic Re input to the Baltic Sea is likely to have increased over the last century due to increased population density, industrialisation, and increased use of catalytic converters. Since 1980 when reducing conditions became more pervasive in the Baltic Sea, the Re budget in seawater is likely to have been depleted due to enhanced drawdown of Re to anoxic sediments (as is indicated by the elevated Re concentration in sediment at a number of locations, Figure 4.4). Therefore, anthropogenic Re may have become a more significant proportion of the Re budget in the Baltic Sea. It is not yet known what the Re isotope composition of anthropogenic Re is, and so it is difficult to estimate the impact it may have on δ^{187}Re recorded in Baltic Sea sediments. Future work to assess the anthropogenic δ^{187}Re signal may include determining δ^{187}Re for a range of known sources of anthropogenic Re, such as catalytic converters. There has been some work on the Os isotopic composition of catalytic converters (Poirier and Gariepy 2005), and

there is a NIST standard made from recycled catalytic converters (Poirier and Gariepy 2005), however there is no Re concentration or δ^{187}Re data available for this standard.

4.4.6 Changes in river runoff into the Baltic Sea since 1960

There has been no significant long-term change in the total river runoff to the Baltic Sea for 500 years, but decadal and regional variability is large (Hansson *et al.* 2011). River runoff into the Baltic Sea is predicted to increase by up to 15 % (predictions range between a decrease of 2 % and an increase of 15 %) in the future due to climate change (Graham 2004). Rainfall and hence river runoff was relatively high during the 1983-1993 stagnation period which supressed the frequency of MBIs (Schinke and Matthäus 1998). The integrated deviations of the runoff to the Baltic Sea indicate that from 1980 to 2010 river runoff increased at a consistent rate by 400 km^3 (Johansson 2017). This indicates that a sudden change in input to the surface of the Baltic Sea could not have caused the major change in the δ^{187}Re values observed in 1993. However, increased anthropogenic Re input to rivers (Colodner *et al.* 1995, Miller *et al.* 2011, Rahaman *et al.* 2012), with a potentially different Re isotope signature, might have altered the Re concentration and δ^{187}Re recorded in the sediment in the Baltic Sea, and the gradual increase in runoff since 1980 (Johansson 2017) could accelerate this process.

4.4.7 Potential impacts of diagenesis on δ^{187}Re

Early diagenesis is likely to have an impact on sediments at the depth analysed in this study (< 16.5 cm depth). Sediment-porewater interaction is likely to occur within the top 4 cm of sediment, which is the depth at which the largest magnitude of δ^{187}Re changes are observed (Figure 4.5). Rhenium is expected to be incorporated into anoxic sediments below the sediment-water interface (Colodner *et al.* 1993), and the depth at which this occurs is likely to change under different redox conditions. Redox or chemical processes involved in the diagenesis may influence the δ^{187}Re recorded in sediment, however the nature and magnitude of this effect remains

unquantified. It is possible that a diagenetic imprint is superimposed on the recorded δ^{187}Re data for sediments from the Baltic Sea. It might be that the changes in δ^{187}Re observed since 1980 show a combination of the shift to a euxinic environment as well as sediment-pore water interaction, and diagenetic effects which increase in effect with depth. Oxic re-mobilisation of Re due to the increased bottom water oxygen concentration during the 1993 and 2003 MBIs may have had an effect on the δ^{187}Re recorded in the sediment; however, the Mo concentration data from the same core (Figure 4.5) indicate that the H_2S in the pore waters buffers the redox conditions in the sediment to some extent (Jilbert and Slomp 2013b). Further work is needed to quantify the effects of diagenesis on the δ^{187}Re of sediment, including the study of δ^{187}Re for both sediment and pore-water samples (similar to the Re concentration work of Colodner *et al.* (1993)), and this is further discussed in Chapter 7.

4.4.8 Summary of potential causes of variation in δ^{187}Re observed at site BY15

The δ^{187}Re data presented in this chapter were used to test two hypotheses to explain the behaviour of δ^{187}Re recorded in Baltic Sea sediment at site BY15: (1) that δ^{187}Re is affected by changing bottom water O_2 concentration; or (2) that δ^{187}Re is affected by the changing areal extent of hypoxia. However, the observed data do not support either of these hypotheses. If changes in δ^{187}Re reflected changing bottom water O_2 concentration, we would expect δ^{187}Re data to track sediment redox conditions recorded in redox-sensitive metal concentrations, or the directly recorded bottom water O_2 data, neither of which correspond directly with changes in our δ^{187}Re data (sections 4.4.1 and 4.4.2). If changes in δ^{187}Re reflected the changing areal extent of hypoxia, we would expect broad-scale changes in δ^{187}Re of similar magnitudes and opposing trends before and after 1993, corresponding to the changes in areal extent of hypoxia observed during this period (section 4.4.3), which again is not reflected in our data. Therefore, neither changing bottom water O_2 conditions nor the changing areal extent of hypoxia have a direct effect

on the $\delta^{187}Re$ recorded in sediment, and it is likely that other factors must be considered to explain the observed changes.

A lag of ~10 years between changes to the bottom water redox conditions and the $\delta^{187}Re$ recorded in the sediment would explain the observed changes if the two negative shifts in $\delta^{187}Re$ track the onset of locally euxinic conditions at site BY15 in 1980, and then the return to euxinic conditions following the 1993 MBI (Figure 4.6). Such a lag is consistent with the findings of Colodner *et al.* (1993), who report that Re is incorporated into the sediment below the sediment water interface, and therefore any changes in local bottom water redox conditions could have a delayed effect on the sediment pore water. Furthermore, a non-linear relationship between oxygen penetration depth and Re concentration in sediment has been observed in a continental margin environment (Morford *et al.* 2012). However, given that the Re concentration (and other redox sensitive metal concentration) data do track the onset of euxinic conditions (Figure 4.5) and therefore do not experience a lag, this hypothesis seems unlikely.

The trends in $\delta^{187}Re$ data presented for sediments from the Gotland Deep could also be explained by the effects of Re budget on the magnitude of changes in $\delta^{187}Re$ which are recorded in the sediment. In this hypothesis, the $\delta^{187}Re$ of sediment is affected by changing bottom water redox conditions, or changing areal extent of hypoxic deposition, only once the Re budget in the water column is sufficiently depleted. In this way, the $\delta^{187}Re$ of sediment becomes more sensitive to redox changes when there is a depleted reservoir of Re in the overlying seawater. The Re budget model would explain why the $\delta^{187}Re$ exhibits a small change (-0.218 ‰) with the onset of euxinic conditions at site BY15 from 1980. This also explains why there is a small $\delta^{187}Re$ change associated with the contraction in areal extent of hypoxia before 1993, and then a large change in $\delta^{187}Re$ associated with a similar magnitude expansion in hypoxic area after 1993 (Figure 4.7, section 4.4.3). A depleted Re budget is likely to occur in a restricted bottom water scenario, such as in the deep basins in the Baltic Sea (Lenz *et al.* 2015a).

Changes in the river runoff (section 4.4.5), anthropogenic Re (section 4.4.4), and diagenetic effects (section 4.4.6) may also affect the δ^{187}Re of sediment, however the direct effect of these factors on δ^{187}Re remains poorly constrained.

If Re is not quantitatively removed to the sediment, then there would be potentially fractionation of Re isotopes in the authigenic incorporation of Re into sediment. If this is the case then δ^{187}Re in sediments is more likely to indicate the severity of the local reducing conditions than seawater δ^{187}Re. Based on the modelling of Miller *et al.* (2015), one would expect that under reducing conditions, δ^{187}Re would be lower than in oxic conditions. However, the exact pathway by which Re is incorporated into the sediment is not known (Miller *et al.* 2015). Even if quantitative drawdown and hence recording of the seawater δ^{187}Re in the reducing sediments of the Baltic Sea occurs, the locally oxic conditions caused by the MBIs, may interrupt the quantitative draw down of Re and hence move the Re isotope composition away from speculated seawater values. This is similar the situation observed in the Mo isotope composition data from the Landsort Deep, where "oxygen flushing" events cause Mo isotope composition lighter than that predicted in a situation of quantitative drawdown of Mo (Noordmann *et al.* 2015).

4.5 Conclusions

- There are large-scale variations in δ^{187}Re in sediment samples from site BY15 in the Gotland Deep of the Baltic Sea between 1960 and 2009 during the modern hypoxic event. The range in δ^{187}Re is 0.826 ‰.
- The changing δ^{187}Re through the BY15 sediment core is characterised by two negative shifts: from 4.25 cm to 2.75 cm depth, δ^{187}Re shifts from - 0.522 ± 0.084 ‰ to - 1.087 ± 0.085 ‰, and from 2.25 cm to 0.5 cm depth, δ^{187}Re shifts from - 0.580 ± 1.25 ‰ to - 1.084 ± 0.125 ‰; these two rapid decreases in δ^{187}Re are interrupted by an increase in δ^{187}Re between 2.75 cm, and 2.25 cm depth from - 1.087 ± 0.085 ‰ to - 0.580 ± 1.25 ‰. The

changes in δ^{187}Re show no clear correlation with changes in redox as indicated by elemental ratio data (section 4.4.2), bottom water O_2 data (section 4.4.3), and areal extent of anoxia (section 4.4.4).

- Anthropogenic Re may have had an impact on the δ^{187}Re recorded in sediments, and the supply of anthropogenic Re to the Baltic Sea is likely to have increased since 1970 due to the widespread use of catalytic converters. The potential effect of anthropogenic Re on the δ^{187}Re of sediment samples from site BY15 in the Gotland Deep requires further study.
- It is possible that the δ^{187}Re recorded in sedimentary samples is altered by diagenesis; however, the magnitude of this potential effect is currently unquantified, and would need further study.
- Variations in δ^{187}Re are larger after 1993 when the Re budget is likely to be significantly depleted due to accumulation of Re in the sediments deposited during the onset of euxinic conditions. Redox changes in the bottom water and changes in the hypoxic area of the Baltic Sea have the capacity to cause larger changes in δ^{187}Re when there is a depleted Re budget in the deep water, because small-scale isotopic changes will have a proportionally larger effect on remaining Re in the seawater.

Chapter 5

Introduction to the Toarcian Oceanic Anoxic Event

Chapter 5 is a literature review of the Toarcian Oceanic Anoxic Event on which there is an extensive and ever growing literature. As this review presents the very wide context which is most relevant to Chapter 6, it has been placed immediately prior to Chapter 6

5.1 Introduction

The Toarcian Oceanic Anoxic Event (T-OAE) was a period of major environmental change that occurred around 183 Ma (Cohen *et al.* 2007, Jenkyns 1988, 2010a, Pálfy and Smith 2000). It involved globally synchronous deposition of organic-rich sediment (Jenkyns 1985) over a geologically short time interval (Boulila *et al.* 2014, Boulila and Hinnov 2017, Kemp *et al.* 2011). This event was associated with major perturbation to the global carbon cycle (Gómez *et al.* 2008, Hermoso *et al.* 2009a, Hesselbo *et al.* 2000, Kemp *et al.* 2011, Schouten *et al.* 2000, Xu *et al.* 2017), elevated global temperatures (Bailey *et al.* 2003, Dera and Donnadieu 2012, Gómez *et al.* 2008), an increase in the areal extent of anoxic deposition in the ocean (Pearce *et al.* 2008), and marine biotic crises (e.g. Caswell and Coe 2013, 2014, Erba 2004, Nikitenko *et al.* 2013, Peti and Thibault 2017). The event coincided with the emplacement of the Karoo-Ferrar Large Igneous Province (LIP) and an increase in seafloor hydrothermal activity due to the break-up of the Pangaea supercontinent (Pálfy and Smith 2000).

The rate of increase in carbon dioxide concentration in the atmosphere during the T-OAE is comparable to the rate of anthropogenic carbon dioxide emissions at the present day (Cohen *et*

al. 2007, Rothman 2017). The study of this event can therefore help us to understand how the Earth's system responded to a period of major climatic change in the geological past, and may be able to inform our predictions of how the system might respond to present-day climate change. The T-OAE has generated much interest because of the extent of environmental change observed across the event. Most study has centred around relatively complete, well-correlated geological sections throughout this time period clustered throughout Northern Europe, and some localities further afield. There is a lack of Toarcian age oceanic crust due to subduction of the denser oceanic crust over the last ~183 Ma, therefore the available sections are largely from the continental crust and were deposited in epicontinental seas, with the exception of some radiolarian cherts from Japan (Hori 1997).

This chapter presents and discusses the key geological, palaeontological and geochemical evidence for environmental change throughout the T-OAE. The discussion covers the following key questions:

- What triggered the event?
- What were the environmental responses to the event?
- How did oceanic anoxia develop?
- What were the biotic responses to the environmental change?
- How long did the environmental and chemical perturbation last?
- How widespread were the environmental changes?

5.2 Geological record of the Toarcian OAE and organic matter deposition

The geological record of the T-OAE is characterised by the deposition of a discrete interval of dark-brown, organic-rich, fine-grained, laminated sediments (often referred to as "black shales"). The identification of the widespread distribution of black shales globally led to the

description of this event as an oceanic anoxic event (Jenkyns 1988). Jenkyns (1988), Schlanger and Jenkyns (1976) hypothesized that this indicated that during the early Toarcian large parts of the global ocean became anoxic.

The stratigraphically complete exposures of Toarcian-age sediments on the Yorkshire coast have been extensively studied (e.g. Caswell and Coe 2013, 2014, Cohen *et al.* 2004, Hesselbo *et al.* 2000, Howarth 1962, 1973, Howarth 1992, Jenkyns 1988, Kemp *et al.* 2011, Pearce *et al.* 2008). Such well-studied sites are particularly useful for the application of a novel palaeoredox proxy which is one of the two case studies in this thesis (Chapter 6) because their key characteristics are already well constrained. Toarcian age strata are exposed close to Whitby at Saltwick Nab (NZ 916111), Hawsker Bottoms (NZ 944082), and Port Mulgrave (NZ 798176). These exposures clearly show a change from fine-grained, grey deposits to very dark brown organic-rich fine-grained laminated deposits in the upper *tenuicostatum*, and the *falciferum* ammonite zones (Howarth 1992). The facies include a series of calcareous concretions, the most distinctive of which are named. The 'Canon balls' concretions occur at the base of the *falciferum* Zone and *exaratum* Subzone and the distinctive 'Top Jet Dogger' cemented layer occurs at the top of the *exaratum* Subzone (see Figure 5.1 for a detailed stratigraphic log, figure after Caswell *et al.* (2009)). The ammonite biostratigraphy (Howarth 1962, 1973, Howarth 1992) can be used to correlate this section with other exposures within the UK and further afield, using comparable ammonite biostratigraphy (Figure 5.2).

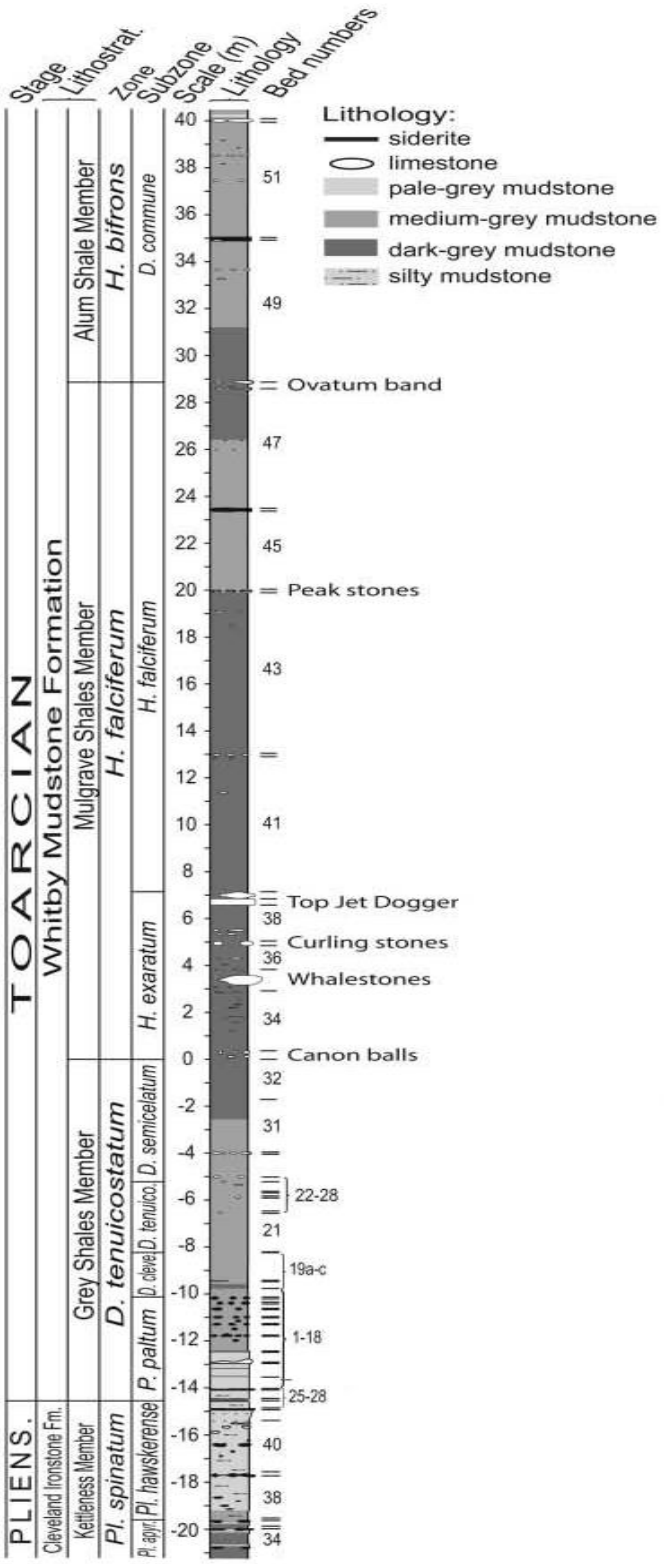

Figure 5.1: Stratigraphical log of the early Toarcian in Yorkshire from Caswell *et al.* (2009). Caswell *et al.* (2009) used: stratigraphy from Kemp *et al.* (2005), Caswell *et al.* (2009) and Hesselbo and Jenkyns (1995); they also used ammonite biostratigraphy from Howarth (1962, 1973) to construct the figure.

<table>
<tr><th colspan="3">Subboreal Province</th><th colspan="3">Submediterranean Province</th><th colspan="3">Mediterranean Province</th></tr>
<tr><th>Chronozone</th><th>Subchronozone</th><th>Biohorizon</th><th>Zonule</th><th>Subchronozone</th><th>Chronozone</th><th>Chronozone</th><th>Subchronozone</th><th>Zonule</th></tr>
<tr><td rowspan="11">Bifrons</td><td rowspan="2">Crassum</td><td>crassum–semipolitum</td><td>Semipolitum</td><td rowspan="4">Bifrons</td><td rowspan="11">Bifrons</td><td rowspan="11">Bifrons</td><td rowspan="4">Bifrons</td><td>Semipolitum</td></tr>
<tr><td>crassum–bifrons</td><td rowspan="2">Bifrons</td><td rowspan="2">Bifrons</td></tr>
<tr><td rowspan="3">Fibulatum</td><td>vortex</td></tr>
<tr><td>braunianus</td><td rowspan="2">Apertum</td><td rowspan="2">Apertum</td></tr>
<tr><td>turriculatum</td></tr>
<tr><td rowspan="3">Commune</td><td>athleticum</td><td>Lusitanicum</td><td rowspan="3">Sublevisoni</td><td rowspan="3">Sublevisoni</td><td>Lusitanicum</td></tr>
<tr><td>commune</td><td>Tethysi</td><td>Tethysi</td></tr>
<tr><td>ovatum</td><td>Sublevisoni</td><td>Sublevisoni</td></tr>
<tr><td rowspan="5">Serpentinum</td><td rowspan="2">Falciferum</td><td>falciferum</td><td>Douvillei</td><td rowspan="2">Falciferum</td><td rowspan="5">Serpentinum</td><td rowspan="5">Levisoni</td><td>Falciferum?</td><td rowspan="4"></td></tr>
<tr><td>pseudoserpentinum</td><td>Pseudoserpentinum</td><td rowspan="4">Levisoni</td></tr>
<tr><td rowspan="3">Exaratum</td><td>elegans</td><td rowspan="2">Strangewaysi</td><td rowspan="3">Elegantulum</td></tr>
<tr><td>exaratum</td></tr>
<tr><td>elegantulum</td><td>Elegantulum</td><td rowspan="2">Striatus</td></tr>
<tr><td rowspan="6">Tenuicostatum</td><td rowspan="2">Semicelatum (I)</td><td>antiquum</td><td rowspan="2">‘Semicelatum’</td><td rowspan="5">‘Semicelatum’ (II)</td><td rowspan="5">Tenuicostatum</td><td rowspan="5">Polymorphum</td><td rowspan="5">‘Semicelatum’ (II)</td></tr>
<tr><td>semicelatum</td></tr>
<tr><td>Tenuicostatum</td><td>tenuicostatum</td><td>Tenuicostatum</td><td rowspan="3">Paltarpites</td></tr>
<tr><td rowspan="2">Clevelandicum</td><td>clevelandicum</td><td rowspan="2">Crosbeyi</td></tr>
<tr><td>crosbeyi</td></tr>
<tr><td>Paltum</td><td>paltum</td><td>Paltum</td><td>Paltum</td><td>Mirabile</td></tr>
</table>

Figure 5.2: Lower Toarcian subdivisions and correlations: Subboreal, Submediterranean and Mediterranean Provinces from Page (2003), and references therein, ammonite biohorizons after (Howarth 1962, 1973, Howarth 1992).

The increased deposition of organic carbon in the Yorkshire section (as identified from the dark- grey to brown colour of the rocks and by subsequent geochemical analyses (e.g. Jenkyns 1988, Kemp *et al*. 2005)) suggests either that greater primary productivity caused greater build-up of organic carbon (Jenkyns *et al*. 2001), and/or that anoxic conditions enhanced preservation of the organic carbon (Jenkyns 2010). High organic carbon content has been observed in the Yorkshire section, with TOC increasing to a maximum of around 15 % in the maximum expression of the OAE (Jenkyns and Clayton 1997, Kemp *et al.* 2011). High TOC has also been recorded in several other sites (*e.g.* up to 10 % in the Paris Basin (Hermoso *et al.* 2012)), though many do not show such high levels as the Yorkshire section (Jenkyns 1988). The disparity between TOC levels in different locations suggests some interplay between the productivity and preservation processes of increased organic carbon deposition, indicating that local controls on both productivity and anoxia may play a role in determining the amount of organic carbon present in the rock record (Jenkyns 2010b).

During the Early Toarcian the Pangaea supercontinent was continuing to break apart, the Panthalassa Ocean lay to the west of the supercontinent, and the Tethys Ocean was partially surrounded by Pangaea (Golonka (2007), Figure 5.3). Lead-lead dating provides places the Early Toarcian at around 183 Ma (Burgess *et al.* 2015, Pálfy and Smith 2000, Sell *et al.* 2014). Coincident with the T-OAE was the main phase of emplacement of the Karoo-Ferrar LIP (Pálfy and Smith 2000). The emplacement of the LIP has been suggested as a cause of major climatic change across the Toarcian, due to the release of volcanogenic CO_2 and the release of thermogenic methane from the intrusion into Gondwanan coals (McElwain *et al.* 2005, Pálfy and Smith 2000, Svensen *et al.* 2007). There is also evidence to indicate that during this period there was an increase in sea-floor hydrothermal activity (Cohen *et al.* 2004), which may have further added to the increased greenhouse gas concentration in the atmosphere, and would have caused changes to ocean chemistry at the time. The causes of the perturbation to the carbon cycle are discussed in more detail in section 5.4.3.

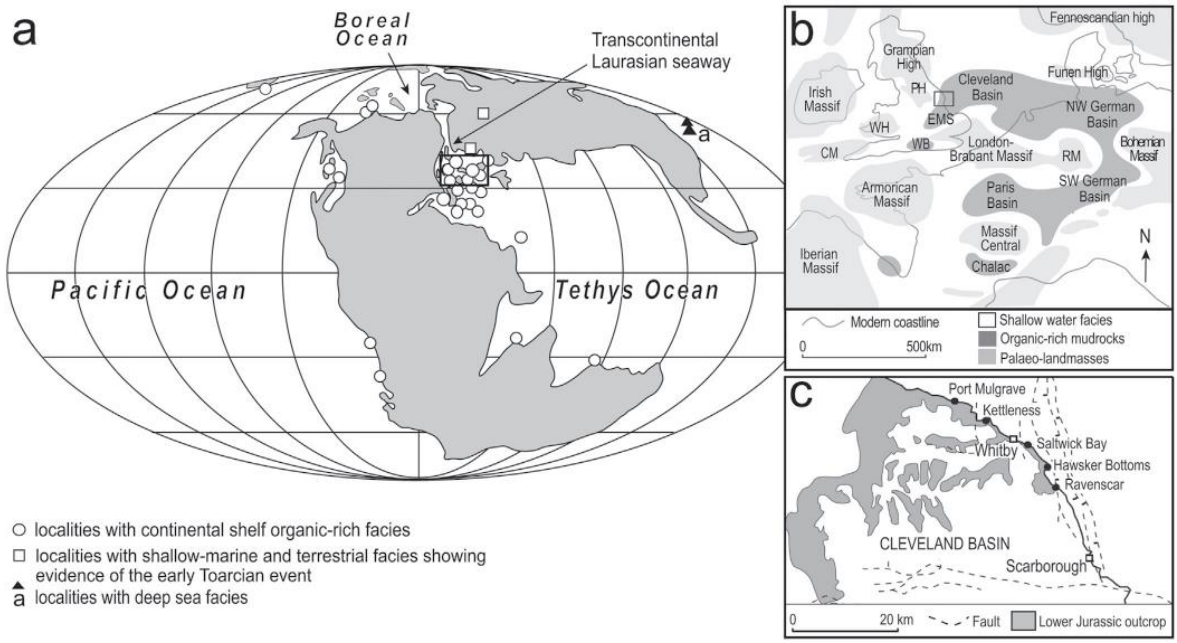

Figure 5.3: Palaeogeographical maps for the early Toarcian from Caswell and Coe (2014). (a) Global palaeogeographical map showing the distribution of the continents, position of the oceans and location of the key sections with different facies. Insert box shows area covered by (b). (b) European palaeogeography showing the widespread distribution of organic-rich facies, and the

present-day coastline. Insert box shows the area covered by (c). Abbreviations: PH – Pennine High, WH – Welsh High, CM – Cornubian Massif, EMS – East Midlands Shelf, WB – Wessex Basin, and RM – Rheinish Massif. (c) Map of the Cleveland basin showing Lower Jurassic outcrops and study sites along the Yorkshire Coast; samples used in this study were collected at Port Mulgrave, Saltwick Bay, and Hawsker Bottoms. Figure caption also from Caswell and Coe (2014).

Several models have been proposed to explain the way in which anoxia developed in the oceans during the T-OAE. The different mechanisms can be summarised as: upwelling of nutrient-rich waters driving high productivity; flooding of epicontinental seaways (Jenkyns 1985) causing a large area of higher productivity; stagnation and stratification of localised oceanic basins (Küspert 1982); or an accelerated hydrological cycle and increased runoff and nutrient supply driving higher primary productivity (this is suggested by the geochemical signal for elevated continental weathering (Cohen *et al.* 2004)).

5.3 Changes to the carbon cycle

The Toarcian OAE is associated with abnormally high levels of TOC, observed in many of the Toarcian sections worldwide (e.g. Al-Suwaidi *et al.* 2010, Jenkyns and Clayton 1997, Kemp *et al.* 2011). A large negative carbon isotope excursion (CIE, initially reported by Küspert (1982)) has also been observed across the event. The negative CIE is recorded in several locations (Figure 5.3 and 5.4) including Yorkshire, UK (Cohen *et al.* 2004, Hesselbo *et al.* 2007, Kemp *et al.* 2005, Kemp *et al.* 2011); the Mochras Borehole, Wales (Jenkyns and Clayton 1997); Poland (Hesselbo and Pieńkowski 2011); Peniche, Portugal (Hesselbo *et al.* 2007); several cores from the Paris basin (e.g. Hermoso *et al.* 2009a); Bornholm, Denmark (Hesselbo *et al.* 2000); Argentina (Al-Suwaidi *et al.* 2010); Haida Gwaii, Canada (Caruthers *et al.* 2011, Caruthers *et al.* 2014); high latitude samples from Northern Siberia (Suan *et al.* 2011); Japan (Gröcke *et al.* 2011, Kemp and Izumi 2014); and lacustrine sediments in the Sichuan Basin, China (Xu *et al.* 2017).The CIE is observed in both the organic carbon, and fossil wood from the same Toarcian age sections: Whitby, UK and Bornholm, Denmark (Hesselbo *et al.* 2000), Peniche, Portugal (Hesselbo *et al.* 2007), Argentina (Al-Suwaidi *et al.* 2010), and Canada (Caruthers *et al.* 2011). The CIE (Figure 5.4) is also observed in the

carbonate record, for example at the Belluno Trough, Italy and Mochras Farm, Wales (Jenkyns *et al.* 2001), and Sancerre, France, and Peniche, Portugal (Hermoso *et al.* 2009b). Furthermore, the negative CIE is observed to a similar magnitude in all molecular carbon groups (Schouten *et al.* 2000), and so is unlikely to be caused by changes in the type of organic matter over time. When studied at a high resolution, the CIE is observed to be stepped in nature (Hermoso *et al.* 2009b, Hesselbo and Pieńkowski 2011, Kemp *et al.* 2005, Kemp *et al.* 2011, Kemp and Izumi 2014).

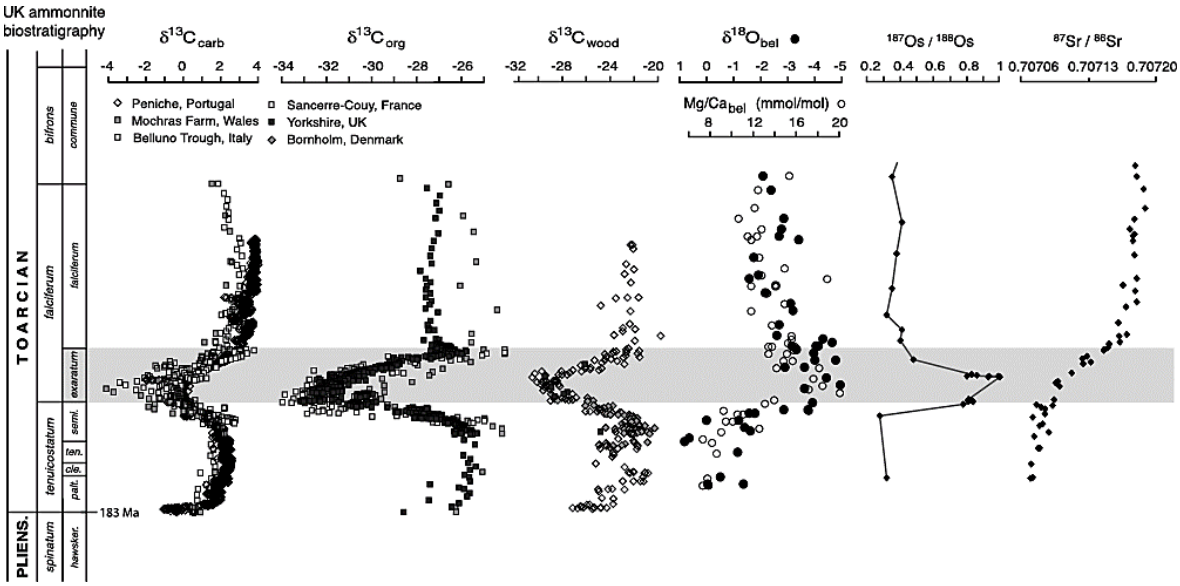

Figure 5.4: Summary of geochemical changes across the early Toarcian OAE from Kemp *et al.* (2011). Kemp *et al.* (2011) used the following sources to construct the figure: stratigraphy of the Yorkshire section from Howarth (1992); Yorkshire $\delta^{13}C_{org}$ data from Kemp *et al.* (2005) and Cohen *et al.* (2004); Belluno Trough and Mochras Farm data from Jenkyns *et al.* (2001); Bornholm and Yorkshire $\delta^{13}C_{fossil\ wood}$ data from Hesselbo *et al.* (2000); Peniche $\delta^{13}C_{fossil\ wood}$ and $\delta^{13}C_{carb}$ data from Hesselbo *et al.* (2007); Sancerre-Couy $\delta^{13}C_{carb}$ data from Hermoso *et al.* (2009); $\delta^{18}O$, Mg/Ca and strontium isotope data measured on belemnites from Yorkshire and published by McArthur *et al.* (2000); Osmium isotope data from Yorkshire and published by Cohen *et al.* (2004). The grey band highlights the *exaratum* subzone which broadly corresponds to the OAE in Yorkshire.

5.3.1 Assessing the global nature of the carbon isotope excursion

A negative excursion is shown in $\delta^{13}C_{org}$, $\delta^{13}C_{carb}$, and in the $\delta^{13}C$ of organic molecule separates and several sites globally (Figure 5.4, section 5.3 above). The CIE therefore affects both the atmospheric and marine carbon reservoirs (Hesselbo *et al.* 2000, Hesselbo *et al.* 2007); and so the perturbation to the carbon cycle is global in nature as the atmosphere is relatively well mixed.

Queries as to the global nature of the CIE have been raised due to discrepancies in the timing of the CIE and therefore the correlation between different European localities (Wignall *et al.* 2005). Whilst there may be differences in timing between the onset of anoxia and the CIE at some localities (Hermoso *et al.* 2009b), and indeed some localities showing evidence of the negative CIE but without conclusive evidence for anoxia (Caruthers *et al.* 2014), it is not unreasonable that local variations in basin parameters and other local conditions could cause slight differences of the expression of the event in the geological record (Thibault *et al.* 2018).

The most likely conclusion is that the T-OAE identified by the large magnitude stepped negative CIE was global in its effect. The global negative CIE requires a global cause such as the rapid destabilisation of methane hydrates (e.g. Hesselbo *et al.* 2000), and discounts suggestions of a local cause for the CIE (e.g. the Küspert model, see section 5.8.4).

5.3.2 Timescales and duration of the T-OAE

The $\delta^{13}C_{org}$, $CaCO_3$ %, and S % record across the T-OAE exposed in Yorkshire, UK exhibit a regular cyclicity (Kemp *et al.* 2011). These proxies contain one dominant cyclicity with a wavelength of 75 cm (revised from the 81 cm estimate of Kemp *et al.* (2005)), which is ascribed to the 36 Kyr obliquity or 21 Kyr precession Milankovitch cycle (Kemp *et al.* 2011). Similarly, Suan *et al.* (2008) assessed the variation in the $CaCO_3$ contents of samples from Peniche, Portugal and the greyscale of laminated sediments from Dotternhausen, Germany. Initially, these data showed three regular cyclicities (Suan *et al.* 2008) within the data interpreted to represent the short-term eccentricity, obliquity and precession cycles (~100 Kyr, ~36 Kyr, and 21 Kyr respectively); however Kemp *et al.* (2011) argue that further analysis of all three datasets reveals only one dominant and statistically significant cyclicity. The most likely astronomical cycle to cause this common dominant wavelength (75 cm in Yorkshire, ~143 cm in Peniche) is either the 36 Kyr obliquity or the 21 Kyr precession cycle (Kemp *et al.* 2011). The cycles observed in the different localities are

likely to have a single cause as the changes in the carbon cycle rapidly affected both the oceanic and atmospheric carbon reservoirs (Hesselbo *et al.* 2000).

The dominant cyclicities calculated across the T-OAE (Boulila and Hinnov 2017) allow us to estimate two key parameters of the event: the time between each shift in the carbon cycle, and the total duration of the event itself. Both of these parameters have implications for our understanding of the causes of the T-OAE, and the rates of geochemical change in the ocean and atmosphere system across the event. Kemp *et al.* (2011) propose that the main $\delta^{13}C_{org}$ excursion lasted 168-324 Kyr (based on either precession or obliquity cycles). Such rapid, relatively large magnitude shifts in the carbon cycle across the T-OAE would require a similarly rapid cause (Boulila and Hinnov 2017, Hesselbo *et al.* 2000), thus supporting the methane hydrate hypothesis (Hesselbo *et al.* 2000, Kemp *et al.* 2011) since this would cause a rapid large magnitude release of isotopically light carbon into the ocean atmosphere system. In this way, the 21 Kyr precession, or 36 Kyr obliquity cycles would cause cyclic breaching of a threshold above which large scale dissociation of methane hydrate would occur (Cohen *et al.* 2007).

5.4 Temperature changes across the T-OAE

Samples from the *tenuicostatum* to lower *falciferum* zones have Mg/Ca, Sr/Ca, and Na/Ca ratios that increase by a factor of between 1.7 to 2.0 (Figure 5.5); this is coincident with a -3 ‰ shift in $\delta^{18}O$ over a period of ~200 Kyr (Bailey *et al.* 2003, McArthur *et al.* 2000). Changes in Mg/Ca and $\delta^{18}O$ in samples from the *tenuicostatum* to lower *falciferum* zones are indicative of a 6-7 ^{o}C increase in global temperatures and a decrease in ocean salinity (Bailey *et al.* 2003), or a 5.7-7.8 ^{o}C increase in temperature using the calculations of Gómez *et al.* (2008). An overall ~6 ^{o}C warming is also inferred from stomatal index data in samples from Bornholm, Denmark (McElwain *et al.* 2005). Increased global temperatures were likely driven by LIP volcanic degassing (e.g. Burgess *et al.* 2015, Cohen and Coe 2007), and methane hydrate destabilisation (e.g. Hesselbo *et*

al. 2000), both of which would increase atmospheric pCO_2. Increased global temperatures caused an accelerated hydrological cycle (Cohen *et al.* 2004), and therefore increase biological productivity in the surface ocean due to increased nutrient supply (Jenkyns 1999).

5.5 Fossil record

Microfossil assemblages before, during and after the T-OAE have been studied by a number of researchers. There is increased biological productivity prior to the event, increased nannofossil speciation, a schizosphaerellid crisis during the onset of the OAE (Erba 2004), and a change in the size distribution of schizophaerella (Peti and Thibault 2017). The increased biological productivity is likely to have been caused by an increased nutrient supply to the surface ocean (Jenkyns 1999).

Macrofossils variations correspond with the major geochemical changes across the T-OAE (Caswell and Coe 2012, 2013, 2014, Caswell *et al.* 2009). There are three *Lagerstätten* locations documented during the T-OAE: the Posidonia Shale (primarily) in Germany, the Strawberry Bank *Lagerstätte* in the UK (Williams *et al.* 2015), and the Ya Ha Tinda biota in Alberta, Canada (Martindale *et al.* 2017). Caswell *et al.* (2009) identified three distinct extinction horizons in the early Toarcian, the first of which corresponds to shifts A and B in $\delta^{13}C_{org}$ identified by Kemp *et al.* (2005). All benthic macro invertebrate species are almost entirely absent for many thousands of years following each of the negative shifts A-C in $\delta^{13}C_{org}$ (Caswell and Coe 2013). Changes in macrofossil abundance are likely to be due to increasingly inhospitable bottom water conditions (Caswell and Coe 2013, 2014, Caswell *et al.* 2009). Four discrete horizons containing fish debris occur consistent with geochemical evidence for oceanic deoxygenation, these are interpreted to represent elevated fish mortality in response to water column deoxygenation (Caswell and Coe 2014). The low abundance of belemnites in the *exaratum* and lower *falciferum* is interpreted to be a result of migration of the belemnites facilitated by increased seawater temperature; ocean

anoxia affecting the food supply; and sea level rise (Caswell and Coe 2014). An increase in the abundance of certain bivalve species indicates that there is a period of relatively increased oxygenation in the upper part of the succession (around 6 m) (Caswell *et al.* 2009). There were changes in abundance, body size, and population dynamics of two bivalve species during the T-OAE (Caswell and Coe 2013). Changes in these features, and their statistical relationship with geochemical data, indicates that changes in primary productivity driven by geochemical changes are closely linked with biotic changes across the T-OAE (Caswell and Coe 2013).

The low abundance of belemnites in the main part of the OAE (Caswell and Coe 2014) may call into question the use of belemnite samples through the T-OAE for geochemical analyses. For instance, a lack of CIE observed in $\delta^{13}C_{org}$ from belemnite samples has been used to question the global nature of the CIE (van de Schootbrugge 2005). However, if it is the case that belemnites simply migrated away from the Cleveland Basin during the peak of the anoxia, then they may not provide a continuous record of the oceanic geochemistry across the T-OAE in that locality (Caswell and Coe 2014).

5.6 Strontium isotope ratio variations across the T-OAE

The strontium (Sr) isotope record of seawater represents a mixture of unradiogenic Sr from the hydrothermal alteration of mid-ocean ridge basalt, and radiogenic Sr from the weathering of ancient continental crust (Cohen and Coe 2007). Across the T-OAE there was a marked increase in $^{87}Sr/^{86}Sr$ ratios (Figure 5.5) recorded in belemnites (Jones and Jenkyns 2001, McArthur *et al.* 2000). The increase in seawater $^{87}Sr/^{86}Sr$ is interpreted to represent an increase in the flux of radiogenic Sr from the chemical weathering of continental crust (Cohen and Coe 2007) because it occurs at the same time interval as a marked excursion in the seawater osmium (Os) isotope composition (Cohen *et al.* 2004, see section 5.7 below), the negative $\delta^{13}C_{(org)}$ excursion (e.g. Kemp *et al.* 2011), and the emplacement of the Karoo-Ferrar LIP (Pálfy and Smith 2000, Sell

et al. 2014). The increase in radiogenic Sr input to seawater indicates an increase in the weathering of the continental crust which would be driven by an accelerated hydrological cycle (Cohen *et al.* 2004). An accelerated hydrological cycle is consistent with evidence for increased average temperatures across the T-OAE (Bailey *et al.* 2003, Them *et al.* 2017) which is likely to be caused by changes in the carbon cycle (Hesselbo *et al.* 2000, Kemp *et al.* 2011). McArthur *et al.* (2000) present an alternative interpretation using the variations in the rate of change of $^{87}Sr/^{86}Sr$, which is to suggest that there is a marked increase in the sedimentation rate across the T-OAE; this is, however, based on the assumption that its ratio would usually change linearly with time which is unlikely to be the case (Cohen *et al.* 2004). Furthermore, Kemp *et al.* (2011) find no evidence for changing sedimentation rate before, during or after the event.

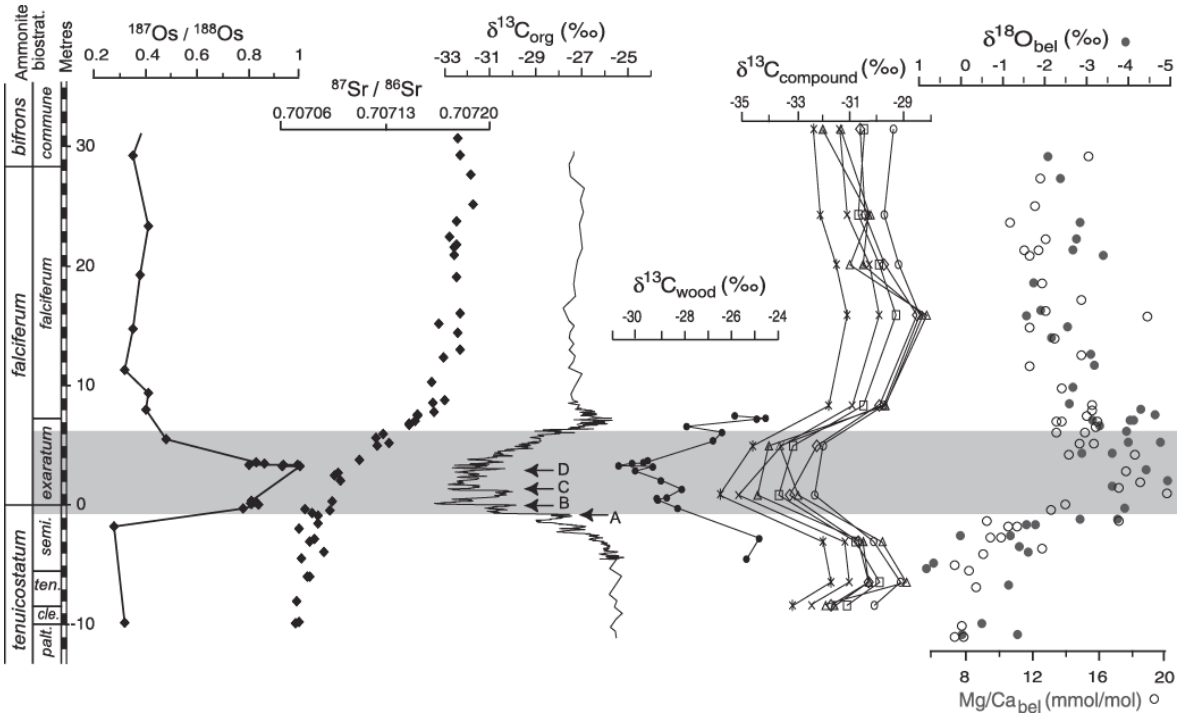

Figure 5.5: Stratigraphic comparison of isotopic and geochemical data from the lower Toarcian section in Yorkshire, UK; figure from Cohen *et al.* (2007). Grey shaded band shows the main part of the T-OAE). Cohen *et al.* (2007) used data from the following sources to compose the figure: $\delta^{13}C$(org) data from Cohen *et al.* (2004) and Kemp *et al.* (2005); Os isotope data from Cohen *et al.* (2004); $^{87}Sr/^{86}Sr$ ratios from McArthur *et al.* (2000); $\delta^{13}C$(wood) data from Hesselbo *et al.* (2007); $\delta^{13}C$(compound) data for a range of organic compounds from Schouten *et al.* (2000); and $\delta^{18}O$ and Mg/Ca data from Bailey *et al.* (2003), McArthur *et al.* (2000).

5.7 Osmium isotope composition changes

There is an excursion of the osmium (Os) isotope ratio ($^{187}Os/^{188}Os$) in contemporaneous seawater from 0.4 to 1.0 concurrent with the -7 ‰ shift in $\delta^{13}C_{org}$ across the T-OAE (Cohen *et al.* 2004), (Figure 5.5). The excursion in Os isotope composition is observed in samples from Yorkshire, UK (Cohen *et al.* 2004), and the Mochras borehole, UK (Percival *et al.* 2016). This excursion is interpreted as resulting from a 400-800 % increase in continental weathering rates as a result of an accelerated hydrological cycle (Cohen *et al.* 2004). The excursion in the $^{187}Os/^{188}Os$ isotope ratio is interpreted (similarly to the increase in the $^{87}Sr/^{86}Sr$ ratio) to represent a change to more radiogenic influence, indicating that it is likely to be caused by an increase in the weathering of ancient continental crust (Cohen and Coe 2007). Recent data showing an excursion in the Os isotope composition of samples from East Tributary of Bighorn Creek in Alberta, Canada are interpreted to show that weathering rates increased by 215 to 530 % (Them *et al.* 2017).

Samples from the *exaratum* and *falciferum* subzones yield Re-Os isochron ages of 181 ± 13 Ma (Cohen *et al.* 1999) and 178 ± 5 Ma (Cohen *et al.* 2004), respectively. These ages are within error of the U-Pb dating of the Karoo-Ferrar LIP: Karoo-Group basalts 183.7 ± 1.9 Ma (Pálfy and Smith 2000); Karoo LIP 183.014 ± 0.13 Ma and lasting for ~2 Ma (Sell *et al.* 2014); Ferrar LIP, magmatism began by 182 ± 0.033 Ma and lasted 349 ± 49 kyr (Burgess *et al.* 2015). Therefore, the geochemical changes of the T-OAE may have been triggered by the Karoo-Ferrar magmatism (e.g. Burgess *et al.* 2015, Sell *et al.* 2014). Weathering of juvenile basalt from the Karoo-Ferrar LIP would increase the input of unradiogenic $^{187}Os/^{188}Os$ into seawater, and so the increase in continental weathering of ancient crust must have been of much greater magnitude to cause the excursion to more radiogenic $^{187}Os/^{188}Os$ values (Cohen and Coe 2007).

5.8 Ocean redox changes during the T-OAE

5.8.1 Organic geochemistry

Specific organic molecules in the geological record act as biomarkers for green, sulphur-reducing bacteria (e.g. Pancost *et al.* 2004, Schwark and Frimmel 2004, van Breugel *et al.* 2006). These bacteria flourished in environments with available sunlight and euxinic conditions, and so their presence indicates photic zone euxinic conditions (PZE). Isorenieratene is the only uniquely defining molecule of green sulphur reducing bacteria; however its derivatives and certain other molecular compounds can also be used as proxies for the presence of these bacteria in the water column (e.g. Brocks and Banfield 2009). Evidence of PZE is also found in samples from Hawsker Bottoms, Yorkshire, UK due to the presence of a biomarker for purple sulphur bacteria (French *et al.* 2014).

There is organic geochemical evidence for PZE during the T-OAE in several locations in the Northern European epicontinental seaway (e.g. French *et al.* 2014, Pancost *et al.* 2004, Schwark and Frimmel 2004, van Breugel *et al.* 2006). Isorenieratene, albeit in relatively low concentrations, has been found in samples from borehole HTM102 in the North East of the Paris Basin (van Breugel *et al.* 2006). Derivatives of both isorenieratene and chlorobactene are present in Toarcian age rocks in the Posidonia Shale, SW-Germany (Schwark and Frimmel 2004). The presence of PZE, as evidenced by the presence of derivatives of isorenieratine in T-OAE samples from the Marche-Umbria region of Italy, reflects either a stratified water column or an intense OMZ which is developed due to enhanced productivity (Pancost *et al.* 2004). These results show that the region of Toarcian PZE extended to large areas of the continental shelf (e.g. Jenkyns 2010b).

A lack of organic geochemical evidence for increased organic productivity contradicts the expanded OMZ model for the development of anoxia in the ocean basin (Farrimond *et al.* 1988, Farrimond *et al.* 1989). Farrimond *et al.* (1988) found no organic geochemical evidence for high

surface productivity, however they do find evidence for oxygen deficient deposition. This evidence contradicts models of anoxia driven by enhanced surface productivity due to increased temperatures (Bailey *et al.* 2003), and increased nutrient supply to the surface ocean (Cohen *et al.* 2004).

In conclusion, there is evidence for PZE in several parts of the NW Europe epicontinental seaway during the T-OAE (e.g. Pancost *et al.* 2004, Schwark and Frimmel 2004, van Breugel *et al.* 2006), suggesting that euxinic conditions developed in this area. There is organic geochemical evidence for two different models of anoxia development during the T-OAE: an expanded OMZ driven by high surface productivity (e.g. van Breugel *et al.* 2006), and intense stratification of a partially restricted basin (Farrimond *et al.* 1989, Farrimond *et al.* 1994, Farrimond and Telnæs 1996). This evidence can better be evaluated when also considering other geochemical evidence for the onset of anoxia across the event as will be discussed in more detail below.

5.8.2 Elemental concentrations

The changes in abundance and relative ratio of redox sensitive metals can be used as proxies for redox changes across the T-OAE (e.g. Jenkyns 2010b). Elemental abundances and their ratios provide evidence for anoxia during the T-OAE in samples from Southern Italy (Lu *et al.* 2010), the Paris Basin (Hermoso *et al.* 2009b), and the Posidonia Shale (Berner *et al.* 2013, Brumsack 1991), and Yorkshire, UK (Harding 2004, Pearce 2007, Pearce *et al.* 2008).

There is evidence from elemental concentration and elemental ratio data for the development of locally anoxic conditions at several sites across the Northern European epicontinental seaway (in Italy, Portugal, UK and Germany) during the T-OAE (Berner *et al.* 2013, Hermoso *et al.* 2009b, Lu *et al.* 2010, Pearce *et al.* 2008). A large drop in the I/Ca ratio in carbonate samples from Southern Italy (Monte Sorgenza) during the T-OAE indicates strong oxygen depletion during the T-OAE (Lu *et al.* 2010). Manganese concentration in rock samples

from the Sancerre borehole, France suggests that the Paris Basin experienced progressive oxygen depletion in the water column and interstitial sediment during the T-OAE (Hermoso *et al.* 2009b). A comparison of Mg/Fe ratio changes, and Mn concentration in samples from the Sancere borehole, and the Peniche section lead Hermoso *et al.* (2009b) to suggest that there were differing redox histories at the two sites, and that local rather than global controls had the most influence on the development of water column anoxia.

The composition (total degree of pyritization, concentration of reactive iron, and total amount of sulphur) of pyrite in samples throughout the Posidonia Shale, Germany is interpreted to show the progression to fully euxinic conditions in the *falciferum* Zone, with the onset of anoxic/dysoxic bottom water conditions in the *tenuicostatum* Zone (Berner *et al.* 2013). There are geochemical similarities between the major and trace element profiles of the Posidonia Shale, and Black Sea sapropels (Brumsack 1991). An enrichment of Mn in the Posidonia shale, is interpreted to be caused by an oxic layer above the anoxic water in a relatively restricted basin (Brumsack 1991). Brumsack (1991) proposes that the environment of deposition is an intermittently anoxic, saline epicontinental sea water mass, overlain by a less saline, more oxic water mass.

During the T-OAE, changes in the concentration of Re and Mo, and changes in the Re/Mo ratio (Figure 5.6) indicate the development of locally reducing conditions (Pearce *et al.* 2008). The Re/Mo ratio in particular indicates that locally euxinic conditions continue for most of the *exaratum* and *falciferum* Subzones.

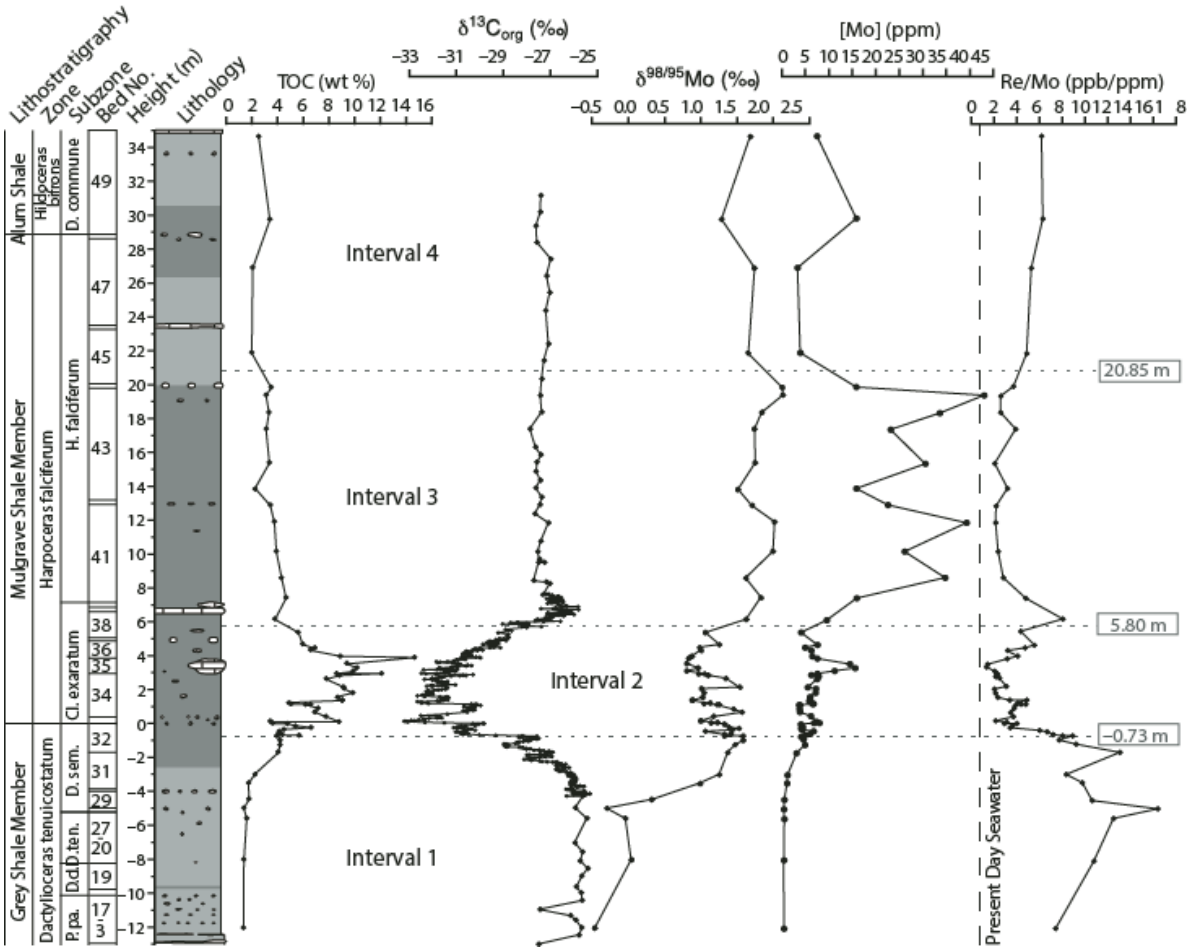

Figure 5.6: $\delta^{98/85}$Mo variations across the T-OAE, shown with Re/Mo ratio, Mo concentration, total organic carbon, and δ^{13}C. Figure, and data from Pearce *et al.* (2008) and references therein.

5. 8. 3 Isotopic evidence for redox changes

5.8.3.1 Molybdenum isotopes

Variations in the $\delta^{98/85}$Mo of samples from Yorkshire, UK (Figures 5.6 and 5.7) have been used to interpret changes in the areal extent of euxinic conditions across the T-OAE (Pearce 2007, Pearce *et al.* 2008). These variations in composition correlate with shifts A to D in the negative CIE (Kemp *et al.* 2011), supporting the idea that the injection of isotopically light carbon into the ocean-atmosphere system was linked to widespread euxinia during the T-OAE. During the OAE *sensu stricto*, $\delta^{98/85}$Mo periodically fluctuated in value, which along with elemental (Mo/Re ratio) data indicating the presence of euxinic conditions throughout the main part of the OAE, indicates

the areal extent of euxinic deposition expanded and contracted periodically four times over a period of ~200 Kyr (Pearce *et al.* 2008).

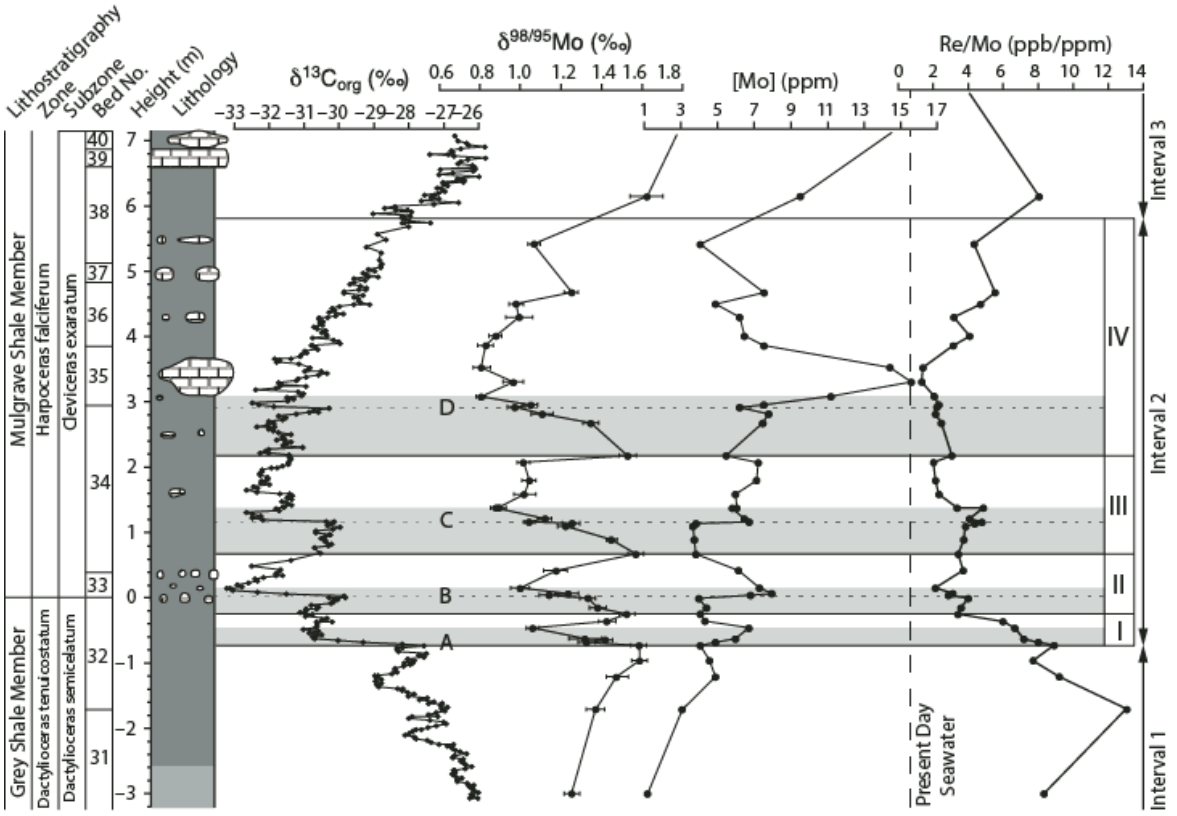

Figure 5.7: An expanded view of $\delta^{98/85}$Mo variations across the T-OAE, shown with Re/Mo ratio, Mo concentration, and δ^{13}C, with shifts A-D highlighted. Figure, and data from Pearce *et al.* (2008) and references therein.

The interpretation of the $\delta^{98/85}$Mo data representing pulsed increases in the areal extent of euxinic conditions across the T-OAE is dependent upon the Mo isotope record representing the geochemistry of the whole ocean basin (Pearce *et al.* 2008). However, McArthur *et al.* (2008) propose that the T-OAE as expressed in Northern Europe is a local event and the product of basin restriction. McArthur *et al.* (2008) note that the ratio of Mo/TOC is 0.5 in the *semicelatum* and *exaratum* Subzones, and 17 in the *falciferum* and *commune* Subzones. They interpret this to indicate that during the main part of the T-OAE, the basin was 10 times more restricted than the present-day Black Sea (Mo/TOC = 4.5) (McArthur *et al.* 2008) and that there was significant drawdown of redox sensitive metals in the *semicelatum* and *exaratum* Subzones. In addition, they

propose that the restricted water mass was made more sensitive to changes in isotopic composition driven by freshwater mixing (McArthur *et al.* 2008). These authors therefore suggest that the palaeoceanographic interpretations of proxies such as the Mo isotope composition are compromised. McArthur *et al.* (2008) suggest that the nature of the isotopic excursions, and their recovery over timescales of a few thousand years are too rapid to reflect whole ocean events. However, the shorter response time of Mo during the T-OAE can be explained by the depleted global inventory (Pearce *et al.* 2008). There is also paleogeographic reconstruction evidence that there was interconnectivity between the epicontinental seas of Northern Europe, and both the Boreal and Tethys oceans (Korte *et al.* 2015), and other geochemical data to suggest that the T-OAE was global in nature (e.g. Kemp *et al.* 2011).

A recent, alternative explanation of the small scale changes in $\delta^{98/85}$Mo observed in the Yorkshire samples is that they are caused by local variations in the Mo cycle caused by changes runoff to the Cleveland basin (Dickson 2017, Dickson *et al.* 2017). These authors compare $\delta^{98/85}$Mo data from four locations across Northern Europe and find that the Cleveland basin samples are the only ones to show the small scale changes in $\delta^{98/85}$Mo which had previously been interpreted to be caused by pulsed expansion and contraction in euxinic deposition by Pearce *et al.* (2008). However the new data are of lower stratigraphical resolution than those of Pearce *et al.* (2008), and rely on an assumption of substantial runoff into the Cleveland basin which is unlikely given the local landmass was of low relief. The Mo isotope composition of seawater at the peak of the T-OAE was probably close to ~1.45 ‰, which suggests that there was a larger extent of global seafloor euxinia compared to the present day (Dickson *et al.* 2017).

5.8.3.2 Nitrogen isotopes

Jenkyns *et al.* (2001) reported a rise in $\delta^{15}N_{tot}$ in epicontinental and pelagic facies across the T-OAE from 3 sites in the UK. These sections show a rise from a background of -2 ‰ to -1 ‰

to maximum $\delta^{15}N_{tot}$ values of +2 ‰ at Hawsker Bottoms, Yorkshire, +1.5 ‰ at the Winterborne Kingston borehole, Dorset, and +2.5 ‰ at the Mochras Borehole, Wales (Jenkyns *et al.* 2001). The high $\delta^{15}N_{tot}$ values correlate with elevated TOC % and negative excursions in $\delta^{13}C_{org}$ and $\delta^{13}C_{carb}$ suggesting that regional upwelling, high organic productivity and an expansion of the OMZ triggered by a climatic optimum was responsible for promoting partial denitrification in the water column (Jenkyns *et al.* 2001). By comparison, Caruthers *et al.* (2014) found no evidence of a positive $\delta^{15}N_{tot}$ excursion in samples from Haida Gwaii (formerly the Queen Charlotte Islands), Canada, and so there is no evidence of ocean anoxia in the North West Panthalassa Ocean (Caruthers *et al.* 2014). However, this result is likely to be influenced by post-depositional alteration of these samples (Robinson *et al.* 2012).

5.8.3.3 Sulphur isotopes

Samples from Yorkshire, UK; Dotternhausen, Germany; and Monte Sorgenza, Italy contain a +5 ‰ to +7 ‰ excursion in the $\delta^{34}S$ composition across the T-OAE. This excursion is associated with increased pyrite burial under euxinic conditions (Gill *et al.* 2011). All three sites show similar S isotope records, and modelling suggests pyrite deposition in the epicontinental seaway was insufficient to cause the observed isotope excursion (Gill *et al.* 2011). This implies that the $\delta^{34}S$ excursion represents a globally significant perturbation in the S cycle, and that increased pyrite burial must have been in action beyond the confines of the epicontinental seaway (Gill *et al.* 2011). Contradicting this hypothesis are the differing S isotope profiles found in samples from Yorkshire and Tibet (Newton *et al.* 2011), which implies that there is a local control on the S isotope composition of samples. However, it is important to note that both Gill *et al.* (2011) and Newton *et al.* (2011) present similar S isotope profiles for samples from Yorkshire, suggesting a good degree of accuracy in the record from this locality.

5.8.3.4 Thallium isotopes

Nielsen *et al.* (2011) present the first use of thallium isotope composition as a palaeoredox proxy for marine sediment samples. They find a large offset between the Tl isotopic composition of early diagenetic pyrite in samples from Peniche, Portugal, and Yorkshire, UK, and attribute the differences to the presence of relatively oxic and euxinic conditions in the two locations, respectively. They take this to imply that significant portions of the shelf remained oxygenated to some degree during the event, and argue against widespread euxinic conditions in the epicontinental sea. Thallium isotope composition is not yet an established palaeoredox proxy, and greater understanding of the behaviour of the behaviour of the Tl isotope system is required to allow for a more detailed interpretation of these data.

5.8.4 Summary

During the T-OAE, there is organic geochemical evidence for photic zone euxinia (Pancost *et al.* 2004, Schwark and Frimmel 2004, van Breugel *et al.* 2006), and elemental and isotopic composition evidence of anoxic/euxinic conditions, largely in the epicontinental seaways of Northern Europe, and parts of the Tethyan continental shelf (Gill *et al.* 2011, Pearce *et al.* 2008) There are some localities without evidence of anoxia, such as the samples from Haida Gwaii, Canada (Caruthers *et al.* 2014), and with evidence for only very weakly developed anoxia, such as Peniche, Portugal (Hermoso *et al.* 2009b), but these are relatively few.

The two main models of the way in which anoxia might have developed in the Toarcian palaeo-ocean are: (i) the expanded OMZ model (Jenkyns *et al.* 2001) based on the idea of enhanced biological productivity in continental shelf areas that drives the expansion of the OMZ; and (ii) a model of intense stratification due to some degree of basin restriction (Küspert 1982). In reality, there is likely to have been some combination of these two mechanisms occurring together driven by the elevated temperatures during the T-OAE. The higher global temperatures

(Bailey *et al.* 2003) will have (1) decreased oxygen levels in seawater because of lower solubility at higher temperatures, (2) caused higher runoff (Cohen *et al.* 2004) and increased productivity (Jenkyns *et al.* 2001), and (3) increased stratification globally (not just locally) because of freshening and a cap of warmer, less dense and less oxic water. There is clear evidence that large areas of the continental shelf, and some globally distributed localised basins, did became anoxic (Al-Suwaidi *et al.* 2010, Pancost *et al.* 2004, Pearce *et al.* 2008). On balance, it seems most likely that during the T-OAE there was an increase in the areal extent of anoxia globally, but that this was in part controlled by local features such as basin geometry, ocean currents, and localised variations in biological productivity.

5.9 Causes of the perturbation to the carbon cycle

The cause of the perturbation to the carbon cycle excursion was a large magnitude flux of isotopically light carbon into the ocean-atmosphere system (e.g. Cohen *et al.* 2007), as evidenced by the large magnitude, globally distributed $\delta^{13}C_{org}$ and $\delta^{13}C_{fossil\ wood}$ excursion, and the newly discovered $\delta^{13}C_{org}$ excursion from an inland lake in the Sichuan Basin, China (Xu *et al.* 2017). Potential sources that have been proposed include methane hydrate release (e.g. Hesselbo *et al.* 2000), volcanic degassing (e.g. Suan *et al.* 2010), and thermogenic methane release due to the intrusion of the Karoo-Ferrar LIP into Gondwanan coals (Svensen *et al.* 2007). The cyclicity observed in the negative CIE suggests that orbital pacing is likely to control or moderate the release of carbon causing the negative CIE (Kemp *et al.* 2011).

The release of methane would account for the negative signature of the excursion, because methane has a negative carbon isotope signal (around - 60 ‰). The most likely candidate for this source of methane is the destabilisation of methane hydrates (e.g. Hesselbo *et al.* 2000, Kemp *et al.* 2011). In this scenario, it is possible that some background warming, perhaps caused by

volcanic degassing, forced the system to a threshold above which orbitally paced warming caused the destabilisation of methane hydrates (Cohen *et al.* 2007).

There is good evidence for volcanism at this time because the Toarcian OAE occurs synchronously with the Karoo-Ferrar LIP (Burgess *et al.* 2015, Pálfy and Smith 2000, Sell *et al.* 2014), and therefore volcanic degassing may be proposed as a cause of the climatic changes in the onset of the OAE and of the negative CIE (Suan *et al.* 2011). The record of the T-OAE from Siberia (Suan *et al.* 2011) suggests that the warming and poorly oxygenated depositional conditions characteristic of the event persisted for around 600 Kyr after the peak of the CIE. Such prolonged warming could only be caused by a longer-term release of carbon into the system such as through volcanic degassing during the LIP volcanism.

A further possible source of isotopically light carbon is thermogenic methane release due to igneous intrusions from the Karoo-Ferrar LIP into organic-rich rocks (Svensen *et al.* 2007) or Gondwana coal deposits (McElwain *et al.* 2005). The observation of breccia pipes in the Gondwanan coals surrounding the Karoo basin suggests that these coals were thermally altered during the emplacement of the LIP (McElwain *et al.* 2005). Svensen *et al.* (2007) estimate that 1800 GT of CO_2 was released from the western Karoo Basin, but that up to ten times that value could have been released from the whole basin. Since the Karroo-Ferrar LIP intruded into large volumes of organic-rich Gondwanan coals, and the LIP occurred synchronously with the Toarcian OAE (Burgess *et al.* 2015, Pálfy and Smith 2000, Sell *et al.* 2014), it seems likely that at least some of the contemporaneous warming would have been caused by the release of thermogenic methane in this manner. Furthermore this thermogenic methane would have had a significantly lighter (- 60 ‰) isotopic signal than the CO_2 degassed from the LIP and so could account at least in part for the large magnitude of the negative CIE. However, this mechanism does not account for the cyclicity observed in the $\delta^{13}C_{org}$ record (Cohen *et al.* 2007).

It seems most likely that the cause of the warming and negative CIE observed at the T-OAE is some combination of methane hydrate release, volcanic degassing, and thermogenic methane release. The methane hydrate hypothesis best accounts for the negative CIE, and the cyclical changes observed in the carbon cycle. However, methane hydrate destabilisation would have required a mechanism for background warming to reach a threshold above which the orbitally forced warming could take effect (Hesselbo *et al.* 2000). The release of CO_2 and methane from the LIP, and from the thermal altering of the organic-rich rocks into which the LIP emplaced, is a suitable mechanism to cause such warming (Cohen *et al.* 2007).

5.10 Conclusion

This chapter presents the main published evidence for geochemical (sections 5.4 to 5.8) and biotic (section 5.3) changes across the T-OAE, with a view to answering the key questions set out in the introduction (section 5.1). A brief summary of the most likely answer to those questions is presented below:

- What triggered the event?
    - The large negative CIE and elevated global temperatures associated with the T-OAE were caused by large magnitude methane hydrate destabilisation (section 5.3), which would have caused a rapid increase in atmospheric pCO_2. Methane hydrate destabilisation was controlled by orbital pacing (Kemp *et al.* 2011) driving temperatures above threshold conditions reached by background warming. Elevated global temperatures overall are also likely to have been driven by the release of CO_2 as well as methane from the Karoo-Ferrar LIP (Pálfy and Smith 2000, Sell *et al.* 2014); the release of thermogenic methane from the intrusion of the LIP into Gondwana coals (Svensen *et al.* 2007).
- What were the environmental responses to the event?

  - The T-OAE is associated with an increase in the areal extent of marine anoxia globally, identified by the widespread deposition of organic rich mudrocks globally (Jenkyns 1988), and evidenced by Mo isotope data (Dickson *et al.* 2017, Pearce *et al.* 2008); increases in characteristic organophile element abundances at various sites (e.g. Pearce *et al.* 2008); and the fossil record of extinctions, major changes in abundance and diversity, and the composition of ecosystems (e.g.Caswell and Coe 2013).
  - Some areas developed anoxia differently to others, *e.g.* differences between the Paris basin and Peniche, Portugal (Hermoso *et al.* 2009b); and samples from Canada, which contain no evidence of denitrification (Caruthers *et al.* 2011).
  - There is organic geochemical evidence for PZE in several locations (e.g. Schwark and Frimmel 2004) suggesting that euxinic conditions extended into the water column at least in parts of the Northern European epicontinental seaway and the Tethys continental shelf.

- What caused anoxia to develop?
  - It is likely that the increased global temperatures (Bailey *et al.* 2003) and accelerated hydrological cycle played a major role in driving enhanced productivity in the surface ocean (Them *et al.* 2017). This would have increased the rate of organic carbon burial, particularly in continental shelf-type environments, and driven an expansion of the OMZ. Increased ocean temperature would have also decreased the solubility of oxygen in the ocean. There is still some debate as to whether the record of anoxia can only be interpreted as occurring in restricted basin type environments, but evidence from globally distributed anoxic sediments (Figure 5.3) suggest a global distribution of anoxic deposition.

- What were the marine biotic responses to the environmental change?
    - Major biotic crises in nanno- and macrofossils, as well as periods of low abundance of ammonites and bivalves, suggest relatively inhospitable bottom-water conditions during the T-OAE (e.g. Caswell and Coe 2014).
- How long did the environmental and chemical perturbation last?
    - The most accurate estimation of the duration of the main part of the OAE can be found using cyclostratigraphic analysis of the carbon isotope record (Boulila and Hinnov 2017). This gives an estimate of the duration of the excursion to the most negative $\delta^{13}C_{org}$ values of between ~168 Kyr and 324 Kyr (Kemp *et al.* 2011).
- Was the T-OAE a truly global event?
    - The CIE appears to be global as it is recorded in globally widespread locations and in samples reflecting both the ocean and atmosphere carbon reservoirs.
    - Evidence for anoxia is available from a wide variety of locations, and the Mo isotope record suggests that there was a significant increase in the global extent of anoxic conditions across the T-OAE. However, it also seems likely that the extent to which anoxia developed in specific areas was locally modulated by basin geometry, and ocean current conditions. This effect would be quite similar to the expected pattern of increased anoxia in the present-day oceans, with restricted basins, continental shelves susceptible to runoff and temperature increase, and upwelling continental margins with already low oxygen levels being the most vulnerable to future changes in marine oxygen concentrations.

Chapter 6

The Toarcian Oceanic Anoxic Event: A rhenium isotope perspective

This chapter of the thesis presents the application of the method (Chapter 3) to the Toarcian Oceanic Anoxic Event. The aim is to evaluate the use of Re isotopes as a palaeo redox indicator on a well-known and extreme de-oxygenation event in Earth history. The study utilises part of the same set samples measured for Mo–isotopes within supervisor's (ALC) research group (Pearce *et al.* 2008).

Note on contributions: The samples were identified and supplied by supervisor ALC together with the stratigraphy. FR measured and processed the samples under the guidance of MF. FR and the supervisors (ALC and MF) interpreted the results. This chapter also benefitted from the early supervision of Anthony Cohen. FR wrote the chapter and prepared the figures and the supervisory team provided guidance, comments and suggested amends.

6.1 Summary

The Toarcian Oceanic Anoxic Event (OAE) is one of eight major deoxygenation events which occurred during the Mesozoic. The extent of anoxic conditions in the ocean during OAEs can be examined using the isotope composition of redox sensitive metals in sedimentary rocks. This study presents the first investigation of the use of Re isotope composition as a proxy for past ocean redox conditions recorded in sedimentary rocks. The rhenium isotope composition, δ^{187}Re, was determined for a suite of marine mudrocks spanning the Toarcian OAE from Yorkshire, UK. The δ^{187}Re results exhibit an excursion of -0.596 ‰ across the Toarcian OAE. The onset of this

excursion consists of two -0.2 ‰ shifts, which broadly correspond to shifts in $\delta^{13}C$. The negative $\delta^{187}Re$ excursion is stratigraphically consistent with redox changes shown by Mo isotope data from the same sections, suggesting that the Re isotope composition is affected by changing redox conditions in the ocean basin. The overall range of $\delta^{187}Re$ in the set of samples is 0.699 ‰, and the average reproducibility of analyses is ± 0.082 ‰ (2 SD).

6.2 Introduction

Ocean deoxygenation is likely to increase as present day global warming progresses (e.g. Gruber 2011, Keeling *et al.* 2010). Ocean deoxygenation alters ocean chemistry and ecosystem balances (Gilly *et al.* 2013). Decreasing oxygen concentration has been recorded in recent years at several open ocean sites (Stramma *et al.* 2010, Whitney *et al.* 2007). Modelling how the Earth system responded to past periods of major environmental change (Beerling and Brentnall 2007) provides information that can help in deciphering and predicting future environmental changes due to anthropogenic carbon dioxide (CO_2) emissions.

Oceanic Anoxic Events (OAEs) represent discrete intervals of major environmental change associated with major changes in ocean chemistry (e.g. Jenkyns 2010b, Thibault *et al.* 2018), and provide an opportunity to study how ocean redox conditions responded to changing atmospheric CO_2 concentrations (e.g. Dickson *et al.* 2017, Kemp and Izumi 2014, Montero-Serrano *et al.* 2015, Pearce *et al.* 2008, Ruebsam *et al.* 2017). The concentration, and relative abundance ratios of various redox sensitive metals provides a proxy for the local redox conditions at the site of deposition (Calvert and Pedersen 1993, Crusius *et al.* 1996, Monien *et al.* 2014, Thibault *et al.* 2018). An insight into the regional and global extent of anoxic can be gained from the isotope ratios of certain trace metals in seawater due to their residence time in the oceans. Recently, the Mo isotope system has been applied as a proxy for the global areal extent of euxinic conditions (Dickson 2017, Dickson *et al.* 2012, Dickson *et al.* 2017, Kendall *et al.* 2017, Pearce *et al.* 2010b,

Pearce *et al.* 2008, Ruebsam *et al.* 2017, Scholz *et al.* 2017). Rhenium is geochemically similar to Mo, but is incorporated into sediment at less reducing conditions than Mo (Crusius *et al.* 1996). Using δ^{187}Re therefore has the potential to reveal new details of the development of reducing conditions during the onset of OAEs, when used in comparison to the Mo isotope system. Based on theoretical calculations, and sample data it is expected that δ^{187}Re could show natural variations of permil scale and possibility of using δ^{187}Re as a past ocean redox proxy has been indicated by Miller *et al.* (2015). Due to the large $\delta^{98/95}$Mo excursion across this event (Dickson 2017, Dickson *et al.* 2017, Pearce *et al.* 2008) and the geochemical similarities of Re with Mo (Crusius *et al.* 1996, Miller *et al.* 2011) δ^{187}Re may also display an excursion across the Toarcian Oceanic Anoxic Event (T-OAE). However, the δ^{187}Re excursion could have a slightly earlier onset due to the greater redox sensitivity of Re compared to Mo.

The T-OAE is a particularly well documented example of past environmental change (e.g. Ait-Itto *et al.* 2018, Cohen *et al.* 2007, Fantasia *et al.* 2018, Han *et al.* 2018, Izumi *et al.* 2018a, Izumi *et al.* 2018b, Jenkyns 1988, Józsa *et al.* 2018, Kemp *et al.* 2005, Kemp *et al.* 2011, Pearce *et al.* 2008, Rosales *et al.* 2018, Ruebsam *et al.* 2018, Thibault *et al.* 2018, Xu *et al.* 2018). The T-OAE occurred 183 Myr ago (Pálfy and Smith 2000), and is characterised by the deposition of fine-grained, organic-rich mudrocks (Jenkyns 1988), and a major carbon isotope excursion (e.g. Ait-Itto *et al.* 2018, Boulila and Hinnov 2017, Caruthers *et al.* 2011, Hermoso *et al.* 2014, Hesselbo *et al.* 2000, Hesselbo and Pieńkowski 2011, Kemp *et al.* 2005, Kemp *et al.* 2011, Metodiev *et al.* 2014, Sandoval *et al.* 2012). Changes in $\delta^{98/95}$Mo across the T-OAE have been interpreted to show the expansion of the areal extent of euxinic deposition globally across the event (Dickson 2017, Dickson *et al.* 2017, Pearce *et al.* 2008). Changes in Mg/Ca and δ^{18}O across this event show increased global temperatures (Bailey *et al.* 2003, Li *et al.* 2012), and changes in the ^{187}Os/^{188}Os ratio indicate an accelerated hydrological cycle (Cohen *et al.* 2004, Percival *et al.* 2016). The T-OAE

is marked by the deposition of organic carbon worldwide (e.g. Jenkyns 1985), and a major crisis in marine biota (Caswell and Coe 2013, 2014, Erba 2004).

The T-OAE $\delta^{13}C$ excursion is global in extent (Figure 6.1) as demonstrated by records from: Argentina (Al-Suwaidi *et al.* 2010), Germany (Schwark and Frimmel 2004), France (Hermoso *et al.* 2009a), Portugal (Hesselbo *et al.* 2007), China (Deng *et al.* 2012), Japan (Izumi *et al.* 2012, Kemp and Izumi 2014), Canada (Caruthers *et al.* 2011) and the United Kingdom (Kemp *et al.* 2011). The sections near Whitby, Yorkshire, UK were chosen to test the new $\delta^{187}Re$ proxy because of the wealth of geochemical data already available from this location. These data include: $\delta^{13}C_{org}$, total organic carbon, sulphur, calcium carbonate (Kemp *et al.* 2005, Kemp *et al.* 2011), and $\delta^{13}C_{fossil\ wood}$ (Hesselbo *et al.* 2000), $\delta^{98/95}Mo$ and Re/Mo ratio (Pearce *et al.* 2008), $^{187}Os/^{188}Os$ (Cohen *et al.* 2004), organic geochemistry (Farrimond *et al.* 1989, French *et al.* 2014), $\delta^{18}O$ and Mg/Ca (Bailey *et al.* 2003). Cyclostratigraphical analysis of regular variations in $\delta^{13}C$, $CaCO_3$ and S concentrations across the event are interpreted to represent the precession or obliquity orbital forcing parameters (Kemp *et al.* 2011). This time series analysis of $\delta^{13}C$ between −4.29 m and +1.30 m gives an estimated duration of the shift from background to minimum $\delta^{13}C$ values of 168 to 324 Kyr (Kemp *et al.* 2011).

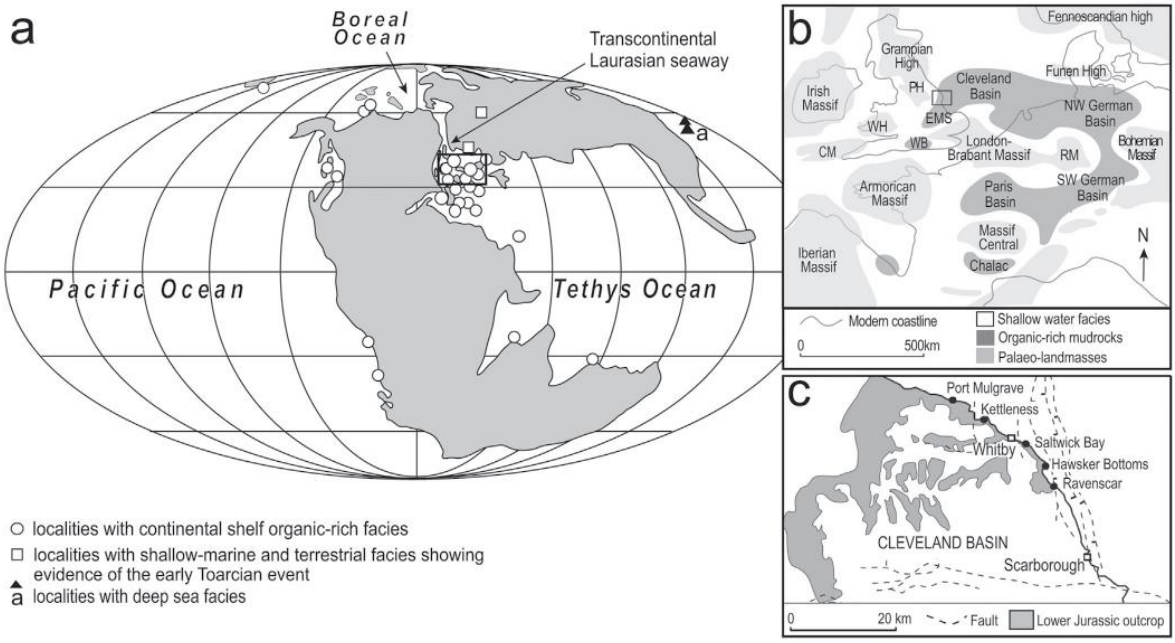

Figure 6.1: Palaeogeographical maps for the early Toarcian from Caswell and Coe (2014). (a) Global palaeogeographical map showing the distribution of the continents, position of the oceans and location of the key sections with different facies. Insert box shows area covered by (b). (b) European palaeogeography showing the widespread distribution of organic-rich facies, and the present-day coastline. Insert box shows the area covered by (c). Abbreviations: PH – Pennine High, WH – Welsh High, CM – Cornubian Massif, EMS – East Midlands Shelf, WB – Wessex Basin, and RM – Rheinish Massif. (c) Map of the Cleveland basin showing Lower Jurassic outcrops and study sites along the Yorkshire Coast, samples used in this study were collected at Port Mulgrave, Saltwick Bay, and Hawsker Bottoms.

The $\delta^{98/95}$Mo variations across the T-OAE allow four distinct intervals to be defined (Figure 6.2, (Pearce *et al.* 2008)). In Interval 1, from -13.0 m to -0.73 m, $\delta^{98/95}$Mo steadily increases from -0.5 ‰ to 1.6 ‰, δ^{13}C decreases from -26 ‰ to -28 ‰, and both Re and Mo concentrations increase (from 3.01 to 35.25 ppb, and from 0.41 to 4.59 ppm, respectively), accompanied by a decrease in the Re/Mo ratio (from ~10 to ~7, but with some variation). In Interval 2, from -0.73 m to 5.80 m, $\delta^{98/95}$Mo fluctuates between 1.6 ‰ and 0.8 ‰, there are low Re and Mo concentrations (averaging 22.74 ppb Re, and 6.38 ppm Mo), and a low Re/Mo ratio (average value 4.01). In Interval 3, from 5.80 m to 20.85 m, $\delta^{98/95}$Mo fluctuates around an average of 1.84 ‰, δ^{13}C values recover to around -27 ‰, the Re/Mo ratio is low (average value 3.35), and the Re and Mo concentration is much higher than in Interval 2 (average 75.21 ppb and 25.82 ppm,

respectively, in Interval 3). In Interval 4, from 20.85 m to 35.00 m, the values of $\delta^{98/95}$Mo and δ^{13}C remain relatively consistent with those in Interval 3, Re and Mo concentrations fall (to average values of 45.57 ppb Re and 7.65 ppm Mo), and the Re/Mo ratio gradually rises to 6. Interval 2 defines the T-OAE *sensu stricto* (Pearce et al. 2008). These intervals will be referred to for comparison when discussing the Re isotope data (section 6.5), and are also labelled in Figures 6.2 and 6.3. The perturbation in $\delta^{98/95}$Mo across the T-OAE is interpreted to indicate an expansion in the areal extent of euxinic deposition equivalent to the entire modern continental shelf becoming euxinic (Pearce *et al.* 2008). The cyclical changes in δ^{13}C (Kemp *et al.* 2005), and the stepped changes in $\delta^{98/95}$Mo (Pearce *et al.* 2008) in Interval 2 are interpreted to be caused by the pulsed input of isotopically light carbon into the ocean-atmosphere system (Pearce *et al.* 2008). Recently the small scale stepped changes in $\delta^{98/95}$Mo across the T-OAE have been interpreted to be caused by local changes in the cycling of Mo in the Cleveland Basin (Dickson 2017, Dickson *et al.* 2017), however the new $\delta^{98/95}$Mo data lack stratigraphical resolution. The most likely source of isotopically light carbon is methane hydrates (Hesselbo *et al.* 2000, Kemp *et al.* 2005); however other sources such as volcanic degassing have also been proposed (e.g. Suan *et al.* 2010). See section 5.4.3 for more discussion of the possible causes of the carbon isotope excursion.

This study presents the first application of changes in the Re isotope composition of sedimentary rocks as a proxy for past ocean redox. As aliquots of the samples analysed for $\delta^{98/95}$Mo (Pearce *et al.* 2008) were used the results can be directly compared with $\delta^{98/95}$Mo.

6.3 Materials and methods

Determination of δ^{187}Re was carried out for a set of 38 organic-rich mudrock samples of Toarcian age from three sites (Saltwick Bay (NZ 916111), Port Mulgrave (NZ 798176) and Hawsker Bottoms (NZ944082)) all close to Whitby, Yorkshire, UK (Figure 6.1). The samples were collected by Angela Coe with direct reference to the graphic log constructed by Angela Coe and David Kemp

and published along with the high-resolution carbon isotope record in Kemp *et al.* (2005). All stratigraphical heights are reported relative to the base of the *exaratum* ammonite Subzone as defined by Howarth (1992). The samples were finely ground and homogenized using an agate planetary ball mill or agate mortar and pestle. Sample aliquots of 0.1 to 1.6 g were selected to aim for 10 ng Re per sample (using Re concentration data presented by Pearce *et al.* (2008)). Where more than 0.5 g of sample was required, samples were processed in separate batches of ~ 0.5 g and combined after the column separation procedure.

All sample processing and δ^{187}Re determinations were carried out at The Open University using the clean lab suite, and Thermo Neptune MC-ICP-MS. Following sample digestion, Re was separated from the samples using a two stage anion exchange chromatographic separation procedure to provide a high purity high (~100 %) yield Re separation. Further details of analytical methods are presented in Chapter 3. Thirty-eight samples, two reference samples, and a single element standard SRM 3143 which had been put through the column processing were analysed between one and fourteen times (Table 6.1).

6.4 Results

6.4.1. Accuracy and reproducibility of Re isotope data

Nine of the 38 investigated Toarcian samples were analysed between 2 and 6 times during the study. The 2 SD reproducibility for these repeats ranges from ± 0.054 ‰ to ± 0.444 ‰. Three analyses of the in-house reference sample 00N118 gave an average δ^{187}Re composition of -0.351 ± 0.053 ‰. The single element standard SRM 3143 was used as bracketing and reference standard for every analysis session. For samples analysed only once, the 2 SD of the bracketing standards (SRM 3143) analysed during the analysis session (at the specific measured concentration) was used as an estimate of the external reproducibility of the sample data.

The accuracy of sample analyses is verified by measurements at the Open University of the geological reference sample SDO-1 and synthetic matrix-test samples as is detailed in Chapter 3. Fourteen measurements of the geological reference sample SDO-1 gave an average δ^{187}Re of -0.153 ± 0.106 ‰ (Table 6.1), which is consistent with data presented by Miller *et al.* (2009) (δ^{187}Re = -0.080 ± 0.130, Table 3.4). Analyses of the SRM 3143 standard displayed a long-term reproducibility (2 SD) of ± 0.082 ‰, similar to that of SDO-1. Twelve analyses of column processed SRM 3143 gave an average δ^{187}Re = -0.022 ± 0.089, the reproducibility of which is similar to the bracketing standard, and the value close to the expected δ^{187}Re = 0 indicating that the column processing does not significantly impact the δ^{187}Re of samples (see Chapter 3 for a more detailed account of the method quality control).

6.4.2. Rhenium isotope data of the Toarcian Oceanic Anoxic Event

The δ^{187}Re of Toarcian age samples shows an overall range of 0.699 ‰ (Table 6.1) and is characterised by a marked negative excursion between - 0.96 m and ~6 m. This excursion is within the stratigraphical interval defined as the T-OAE *sensu stricto* (Figure 6.2; Pearce *et al.* 2008). Between -5.62 m to -0.96 m (Figure 6.2) δ^{187}Re increases from -0.276 ± 0.065 ‰ to -0.057 ± 0.066 ‰; over the same height interval, Re concentration increases from 6.07 ppb to 35.25 ppb, the Re/Mo ratio falls, and δ^{13}C begins to show an overall decrease. Between -0.96 m and 3.31 m, δ^{187}Re decreases from -0.057 ± 0.066 ‰ to a minimum of -0.756 ± 0.085 ‰. This decrease is characterised by two high amplitude fluctuations between -0.96 m and 0.67 m where δ^{187}Re decreases from -0.057 ± 0.066 ‰ to -0.653 ± 0.077 ‰, before the rate of change in δ^{187}Re lowers, and the values fluctuate, but continues to gradually decrease. Between 0.67 m and 3.31 m, the Re isotope composition averages -0.575 ± 0.189 ‰ and fluctuates by up to 0.320 ‰; but some of this fluctuation is based on single values. The overall decrease in δ^{187}Re (-0.96 m to 3.31 m) is coincident with δ^{13}C shifts A to D (Figure 6.3). The δ^{187}Re excursion is also coincident with the previously defined Interval 2, during which $\delta^{98/85}$Mo has high values and shows fluctuations,

Re/Mo is low, and Re and Mo concentrations are higher than in Interval 1 but consistently below the concentrations in Intervals 3 and 4. Within the δ^{187}Re excursion (between -0.96 m and 0.67 m) there are two shifts each with a magnitude of 0.2 ‰ (Figure 6.3). The oldest of these shifts is from -0.057 ± 0.049 ‰ at -0.96 m, to -0.236 ± 0.044 ‰ at -0.63 m; the youngest is from -0.200 ± 0.444 ‰ at -0.16 m, to -0.415 ± 0.052 ‰ at 0.15 m. The δ^{187}Re data show an overall increase between 3.31 m and 6.15 m, and then remains relatively stable between 6.15 m and 29.79 m, with an average composition of -0.343 ± 0.0436 ‰. Over this same interval, δ^{13}C and $\delta^{98/85}$Mo values have recovered following the excursion in the *exaratum* Subzone*;* Re and Mo concentrations are significantly higher in Interval 3 than in Interval 2, but then fluctuate in Interval 4.

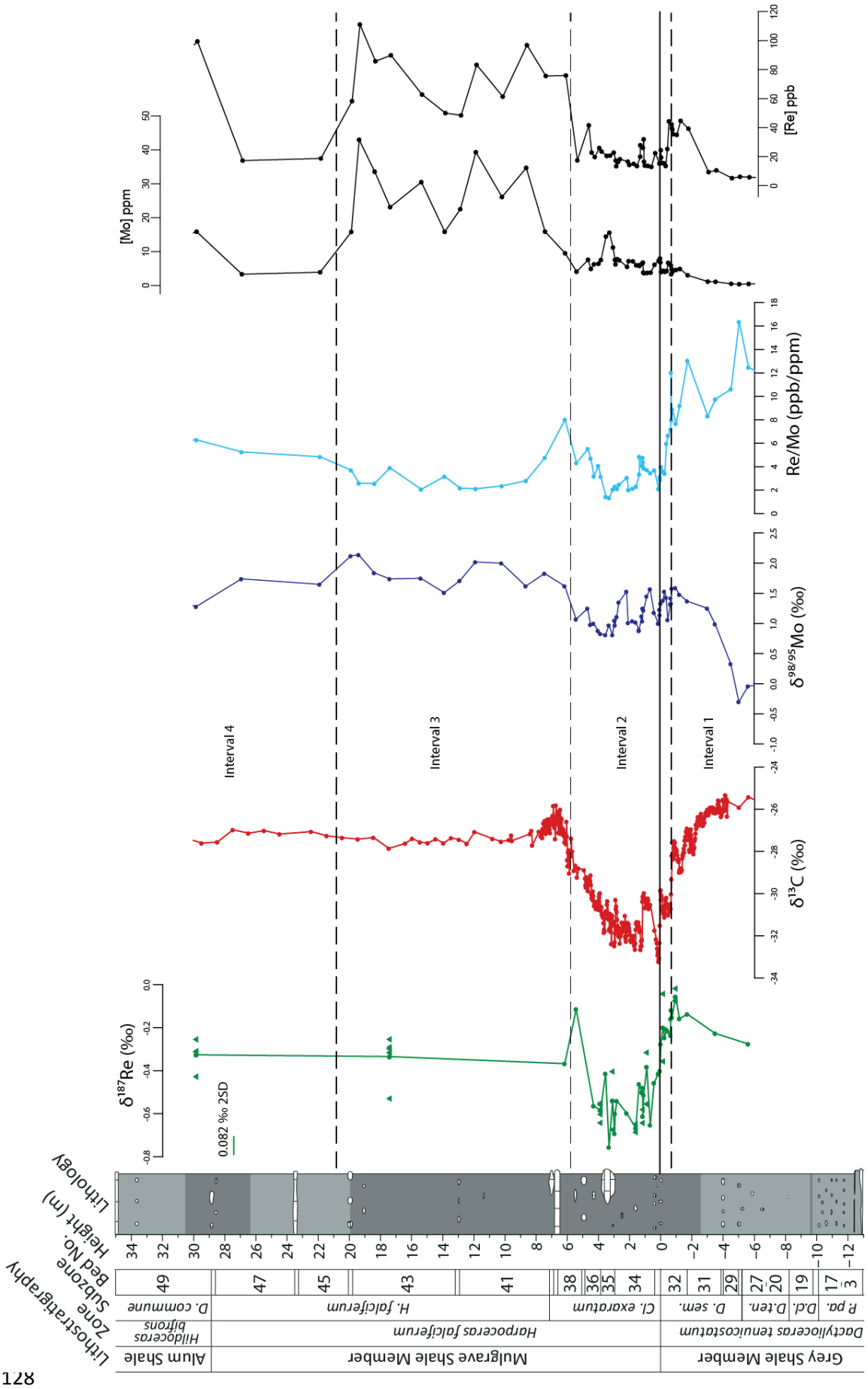
Grey Shale Member
Mulgrave Shale Member
Alum Shale
Dactylioceras tenuicostatum
Harpoceras falciferum
Hildoceras bifrons
P. pa.
D.cl.
D.ten.
D. sem.
Cl. exaratum
H. falciferum
D. commune
Lithostratigraphy
Zone
Subzone
Bed No.
Height (m)
Lithology
Interval 4
Interval 3
Interval 2
Interval 1
δ187Re (‰)
0.082 ‰ 2SD
δ13C (‰)
δ98/95Mo (‰)
Re/Mo (ppb/ppm)
[Mo] ppm
[Re] ppb

Figure 6.2: $\delta^{187}Re$, $\delta^{13}C_{org}$, $\delta^{98/95}Mo$, Re/Mo, [Mo], and [Re] data from the lower Toarcian sedimentary rocks in Yorkshire, UK. Ammonite biostratigraphy, bed numbers from Howarth (1973), $\delta^{13}C_{org}$ data from Cohen *et al.* (2004) and Kemp *et al.* (2005); $\delta^{98/95}Mo$, Re/Mo, [Mo] and [Re] data from Pearce *et al.* (2008). Figure modified from Pearce *et al.* (2008). Divisions based on geochemical characteristics (Intervals 1-4) from Pearce *et al.* (2008). The line at 0.04 m shows the division in interval 2 samples identified in Figure 6.4. The external reproducibility on $\delta^{187}Re$ analyses is 0.082 ‰ based on the long-term reproducibility of single element bracketing standards (SRM 3143) used during analyses. For the $\delta^{187}Re$ data, circles show single analysis data points, or the average of repeat analyses where these were carried out; triangles are used to show the single data points for samples with repeat analyses. Abbreviations: *P.pa – Protogrammoceras paltum; D. – Dactylioceras; cl. – clevelandium; ten. – tenuicostatum; sem. – semicelatum; Cl. – Cleviceras; H- Harpoceras.*

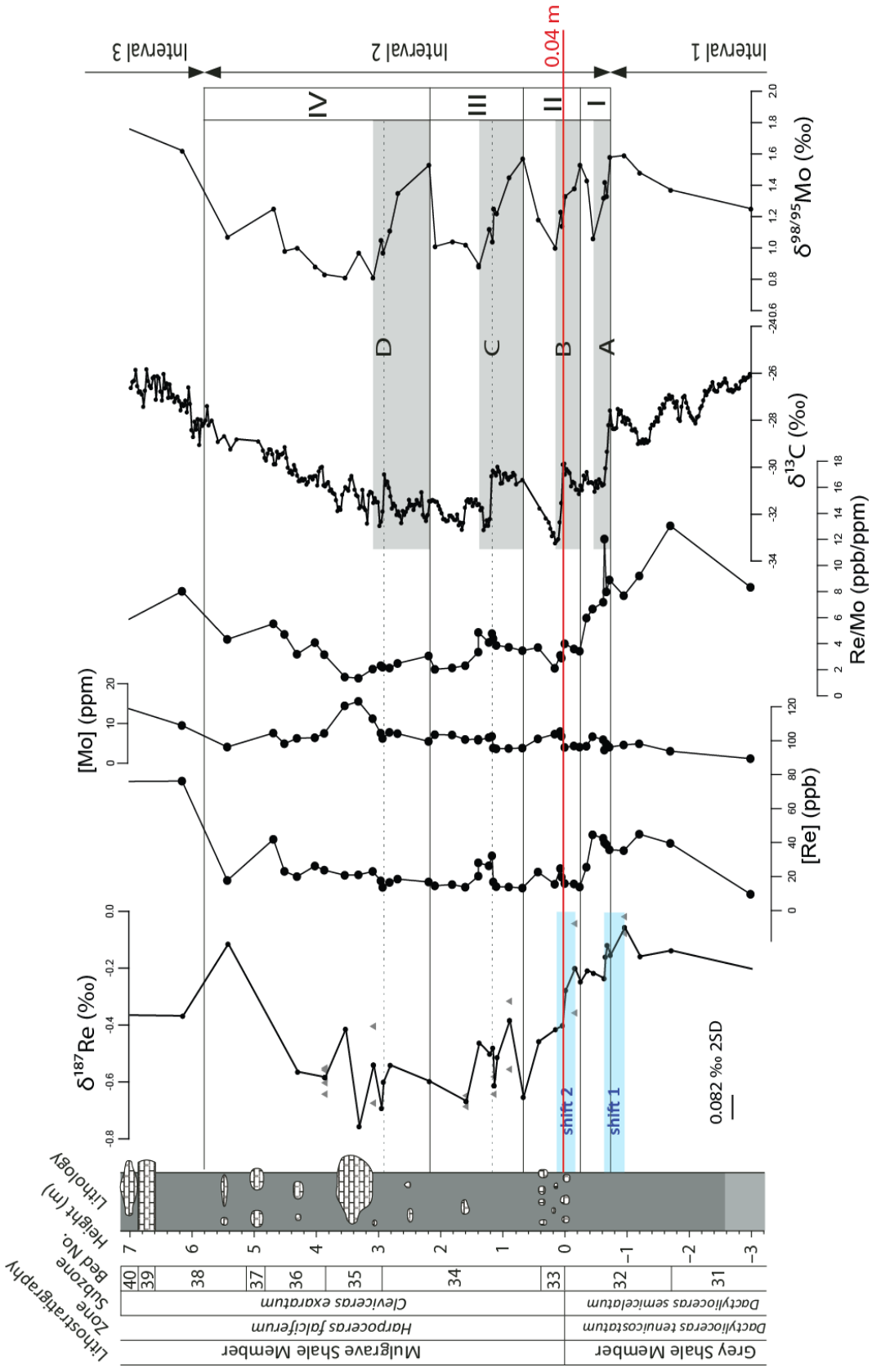

Figure 6.3: A detailed view of geochemical changes in the upper *Dactylioceras semicelatum* and *Cleviceras exaratum* ammonite subzones from Pearce *et al.* (2008) with the Re isotope and [Re]

data added. Ammonite biostratigraphy and bed numbers from Howarth (1973), $\delta^{13}C_{org}$ data and graphic log from Cohen *et al.* (2004) and Kemp *et al.* (2005); $\delta^{98/95}$Mo, Re/Mo, [Mo] and [Re] data and intervals from Pearce *et al.* (2008). Four shifts in $\delta^{13}C_{org}$ labelled A-D (dashed grey lines) are from Cohen and Coe (2007), Kemp *et al.* (2005). Four excursions in $\delta^{98/95}$Mo are labelled I-IV (Pearce *et al.* 2008) and the intervals representing the development of global marine anoxia are shaded in grey. Two abrupt shifts in δ^{187}Re are labelled shift 1 and shift 2 and are highlighted in blue to show the slightly different stratigraphical heights to shifts I and II in $\delta^{98/95}$Mo. The red line at 0.04 m shows the division in interval 2 samples identified in Figure 6.4.

When all samples are considered together, there is a weak positive correlation between δ^{13}C and δ^{187}Re (Figure 6.4; $R^2 = 0.3576$). However, data plotted separately for each interval (as defined by Pearce *et al.* 2008; Figure 2) display separate trends in the data for Interval 1 and Interval 2. Samples in Interval 1 show a negative correlation ($R^2 = 0.541$ or $R^2 = 0.997$ without the single outlier which is highlighted in purple), whereas samples in Interval 2 show a weak positive correlation ($R^2 = 0.357$). Samples in Interval 2 form two distinct groups, those with δ^{187}Re above -0.4 ‰, and those below. Samples in Interval 2 between -0.73 m and -0.01 m (the group with δ^{187}Re above -0.4 ‰) have a very weak positive correlation ($R^2 = 0.407$) between δ^{13}C and δ^{187}Re (Figure 6.4), whereas samples from Interval 2 between 0.04 m and 4.3 m (the group with δ^{187}Re less than -0.4 ‰) show no correlation between δ^{13}C and δ^{187}Re. There is one remaining sample at the top of Interval 2 (5.42 m) which plots closer to the samples in the lower part of Interval 2 due to the lower δ^{187}Re for this sample. Samples in Intervals 3 and 4 plot separately from the other intervals, and the few data points preclude assessment of any possible correlation between variables.

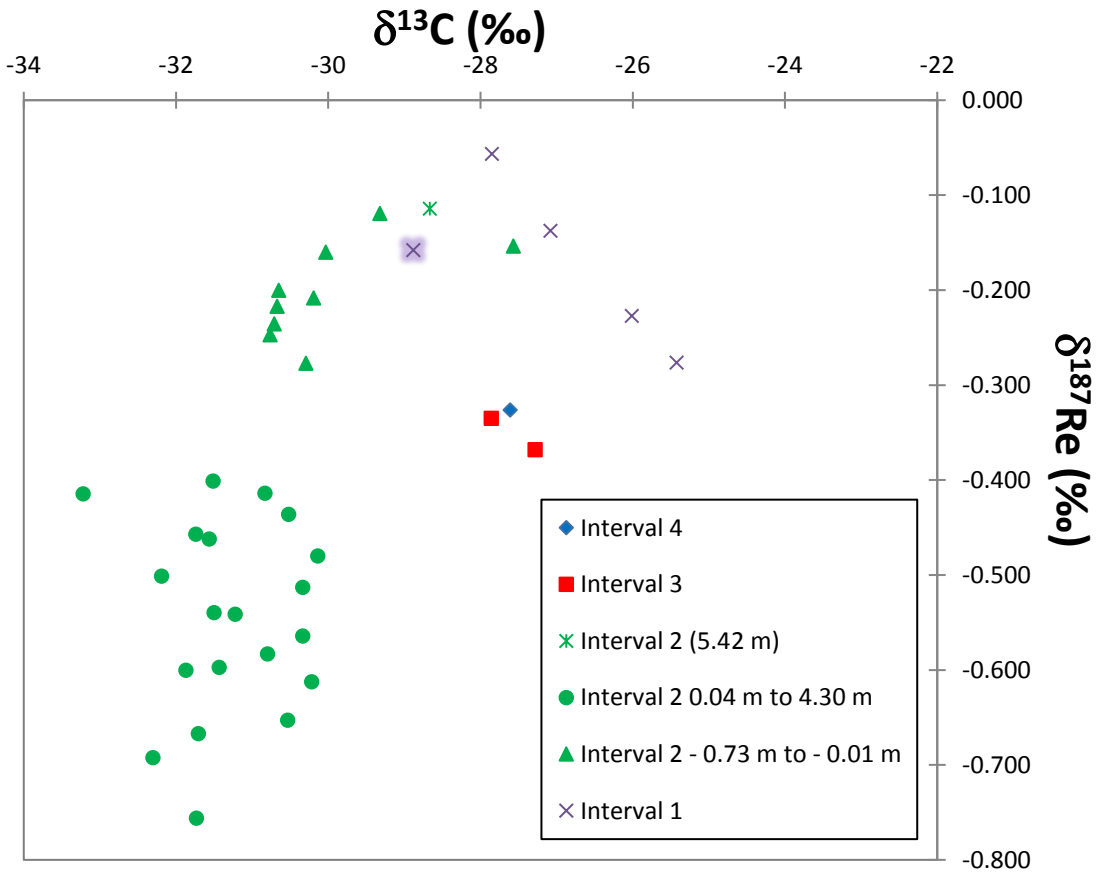

Figure 6.4: The relationship between δ^{187}Re and δ^{13}C, grouped by stratigraphic interval as defined by Pearce *et al.* (2008); $\delta^{13}C_{org}$ data from Cohen *et al.* (2004) and Kemp *et al.* (2005). Samples within Interval 2 were further grouped into three subsets based on their Re isotopic composition, and stratigraphic height. The outlier in Interval 1 is shown with purple shading.

6.5 Discussion

6.5.1 Trends in δ^{187}Re and the behaviour of the Re isotope system

The increase in δ^{187}Re in Interval 1 during the onset of the T-OAE (from -0.276 ± 0.065 ‰ to -0.057 ± 0.066 ‰) corresponds with the onset of locally anoxic conditions, indicated by other redox proxies *e.g* $\delta^{98/95}$Mo, Re/Mo (Figure 6.2, Pearce *et al.* 2008). The lower δ^{187}Re values in Interval 2 during the onset of the negative excursion (Figures 6.2 and 6.3) would therefore imply a recovery in the local redox conditions. However, all other proxies for reducing conditions indicate that the local conditions remained anoxic, including the Re/Mo ratio (Pearce *et al.* 2008), sedimentary facies (Kemp *et al.* 2005), pyrite framboids (Newton 1998) and biota (Caswell and

Coe 2014). An alternative explanation that reconciles these apparently opposing sets of data is that the decrease in δ^{187}Re indicates a reduction in the δ^{187}Re of contemporaneous seawater due to the increased drawdown of Re during widespread anoxic conditions. This is similar to the behaviour of the Mo isotope system, which has been interpreted to exhibit a different behaviour depending on whether the local or global conditions are the dominant control on the isotopic composition (Pearce *et al.* 2008). Increased drawdown of Re from the oceans would have also led to a decrease in the residence time of Re in the ocean basin, which is consistent with the lower Re concentration during the T-OAE *sensu stricto* (Interval 2) when more widespread anoxic conditions would have led to a greater areal extent of Re deposition.

There are opposing trends in the plot of δ^{187}Re against δ^{13}C in Interval 1 compared to interval 2 (Figure 6.4). During Interval 1, the inverse correlation between δ^{187}Re and δ^{13}C suggests that anoxia was increasing as productivity increased. The weak positive correlation between δ^{187}Re and δ^{13}C during Interval 2, particularly the lower part, is interpreted to have occurred because the extra input of light carbon into the ocean atmosphere system led to the widespread occurrence of anoxic conditions and the reduction of δ^{187}Re of seawater.

6.5.2 Detailed changes during the onset of the δ^{187} Re excursion

Each of the 0.2 ‰ steps in δ^{187}Re (Figure 6.3) occur over a similar stratigraphic interval as δ^{13}C shifts A and B. The synchronicity between the δ^{187}Re and δ^{13}C shifts suggests that the pulsed changes in δ^{187}Re are directly related to the input of isotopically light carbon. Shifts C and D in the δ^{13}C record are not clearly resolved in the δ^{187}Re record, though there is clear variation in δ^{187}Re over these stratigraphic intervals (Figure 6.3) and higher resolution analyses may reveal a more coherent pattern. There is also the suggestion of a slight stratigraphical lead between shifts 1 and 2 in δ^{187}Re compared to shifts A and B in δ^{13}C, but this is not resolvable within the stratigraphic resolution and analytical precision of the δ^{187}Re data.

The stepped onset of the δ^{187}Re excursion to lower values in Interval 2 shows similarities to the way in which the $\delta^{98/95}$Mo values fluctuate. In particular, the two steps in δ^{187}Re occur in the same stratigraphic interval as the first two steps in $\delta^{98/95}$Mo. However, the δ^{187}Re values continue to decrease, whereas across the same interval $\delta^{98/95}$Mo values fluctuate between 1.5 ‰ and 1.0 ‰. One possible explanation for the different characteristics of the δ^{187}Re and $\delta^{98/95}$Mo excursions is their differing redox sensitivities, as Re is preferentially incorporated into sediment in less reducing conditions than Mo (Crusius *et al.* 1996). Throughout Interval 2, the Re/Mo ratio, and the Re and Mo concentration data all indicate that euxinic conditions are locally persistent, and continue into Interval 3 (Pearce *et al.* 2008). This is consistent with local palaeoredox proxies (Raiswell *et al.* 1993) and organic geochemistry data (Pancost *et al.* 2004, van Breugel *et al.* 2006) which indicate persistently euxinic conditions during this time. Globally the conditions remained anoxic, therefore not allowing for the intermittent reduction in areal extent of the anoxic conditions and causing δ^{187}Re to continue to decrease. However, the return of the $\delta^{98/95}$Mo values to those immediately before interval 2 indicates that euxinic, rather than anoxic conditions did not persist between the two pulsed changes in the carbon cycle and that there was a brief recovery. Since the Re isotope composition over this same interval continues to progress to lower values, rather than showing short term recovery, a progressive expansion in the areal extent of anoxic deposition is interpreted.

A more recent interpretation of the $\delta^{98/95}$Mo data across the T-OAE indicates that the small scale fluctuations in $\delta^{98/95}$Mo may be caused by changing amounts of open water exchange with the Cleveland basin, particularly since the small scale changes in $\delta^{98/95}$Mo are not observed at other Northern European sites (Dickson *et al*. 2017). Therefore based on the assumed similarity between the two systems, the stepped changes observed in δ^{187}Re may be caused by changes in water exchange between the Cleveland basin and the open ocean. In this case, there is not a clear reason to account for the differing trends in their isotope composition (fluctuating vs. progressing

to lower values). The new interpretation of the $\delta^{98/95}$Mo data across the T-OAE (Dickson *et al.* 2017, Dickson 2017) highlights the potential for factors other than global redox controls to have influence on trace metal isotope proxies for redox, though evidence to support either interpretation is limited by the differing palaeogeography of each site considered. Furthermore, the new $\delta^{98/95}$Mo data lack stratigraphical resolution, and there is no evidence for high runoff into the Cleveland basin since the local land masses were of low relief.

6.5.3 δ^{187}Re variations between 0.67 m and 3.31 m

The fluctuations in δ^{187}Re in the upper part of the δ^{13}C excursion (0.67 m to 3.31 m) do not show any coherent small-scale trends (Figure 6.3), but the fluctuation suggests that the areal extent of anoxic deposition or the severity of the anoxic conditions was not constant. This is consistent with the $\delta^{98/95}$Mo data exhibiting two further shifts (III and IV, Figure 6.3) which either show two further pulsed expansions and contractions in the areal extent of euxinic deposition (Pearce *et al.* 2008) or fluctuations in the rate of open ocean water exchange (Dickson *et al.* 2017). The δ^{187}Re values reach their lowest values over this part of the section. This suggests that widespread anoxic conditions were present for most of the *exaratum* Subzone and at their most extensive over this interval. The minimum δ^{187}Re value reached at 3.31 m is interpreted to indicate the maximum extent of anoxic conditions globally during the T-OAE.

6.5.4 The recovery in δ^{187}Re

The increase in the δ^{187}Re values from about - 0.7 ‰ to about - 0.2 ‰ between 3.31 m and 6.15 m is interpreted to represent a recovery in the Re isotope composition of the palaeo-ocean. This recovery in Re isotope composition occurs over the same stratigraphical interval as the recovery phase of the $\delta^{98/95}$Mo excursion. The relatively stable δ^{187}Re values in the upper part of the section (*falciferum* Subzone and above) shows that the severity of the anoxia has decreased.

6.6 Conclusions

- It is possible to determine the δ^{187}Re of organic-rich sedimentary rocks to high precision. The average reproducibility of analyses in this study is ± 0.082 ‰ (2 SD).
- The δ^{187}Re in Toarcian age sedimentary rock samples is characterised by a marked - 0.596 ‰ excursion. This perturbation in the Re isotope system is consistent with an expansion of the global areal extent of reducing conditions in seawater across the T-OAE. The excursion in the Re isotope composition correlates broadly with the excursion in the carbon cycle and $\delta^{98/95}$ Mo, indicating that the observed changes in ocean redox and the perturbation to the carbon cycle were driven by the same change in Earth processes.
- The onset of the δ^{187}Re excursion is stepped in nature, defined by at least two intervals of more rapid change with a magnitude of - 0.2 ‰. These steps correlate approximately with shifts A and B in the carbon isotope excursion, strengthening the link between the perturbation in the carbon cycle and significant changes in ocean redox across the T-OAE.
- Re responds differently than Mo to the redox changes across the T-OAE. During the excursion, the δ^{187}Re values continue to decrease indicating that the area of anoxic deposition is likely to be expanding, whereas the area of euxinic deposition expands and contracts. Alternatively the small scale changes in δ^{187}Re may be caused by changes in water exchange between the Cleveland basin and the open ocean, as has been proposed for the small scale changes in $\delta^{98/95}$ Mo observed in the Yorkshire section (Dickson *et al.* 2017).
- The minimum δ^{187}Re value is observed at 3.31 m with δ^{187}Re = -0.756 ± 0.085 ‰, this is interpreted to indicate that the maximum extent of anoxic depositional area was near the middle of the *exaratum* Subzone in Yorkshire.

Table 6.1: δ^{187}Re calculated by bracketing for reference samples, processed single element standard SRM 3143, and Toarcian age samples collected from Port Mulgrave, Saltwick Bay, and Hawsker Bottoms, all in Yorkshire.

Standards and reference samples	Exposure[e]	Ammonite subzone	Processing No.	Analysis	Stratigraphic height (m)[c]	Interval[d]	[Re] [a] (ppb)	δ^{187}Re (‰)	2SD [b]
0N118			1	a			10	-0.381	0.130
00N118			1	b			10	-0.337	0.130
00N118			2	a			10	-0.335	0.119
Average 00N118								**-0.351**	**0.053**
Processed SRM 3143			1	a			10	-0.134	0.119
Processed SRM 3143			1	b			10	-0.016	0.074
Processed SRM 3143			2	a			20	0.006	0.044
Processed SRM 3143			2	b			10	-0.026	0.096
Processed SRM 3143			2	c			10	-0.013	0.096
Processed SRM 3143			3	a			15	-0.032	0.052
Processed SRM 3143			3	b			9	-0.032	0.065
Processed SRM 3143			4	a			15	0.015	0.085
Processed SRM 3143			4	b			15	0.009	0.067
Processed SRM 3143			5	a			20	-0.075	0.053
Processed SRM 3143			5	b			15	0.003	0.085
Processed SRM 3143			6	a			20	0.029	0.088
Average Processed SRM 3143								**-0.022**	**0.089**
SD0-1			1	a			20	-0.162	0.052
SD0-1			1	b			10	-0.066	0.074
SD0-1			2	a			20	-0.160	0.044
SD0-1			3	a			15	-0.175	0.085
SD0-1			3	b			15	-0.103	0.085
SD0-1			3	c			15	-0.241	0.067
SD0-1			4	a			20	-0.234	0.053
SD0-1			5	a			20	-0.168	0.053
SD0-1			5	b			15	-0.168	0.078
SD0-1			5	c			15	-0.174	0.085
SD0-1			5	d			10	-0.060	0.077
SD0-1			5	e			10	-0.128	0.077
SD0-1			6	a			15	-0.124	0.081
SD0-1			7	b			20	-0.180	0.088
Average SD0-1								**-0.153**	**0.106**

Toarcian Sample	Exposure[e]	Ammonite subzone	Processing No.	Analysis	Stratigraphic height (m)[c]	Interval[d]	[Re][f] (ppb)	[Re] [a] (ppb)	δ^{187}Re (‰)	2SD [b]
Tco 01-50	S.B.	*commune*	1	a	29.79	4	99.74	10	-0.255	0.119
Tco 01-50	S.B.	*commune*	2	a	29.79	4	99.74	10	-0.310	0.119
Tco 01-50	S.B.	*commune*	3	a	29.79	4	99.74	10	-0.428	0.119
Tco 01-50	S.B.	*commune*	3	b	29.79	4	99.74	10	-0.312	0.119
Average Tco 01-50	S.B.	*commune*							**-0.326**	**0.146**
Tfa 01-25	S.B.	*falciferum*	1	a	17.38	3	90.15	10	-0.317	0.119
Tfa 01-25	S.B.	*falciferum*	2	a	17.38	3	90.15	10	-0.530	0.119
Tfa 01-25	S.B.	*falciferum*	3	a	17.38	3	90.15	10	-0.316	0.119
Tfa 01-25	S.B.	*falciferum*	3	b	17.38	3	90.15	10	-0.291	0.074
Tfa 01-25	S.B.	*falciferum*	4	a	17.38	3	90.15	10	-0.299	0.119
Tfa 01-25	S.B.	*falciferum*	4	b	17.38	3	90.15	10	-0.255	0.074
Average Tfa 01-25	S.B.	*falciferum*							**-0.335**	**0.197**
Tex 00-81	H.B.	*exaratum*	1	a	6.15	3	76.21	15	-0.368	0.080
Tex 97-46	P.M.	*exaratum*	1	a	5.42	2	17.71	15	-0.114	0.085
Tex 00-25	P.M.	*exaratum*	1	a	4.30	2	19.97	15	-0.564	0.085
Tex 06-28	P.M.	*exaratum*	1	a	3.86	2	23.75	9	-0.559	0.023
Tex 06-28	P.M.	*exaratum*	2	a	3.86	2	23.75	10	-0.556	0.119
Tex 06-28	P.M.	*exaratum*	2	b	3.86	2	23.75	10	-0.603	0.074
Tex 06-28	P.M.	*exaratum*	3	a	3.86	2	23.75	10	-0.586	0.119
Tex 06-28	P.M.	*exaratum*	4	a	3.86	2	23.75	10	-0.643	0.119
Tex 06-28	P.M.	*exaratum*	4	b	3.86	2	23.75	10	-0.551	0.119
Average Tex 06-28	P.M.	*exaratum*							**-0.583**	**0.071**
Tex 97-39	P.M.	*exaratum*	1	a	3.53	2	20.76	10	-0.414	0.077
Tex 97-27	P.M.	*exaratum*	1	a	3.31	2	20.99	15	-0.756	0.085
Tex 06-16	P.M.	*exaratum*	1	a	3.08	2	23.02	10	-0.404	0.096
Tex 06-16	P.M.	*exaratum*	2	a	3.08	2	23.02	20	-0.675	0.053
Average Tex 06-16	P.M.	*exaratum*							**-0.539**	**0.382**
Tex 06-08	P.M.	*exaratum*	1	a	2.95	2	17.5	10	-0.692	0.077
Tex 06-06	P.M.	*exaratum*	1	a	2.92	2	13.63	15	-0.600	0.067
Tex 06-01	P.M.	*exaratum*	1	a	2.81	2	16.56	15	-0.541	0.067
Tex 00-73	H.B.	*exaratum*	1	a	2.18	2	16.82	9	-0.597	0.065
Tex 00-72	H.B.	*exaratum*	1	a	1.59	2	13.77	9	-0.648	0.065
Tex 00-72	H.B.	*exaratum*	2	a	1.59	2	13.77	15	-0.686	0.067
Average Tex 00-72	H.B.	*exaratum*							**-0.667**	**0.054**
Tex 97-09	P.M.	*exaratum*	1	a	1.38	2	20.23	15	-0.462	0.080
TC05-A01	P.M.	*exaratum*	1	a	1.21	2	26.33	15	-0.501	0.080
Tex 00-14	P.M.	*exaratum*	1	a	1.16	2	32.2	10	-0.480	0.074
Tex 00-71	H.B.	*exaratum*	1	a	1.14	2	16.8	8	-0.643	0.074

Toarcian Sample	Exposure[e]	Ammonite subzone	Processing No.	Analysis	Stratigraphic height (m)[c]	Interval[d]	[Re][f] (ppb)	[Re] [a] (ppb)	δ^{187}Re (‰)	2SD [b]
Tex 00-71	H.B.	*exaratum*	2	a	1.14	2	16.8	15	-0.581	0.067
Average Tex 00-71	H.B.	*exaratum*							**-0.612**	**0.087**
TC05 - A02	P.M.	*exaratum*	1	a	1.09	2	14.06	15	-0.513	0.067
TC05 - A03	P.M.	*exaratum*	1	a	0.89	2	13.88	15	-0.316	0.052
TC05 - A03	P.M.	*exaratum*	3	a	0.89	2	13.88	20	-0.556	0.053
Average TC05 - A03	P.M.	*exaratum*							**-0.436**	**0.339**
Tex 00-13	P.M.	*exaratum*	1	a	0.67	2	13.21	10	-0.653	0.077
Tex 97-28	P.M.	*exaratum*	1	a	0.42	2	22.66	20	-0.457	0.052
Tex 97-32	P.M.	*exaratum*	1	a	0.15	2	15.47	15	-0.415	0.052
TC05-B02	P.M.	*exaratum*	1	a	0.04	2	19.68	15	-0.401	0.052
TCO5-B03	P.M.	*semicelatum*	1	a	-0.01	2	15.91	15	-0.277	0.081
TC05-B04	P.M.	*semicelatum*	1	a	-0.16	2	15.64	10	-0.043	0.096
TC05-B04	P.M.	*semicelatum*	2	a	-0.16	2	15.64	15	-0.357	0.085
Average TC05-B04	P.M.	*semicelatum*							**-0.200**	**0.444**
Tse 97-36 a	P.M.	*semicelatum*	1	a	-0.25	2	13.87	10	-0.247	0.096
TC05-C01	H.B.	*semicelatum*	1	a	-0.36	2	25.55	10	-0.208	0.096
Tse 00-68	H.B.	*semicelatum*	1	a	-0.46	2	44.59	20	-0.217	0.044
TC05-C02	H.B.	*semicelatum*	1	a	-0.63	2	42.55	20	-0.236	0.044
Tex 00-15	P.M.	*semicelatum*	1	a	-0.65	2	39.97	10	-0.160	0.096
TC05-C03	H.B.	*semicelatum*	1	a	-0.68	2	38.88	10	-0.119	0.096
TC05-C04	H.B.	*semicelatum*	1	a	-0.73	2	35.79	10	-0.154	0.096
Tse 00-67	H.B.	*semicelatum*	1	a	-0.96	1	35.25	15	-0.019	0.080
Tse 00-67	H.B.	*semicelatum*	2	a	-0.96	1	35.25	15	-0.073	0.067
Tse 00-67	H.B.	*semicelatum*	2	b	-0.96	1	35.25	15	-0.078	0.067
Average Tse 00-67	H.B.	*semicelatum*							**-0.057**	**0.066**
Tse 00-66	H.B.	*semicelatum*	1	a	-1.21	1	44.95	20	-0.158	0.044
Tse 00-65	H.B.	*semicelatum*	1	a	-1.71	1	39.54	20	-0.137	0.052
Tse 00-62	H.B.	*semicelatum*	1	a	-3.50	1	10.78	15	-0.227	0.085
Tte 00-58	H.B.	*tenuicostatum*	1	a	-5.62	1	6.07	9	-0.276	0.065

[a] [Re] is the concentration in the analysed sample solution aliquots, and the Ir concentration in all aliquots analysed is 200ppb.

[b] For single analyses, 2SD is the reproducibility of bracketing standards. For the averages of repeat analyses, 2SD is the reproducibility of the individual values.

[c] Stratigraphic heights are given relative to the base of the *exaratum* Subzone, defined as the base of bed 33 (Howarth, 1962, 1992)

[d] Interval indicates the previously defined stratigraphical intervals from Pearce *et al.* (2008)

[e] Exposure S.B = Saltwick Bay (NZ 916111); P.M = Port Mulgrave (NZ 798176); H.B. = Hawsker Bottoms (NZ944082).

[f] [Re] is the concentration of Re in the sample from Pearce *et al.* (2008).

Chapter 7

Conclusions and future work

This chapter presents the main conclusions of the thesis (sections 7.1 and 7.2), and suggestions for future work (section 7.3).

7.1 Conclusions

The overall aim of the thesis was to develop δ^{187}Re as a new proxy for ocean redox conditions, to evaluate the behaviour of the proxy in a modern day setting and to apply the proxy to the study of the T-OAE (section 1.3). The key objectives of the thesis were (section 1.4):

1. To develop a method to determine the Re isotope composition of natural samples at high precision.
2. To determine δ^{187}Re for samples across the T-OAE, to deduce whether any variations in Re isotopes correspond to changing redox conditions, and to assess whether the data show new features in the onset of the redox changes across the T-OAE.
3. To determine whether there are variations in δ^{187}Re corresponding with recent changes in hypoxia in the Baltic Sea, and to understand the behaviour of Re isotopes in a modern-day anoxic environment where the bottom-water O_2 concentration is known.

The following three sections (7.1.1, 7.1.2, 7.1.3) outline the key findings addressing each of these objectives in turn, and section 7.2 draws together the key findings of the thesis.

7.1.1 Determination of δ^{187}Re in geological materials

Chapter 3 described a new method to determine δ^{187}Re of geological materials, and the experiments involved in setting up that method. The key findings from Chapter 3 are as follows:

- The method developed in this research project allows for the extraction of Re from geological materials with high purity and ~100 % yield using a two-stage chromatographic separation procedure (section 3.4.1). This method requires 1.5 – 6.0 ng of Re per δ^{187}Re determination (compared to a minimum of 10 ng required for the previous method developed by Miller *et al.* (2009)), making it possible to precisely determine δ^{187}Re of samples with lower concentrations of Re than previously possible (section 3.4.6).
- "Matrix test" samples (consisting of Re-free sediment sample matrix and addition of SRM 3143 Re with a δ^{187}Re = 0 before the ion-exchange separation procedure) had an average δ^{187}Re of - 0.035 ± 0.112 ‰ and the average of column processed SRM 3143 had δ^{187}Re = - 0.042 ± 0.108 ‰. Therefore, no fractionation was induced by the separation procedure and matrix elements were successfully decreased to low levels allowing for accurate determination of the Re isotope composition of samples (section 3.4.4).
- Determination of δ^{187}Re using Ir for mass bias correction is sensitive to bias by small residual levels of Hf in the Re fraction (section 3.4.2). The method described in Chapter 3 provides a high purity Re separation (sections 3.4.1, 3.4.2) such that the measured δ^{187}Re data are free from bias.
- The overall reproducibility of 306 analyses of SRM 3143 at Re concentrations of 5 - 12 ng ml^{-1} performed during method development was ± 0.084 ‰ (2 SD). Average δ^{187}Re of an in-house single element Re standard (Specpure®) solution over a 11-month period was - 0.202 ± 0.097 ‰ for 21 individual measurements during 9 analytical sessions. The reproducibility of δ^{187}Re determinations is sufficient to resolve small-scale variations in δ^{187}Re of natural samples (section 3.4.5).
- During method development, determination of δ^{187}Re was carried out for an in-house reference material 00N118, reference sample SDO-1, and Toarcian age samples (Tco 01-50, Tfa 01-25, Tex 06-28). The range in δ^{187}Re of these Toarcian samples was 0.257 ‰,

indicating that there are natural variations in δ^{187}Re of Toarcian age mudrocks. Our analyses of SDO-1 are indistinguishable within analytical uncertainty from the results reported by Miller *et al.* (2009), and with the exception of one outlier, the reproducibility of δ^{187}Re determination for natural samples was sufficient to resolve the observed range in δ^{187}Re of Toarcian samples (section 3.4.6).

7.1.2 Behaviour of Re in modern sediments

Chapter 4 presented the determination of δ^{187}Re for a sediment depth profile (16.5 cm to 0.25 cm) from site BY15 in the Gotland Deep of the Baltic Sea. An age model for the samples calculated using ^{210}Pb chronometry, and subsequent tuning using peaks in the high-resolution Mo/Al data for the core (Jilbert and Slomp 2013b), indicates that the samples correspond to a 50-year period from ~1960 to 2009. Variations in δ^{187}Re were observed in anoxic sediments from site BY15, with a maximum range in sample δ^{187}Re of 0.826 ‰. These samples include the lowest δ^{187}Re values of any samples studied in this project (and indeed reported anywhere), at δ^{187}Re = - 1.087 ± 0.084 ‰ (section 4.3.1).

The δ^{187}Re data presented in this chapter were compared to *a)* changing sedimentary redox conditions indicated by elemental data (Jilbert and Slomp 2013b, Lenz *et al.* 2015b), enrichment in TOC % (Lenz *et al.* 2015b), Re concentration data for samples from site BY15 from this study (section 4.4.2), and Re concentration data from other sites in the Baltic Sea (Caroline Slomp, *pers. comm.*); *b)* changing bottom water oxygen concentration data from site BY15 (data assimilated from Baltic Environmental Database by Gustafsson and Medina (2011), and presented by Jilbert and Slomp (2013b), section 4.4.3); and *c)* the changing areal extent of bottom water hypoxia (Conley *et al.* 2009, section 5.4.3). This allowed the following hypotheses to be examined:

1) That δ^{187}Re is affected by bottom water redox conditions at site BY15 (sections 4.4.2, 4.4.3)

2) That δ^{187}Re is affected by the changing areal extent of bottom water hypoxia in the Baltic Sea (section 4.4.4)

The δ^{187}Re data do not fully support either hypothesis, indicating that either δ^{187}Re is not solely controlled by the bottom water redox conditions, or areal extent of hypoxia (section 4.4.8), or that these and/or other factors influence the δ^{187}Re of the sediment samples. Possible alternative factors for the observed changes in δ^{187}Re are:

a) A lag time of 10 years between the changes in local redox conditions and changes in δ^{187}Re recorded in the sediment (section 4.4.8);

b) A change in the sensitivity of the δ^{187}Re recorded in the sediment in 1993, after significant drawdown of Re after the onset of euxinic conditions (from 1980), and the peak in Re concentration recorded in the sediment (section 4.4.8).

c) Influxes of anthropogenic Re may have an effect on the δ^{187}Re recorded in sediment. The amount of anthropogenic Re in river sources globally has increased since pre-industrial times (Miller *et al.* 2011), and is likely to continue to increase (Colodner *et al.* 1995). However, the δ^{187}Re of anthropogenic Re into the Baltic Sea is as yet unquantified and therefore it is not possible to establish whether the increasing contribution of anthropogenic Re has had a significant effect on the δ^{187}Re recorded in sediment at site BY15 (section 4.4.5).

d) Changing river runoff may impact the δ^{187}Re recorded in sediments, particularly if the Re from this source has a different isotopic signature than that already present in the Baltic Sea (either due to weathering of different continental sources or increased anthropogenic Re input). However, there are no sudden major changes in river runoff during the studied time period (Hansson *et al.* 2011), and therefore this factor is unlikely to have a significant effect on the composition of δ^{187}Re (section 4.4.6).

e) Diagenesis may alter the δ^{187}Re recorded in sedimentary samples. However, it is not clear whether, how or to what magnitude diagenetic changes may alter δ^{187}Re observed in samples at site BY15 (section 4.4.7).

Factors (a) to (c) above and to a certain extent (d) are particular to the recent past and the Baltic Sea samples but do not apply to the Toarcian. This is because in the case of (a), a lag of 10 years, the sampling resolution of the Baltic Sea samples is two orders of magnitude higher than is possible from the Cleveland basin section and most Mesozoic records. In addition the geological record will time average the isotopic composition over at least the decadal time scale. The restricted nature of the modern day Baltic Sea, compared to the Cleveland basin of the T-OAE is more likely to cause the change in sensitivity (b). Anthropogenic input (c) is not relevant to the Toarcian and furthermore, the unquantified effect of anthropogenic Re in the modern-day Baltic Sea adds a significant further unknown. (d), changes in riverine input, are also unlikely to have influenced the Toarcian signal because the adjacent landmasses were very low lying (Cope *et al.* 1980). These possible factors all appear to mask a clear relationship in the Baltic Sea samples. This is further confounded by the assumptions and errors on the two age models. In contrast, T-OAE samples from the Cleveland Basin (Chapter 6), show a much clearer and unambiguous relationship between δ^{187}Re and changing redox conditions as is summarised below.

7.1.3 The δ^{187}Re of Toarcian age sedimentary rocks

Chapter 6 presented the determination of δ^{187}Re for a suite of T-OAE samples. The key findings of Chapter 6 are as follows:

- It is possible to determine δ^{187}Re of organic-rich sedimentary rocks to high precision; average reproducibility of analyses in this study is ± 0.082 ‰ (2 SD) (Table 6.1).
- Broad changes in δ^{187}Re observed across the T-OAE are characterised by a - 0.596 ‰ excursion; between -0.96 m and 3.31 m, δ^{187}Re decreases from -0.057 ± 0.066 ‰ to a minimum of -0.756 ± 0.085 ‰, which is coincident with previously observed redox

changes across the event (section 6.5.1). The marked negative excursion is interpreted to have been driven by the expansion in the areal extent of anoxic deposition. Prior to the marked negative excursion in δ^{187}Re, there is a gradual 0.219 ‰ increase in δ^{187}Re between – 0.276 ± 0.065 ‰ at -5.62 m and – 0.057 ± 0.066 ‰ at -0.96 m. This could be interpreted as a decrease in the anoxic area, or more likely a trend towards the quantitative removal of Re from seawater, and hence the recording of seawater δ^{187}Re values in the sediment.

- The change in trend in δ^{187}Re during the onset of the OAE from an increase to a rapid negative excursion with continued increases in the severity of locally anoxic conditions may indicate a change in the response of δ^{187}Re with respect to local or regional controls.
- There are two distinct 0.2 ‰ steps in δ^{187}Re over a similar stratigraphic interval as shifts A and B in δ^{13}C (section 6.5.2).
- The 0.2 ‰ steps in δ^{187}Re show similarities to the fluctuations in $\delta^{98/95}$Mo; however the δ^{187}Re values continue to decrease where the $\delta^{98/95}$Mo values fluctuate between two extremes. The rapid fluctuations in the $\delta^{98/95}$Mo have been interpreted to represent the pulsed expansion and contraction of globally euxinic conditions across the T-OAE (Pearce *et al.* 2008); if this is the case, then the progressive changes in δ^{187}Re could indicate that the area of anoxic deposition expanded whilst the euxinic area expanded and contracted (section 6.5.2). Whilst new $\delta^{98/95}$Mo data from several sites in Northern Europe (Dickson *et al.* 2017) support the findings of Pearce *et al.* (2008) indicating that broad changes in $\delta^{98/95}$Mo are caused by an expanded area of euxinic conditions globally, the authors have also suggested that the small-scale changes observed in samples from Yorkshire could be caused by redox changes in the Cleveland basin (Dickson *et al.* 2017). However the new data lack stratigraphical resolution and there is no evidence for substantial runoff into the Cleveland basin at this time as the local landmass was of low relief. Further high

resolution studies are required to resolve this and to determine the cause of the small scale (0.2 ‰) steps in δ^{187}Re.

- The minimum δ^{187}Re is observed at 3.31 m above the base of the *exaratum* Subzone (δ^{187}Re = - 0.756 ± 0.085 ‰). Assuming that an excursion in δ^{187}Re in sedimentary rocks is caused by global redox changes in the ocean, and that low δ^{187}Re values correspond with anoxic deposition conditions, the Re isotope data may indicate that the maximum extent of anoxic depositional area globally was observed at 3.31 m during the T-OAE (sections 6.5.2, 6.5.3).
- The application of the newly developed δ^{187}Re redox proxy to the T-OAE has shown that the δ^{187}Re of sedimentary rocks has the potential to become a new proxy for past ocean redox conditions (Chapter 6).

7.2 Rhenium isotope composition as a new proxy for past ocean redox conditions

The investigated mudrock samples across the T-OAE from Yorkshire, and sediment samples from site BY15 in the Gotland Deep of the Baltic Sea, overall show a variation in δ^{187}Re of 1.030 ‰ (Figure 1.2). This is consistent with the predictions presented by Miller *et al.* (2015) that there are likely natural variations in δ^{187}Re of geological materials with a magnitude of ~1 ‰. The data presented in this thesis significantly expand the available data on the δ^{187}Re of sedimentary materials (Figure 1.2). The δ^{187}Re values for the reference standard SDO-1 presented in this thesis are equal (within prescribed analytical uncertainty) to the δ^{187}Re values presented for the same standard by Miller *et al.* (2009). The δ^{187}Re values reported for the New Albany Shale weathering profile (Miller *et al.* 2015) overlap the range of values observed in Interval 2 of the T-OAE (Chapter 6), and those observed in the modern day Baltic Sea (Chapter 4); however the lower δ^{187}Re values are observed in the most weathered samples from the NAS profile, which cannot explain the low values seen in Interval 2 of the T-OAE or the Baltic Sea samples. Both the data points for sediment

samples from the Black Sea are single data points from a conference abstract presented by Neubert *et al.* (2010a), and so any comparison with the data presented in this thesis must be approached with caution.

The rapid shifts in δ^{187}Re observed in the Baltic Sea samples (a - 0.608 ‰ shift between 3.75 cm and 2.75 cm depth (between 1991.3 and 1999.3 yr, based on Mo-tuned age), and a - 0.504 ‰ shift between 2.25 cm and 0.5 cm depth (between 2002.2 and 2008.0 yr, based on Mo-tuned age; section 4.4.2, Figure 4.7) suggest that the Re isotope composition in the Baltic Sea is sensitive on short timescales in the order of 10 years. These timescales are much shorter than the likely sampling resolution of the T-OAE samples where a few centimetres represents thousands of years. These 10-year shifts are also much shorter than the current estimates of residence time of Re in the open ocean (estimated to be 750,000 years by Colodner *et al.* (1993), and 130,000 years by Miller *et al.* (2011)), which suggests that the residence time of Re in a restricted anoxic basin such as the Baltic Sea may be significantly lower than the open ocean, although we cannot discount the possibility that these shifts in δ^{187}Re may be caused by an increased flux of anthropogenic Re to the Baltic Sea, or diagenesis (section 7.1.2).

If Re in the Cleveland Basin (where T-OAE samples from Yorkshire, UK were deposited) had a similarly short residence time to that proposed above for Re in the Baltic Sea, this would also indicate that the δ^{187}Re data for samples from the T-OAE (Chapter 6) may be affected by basinal redox changes on a short timescale, as well as the global changes in redox conditions that occurred over longer timescales during the T-OAE (Figure 6.2). However such high resolution sampling would be impossible for the Cleveland basin, given that samples at 1 cm resolution represent thousands of years, so a more expanded section would be required.

The large (- 0.596 ‰) excursion in δ^{187}Re observed across the T-OAE (Figure 6.2) coincides with a known large-scale global expansion in the area of anoxic sediment deposition (section

6.5.1). Assuming that δ^{187}Re behaves similarly to $\delta^{98/95}$Mo (Miller *et al.* 2015), and therefore that δ^{187}Re records the isotope composition of contemporaneous seawater, then this finding suggests that the expanded area of anoxic sediment deposition across the T-OAE caused a decrease in the δ^{187}Re values of seawater. Below the main negative δ^{187}Re excursion there is a small increase (from -0.276 ± 0.065 ‰ to -0.057 ± 0.066 ‰) in δ^{187}Re values which is shown by $\delta^{98/95}$Mo and other proxies to be associated with the onset of locally anoxic conditions (section 6.5.1). This interpretation of a change in behaviour of δ^{187}Re between responding to locally anoxic conditions and subsequently responding to expanded global hypoxia was based on similarities between Re and Mo geochemistry, and the interpretation of $\delta^{98/95}$Mo data from Pearce *et al.* (2008).

The findings presented in Chapter 6 show that during the expansion of areal extent of anoxia across the T-OAE, the δ^{187}Re of anoxic sediment decreases from -0.057 ± 0.066 ‰ to -0.756 ± 0.085 ‰. Assuming that Re is quantitatively removed to anoxic sediment, and therefore that the δ^{187}Re of anoxic sediment records that of seawater, then this finding indicates that the δ^{187}Re of seawater became lower when the areal extent of anoxic deposition expanded during the T-OAE (Figure 7.1a). This finding contradicts the expected behaviour of δ^{187}Re modelled by Miller *et al.* (2015). The modelling of the expected fractionation of Re during reduction of $Re^{VII}O_4^-$ (the dominant Re species in seawater) to various Re^{IV} species predicts that $Re^{VII}O_4^-$ is ^{187}Re enriched by up to 1.52 ‰ compared to any of the more reduced species (Miller *et al.* 2015). Assuming again that Re is quantitatively removed to anoxic sediment, based on assumed similarities with the behaviour of $\delta^{98/95}$Mo, Miller *et al.* (2015) therefore propose that a decrease in δ^{187}Re recorded in organic rich sediments would be caused by a diminished anoxic or euxinic area (Figure 7.1b).

The apparent contradiction between the empirical data presented in this thesis and the modelling presented in Miller *et al.* (2015) highlights the remaining uncertainties about the exact chemical mechanism by which Re is incorporated into sediments (Miller 2009, Miller *et al.* 2011,

2015). Whilst our evidence from the T-OAE indicates that in anoxic settings Re is quantitatively removed to sediment, and hence δ^{187}Re of sediment reflects that of seawater, it remains possible that there are situations where Re is not quantitatively removed to the sediment. If there are situations in which Re is not quantitatively removed to the sediment, but conditions are still anoxic, then the modelling of Miller *et al.* (2015) predicts that the δ^{187}Re of the sediment would be isotopically lighter than the seawater it is being removed from (this is similar to the behaviour of Mo isotopes). It is possible that the samples in Interval 1 of the T-OAE (section 6.5.1), where δ^{187}Re values increase despite an increase in local anoxia, could represent a change from lower, fractionated δ^{187}Re towards quantitative removal of Re, and hence the recording of seawater δ^{187}Re in the sediment. Further work is required to establish with greater certainty whether Re is quantitatively removed to anoxic sediment in all cases of anoxia or only where anoxia is globally widespread, and hence whether the δ^{187}Re of anoxic sediment reflects the Re isotope composition of seawater (section 7.3).

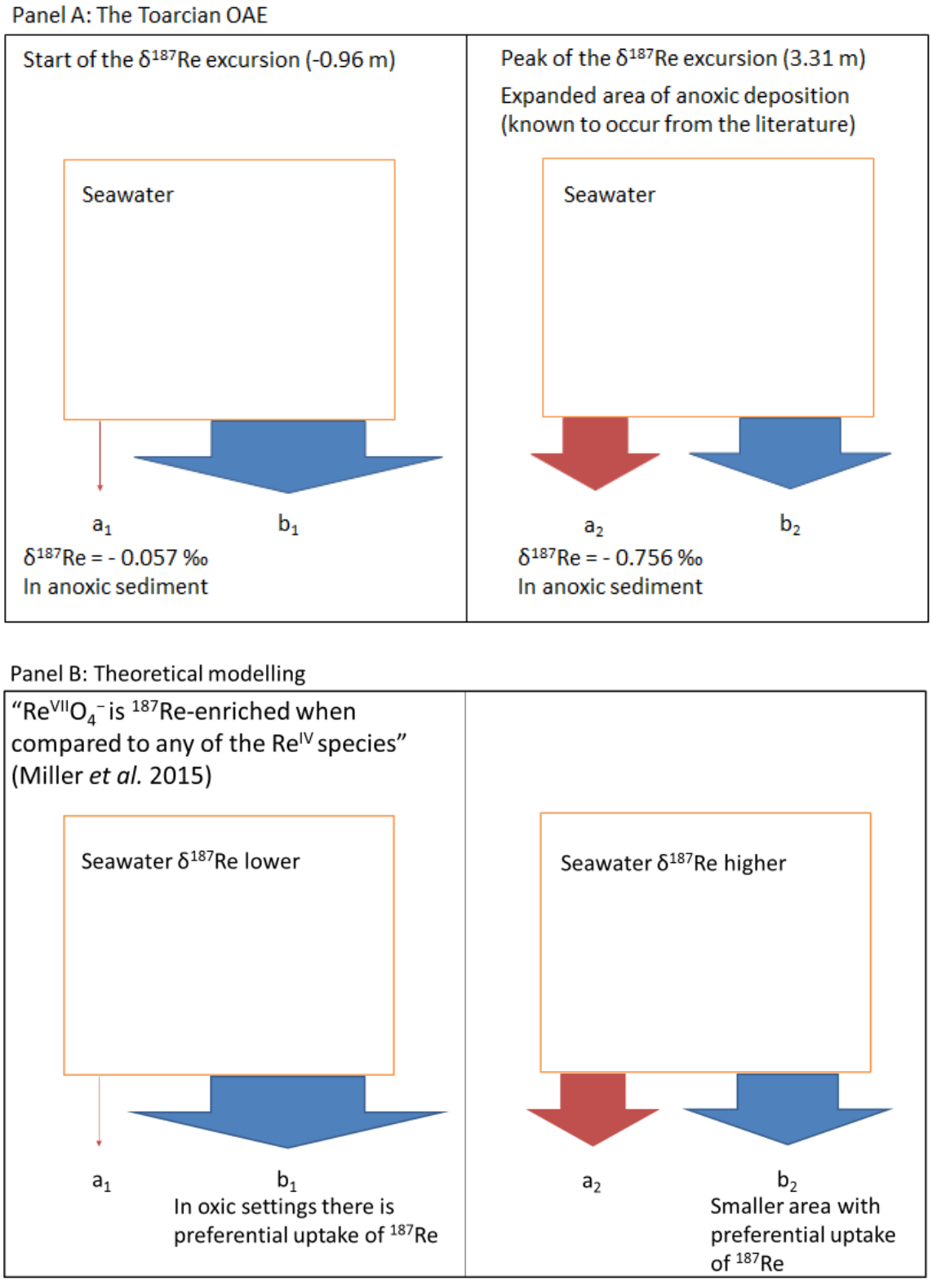

Figure 7.1: Considering the effects on changing areal extent of hypoxic deposition during the T-OAE. a = areal extent of anoxic deposition, b = areal extent of oxic deposition. $a_1 < a_2$ and $b_1 > b_2$. Panel A shows what is known in the Toarcian (that the anoxic area expanded during the T-OAE), and the empirical evidence for how that affects $\delta^{187}Re$ presented in this thesis. Panel B shows the

implications of the modelling of Miller *et al.* (2015). In the present day, the area of anoxic deposition is 0.3 % of the global seafloor area, and is thought to remove the equivalent of 43 % of the Re which is input into the ocean from river sources (Miller *et al.* 2011).

Data from the Baltic Sea are inconclusive as to whether reducing conditions cause isotopically light or heavy Re to be recorded in sediment (Chapter 4). The expansion in the areal extent of hypoxia between 1993 and 2010 is associated with the lowest δ^{187}Re values observed in the section, but also the greatest range in δ^{187}Re. However, the decrease in hypoxic area between 1970 and 1993 does not have a significant effect on the δ^{187}Re of sediments from site BY15 of the Gotland Deep in the Baltic Sea. Furthermore, there is relatively little change in δ^{187}Re associated with the onset of local euxinic conditions at site BY15 in the Baltic Sea from 1980, which further complicates our understanding of the relationship between changing redox conditions and the direction of change in δ^{187}Re values. The lowest O_2 concentration recorded in the studied interval of the Gotland Deep (Baltic Sea) corresponds stratigraphically to higher δ^{187}Re values which may suggest that reducing conditions cause isotopically heavy Re to be recorded in the sediment. Furthermore, the correlation of δ^{187}Re to bottom water O_2 is vulnerable to potential errors in the age model (discussed in section 4.4.3). It is therefore difficult to accurately correlate the direction of changes in δ^{187}Re with the known redox changes that occurred during the 1993 and 2003 MBIs at this resolution. It is also possible that the correlation may be affected by a lag time between the changes in local redox conditions and the δ^{187}Re recorded in the sediment, or the effects of anthropogenic inputs, or diagenetic factors.

The δ^{187}Re data presented in this thesis from both recent sediment from the Baltic Sea (Chapter 4), and T-OAE samples from Yorkshire, UK (Chapter 6) show that δ^{187}Re is likely to be highly vulnerable to changing local and basin wide redox conditions. The large magnitude negative excursion in δ^{187}Re observed across the T-OAE occurred during a time of known expansion in areal extent of anoxic deposition; based on the assumption that Re isotopes behave

similarly to Mo isotopes (and therefore assuming that the δ^{187}Re of organic-rich mudrocks records the δ^{187}Re of contemporaneous seawater), this excursion in δ^{187}Re recorded is likely to be caused by a decrease in the δ^{187}Re of seawater caused by the global expansion of anoxic deposition. The δ^{187}Re data from the Baltic Sea have many possible interpretations (section 7.1.2). These findings highlight the need to understand the cycling of Re isotopes in the ocean in order to develop δ^{187}Re as a palaeoredox proxy, through further study of the Re isotope system in seawater and sediment, discussed in more detail below.

7.3 Future work

The Re isotope composition of sedimentary rocks is a new and under-studied palaeoredox proxy (Chapters 2 and 3). Whilst we have successfully shown that the Re isotope composition of sedimentary rocks has great potential as a palaeoredox proxy (Chapter 6), more work is needed to develop our understanding of Re isotope systematics in the modern ocean and to further investigate the origin of Re isotope variations documented for recent Baltic Sea sediments (Chapter 4). Some suggestions for future work to explore δ^{187}Re as a palaeoredox proxy are:

- Determination of δ^{187}Re in seawater in a range of settings:
    - An initial attempt to constrain the behaviour of Re isotopes in modern-day anoxic settings was conducted using sediment from the Baltic Sea (Chapter 4). By conducting a study of δ^{187}Re in seawater from the Baltic Sea it will be possible to better understand the Re reservoir from which Re in these sediments is precipitated. This could be achieved by determining δ^{187}Re for a depth profile of seawater samples collected at site BY15 to provide comparison with sediment data presented in Chapter 4; this would demonstrate whether there are any depth variations in δ^{187}Re, for instance due to the addition of anthropogenic Re at the surface and/or the removal of isotopically light Re into anoxic sediments in

the deep water. The determination of δ^{187}Re in seawater samples would require some further method development. The determination of δ^{187}Re in seawater would require around a litre of seawater per analysis.

  - Further work to determine the δ^{187}Re of seawater in the open ocean, where the effects of anthropogenic Re are likely to be less significant than in the Baltic Sea, will enable us to understand whether there are variations in δ^{187}Re spatially due to varying proximity to anthropogenic sources of Re. Comparison of these data with the δ^{187}Re of seawater from BY15 (see above) would further our understanding of Re isotope budgets in the ocean.

- At present there is no commercially available isotopically certified single element Re standard, since SRM 989 is no longer commercially available (section 2.6). To allow for easier comparison of future δ^{187}Re determinations, a new isotopically certified Re standard is required.
- Rhenium isotope fractionation in the authigenic enrichment of Re in anoxic sediments may affect the δ^{187}Re of sedimentary rocks and modern-day sediments. The exact mechanism for this process is still poorly understood. The determination of δ^{187}Re for pore water samples and their corresponding sediment may illuminate more details of this process, and help us to understand how diagenetic effects may impact the Re isotope composition of sedimentary rocks. The δ^{187}Re data from the T-OAE samples from Yorkshire, UK appear to indicate that the Re isotope composition of seawater is recorded without fractionation during the OAE, based on similarities with the Mo isotope record from the same site (section 6.5.1).
- Furthermore, Re precipitation experiments under a range of different redox conditions may help us to understand how, and if, Re isotope composition is affected by the precipitation of Re from seawater.

- A significant unknown highlighted by the work presented in Chapter 4 is the Re isotope composition of anthropogenic Re. Since catalytic converters are likely to be a major source of anthropogenic Re, it would be useful to determine δ^{187}Re of catalytic converters. Furthermore, it would be necessary to investigate further anthropogenic Re sources by *e.g.* collecting fumes from coal power stations or internal combustion engines to determine δ^{187}Re for Re from a variety of anthropogenic sources. An understanding of δ^{187}Re of anthropogenic Re would allow us to consider the effect of changing anthropogenic Re inputs on the Re isotope composition of modern-day sediments. Once we have an estimate of δ^{187}Re for anthropogenic Re, the study of δ^{187}Re through ocean depth profiles (discussed below) will allow us to consider how, and how much, anthropogenic Re is incorporated into modern-day sediment.
- The overall budget of Re concentration and cycling has been evaluated in detail by Miller *et al.* (2011). However, the isotope composition of the various sources of Re to seawater remains poorly constrained, and it is therefore difficult to quantify a mass balance model for the δ^{187}Re recorded in sediment. Further research to constrain the δ^{187}Re of non-anthropogenic riverine Re sources (weathering of sedimentary rocks), and comparison of this to the magnitude and δ^{187}Re of anthropogenic sources to riverine Re, will enable an estimate of the isotopic budget of Re sources to seawater, and allow mass balance equations for changing δ^{187}Re in sediment to be constructed.
- Once the behaviour of Re isotopes in seawater has been better constrained (as above), and the Re budgets of the Baltic Sea and causes for δ^{187}Re changes observed since 1960 have been identified, the method developed in this project can be applied to the study of other modern-day anoxic basins to further our understanding of Re isotope cycling in the modern ocean.

We have found variations in δ^{187}Re across the T-OAE for a suite of samples from Yorkshire, UK (Chapter 6). Once the Re isotope cycling in the ocean is better constrained (as above), the Re isotope composition of sedimentary rocks may become a useful palaeoredox proxy. This proxy may be applied to other OAEs, and indeed a wide range of samples from the T-OAE from other sites, in order to provide new detail of the redox histories of these events.

References

Ait-Itto, F.-Z., Martinez, M., Price, G. D. and Ait Addi, A. (2018) 'Synchronization of the astronomical time scales in the Early Toarcian: A link between anoxia, carbon-cycle perturbation, mass extinction and volcanism', *Earth and Planetary Science Letters*, vol. 493, p.1-11.

Al-Suwaidi, A. H., Angelozzi, G. N., Baudin, F., Damborenea, S. E., Hesselbo, S. P., Jenkyns, H. C., Mancenido, M. O. and Riccardi, A. C. (2010) 'First record of the Early Toarcian Oceanic Anoxic Event from the Southern Hemisphere, Neuquen Basin, Argentina', *Journal of the Geological Society*, vol. 167, p.633-636.

Albarède, F., Telouk, P., Blichert-Toft, J., Boyet, M., Agranier, A. and Nelson, B. (2004) 'Precise and accurate isotopic measurements using multiple-collector ICPMS', *Geochimica et Cosmochimica Acta*, vol. 68, p.2725-2744.

Algeo, T. J. and Rowe, H. (2012) 'Paleoceanographic applications of trace-metal concentration data', *Chemical Geology*, vol. 324-325, p.6-18.

Algeo, T. J. and Tribovillard, N. (2009) 'Environmental analysis of paleoceanographic systems based on molybdenum–uranium covariation', *Chemical Geology*, vol. 268, p.211-225.

Allen, M. R., Scott, P. A., Mitchell, J. F. B., Schnur, R. and Delworth, T. L. (2000) 'Quantifying the uncertainty in forecasts of anthropogenic climate change', *Nature*, vol. 407, p.617-620.

Anbar, A. D. (2004) 'Molybdenum Stable Isotopes: Observations, Interpretations and Directions', *Reviews in Mineralogy and Geochemistry*, vol. 55, p.429-454.

Anbar, A. D., Creaser, R. A., Papanastassiou, D. A. and Wasserburg, G. J. (1992) 'Rhenium in seawater: Confirmation of generally conservative behavior', *Geochimica et Cosmochimica Acta*, vol. 56, p.4099-4103.

Anbar, A. D. and Gordon, W. W. (2008) 'Redox Renaissance', *The Geological Society of America*, vol. 36, p.271-272.

Anbar, A. D. and Rouxel, O. (2007) 'Metal Stable Isotopes in Paleoceanography', *Annual Review of Earth and Planetary Sciences*, vol. 35, p.717-746.

Andersen, J. H., Carstensen, J., Conley, D. J., Dromph, K., Fleming-Lehtinen, V., Gustafsson, B. G., Josefson, A. B., Norkko, A., Villnas, A. and Murray, C. (2017a) 'Long-term temporal and spatial trends in eutrophication status of the Baltic Sea', *Biological Reviews Cambridge Philosophical Society*, vol. 92, p.135-149.

Andersen, M. B., Romaniello, S., Vance, D., Little, S. H., Herdman, R. and Lyons, T. W. (2014) 'A modern framework for the interpretation of 238U/235U in studies of ancient ocean redox', *Earth and Planetary Science Letters*, vol. 400, p.184-194.

Andersen, M. B., Stirling, C. H. and Weyer, S. (2017b) 'Uranium Isotope Fractionation', *Reviews in Mineralogy and Geochemistry*, vol. 82, p.799-850.

Archer, C. and Vance, D. (2008) 'The isotopic signature of the global riverine molybdenum flux and anoxia in the ancient oceans', *Nature Geoscience*, vol. 1, p.597-600.

Arnold, G. L., Anbar, A. D., Barling, J. and Lyons, T. (2004) 'Molybdenum isotope evidence for widespread anoxia in Mid-Proterozoic Oceans', *Science*, vol. 304, p.87-90.

Bailey, T. R., Rosenthal, Y., McArthur, J. M., van de Schootbrugge, B. and Thirlwall, M. F. (2003) 'Paleoceanographic changes of the Late Pliensbachian-Early Toarcian interval: A possible

link to the genesis of an Oceanic Anoxic Event', *Earth and Planetary Science Letters*, vol. 212, p.307-320.

Barling, J. and Anbar, A. D. (2004) 'Molybdenum isotope fractionation during adsorption by manganese oxides', *Earth and Planetary Science Letters*, vol. 217, p.315-329.

Barling, J., Arnold, G. L. and Anbar, A. D. (2001) 'Natural mass-dependent variations in the isotopic composition of molybdenum', *Earth and Planetary Science Letters*, vol. 193, p.447-457.

Beerling, D. J. and Brentnall, S. J. (2007) 'Numerical evaluation of mechanisms driving Early Jurassic changes in global carbon cycling', *Geology*, vol. 35, p.247.

Beerling, D. J. L. M. R., Grocke D.R. (2002) 'On the nature of methane gas-hydrate dissociation during the Toarcian and Aptian Oceanic Anoxic Events', *American Journal of Science*, vol. 302, p.28-49.

Bendtsen, J., Gustafsson, K. E., Söderkvist, J. and Hansen, J. L. S. (2009) 'Ventilation of bottom water in the North Sea–Baltic Sea transition zone', *Journal of Marine Systems*, vol. 75, p.138-149.

Berner, Z. A., Puchelt, H., Nöltner, T. and Kramar, U. T. Z. (2013) 'Pyrite geochemistry in the Toarcian Posidonia Shale of south-west Germany: Evidence for contrasting trace-element patterns of diagenetic and syngenetic pyrites', *Sedimentology*, vol. 60, p.548-573.

Bopp, L., Resplandy, L., Untersee, A., Le Mezo, P. and Kageyama, M. (2017) 'Ocean (de)oxygenation from the Last Glacial Maximum to the twenty-first century: insights from Earth System models', *Philosophical Transactions of the Royal Society A: Mathematical, Physical and Engineering Sciences*, vol. 375, p.1-15.

Boulila, S., Galbrun, B., Huret, E., Hinnov, L. A., Rouget, I., Gardin, S. and Bartolini, A. (2014) 'Astronomical calibration of the Toarcian Stage: Implications for sequence stratigraphy and duration of the early Toarcian OAE', *Earth and Planetary Science Letters*, vol. 386, p.98-111.

Boulila, S. and Hinnov, L. (2017) 'A review of tempo and scale of the early Jurassic Toarcian OAE: Implications for carbon cycle and sea level variations', *Newsletters on Stratigraphy*, vol. 50, p.363-389.

Brocks, J. J. and Banfield, J. (2009) 'Unravelling ancient microbial history with community proteogenomics and lipid geochemistry', *Nature reviews: Microbiology*, vol. 7, p.601-609.

Brumsack, H.-J. (1991) 'Inorganic Geochemistry of the German 'Posidonia Shale' palaeoenvironmental consequences', *Geological Society, London, Special Publication*, vol., p.353-362.

Brumsack, H.-J. (2006) 'The trace metal content of recent organic carbon-rich sediments: Implications for Cretaceous black shale formation', *Palaeogeography, Palaeoclimatology, Palaeoecology*, vol. 232, p.344-361.

Burgess, S. D., Bowring, S. A., Fleming, T. H. and Elliot, D. H. (2015) 'High-precision geochronology links the Ferrar large igneous province with early-Jurassic ocean anoxia and biotic crisis', *Earth and Planetary Science Letters*, vol. 415, p.90-99.

Calvert, S. E. and Pedersen, T. F. (1993) 'Geochemistry of Recent oxic and anoxic marine sediments: Implications for the geological record', *Marine Geology*, vol. 113, p.67-88.

Calvert, S. E. and Pedersen, T. F. (2007) *'Chapter Fourteen: Elemental Proxies for Palaeoclimatic and Palaeoceanographic Variability in Marine Sediments: Interpretation and Application'*,

in: Hillaire-Marcel, C. and Vernal, A. d. (eds), *Palaeoceanography of the Late Cenozoic, Part 1, Methods*. (New York) Elsevier, p.567-644.

Cao, L., Wang, S., Zheng, M. and Zhang, H. (2014) 'Sensitivity of ocean acidification and oxygen to the uncertainty in climate change', *Environmental Research Letters*, vol. 9, p.1-10.

Carstensen, J., Andersen, J. H., Gustafsson, B. G. and Conley, D. J. (2014a) 'Deoxygenation of the Baltic Sea during the last century', *Proceedings of the National Academy of Sciences of the United States of America*, vol. 111, p.5628-5633.

Carstensen, J., Conley, D. J., Bonsdorff, E., Gustafsson, B. G., Hietanen, S., Janas, U., Jilbert, T., Maximov, A., Norkko, A., Norkko, J., Reed, D. C., Slomp, C. P., Timmermann, K. and Voss, M. (2014b) 'Hypoxia in the Baltic Sea: biogeochemical cycles, benthic fauna, and management', *Ambio*, vol. 43, p.26-36.

Caruthers, A. H., Gröcke, D. R. and Smith, P. L. (2011) 'The significance of an Early Jurassic (Toarcian) carbon-isotope excursion in Haida Gwaii (Queen Charlotte Islands), British Columbia, Canada', *Earth and Planetary Science Letters*, vol. 307, p.19-26.

Caruthers, A. H., Smith, P. L. and Gröcke, D. R. (2014) The Pliensbachian-Toarcian (Early Jurassic) extinction: A North American perspective. Special Paper of the Geological Society of America, p.225-243.

Caswell, B. A. and Coe, A. L. (2012) 'A high-resolution shallow marine record of the Toarcian (Early Jurassic) Oceanic Anoxic Event from the East Midlands Shelf, UK', *Palaeogeography, Palaeoclimatology, Palaeoecology*, vol. 365-366, p.124-135.

Caswell, B. A. and Coe, A. L. (2013) 'Primary productivity controls on opportunistic bivalves during Early Jurassic oceanic deoxygenation', *Geology*, vol. 41, p.1163-1166.

Caswell, B. A. and Coe, A. L. (2014) 'The impact of anoxia on pelagic macrofauna during the Toarcian Oceanic Anoxic Event (Early Jurassic)', *Proceedings of the Geologists' Association*, vol., p.1-9.

Caswell, B. A., Coe, A. L. and Cohen, A. S. (2009) 'New range data for marine invertebrate species across the early Toarcian (Early Jurassic) mass extinction', *Journal of the Geological Society*, vol. 166, p.859-872.

Chappaz, A., Gobeil, C. and Tessier, A. (2008) 'Sequestration mechanisms and anthropogenic inputs of rhenium in sediments from Eastern Canada lakes', *Geochimica et Cosmochimica Acta*, vol. 72, p.6027-6036.

Chappaz, A., Lyons, T. W., Gregory, D. D., Reinhard, C. T., Gill, B. C., Li, C. and Large, R. R. (2014) 'Does pyrite act as an important host for molybdenum in modern and ancient euxinic sediments?', *Geochimica et Cosmochimica Acta*, vol. 126, p.112-122.

Chen, C., Sedwick, P. N. and Sharma, M. (2009) 'Anthropogenic osmium in rain and snow reveals global-scale atmospheric contamination', *Proc Natl Acad Sci U S A*, vol. 106, p.7724-8.

Chen, X., Romaniello, S. J., Herrmann, A. D., Wasylenki, L. E. and Anbar, A. D. (2016) 'Uranium isotope fractionation during coprecipitation with aragonite and calcite', *Geochimica et Cosmochimica Acta*, vol. 188, p.189-207.

Cheng, M., Li, C., Zhou, L., Algeo, T. J., Zhang, F., Romaniello, S., Jin, C.-S., Lei, L.-D., Feng, L.-J. and Jiang, S.-Y. (2016) 'Marine Mo biogeochemistry in the context of dynamically euxinic mid-depth waters: A case study of the lower Cambrian Niutitang shales, South China', *Geochimica et Cosmochimica Acta*, vol. 183, p.79-93.

Clarkson, M. O., Stirling, C. H., Jenkyns, H. C., Dickson, A. J., Porcelli, D., Moy, C. M., Strandmann, P. A. E. P. v., Cooke, I. R. and Lenton, T. M. (2018) 'Uranium isotope evidence for two

episodes of deoxygenation during Oceanic Anoxic Event 2', *Proceedings of the National Academy of Sciences*, vol. 115, p.2918-2923.

Cohen, A. S. and Coe, A. L. (2007) 'The impact of the Central Atlantic Magmatic Province on climate and on the Sr- and Os-isotope evolution of seawater', *Palaeogeography, Palaeoclimatology, Palaeoecology*, vol. 244, p.374-390.

Cohen, A. S., Coe, A. L., Bartlett, J. M. and Hawkesworth, C. J. (1999) 'Precise Re–Os ages of organic-rich mudrocks and the Os isotope composition of Jurassic seawater', *Earth and Planetary Science Letters*, vol. 167, p.159-173.

Cohen, A. S., Coe, A. L., Harding, S. M. and Schwark, L. (2004) 'Osmium isotope evidence for the regulation of atmospheric CO2 by continental weathering', *Geology*, vol. 32, p.157-160.

Cohen, A. S., Coe, A. L. and Kemp, D. B. (2007) 'The Late Palaeocene - Early Eocene and Toarcian (Early Jurassic) carbon isotope excursions: A comparison of their time scales, associated environmental changes, causes and consequences', *Journal of the Geological Society*, vol. 164, p.1093-1108.

Cohen, A. S. and Waters, F. G. (1996) 'Separation of osmium from geological materials by solvent extraction for analysis by thermal ionisation mass spectrometry', *Analytica Chimica Acta*, vol. 332, p.269-275.

Collier, R. (1985) 'Molybdenum in the Northeast Pacific-Ocean', *Limnol Oceanogr*, vol. 30, p.1351-1354.

Colodner, D., Edmond, J. and Boyle, E. (1995) 'Rhenium in the Black Sea: comparison with molybdenum and uranium', *Earth and Planetary Science Letters*, vol. 131, p.1-15.

Colodner, D., Sachs, J., Ravizza, G., Turekian, K., Edmond, J. and Boyle, E. (1993) 'The geochemical cycle of rhenium: a reconnaissance', *Earth and Planetary Science Letters*, vol. 117, p.205-221.

Conley, D. J., Bjorck, S. and E, B. (2009) 'Hypoxia related processes in the Baltic Sea', *American Chemical Society*, vol. 43, p.3412-3420.

Conley, D. J., Humborg, C., Rahm, L., Savchuk, O. P. and Wulff, F. (2002) 'Hypoxia in the Baltic Sea and Basin-Scale Changes in Phosphorus Biogeochemistry', *Environ Sci Technol*, vol. 36, p.5315-5320.

Cope, J., Getty, T. A., Howarth, M. K., Morton, N. and Torrens, H. S. (1980) *A correlation of Jurassic rocks in the British Isles. Part 1: introduction and Lower Jurassic*.

Crusius, J., Calvert, S., Pedersen, T. and Sage, D. (1996) 'Rhenium and molybdenum enrichments in sediments as indicators of oxic, suboxic and sulfidic conditions of deposition', *Earth and Planetary Science Letters*, vol. 145, p.65-78.

Day, J. M. D., Pearson, D. G. and Nowell (2003) 'High precision rhenium and platinum isotope dilution analyses by plasma ionisation multi-collector mass spectrometry', *In: Holland G., Tanner S.D. (Eds.) Plasma Source Mass Spectrometry: applications and emerging technologies. The Royal Society of Chemistry Sepcial Publication*, vol., p.374-390.

Deng, S. H., Lu, Y. Z., Fan, R., Fang, L. H., Li, X. and Liu, L. (2012) 'Toarcian (Early Jurassic) oceanic anoxic event and the responses in terrestrial ecological system', *Diqiu Kexue - Zhongguo Dizhi Daxue Xuebao/Earth Science - Journal of China University of Geosciences*, vol. 37, p.23-38.

Dera, G. and Donnadieu, Y. (2012) 'Modeling evidences for global warming, Arctic seawater freshening, and sluggish oceanic circulation during the Early Toarcian anoxic event', *Paleoceanography*, vol. 27.

Dichiarante, A. M., Holdsworth, R. E., Dempsey, E. D., Selby, D., McCaffrey, K. J. W., Michie, U., Morgan, G. and Bonniface, J. (2016) 'New structural and Re–Os geochronological evidence constraining the age of faulting and associated mineralization in the Devonian Orcadian Basin, Scotland', *Journal of the Geological Society*, vol. 173, p.457 - 473.

Dickson, A. J. (2017) 'A Molybdenum-isotope perspective on Phanerozoic deoxygenation events', *Nature Geoscience*, vol. 10, p.722-726.

Dickson, A. J., Cohen, A. S. and Coe, A. L. (2012) 'Seawater oxygenation during the Paleocene-Eocene Thermal Maximum', *Geology*, vol. 40, p.639-642.

Dickson, A. J., Gill, B. C., Ruhl, M., Jenkyns, H. C., Porcelli, D., Idiz, E., Lyons, T. W. and van den Boorn, S. H. J. M. (2017) 'Molybdenum-isotope chemostratigraphy and paleoceanography of the Toarcian Oceanic Anoxic Event (Early Jurassic)', *Paleoceanography*, vol. 32, p.813-829.

Dickson, A. J., Jenkyn, H. C., Porcelli, D., van den Boorn, S. and Idiz, E. F. (2016) 'Basin-scale controls on the molybdenum-isotope composition of seawater during Oceanic Anoxic Event 2 (Late Cretaceous)', *Geochimica et Cosmochimica Acta*, vol. 178, p.291-306.

Doney, S. C. (2010) 'The Growing Human Footprint on Coastal and Open-Ocean Biogeochemistry', *Science*, vol. 328, p.1512-1516.

Døssing, L. N., Dideriksen, K., Stipp, S. L. S. and Frei, R. (2011) 'Reduction of hexavalent chromium by ferrous iron: A process of chromium isotope fractionation and its relevance to natural environments', *Chemical Geology*, vol. 285, p.157-166.

Duan, Y., Anbar, A. D., Arnold, G. L., Lyons, T. W., Gordon, G. W. and Kendall, B. (2010) 'Molybdenum isotope evidence for mild environmental oxygenation before the Great Oxidation Event', *Geochimica et Cosmochimica Acta*, vol. 74, p.6655-6668.

Dubin, A. and Peucker-Ehrenbrink, B. (2015) 'The importance of organic-rich shales to the geochemical cycles of rhenium and osmium', *Chemical Geology*, vol. 403, p.111-120.

Ellis, A. S., Johnson, T. M. and Bullen, T. D. (2002) 'Chromium isotopes and the fate of hexavalent chromium in the environment', *Science*, vol. 295, p.2060-2062.

Emerson, S. and Huested, S. (1991) 'Ocean anoxia and the concentrations of molybdenum and vanadium in seawater', *Marine Chemistry*, vol. 34, p.177-196.

Erba, E. (2004) 'Calcareous nannofossils and Mesozoic oceanic anoxic events', *Marine Micropaleontology*, vol. 52, p.85-106.

Fantasia, A., Föllmi, K. B., Adatte, T., Spangenberg, J. E. and Montero-Serrano, J.-C. (2018) 'The Early Toarcian oceanic anoxic event: Paleoenvironmental and paleoclimatic change across the Alpine Tethys (Switzerland)', *Global and Planetary Change*, vol. 162, p.53-68.

Farrimond, P., Eglinton, G., Brassell, S. C. and Jenkyns, H. C. (1988) 'The Toarcian black shale event in northern Italy', *Organic Geochemistry*, vol. 13, p.823-832.

Farrimond, P., Eglinton, G., Brassell, S. C. and Jenkyns, H. C. (1989) 'Toarcian anoxic event in Europe: An organic geochemical study', *Marine and Petroleum Geology*, vol. 6, p.136-147.

Farrimond, P., Stoddart, D. P. and Jenkyns, H. C. (1994) 'An organic geochemical profile of the Toarcian anoxic event in northern Italy', *Chemical Geology*, vol. 111, p.17-33.

Farrimond, P. and Telnæs, N. (1996) 'Three series of rearranged hopanes in Toarcian sediments (northern Italy)', *Organic Geochemistry*, vol. 25, p.165-177.

Fehr, M. A., Andersson, P. S., Hålenius, U., Gustafsson, Ö. and Mörth, C.-M. (2010) 'Iron enrichments and Fe isotopic compositions of surface sediments from the Gotland Deep, Baltic Sea', *Chemical Geology*, vol. 277, p.310-322.

Fehr, M. A., Andersson, P. S., Hålenius, U. and Mörth, C.-M. (2008) 'Iron isotope variations in Holocene sediments of the Gotland Deep, Baltic Sea', *Geochimica et Cosmochimica Acta*, vol. 72, p.807-826.

Frei, R., Gaucher, C., Døssing, L. N. and Sial, A. N. (2011) 'Chromium isotopes in carbonates — A tracer for climate change and for reconstructing the redox state of ancient seawater', *Earth and Planetary Science Letters*, vol. 312, p.114-125.

French, K. L., Sepúlveda, J., Trabucho-Alexandre, J., Gröcke, D. R. and Summons, R. E. (2014) 'Organic geochemistry of the early Toarcian oceanic anoxic event in Hawsker Bottoms, Yorkshire, England', *Earth and Planetary Science Letters*, vol. 390, p.116-127.

Georgiev, S. V., Zimmerman, A., Yang, G., Goswami, V., Hurtig, N. C., Hannah, J. L. and Stein, H. J. (2018) 'Comparison of chemical procedures for Re-isotopic measurements by N-TIMS', *Chemical Geology*, vol. 483, p.151-161.

Gill, B. C., Lyons, T. W. and Jenkyns, H. C. (2011) 'A global perturbation to the sulfur cycle during the Toarcian Oceanic Anoxic Event', *Earth and Planetary Science Letters*, vol. 312, p.484-496.

Gilly, W. F., Beman, J. M., Litvin, S. Y. and Robison, B. H. (2013) 'Oceanographic and Biological Effects of Shoaling of the Oxygen Minimum Zone', *Annual Review of Marine Science*, vol. 5, p.393-420.

Goldberg, T., Gordon, G., Izon, G., Archer, C., Pearce, C. R., McManus, J., Anbar, A. D. and Rehkämper, M. (2013) 'Resolution of inter-laboratory discrepancies in Mo isotope data: an intercalibration', *Journal of Analytical Atomic Spectrometry*, vol. 28, p.724.

Golonka, J. (2007) 'Late Triassic and Early Jurassic palaeogeography of the world', *Palaeogeography, Palaeoclimatology, Palaeoecology*, vol. 244, p.297-307.

Gómez, J. J., Goy, A. and Canales, M. L. (2008) 'Seawater temperature and carbon isotope variations in belemnites linked to mass extinction during the Toarcian (Early Jurassic) in Central and Northern Spain. Comparison with other European sections', *Palaeogeography, Palaeoclimatology, Palaeoecology*, vol. 258, p.28-58.

Graham, L. P. (2004) 'Climate Change Effects on River Flow to the Baltic Sea', *AMBIO: A Journal of the Human Environment*, vol. 33, p.235-241.

Gramlich, J. W., Murphy, T. J., Garner, E. L. and Shields, W. R. (1973) 'Absolute Isotopic Abundance Ratio and Atomic Weight of a Reference Sample of Rhenium', *Journal of Research of the National Bureau of Standards - A. Physics and Chemistry*, vol. 77A, p.691 -689.

Gröcke, D. R., Hori, R. S., Trabucho-Alexandre, J., Kemp, D. B. and Schwark, L. (2011) 'An open ocean record of the Toarcian oceanic anoxic event', *Solid Earth*, vol. 2, p.245-257.

Gruber, N. (2011) 'Warming up, turning sour, losing breath: ocean biogeochemistry under global change', *Philosophical Transactions of the Royal Society A: Mathematical, Physical and Engineering Sciences*, vol. 369, p.1980-1996.

Gustafsson, B. G. and Medina, M. R. (2011) Validation data set compiled from Baltic Environmental Database, Version 2. Stockholm University Baltic Nest Institute, p.25.

Gustafsson, E. (2012) 'Modelled long-term development of hypoxic area and nutrient pools in the Baltic Proper', *Journal of Marine Systems*, vol. 94, p.120-134.

Han, Z., Hu, X., Kemp, D. B. and Li, J. (2018) 'Carbonate-platform response to the Toarcian Oceanic Anoxic Event in the southern hemisphere: Implications for climatic change and biotic platform demise', *Earth and Planetary Science Letters*, vol. 489, p.59-71.

Hansson, D., Eriksson, C., Omstedt, A. and Chen, D. (2011) 'Reconstruction of river runoff to the Baltic Sea, AD 1500-1995', *International Journal of Climatology*, vol. 31, p.696-703.

Hansson, D. and Gustafsson, E. (2011) 'Salinity and hypoxia in the Baltic Sea since A.D. 1500', *Journal of Geophysical Research*, vol. 116.

Harding, S. M. (2004) *The Toarcian oceanic anoxic event: organic and inorganic ceochemical anomalies in organic-carbon-rich mudrocks from the North Yorkshire Coast, UK and Dotternhausen Quarry, SW Germany,* PhD thesis, Milton Keynes, The Open University.

Helz, G. R. and Adelson, J. M. (2013) 'Trace element profiles in sediments as proxies of dead zone history; rhenium compared to molybdenum', *Environmental Science and Technology*, vol. 47, p.1257-64.

Helz, G. R., Bura-Nakić, E., Mikac, N. and Ciglenečki, I. (2011) 'New model for molybdenum behavior in euxinic waters', *Chemical Geology*, vol. 284, p.323-332.

Helz, G. R. and Dolor, M. K. (2012) 'What regulates rhenium deposition in euxinic basins?', *Chemical Geology*, vol. 304-305, p.131-141.

Hermoso, M., Delsate, D., Baudin, F., Le Callonnec, L., Minoletti, F., Renard, M. and Faber, A. (2014) 'Record of Early Toarcian carbon cycle perturbations in a nearshore environment: The Bascharage section (easternmost Paris Basin)', *Solid Earth*, vol. 5, p.793-804.

Hermoso, M., Le Callonnec, L., Minoletti, F., Renard, M. and Hesselbo, S. P. (2009a) 'Expression of the Early Toarcian negative carbon-isotope excursion in separated carbonate microfractions (Jurassic, Paris Basin)', *Earth and Planetary Science Letters*, vol. 277, p.194-203.

Hermoso, M., Minoletti, F., Le Callonnec, L., Jenkyns, H. C., Hesselbo, S. P., Rickaby, R. E. M., Renard, M., de Rafélis, M. and Emmanuel, L. (2009b) 'Global and local forcing of Early Toarcian seawater chemistry: A comparative study of different paleoceanographic settings (Paris and Lusitanian basins)', *Paleoceanography*, vol. 24, p.1-15.

Hermoso, M., Minoletti, F., Rickaby, R. E. M., Hesselbo, S. P., Baudin, F. and Jenkyns, H. C. (2012) 'Dynamics of a stepped carbon-isotope excursion: Ultra high-resolution study of Early Toarcian environmental change', *Earth and Planetary Science Letters*, vol. 319-320, p.45-54.

Hesselbo, S. P., Grocke, D. R., Jenkyns, H. C., Bjerrum, C. J., Farrimond, P., Morgans Bell, H. S. and Green, O. R. (2000) 'Massive dissociation of gas hydrate during a Jurassic oceanic anoxic event', *Nature*, vol. 406, p.392-395.

Hesselbo, S. P. and Jenkyns, H. C. (1995) *'A comparison of the Hettangian to Bajocian successions of Dorset and Yorkshire'*, in: Taylor, P. D. (ed), *Field Geology of the British Jurassic*. (London) Geological Society, p.105-150.

Hesselbo, S. P., Jenkyns, H. C., Duarte, L. V. and Oliveira, L. C. V. (2007) 'Carbon-isotope record of the Early Jurassic (Toarcian) Oceanic Anoxic Event from fossil wood and marine carbonate (Lusitanian Basin, Portugal)', *Earth and Planetary Science Letters*, vol. 253, p.455-470.

Hesselbo, S. P. and Pieńkowski, G. (2011) 'Stepwise atmospheric carbon-isotope excursion during the Toarcian Oceanic Anoxic Event (Early Jurassic, Polish Basin)', *Earth and Planetary Science Letters*, vol. 301, p.365-372.

Hoegh-Guldberg, O. and Bruno, J. F. (2010) 'The Impact of Climate Change on the World's Marine Ecosystems', *Science*, vol. 328, p.1523-1528.

Holland, H. (1984) *The Cheical Evolution of the Atmosphere and Oceans*. (Princeton) Princeton University Press.

Hori, R. S. (1997) 'The Toarcian radiolarian event in bedded cherts from southwestern Japan', *Marine Micropaleontology*, vol. 30, p.159-169.

Howarth, M. K. (1962) 'The Jet Rock Series and the Alum Shales Series of the Yorkshire coast', *Proceedings of the Yorkshire Geological Society*, vol. 33, p.381-422.

Howarth, M. K. (1973) 'The stratigraphy and ammonite fauna of the Upper Liassic Grey Shales of the Yorkshire coast', *Bulletin of the British Museum (Natural History), Geology Series*, vol. Vol.29, p.235-288.

Howarth, M. K. (1992) 'The ammonite family Hildoceratidae in the Lower Jurassic of Britain', *Monograph of the Palaeontographical Society London*, vol. 145, p.1-106.

Ingri, J., Widerlund, A., Suteerasak, T., Bauer, S. and Elming, S.-Å. (2014) 'Changes in trace metal sedimentation during freshening of a coastal basin', *Marine Chemistry*, vol. 167, p.2-12.

IPCC (2014) 'Climate Change 2014: Synthesis Report. Contribution of Working Groups I, II and III to the Fifth Assessment Report of the Intergovernmental Panel on Climate Change [Core Writing Team, R.K. Pachauri and L.A. Meyer (eds.)]. IPCC, Geneva, Switzerland, p.1-151', vol.

Izon, G. J. (2012) *A Mo-isotope appraisal of ocean oxygen deficiency: Examples from the Cretaceous and Miocene,* PhD thesis, MIlton Keynes, The Open University.

Izumi, K., Endo, K., Kemp, D. B. and Inui, M. (2018a) 'Oceanic redox conditions through the late Pliensbachian to early Toarcian on the northwestern Panthalassa margin: Insights from pyrite and geochemical data', *Palaeogeography, Palaeoclimatology, Palaeoecology*, vol. 493, p.1-10.

Izumi, K., Kemp, D. B., Itamiya, S. and Inui, M. (2018b) 'Sedimentary evidence for enhanced hydrological cycling in response to rapid carbon release during the early Toarcian oceanic anoxic event', *Earth and Planetary Science Letters*, vol. 481, p.162-170.

Izumi, K., Miyaji, T. and Tanabe, K. (2012) 'Early Toarcian (Early Jurassic) oceanic anoxic event recorded in the shelf deposits in the northwestern Panthalassa: Evidence from the Nishinakayama Formation in the Toyora area, west Japan', *Palaeogeography, Palaeoclimatology, Palaeoecology*, vol. 315-316, p.100-108.

Jenkyns, H. C. (1985) 'The Early Toarcian and Cenomanian-Turonian anoxic events in Europe: Comparisons and Contrasts', *Geologische Rundschau*, vol. 74, p.505-518.

Jenkyns, H. C. (1988) 'The early Toarcian (Jurassic) anoxic event; stratigraphic, sedimentary and geochemical evidence', *American Journal of Science*, vol. 288, p.101-151.

Jenkyns, H. C. (1999) 'Mesozoic anoxic events and palaeoclimate', *Zentralbl. Geol. Palaeontol. Teil*, vol., p.943 - 949.

Jenkyns, H. C. (2010a) 'Geochemistry of oceanic anoxic events', *Geochemistry Geophysics Geosystems*, vol. 11.

Jenkyns, H. C. (2010b) 'Geochemistry of oceanic anoxic events', *Geochemistry, Geophysics, Geosystems*, vol. 11, p.1-30.

Jenkyns, H. C. and Clayton, C. J. (1997) 'Lower Jurassic epicontinental carbonates and mudstones from England and Wales: chemostratigraphic signals and the early Toarcian anoxic event', *Sedimentology*, vol. 44, p.687-706.

Jenkyns, H. C., Gröcke, D. R. and Hesselbo, S. P. (2001) 'Nitrogen isotope evidence for water mass denitrification during the Early Toarcian (Jurassic) oceanic anoxic event', *Paleoceanography*, vol. 16, p.593-603.

Jilbert, T. and Slomp, C. P. (2013a) 'Iron and manganese shuttles control the formation of authigenic phosphorus minerals in the euxinic basins of the Baltic Sea', *Geochimica et Cosmochimica Acta*, vol. 107, p.155-169.

Jilbert, T. and Slomp, C. P. (2013b) 'Rapid high-amplitude variability in Baltic Sea hypoxia during the Holocene', *Geology*, vol. 41, p.1183-1186.

Jilbert, T., Slomp, C. P., Gustafsson, B. G. and Boer, W. (2011) 'Beyond the Fe-P-redox connection: preferential regeneration of phosphorus from organic matter as a key control on Baltic Sea nutrient cycles', *Biogeosciences*, vol. 8, p.1699-1720.

Johansson, J. (2017) Total and regional runoff to the Baltic Sea. HELCOM Baltic Sea Environment Fact Sheets(Online).

Jones, C. E. and Jenkyns, H. C. (2001) 'Seawater strontium isotopes, oceanic anoxic events, and seafloor hydrothermal activity in the Jurassic and Cretaceous', *American Journal of Science*, vol. 301, p.112-149.

Józsa, Š., Suan, G. and Schlögl, J. (2018) 'Benthic foraminiferal bioevents in lower to upper Toarcian strata of Southern Beaujolais (SE France)', *Geobios*, vol. 51, p.137-150.

Kabel, K., Moros, M., Porsche, C., Neumann, T., Adolphi, F., Andersen, T. J., Siegel, H., Gerth, M., Leipe, T., Jansen, E. and Sinninghe Damste, J. S. (2012) 'Impact of climate change on the Baltic Sea ecosystem over the past 1,000 years', *Nature Clim. Change*, vol. 2, p.871-874.

Kane, J. S., Arbogast, B. and Leventhal, J. (1990) 'Characterization of Devonian Ohio Shale SDO-1 as a USGS Geochemical Reference Sample', *Geostandards Newsletter*, vol. 14, p.169-196.

Karl, T. R. and Trenberth, K. E. (2003) 'Modern Global Climate Change', *Science*, vol. 302, p.1719-1723.

Keeling, R. F., Körtzinger, A. and Gruber, N. (2010) 'Ocean Deoxygenation in a Warming World', *Annual Review of Marine Science*, vol. 2, p.199-229.

Kemp, D. B., Coe, A. L., Cohen, A. S. and Schwark, L. (2005) 'Astronomical pacing of methane release in the Early Jurassic period', *Nature*, vol. 437, p.396-399.

Kemp, D. B., Coe, A. L., Cohen, A. S. and Weedon, G. P. (2011) 'Astronomical forcing and chronology of the early Toarcian (Early Jurassic) oceanic anoxic event in Yorkshire, UK', *Paleoceanography*, vol. 26, p.1-17.

Kemp, D. B. and Izumi, K. (2014) 'Multiproxy geochemical analysis of a Panthalassic margin record of the early Toarcian oceanic anoxic event (Toyora area, Japan)', *Palaeogeography, Palaeoclimatology, Palaeoecology*, vol. 414, p.332-341.

Kendall, B., Dahl, T. W. and Anbar, A. D. (2017) 'The Stable Isotope Geochemistry of Molybdenum', *Reviews in Mineralogy and Geochemistry*, vol. 82, p.683-732.

Kennedy, C. (2016) Climate Change: Atmospheric Carbon Dioxide. NOAA (https://www.climate.gov/news-features/understanding-climate/climate-change-atmospheric-carbon-dioxide).

Korte, C., Hesselbo, S. P., Ullmann, C. V., Dietl, G., Ruhl, M., Schweigert, G. and Thibault, N. (2015) 'Jurassic climate mode governed by ocean gateway', *Nat Commun*, vol. 6, p.1-7.

Küspert, W. (1982) *'Environmental changes during oil shale deposition as deduced from stable isotope ratios'*, in: Einsele, G. and Seilacher, A. (eds), *Cyclic and event stratification*. (Berlin) Springer, p.482-501.

Le Quéré, C., Andrew, R. M., Canadell, J. G., Sitch, S., Korsbakken, J. I., Peters, G. P., Manning, A. C., Boden, T. A., Tans, P. P., Houghton, R. A., Keeling, R. F., Alin, S., Andrews, O. D., Anthoni, P., Barbero, L., Bopp, L., Chevallier, F., Chini, L. P., Ciais, P., Currie, K., Delire, C., Doney, S. C., Friedlingstein, P., Gkritzalis, T., Harris, I., Hauck, J., Haverd, V., Hoppema, M., Klein Goldewijk, K., Jain, A. K., Kato, E., Körtzinger, A., Landschützer, P., Lefèvre, N., Lenton, A., Lienert, S., Lombardozzi, D., Melton, J. R., Metzl, N., Millero, F., Monteiro, P. M. S., Munro, D. R., Nabel, J. E. M. S., Nakaoka, S.-i., amp, apos, Brien, K., Olsen, A., Omar, A. M., Ono, T., Pierrot, D., Poulter, B., Rödenbeck, C., Salisbury, J., Schuster, U., Schwinger, J., Séférian, R., Skjelvan, I., Stocker, B. D., Sutton, A. J., Takahashi, T., Tian, H., Tilbrook, B., van der Laan-Luijkx, I. T., van der Werf, G. R., Viovy, N., Walker, A. P., Wiltshire, A. J. and Zaehle, S. (2016) 'Global Carbon Budget 2016', *Earth System Science Data*, vol. 8, p.605-649.

Lenz, C., Jilbert, T., Conley, D. J. and Slomp, C. P. (2015a) 'Hypoxia-driven variations in iron and manganese shuttling in the Baltic Sea over the past 8Kyr', *Geochemistry Geophysics Geosystems*, vol. 16, p.3754-3766.

Lenz, C., Jilbert, T., Conley, D. J., Wolthers, M. and Slomp, C. P. (2015b) 'Are recent changes in sediment manganese sequestration in the euxinic basins of the Baltic Sea linked to the expansion of hypoxia?', *Biogeosciences*, vol. 12, p.4875-4894.

Li, Q., McArthur, J. M. and Atkinson, T. C. (2012) 'Lower Jurassic belemnites as indicators of palaeo-temperature', *Palaeogeography, Palaeoclimatology, Palaeoecology*, vol. 315-316, p.38-45.

Liu, R., Hu, L. and Humayun, M. (2017) 'Natural variations in the rhenium isotopic composition of meteorites', *Meteoritics & Planetary Science*, vol. 52, p.479-492.

Lu, Z., Jenkyns, H. C. and Rickaby, R. E. M. (2010) 'Iodine to calcium ratios in marine carbonate as a paleo-redox proxy during oceanic anoxic events', *Geology*, vol. 38, p.1107-1110.

Lyons, T. W., Anbar, A. D., Severmann, S., Scott, C. and Gill, B. C. (2009) 'Tracking Euxinia in the Ancient Ocean: A Multiproxy Perspective and Proterozoic Case Study', *Annual Review of Earth and Planetary Sciences*, vol. 37, p.507-534.

Martindale, R. C., Them, T. R., Gill, B. C., Marroquín, S. M. and Knoll, A. H. (2017) 'A new Early Jurassic (ca. 183 Ma) fossil Lagerstätte from Ya Ha Tinda, Alberta, Canada', *Geology*, vol. 45, p.255-258.

Matthäus, W. and Franck, H. (1992) 'Characteristics of major Baltic inflows - a statistical analysis', *Continental shelf research*, vol. 12, p.1375-1400.

McArthur, J. M., Algeo, T. J., van de Schootbrugge, B., Li, Q. and Howarth, R. J. (2008) 'Basinal restriction, black shales, Re-Os dating, and the Early Toarcian (Jurassic) oceanic anoxic event', *Paleoceanography*, vol. 23, p.1-22.

McArthur, J. M., Donovan, D. T., Thirlwall, M. F., Fouke, B. W. and Mattey, D. (2000) 'Strontium isotope profile of the early Toarcian (Jurassic) oceanic anoxic event, the duration of ammonite biozones, and belemnite palaeotemperatures', *Earth and Planetary Science Letters*, vol. 179, p.269-285.

McCormick, L. R. and Levin, L. A. (2017) 'Physiological and ecological implications of ocean deoxygenation for vision inmarine organisms', *Philosophical Transactions of the Royal Society A: Mathematical, Physical and Engineering Sciences*, vol. 375, p.1-26.

McElwain, J. C., Wade-Murphy, J. and Hesselbo, S. P. (2005) 'Changes in carbon dioxide during an oceanic anoxic event linked to intrusion into Gondwana coals', *Nature*, vol. 435, p.479-482.

McLennan, S. M. (2001) 'Relationships between the trace element composition of sedimentary rocks and upper continental crust', *Geochemistry Geophysics Geosystems*, vol. 2.

McManus, J., Berelson, W. M., Severmann, S., Poulson, R. L., Hammond, D. E., Klinkhammer, G. P. and Holm, C. (2006) 'Molybdenum and uranium geochemistry in continental margin sediments: Paleoproxy potential', *Geochimica et Cosmochimica Acta*, vol. 70, p.4643-4662.

McManus, J., Nagler, T., Siebert, C., Wheat, C. G. and Hammond, D. E. (2002) 'Oceanic molybdenum isotope fractionation: diagenesis and hydrothermal ridge-flank alteration', *Geochemistry Geophysics Geosystems*, vol. 3, p.1078.

Metodiev, L. S., Savov, I. P., Gröcke, D. R., Wignall, P. B., Newton, R. J., Andreeva, P. V. and Koleva-Rekalova, E. K. (2014) 'Palaeoenvironmental conditions recorded by 87Sr/86Sr, δ13C and δ18O in late Pliensbachian–Toarcian (Jurassic) belemnites from Bulgaria', *Palaeogeography, Palaeoclimatology, Palaeoecology*, vol.

Miller, C. A. (2009) *Surface-cycling of rhenium and its isotopes,* PhD thesis, Cambridge, Massachusetts, MIT/WHOI.

Miller, C. A., Peucker-Ehrenbrink, B. and Ball, L. (2009) 'Precise determination of rhenium isotope composition by multi-collector inductively-coupled plasma mass spectrometry', *Journal of Analytical Atomic Spectrometry*, vol. 24, p.1069-1078.

Miller, C. A., Peucker-Ehrenbrink, B. and Schauble, E. A. (2015) 'Theoretical modeling of rhenium isotope fractionation, natural variations across a black shale weathering profile, and potential as a paleoredox proxy', *Earth and Planetary Science Letters*, vol. 430, p.339-348.

Miller, C. A., Peucker-Ehrenbrink, B., Walker, B. D. and Marcantonio, F. (2011) 'Re-assessing the surface cycling of molybdenum and rhenium', *Geochimica et Cosmochimica Acta*, vol. 75, p.7146-7179.

Mohrholz, V., Naumann, M., Nausch, G., Krüger, S. and Gräwe, U. (2015) 'Fresh oxygen for the Baltic Sea — An exceptional saline inflow after a decade of stagnation', *Journal of Marine Systems*, vol. 148, p.152-166.

Monien, P., Lettmann, K. A., Monien, D., Asendorf, S., Wölfl, A.-C., Lim, C. H., Thal, J., Schnetger, B. and Brumsack, H.-J. (2014) 'Redox conditions and trace metal cycling in coastal sediments from the maritime Antarctic', *Geochimica et Cosmochimica Acta*, vol. 141, p.26-44.

Montero-Serrano, J.-C., Föllmi, K. B., Adatte, T., Spangenberg, J. E., Tribovillard, N., Fantasia, A. and Suan, G. (2015) 'Continental weathering and redox conditions during the early Toarcian Oceanic Anoxic Event in the northwestern Tethys: Insight from the Posidonia Shale section in the Swiss Jura Mountains', *Palaeogeography, Palaeoclimatology, Palaeoecology*, vol. 429, p.83-99.

Montoya-Pino, C., Weyer, S., Anbar, A. D., Pross, J., Oschmann, W., van de Schootbrugge, B. and Arz, H. W. (2010) 'Global enhancement of ocean anoxia during Oceanic Anoxic Event 2: A quantitative approach using U isotopes', *Geology*, vol. 38, p.315-318.

Morford, J. L. and Emerson, S. (1999) 'The geochemistry of redox sensitive trace metals in sediments', *Geochimica et Cosmochimica Acta*, vol. 63, p.1735-1750.

Morford, J. L., Emerson, S. R., Breckel, E. J. and Kim, S. H. (2005) 'Diagenesis of oxyanions (V, U, Re, and Mo) in pore waters and sediments from a continental margin', *Geochimica et Cosmochimica Acta*, vol. 69, p.5021-5032.

Morford, J. L., Martin, W. R. and Carney, C. M. (2012) 'Rhenium geochemical cycling: Insights from continental margins', *Chemical Geology*, vol. 324-325, p.73-86.

Morford, J. L., Martin, W. R., François, R. and Carney, C. M. (2009) 'A model for uranium, rhenium, and molybdenum diagenesis in marine sediments based on results from coastal locations', *Geochimica et Cosmochimica Acta*, vol. 73, p.2938-2960.

Morford, J. L., Martin, W. R., Kalnejais, L. H., Francois, R., Bothner, M. and Karle, I.-M. (2007) 'Insights on geochemical cycling of U, Re and Mo from seasonal sampling in Boston Harbor, Massachusetts, USA', *Geochimica et Cosmochimica Acta*, vol. 71, p.895-917.

Morris, A. (1975) 'Dissolved molybdenum and vanadium in the northeast Atlantic Ocean', *Deep Sea Research*, vol. 22, p.49-54.

Mort, H. P., Slomp, C. P., Gustafsson, B. G. and Andersen, T. J. (2010) 'Phosphorus recycling and burial in Baltic Sea sediments with contrasting redox conditions', *Geochimica et Cosmochimica Acta*, vol. 74, p.1350-1362.

Nägler, T. F., Neubert, N., Bottcher, M. E., Dellwig, O. and Schnetger, B. (2011) 'Molybdenum isotope fractionation in pelagic euxinia: evidence from the modern Black and Baltic Seas. ', *Chemical Geology*, vol. 289, p.1-11.

Nakagawa, Y., Takano, S., Firdaus, M. L., Norisuye, K., Hirata, T., Vance, D. and Sohrin, Y. (2012) 'The molybdenum isotopic composition of the modern ocean', *Journal of Geochemistry*, vol. 46, p.131-141.

Neubert, N., Heri, A., Voegelin, A. R., Nagler, T., Schlunegger, F. and Villa, I. (2011) 'The molybdenum isotopic composition in river water: constraints from small catchments', *Earth and Planetary Science Letters*, vol. 304, p.180-190.

Neubert, N., Miller, C. A., Peucker-Ehrenbrink, B. and Schubert, M. (2010a) Rhenium isotope variations in modern environments. Goldschmidt conference abstract, p.A754.

Neubert, N., Miller, C. A., Peucker-Ehrenbrink, B. and Schubert, M. (2010b) Rhenium isotopes: applications to modern environments. EGU General Assembly

Neubert, N., Nägler, T. F. and Böttcher, M. E. (2008) 'Sulfidity controls molybdenum isotope fractionation into euxinic sediments: Evidence from the modern Black Sea', *Geology*, vol. 36, p.775.

Neumann, T., Heiser, U., Leosson, M. A. and Kersten, M. (2002) 'Early diagenetic processes during Mn-carbonate formation: evidence from the isotopic composition of authigenic Ca-rhodochrosites of the Baltic Sea', *Geochimica et Cosmochimica Acta*, vol. 66, p.867-879.

Newton, P. B. W. a. R. (1998) 'Pyrite framboid diameter as a measure of oxygen deficiency in ancient mudrocks', *American Journal of Science*, vol. 298, p.537-552.

Newton, R. J., Reeves, E. P., Kafousia, N., Wignall, P. B., Bottrell, S. H. and Sha, J. G. (2011) 'Low marine sulfate concentrations and the isolation of the European epicontinental sea during the Early Jurassic', *Geology*, vol. 39, p.7-10.

Nielsen, S. G., Goff, M., Hesselbo, S. P., Jenkyns, H. C., LaRowe, D. E. and Lee, C.-T. A. (2011) 'Thallium isotopes in early diagenetic pyrite – A paleoredox proxy?', *Geochimica et Cosmochimica Acta*, vol. 75, p.6690-6704.

Nikitenko, B. L., Reolid, M. and Glinskikh, L. (2013) 'Ecostratigraphy of benthic foraminifera for interpreting Arctic record of Early Toarcian biotic crisis (Northern Siberia, Russia)', *Palaeogeography, Palaeoclimatology, Palaeoecology*, vol. 376, p.200-212.

Noddack, I. and Noddack, W. (1929) 'Die Sauerstoffverbindungen des Rheniums', *Die Naturwissenschaften*, vol. 17, p.93-94.

Noordmann, J., Weyer, S., Montoya-Pino, C., Dellwig, O., Neubert, N., Eckert, S., Paetzel, M. and Böttcher, M. E. (2015) 'Uranium and molybdenum isotope systematics in modern euxinic basins: Case studies from the central Baltic Sea and the Kyllaren fjord (Norway)', *Chemical Geology*, vol. 396, p.182-195.

Oschlies, A., Duteil, O., Getzlaff, J., Koeve, W., Landolfi, A. and Schmidtko, S. (2017) 'Patterns of deoxygenation: sensitivity to natural and anthropogenic drivers', *Philosophical Transactions of the Royal Society A: Mathematical, Physical and Engineering Sciences*, vol. 375, p.1-16.

Owens, J. D., Nielsen, S. G., Horner, T. J., Ostrander, C. M. and Peterson, L. C. (2017) 'Thallium-isotopic compositions of euxinic sediments as a proxy for global manganese-oxide burial', *Geochimica et Cosmochimica Acta*, vol. 213, p.291-307.

Page, K. N. (2003) 'The Lower Jurassic of Europe: its subdivision and correlation', *Geological Survey of Denmark and Greenland Bulletin*, vol. 1, p.23-59.

Pálfy, J. and Smith, P. L. (2000) 'Synchrony between Early Jurassic extinction, oceanic anoxic event, and the Karoo-Ferrar flood basalt volcanism', *Geology*, vol. 28, p.747-750.

Pancost, R. D., Crawford, N., Magness, S., Turner, A., Jenkyns, H. C. and Maxwell, J. R. (2004) 'Further evidence for the development of photic-zone euxinic conditions during Mesozoic oceanic anoxic events', *Journal of the Geological Society*, vol. 161, p.353-364.

Pearce, C. R. (2007) *The development and application of the molybdenum stable isotope system as a proxy for changes in marine anoxia,* PhD thesis, Milton Keynes, The Open University.

Pearce, C. R., Burton, K. W., E., P. v. S. P. A., H., J. R. and R., G. S. (2010a) 'Molybdenum isotope behaviour acompanying weathering and riverine transport in a basaltic terrain', *Earth and Planetary Science Letters*, vol. 295, p.104-114.

Pearce, C. R., Coe, A. L. and Cohen, A. S. (2010b) 'Seawater redox variations during the deposition of the Kimmeridge Clay Formation, United Kingdom (Upper Jurassic): Evidence from molybdenum isotopes and trace metal ratios', *Paleoceanography*, vol. 25, p.1-15.

Pearce, C. R., Cohen, A. S., Coe, A. L. and Burton, K. W. (2008) 'Molybdenum isotope evidence for global ocean anoxia coupled with perturbations to the carbon cycle during the early Jurassic', *Geology*, vol. 36, p.231-234.

Pearce, C. R., Cohen, A. S. and Parkinson, I. J. (2009) 'Quantitative Separation of Molybdenum and Rhenium from Geological Materials for Isotopic Determination by MC-ICP-MS', *Geostandards and Geoanalytcal Research*, vol. 33, p.219-229.

Percival, L. M. E., Cohen, A. S., Davies, M. K., Dickson, A. J., Hesselbo, S. P., Jenkyns, H. C., Leng, M. J., Mather, T. A., Storm, M. S. and Xu, W. (2016) 'Osmium isotope evidence for two pulses of increased continental weathering linked to Early Jurassic volcanism and climate change', *Geology*, vol. 44, p.759-762.

Peti, L. and Thibault, N. (2017) 'Abundance and size changes in the calcareous nannofossil Schizosphaerella – Relation to sea-level, the carbonate factory and palaeoenvironmental change from the Sinemurian to earliest Toarcian of the Paris Basin', *Palaeogeography, Palaeoclimatology, Palaeoecology*, vol. article in press, p.1-12.

Poirier, A. and Doucelance, R. (2009) 'Effective Correction of Mass Bias for Rhenium Measurements by MC-ICP-MS', *Geostandards and Geoanalytcal Research*, vol. 33, p.195 - 204.

Poirier, A. and Gariepy, C. (2005) 'Isotopic Signature and Impact of Car Catalysts on the Anthropogenic Osmium Budget', *Environ Sci Technol*, vol. 39, p.4431-4434.

Poulson Brucker, R. L., McManus, J., Severmann, S. and Berelson, W. M. (2009) 'Molybdenum behavior during early diagenesis: Insights from Mo isotopes', *Geochemistry, Geophysics, Geosystems*, vol. 10, p.Q06010.

Poulson, R. L., Siebert, C., McManus, J. and Berelson, W. M. (2006) 'Authigenic molybdenum isotope signatures in marine sediments', *Geology*, vol. 34, p.617-620.

Racionero-Gómez, B., Sproson, A. D., Selby, D., Grocke, D. R., Redden, H. and Greenwell, H. C. (2016) 'Rhenium uptake and distribution in phaeophyceae macroalgae, Fucus vesiculosus', *Royal Society Open Science*, vol. 3, p.1-18.

Rahaman, W., Singh, S. K. and Shukla, A. D. (2012) 'Rhenium in Indian rivers: Sources, fluxes, and contribution to oceanic budget', *Geochemistry, Geophysics, Geosystems*, vol. 13, p.1-21.

Raiswell, R., Bottrell, S. H., Al-Biatty, H. J. and Tan, M. M. (1993) 'The influence of bottom water oxygenation and reactive iron content on sulfur incorporation into bitumens from Jurassic marine shales', *American Journal of Science*, vol. 293, p.569-596.

Rampino, M. R. and Caldeira, K. (2017) 'Comparison of the ages of large-body impacts, flood-basalt eruptions, ocean-anoxic events and extinctions over the last 260 million years: a statistical study', *International Journal of Earth Sciences*, vol. 107, p.601-606.

Reisberg, L. and Meisel, T. (2002) 'The Re-Os isotopic system: A review of analytical techniques', *Geostandards Newsletter: The Journal of Geostandards and Geoanalysis*, vol. 26, p.249 - 267.

Robinson, R. and Thoennessen, M. (2012) 'Discovery of tantalum, rhenium, osmium, and iridium isotopes', *Atomic Data and Nuclear Data Tables*, vol. 98, p.911-932.

Robinson, R. S., Kienast, M., Luiza Albuquerque, A., Altabet, M., Contreras, S., De Pol Holz, R., Dubois, N., Francois, R., Galbraith, E., Hsu, T.-C., Ivanochko, T., Jaccard, S., Kao, S.-J., Kiefer, T., Kienast, S., Lehmann, M., Martinez, P., McCarthy, M., Möbius, J., Pedersen, T., Quan, T. M., Ryabenko, E., Schmittner, A., Schneider, R., Schneider-Mor, A., Shigemitsu, M., Sinclair, D., Somes, C., Studer, A., Thunell, R. and Yang, J.-Y. (2012) 'A review of nitrogen isotopic alteration in marine sediments', *Paleoceanography*, vol. 27, p.1-13.

Rolison, J. M., Stirling, C. H., Middag, R. and Rijkenberg, M. J. A. (2017) 'Uranium stable isotope fractionation in the Black Sea: Modern calibration of the 238 U/ 235 U paleo-redox proxy', *Geochimica et Cosmochimica Acta*, vol. 203, p.69-88.

Rosales, I., Barnolas, A., Goy, A., Sevillano, A., Armendáriz, M. and López-García, J. M. (2018) 'Isotope records (C-O-Sr) of late Pliensbachian-early Toarcian environmental

perturbations in the westernmost Tethys (Majorca Island, Spain)', *Palaeogeography, Palaeoclimatology, Palaeoecology*, vol. 497, p.168-185.

Rosenzweig, C., Karoly, D., Vicarelli, M., Neofotis, P., Wu, Q., Casassa, G., Menzel, A., Root, T. L., Estrella, N., Seguin, B., Tryjanowski, P., Liu, C., Rawlins, S. and Imeson, A. (2008) 'Attributing physical and biological impacts to anthropogenic climate change', *Nature*, vol. 453, p.353-357.

Rothman, D. H. (2017) 'Thresholds of catastrophe in the Earth system', *Science Advances*, vol. 3, p.1-12.

Ruebsam, W., Dickson, A. J., Hoyer, E.-M. and Schwark, L. (2017) 'Multiproxy reconstruction of oceanographic conditions in the southern epeiric Kupferschiefer Sea (Late Permian) based on redox-sensitive trace elements, molybdenum isotopes and biomarkers', *Gondwana Research*, vol. 44, p.205-218.

Ruebsam, W., Müller, T., Kovács, J., Pálfy, J. and Schwark, L. (2018) 'Environmental response to the early Toarcian carbon cycle and climate perturbations in the northeastern part of the West Tethys shelf', *Gondwana Research*, vol. 59, p.144-158.

Sandoval, J., Bill, M., Aguado, R., O'Dogherty, L., Rivas, P., Morard, A. and Guex, J. (2012) 'The Toarcian in the Subbetic basin (southern Spain): Bio-events (ammonite and calcareous nannofossils) and carbon-isotope stratigraphy', *Palaeogeography, Palaeoclimatology, Palaeoecology*, vol. 342-343, p.40-63.

Savchuk, O. P., Wulff, F., Hille, S., Humborg, C. and Pollehne, F. (2008) 'The Baltic Sea a century ago — a reconstruction from model simulations, verified by observations', *Journal of Marine Systems*, vol. 74, p.485-494.

Schinke, H. and Matthäus, W. (1998) 'On the causes of major Baltic inflows —an analysis of long time series', *Continental shelf research*, vol. 18, p.67-97.

Schlanger, S. O. and Jenkyns, H. C. (1976) 'Cretaceous Oceanic Anoxic Events: Causes and Consequences', *Geologie en Mijnbouw*, vol. 55, p.179-184.

Schmidtko, S., Stramma, L. and Visbeck, M. (2017) 'Decline in global oceanic oxygen content during the past five decades', *Nature*, vol. 542, p.335-339.

Scholz, F., Siebert, C., Dale, A. W. and Frank, M. (2017) 'Intense molybdenum accumulation in sediments underneath a nitrogenous water column and implications for the reconstruction of paleo-redox conditions based on molybdenum isotopes', *Geochimica et Cosmochimica Acta*, vol. 213, p.400-417.

Schouten, S., Van Kaam-Peters, H. M. E., Rijpstra, W. I. C., Schoell, M. and Sinninghe Damste, J. S. (2000) 'Effects of an oceanic anoxic event on the stable carbon isotopic composition of early Toarcian carbon', *American Journal of Science*, vol. 300, p.1-22.

Schwark, L. and Frimmel, A. (2004) 'Chemostratigraphy of the Posidonia Black Shale, SW-Germany', *Chemical Geology*, vol. 206, p.231-248.

Scott, C. T. and Lyons, T. (2012) 'Contrasting molybdenum cycling and isotopic properties in euxinic versus non-euxinic sediments and sedimentary rocks: Refining the paleoproxies', *Chemical Geology*, vol. 324-325, p.19-27.

Selby, D. and Creaser, R. A. (2003) 'Re–Os geochronology of organic rich sediments: an evaluation of organic matter analysis methods', *Chemical Geology*, vol. 200, p.225-240.

Selby, D., Creaser, R. A., Stein, H. J., Markey, R. J. and Hannah, J. L. (2007) 'Assessment of the 187Re decay constant by cross calibration of Re–Os molybdenite and U–Pb zircon

chronometers in magmatic ore systems', *Geochimica et Cosmochimica Acta*, vol. 71, p.1999-2013.

Sell, B., Ovtcharova, M., Guex, J., Bartolini, A., Jourdan, F., Spangenberg, J. E., Vicente, J.-C. and Schaltegger, U. (2014) 'Evaluating the temporal link between the Karoo LIP and climatic–biologic events of the Toarcian Stage with high-precision U–Pb geochronology', *Earth and Planetary Science Letters*, vol. 408, p.48-56.

Shepherd, J. G., Brewer, P. G., Oschlies, A. and Watson, A. J. (2017) 'Ocean ventilation and deoxygenation in a warming world: introduction and overview', *Philosophical Transactions of the Royal Society A: Mathematical, Physical and Engineering Sciences*, vol. 375, p.1-12.

Siebert, C., Kramers, J. D., Meisel, T., Morel, P. and Nagler, T. (2005) 'PGE, Re-Os, and Mo isotope systematics in Archean and early Proterozoic sedimentary systems as proxies for redox conditions of the early Earth. ', *Geochimica et Cosmochimica Acta*, vol. 69, p.1787-1801.

Siebert, C., McManus, J., Bice, A., Poulson, R. L. and Berelson, W. M. (2006) 'Molybdenum isotope signatures in continental margin sediments', *Earth and Planetary Science Letters*, vol. 241, p.723-733.

Siebert, C., Nägler, T. F., von Blanckenburg, F. and Kramers, J. D. (2003) 'Molybdenum isotope records as a potential new proxy for paleoceanography', *Earth and Planetary Science Letters*, vol. 211, p.159-171.

Siebert, C., Pett-Ridge, J. C., Opfergelt, S., Guicharnaud, R. A., Halliday, A. N. and Burton, K. W. (2015) 'Molybdenum isotope fractionation in soils: Influence of redox conditions, organic matter, and atmospheric inputs', *Geochimica et Cosmochimica Acta*, vol. 162, p.1-24.

Slomp, C. P. (2016) Personal communication. (unpublished).

Stendardo, I. and Gruber, N. (2012) 'Oxygen trends over five decades in the North Atlantic', *Journal of Geophysical Research: Oceans*, vol. 117, p.1-18.

Stramma, L., Schmidtko, S., Levin, L. A. and Johnson, G. C. (2010) 'Ocean oxygen minima expansions and their biological impacts', *Deep Sea Research Part I: Oceanographic Research Papers*, vol. 57, p.587-595.

Suan, G., Mattioli, E., Pittet, B., Lécuyer, C., Suchéras-Marx, B., Duarte, L. V., Philippe, M., Reggiani, L. and Martineau, F. (2010) 'Secular environmental precursors to Early Toarcian (Jurassic) extreme climate changes', *Earth and Planetary Science Letters*, vol. 290, p.448-458.

Suan, G., Nikitenko, B. L., Rogov, M. A., Baudin, F., Spangenberg, J. E., Knyazev, V. G., Glinskikh, L. A., Goryacheva, A. A., Adatte, T., Riding, J. B., Föllmi, K. B., Pittet, B., Mattioli, E. and Lécuyer, C. (2011) 'Polar record of Early Jurassic massive carbon injection', *Earth and Planetary Science Letters*, vol. 312, p.102-113.

Suan, G., Pittet, B., Bour, I., Mattioli, E., Duarte, L. and Mailliot, S. (2008) 'Duration of the Early Toarcian carbon isotope excursion deduced from spectral analysis: Consequence for its possible causes', *Earth and Planetary Science Letters*, vol. 267, p.666-679.

Svensen, H., Planke, S., Chevallier, L., Malthe-Sørenssen, A., Corfu, F. and Jamtveit, B. (2007) 'Hydrothermal venting of greenhouse gases triggering Early Jurassic global warming', *Earth and Planetary Science Letters*, vol. 256, p.554-566.

Them, T. R., Gill, B. C., Caruthers, A. H., Gerhardt, A. M., Gröcke, D. R., Lyons, T. W., Marroquín, S. M., Nielsen, S. G., Trabucho Alexandre, J. P. and Owens, J. D. (2018) 'Thallium isotopes reveal protracted anoxia during the Toarcian (Early Jurassic) associated with volcanism,

carbon burial, and mass extinction', *Proceedings of the National Academy of Sciences*, vol. 115, p.6596-6601.

Them, T. R., Gill, B. C., Selby, D., Grocke, D. R., Friedman, R. M. and Owens, J. D. (2017) 'Evidence for rapid weathering response to climatic warming during the Toarcian Oceanic Anoxic Event', *Nature Scientific Reports*, vol. 7, p.5003.

Thibault, N., Ruhl, M., Ullmann, C. V., Korte, C., Kemp, D. B., Gröcke, D. R. and Hesselbo, S. P. (2018) 'The wider context of the Lower Jurassic Toarcian oceanic anoxic event in Yorkshire coastal outcrops, UK', *Proceedings of the Geologists' Association*, vol. 129, p.372-391.

Tribovillard, N., Algeo, T. J., Baudin, F. and Riboulleau, A. (2012) 'Analysis of marine environmental conditions based onmolybdenum–uranium covariation—Applications to Mesozoic paleoceanography', *Chemical Geology*, vol. 324–325, p.46-58.

Tribovillard, N., Algeo, T. J., Lyons, T. and Riboulleau, A. (2006) 'Trace metals as paleoredox and paleoproductivity proxies: An update', *Chemical Geology*, vol. 232, p.12-32.

van Breugel, Y., Baas, M., Schouten, S., Mattioli, E. and Damsté, J. S. S. (2006) 'Isorenieratane record in black shales from the Paris Basin, France: Constraints on recycling of respired CO2 as a mechanism for negative carbon isotope shifts during the Toarcian oceanic anoxic event', *Paleoceanography*, vol. 21.

van de Schootbrugge, B. (2005) 'Toarcian oceanic anoxic event: An assessment of global causes using belemnite C isotope records', *Paleoceanography*, vol. 20, p.1-10.

Walker, R. J. (1988) 'Low-blank chemical separation of rhenium and osmium from gram quantities of silicate rock for measurement by resonance ionization mass spectrometry', *Analytical Chemistry*, vol. 60, p.1231-1234.

Watson, A. J., Lenton, T. M. and Mills, B. J. W. (2017) 'Ocean deoxygenation, the global phosphorus cycle and the possibility of human-caused large-scale ocean anoxia', *Philosophical Transactions of the Royal Society A: Mathematical, Physical and Engineering Sciences*, vol. 375, p.1-14.

Wedepohl, K. H. (1976) *'Handbook of Geochemistry'*, in: Morris, D. F. C. and Short, E. L. (eds), *Handbook of Geochemistry*. (Berlin) Springer-Verlag, p.75-113.

Weyer, S., Anbar, A. D., Gerdes, A., Gordon, G. W., Algeo, T. J. and Boyle, E. A. (2008) 'Natural fractionation of 238U/235U', *Geochimica et Cosmochimica Acta*, vol. 72, p.345-359.

Whitney, F. A., Freeland, H. J. and Robert, M. (2007) 'Persistently declining oxygen levels in the interior waters of the eastern subarctic Pacific', *Progress in Oceanography*, vol. 75, p.179-199.

Wignall, P. B., Newton, R. J. and Little, C. T. S. (2005) 'The timing of paleoenvironmental change and cause-and-effect relationships during the early Jurassic mass extinction in Europe', *American Journal of Science*, vol. 305, p.1014-1032.

Williams, M., Benton, M. J. and Ross, A. (2015) 'The Strawberry Bank Lagerstatte reveals insights into Early Jurassic life', *Journal of the Geological Society*, vol. 172, p.683-692.

Xu, W., Ruhl, M., Jenkyns, H. C., Hesselbo, S. P., Riding, J. B., Selby, D., Naafs, B. D. A., Weijers, J. W. H., Pancost, R. D., Tegelaara, E. W. and Idiz, E. F. (2017) 'Carbon sequestration in an expanded lake system during the Toarcian oceanic anoxic event', *Nature Geoscience*, vol. 10, p.129-134.

Xu, W., Ruhl, M., Jenkyns, H. C., Leng, M. J., Huggett, J. M., Minisini, D., Ullmann, C. V., Riding, J. B., Weijers, J. W. H., Storm, M. S., Percival, L. M. E., Tosca, N. J., Idiz, E. F., Tegelaar, E. W. and Hesselbo, S. P. (2018) 'Evolution of the Toarcian (Early Jurassic) carbon-cycle and

global climatic controls on local sedimentary processes (Cardigan Bay Basin, UK)', *Earth and Planetary Science Letters*, vol. 484, p.396-411.

Zillén, L. and Conley, D. J. (2010) 'Hypoxia and cyanobacteria blooms - are they really natural features of the late Holocene history of the Baltic Sea?', *Biogeosciences*, vol. 7, p.2567-2580.

Zillén, L., Conley, D. J., Andrén, T., Andrén, E. and Björck, S. (2008) 'Past occurrences of hypoxia in the Baltic Sea and the role of climate variability, environmental change and human impact', *Earth-Science Reviews*, vol. 91, p.77-92.

Zimmerman, A., Georgiev, S., Yang, G., Stein, H. J. and Hannah, J. L. (2011) Possible rhenium fractionation during standard Re-Os dissolution and chemical separation procedures. Goldschmidt. Mineralogical magazine, p.2287.

Zimmerman, A., Stein, H. and Hannah, J. (2013) Additional insight into natural $^{185}Re/^{187}Re$ of various materials. Goldschmidt. Mineralogical magazine, p.2619.

Appendix

Standard data for SRM3143

This appendix contains the data for all SRM3143 analysed during the Re isotope composition determinations in this thesis. The single element standard SRM3143 was used as a bracketing standard for δ^{187}Re determinations, and to provide an estimate of the external reproducibility of analyses. The data are presented in three tables with Tables A1, A2, and A3 showing all SRM3143 data relating to Chapters 3, 6 and 4 respectively.

Table A1: Table of Re isotope composition data for all analyses of standard SRM3143 carried out during the development of the method presented in Chapter 3. For all standards analysed, Ir was added to make Ir concentration of 200 ppb.

Analysis no.	Date	[Re][1] (ppb)	$^{187}Re/^{185}Re$[2]	Raw $^{193}Ir/^{191}Ir$	Raw $^{187}Re/^{185}Re$	$\delta^{187}Re$[3]
1	22.04.2013	20	1.669980	1.707024	1.694619	-
2	22.04.2013	20	1.670135	1.706876	1.694584	0.106
3	22.04.2013	20	1.669936	1.707122	1.694663	-0.081
4	22.04.2013	20	1.670009	1.707014	1.694626	0.007
5	22.04.2013	20	1.670059	1.706944	1.694583	0.000
6	22.04.2013	20	1.670107	1.706981	1.694716	0.014
7	22.04.2013	20	1.670109	1.706978	1.694718	0.047
8	22.04.2013	20	1.669955	1.707151	1.694713	-0.092
9	22.04.2013	20	1.670109	1.706948	1.694683	0.014
10	22.04.2013	20	1.670217	1.706830	1.694655	0.096
11	22.04.2013	20	1.670004	1.707123	1.694780	-0.055
12	22.04.2013	20	1.669974	1.707063	1.694669	-0.003
13	22.04.2013	20	1.669956	1.707064	1.694631	-0.037
14	22.04.2013	20	1.670059	1.707073	1.694766	0.068
15	22.04.2013	20	1.669934	1.707105	1.694679	-0.031
16	22.04.2013	20	1.669911	1.707061	1.694617	-0.009
17	22.04.2013	20	1.669918	1.707050	1.694595	-0.011
18	22.04.2013	20	1.669962	1.707055	1.694600	-
20	30.04.2013	20	1.669937	1.706290	1.693812	-
21	30.04.2013	20	1.669970	1.706146	1.693702	-0.018
22	30.04.2013	20	1.670065	1.705845	1.693477	0.045
23	30.04.2013	20	1.670007	1.705869	1.693458	-0.019
24	30.04.2013	20	1.670013	1.705860	1.693447	0.007
25	30.04.2013	20	1.669995	1.705704	1.693286	-0.026
26	30.04.2013	20	1.670062	1.705514	1.693169	0.044
27	30.04.2013	20	1.669982	1.705674	1.693271	-0.047
28	30.04.2013	20	1.670059	1.705246	1.692893	0.028
29	30.04.2013	20	1.670043	1.705382	1.692987	-0.010
30	30.04.2013	20	1.670060	1.705354	1.692981	-0.006
31	30.04.2013	20	1.670099	1.705362	1.693049	0.067
32	30.04.2013	20	1.669916	1.706396	1.693914	-0.089
33	30.04.2013	20	1.670030	1.705741	1.693344	0.070
34	30.04.2013	20	1.669910	1.706522	1.694028	-0.028
35	30.04.2013	20	1.669884	1.706584	1.694097	-0.010
36	30.04.2013	20	1.669891	1.706806	1.694270	-
38	30.04.2013	9	1.669929	1.706820	1.694362	-
39	30.04.2013	9	1.669831	1.706836	1.694264	-0.018
40	30.04.2013	9	1.669794	1.706797	1.694163	-0.006
41	30.04.2013	9	1.669776	1.707058	1.694407	-0.028
42	30.04.2013	9	1.669852	1.707007	1.694422	-
44	01.07.2013	15	1.669875	1.704800	1.692220	-
45	01.07.2013	15	1.669883	1.704956	1.692404	-0.017
46	01.07.2013	15	1.669949	1.705118	1.692620	0.031
47	01.07.2013	15	1.669910	1.705476	1.692922	0.011

Analysis no.	Date	[Re][1] (ppb)	$^{187}Re/^{185}Re$[2]	Raw $^{193}Ir/^{191}Ir$	Raw $^{187}Re/^{185}Re$	$\delta^{187}Re$[3]
48	01.07.2013	15	1.669834	1.705904	1.693358	-0.038
49	01.07.2013	15	1.669885	1.705655	1.693090	-
51	01.07.2013	15	1.669750	1.706795	1.694150	-
52	01.07.2013	15	1.669875	1.706804	1.694279	0.061
53	01.07.2013	15	1.669796	1.707132	1.694493	-0.015
54	01.07.2013	15	1.669769	1.707149	1.694524	-0.020
55	01.07.2013	15	1.669809	1.707052	1.694459	0.020
56	01.07.2013	15	1.669782	1.707164	1.694585	-0.012
57	01.07.2013	15	1.669796	1.707253	1.694652	-0.006
58	01.07.2013	15	1.669829	1.707204	1.694655	0.010
59	01.07.2013	15	1.669829	1.707303	1.694730	0.006
60	01.07.2013	15	1.669808	1.707347	1.694764	0.015
61	01.07.2013	15	1.669740	1.707245	1.694570	-0.030
62	01.07.2013	15	1.669772	1.707030	1.694434	-0.002
63	01.07.2013	15	1.669810	1.706808	1.694214	-
65	22.07.2013	10	1.669706	1.708848	1.696196	-
66	22.07.2013	10	1.669737	1.708913	1.696281	-0.034
67	22.07.2013	10	1.669882	1.708983	1.696487	0.077
68	22.07.2013	10	1.669769	1.708916	1.696340	-0.060
69	22.07.2013	10	1.669855	1.708975	1.696448	0.069
70	22.07.2013	10	1.669712	1.708985	1.696347	-0.068
71	22.07.2013	10	1.669794	1.708949	1.696354	0.048
72	22.07.2013	10	1.669718	1.708942	1.696326	0.002
73	22.07.2013	10	1.669634	1.708918	1.696170	-0.085
74	22.07.2013	10	1.669832	1.708856	1.696359	0.048
75	22.07.2013	10	1.669870	1.708784	1.696311	0.021
76	22.07.2013	10	1.669838	1.708815	1.696288	0.047
77	22.07.2013	10	1.669651	1.708417	1.695699	-0.121
78	22.07.2013	10	1.669868	1.708358	1.695895	-
80	23.07.2013	10	1.669590	1.708003	1.695218	-
81	23.07.2013	10	1.669700	1.708073	1.695382	0.021
82	23.07.2013	10	1.669741	1.708109	1.695498	0.054
83	23.07.2013	10	1.669602	1.708143	1.695306	-0.104
84	23.07.2013	10	1.669812	1.708121	1.695577	0.089
85	23.07.2013	10	1.669724	1.708100	1.695461	-0.016
86	23.07.2013	10	1.669691	1.708076	1.695327	0.004
87	23.07.2013	10	1.669643	1.708080	1.695363	-0.067
88	23.07.2013	10	1.669821	1.708123	1.695539	0.059
89	23.07.2013	10	1.669801	1.708166	1.695622	0.024
90	23.07.2013	10	1.669700	1.708115	1.695439	0.010
91	23.07.2013	10	1.669567	1.708106	1.695299	-0.084
92	23.07.2013	10	1.669714	1.708035	1.695376	0.015
93	23.07.2013	10	1.669811	1.708023	1.695470	0.062
94	23.07.2013	10	1.669700	1.708031	1.695359	-0.034
95	23.07.2013	10	1.669701	1.708028	1.695346	-0.071
96	23.07.2013	10	1.669940	1.708028	1.695612	0.131
97	23.07.2013	10	1.669741	1.708128	1.695518	-0.032

Analysis no.	Date	[Re][1] (ppb)	$^{187}Re/^{185}Re$[2]	Raw $^{193}Ir/^{191}Ir$	Raw $^{187}Re/^{185}Re$	$\delta^{187}Re$[3]
98	23.07.2013	10	1.669649	1.708081	1.695354	-0.053
99	23.07.2013	10	1.669734	1.708084	1.695447	0.057
100	23.07.2013	10	1.669628	1.708163	1.695518	-0.063
101	23.07.2013	10	1.669734	1.708161	1.695523	0.022
102	23.07.2013	10	1.669766	1.708084	1.695497	0.047
103	23.07.2013	10	1.669640	1.708064	1.695332	-0.048
104	23.07.2013	10	1.669674	1.708064	1.695418	-0.001
105	23.07.2013	10	1.669712	1.708111	1.695470	-
107	12.09.2013	20	1.669957	1.706128	1.693685	-0.029
108	12.09.2013	20	1.669988	1.706112	1.693702	0.017
109	12.09.2013	20	1.669961	1.706078	1.693621	0.000
110	12.09.2013	20	1.669934	1.705934	1.693481	-0.012
111	12.09.2013	20	1.669948	1.706029	1.693580	-0.009
112	12.09.2013	20	1.669991	1.706021	1.693566	0.026
113	12.09.2013	20	1.669946	1.706043	1.693552	-0.029
114	12.09.2013	20	1.669998	1.705974	1.693535	0.036
115	12.09.2013	20	1.669929	1.705998	1.693521	-0.029
116	12.09.2013	20	1.669956	1.705981	1.693514	0.005
117	12.09.2013	20	1.669965	1.705968	1.693485	0.004
118	12.09.2013	20	1.669961	1.705982	1.693521	-0.014
119	12.09.2013	20	1.670005	1.705967	1.693505	-0.003
120	12.09.2013	20	1.670060	1.705967	1.693604	0.034
121	12.09.2013	20	1.670002	1.705972	1.693551	-0.036
122	12.09.2013	20	1.670063	1.705989	1.693621	0.041
123	12.09.2013	20	1.669986	1.705988	1.693563	-0.032
124	12.09.2013	20	1.670017	1.705977	1.693601	0.006
125	12.09.2013	20	1.670028	1.705991	1.693587	-
127	12.09.2013	20	1.670049	1.705955	1.693611	-
128	12.09.2013	20	1.669908	1.706082	1.693582	-0.044
129	12.09.2013	20	1.669912	1.706188	1.693720	-0.019
130	12.09.2013	20	1.669981	1.706337	1.693903	0.037
131	12.09.2013	20	1.669928	1.705887	1.693369	0.008
132	12.09.2013	15	1.669848	1.705911	1.693366	-0.039
133	12.09.2013	15	1.669901	1.705881	1.693358	-0.003
134	12.09.2013	15	1.669964	1.705902	1.693423	-0.007
135	12.09.2013	15	1.670052	1.705881	1.693546	0.088
136	12.09.2013	15	1.669847	1.705845	1.693267	-0.085
137	12.09.2013	15	1.669924	1.705876	1.693384	0.036
138	12.09.2013	15	1.669882	1.705848	1.693275	-0.008
139	12.09.2013	15	1.669866	1.705832	1.693268	-0.028
140	12.09.2013	15	1.669944	1.705841	1.693366	0.006
141	12.09.2013	15	1.670002	1.705808	1.693412	0.021
142	12.09.2013	15	1.669991	1.705890	1.693498	0.023
143	12.09.2013	15	1.669902	1.705847	1.693307	-0.032
144	12.09.2013	15	1.669919	1.705902	1.693421	0.000
145	12.09.2013	15	1.669938	1.705882	1.693413	-0.021
146	12.09.2013	15	1.670026	1.706068	1.693671	0.058
147	12.09.2013	15	1.669922	1.706152	1.693638	-0.031
148	12.09.2013	15	1.669920	1.706119	1.693621	-0.020

Analysis no.	Date	[Re][1] (ppb)	$^{187}Re/^{185}Re$[2]	Raw $^{193}Ir/^{191}Ir$	Raw $^{187}Re/^{185}Re$	$\delta^{187}Re$[3]
149	12.09.2013	10	1.669986	1.706023	1.693606	0.060
150	12.09.2013	10	1.669852	1.705966	1.693406	-0.075
151	12.09.2013	10	1.669967	1.705953	1.693458	0.043
152	12.09.2013	10	1.669938	1.705938	1.693470	-0.015
153	12.09.2013	10	1.669958	1.705969	1.693506	0.010
154	12.09.2013	10	1.669945	1.705911	1.693452	-0.015
155	12.09.2013	10	1.669982	1.705911	1.693490	0.022
156	12.09.2013	10	1.669947	1.705938	1.693413	0.008
157	12.09.2013	10	1.669883	1.705922	1.693368	-0.043
158	12.09.2013	10	1.669963	1.706108	1.693699	0.019
159	12.09.2013	10	1.669979	1.706065	1.693662	0.028
160	12.09.2013	10	1.669903	1.706009	1.693479	-0.035
161	12.09.2013	10	1.669943	1.705925	1.693457	-0.012
162	12.09.2013	10	1.670025	1.706151	1.693765	0.035
163	12.09.2013	10	1.669989	1.705989	1.693561	-
166	26.11.2013	20	1.670223	1.705199	1.692977	-
167	26.11.2013	20	1.670205	1.705130	1.692915	0.006
168	26.11.2013	20	1.670166	1.705134	1.692862	-0.025
169	26.11.2013	20	1.670211	1.705192	1.692984	0.022
170	26.11.2013	20	1.670182	1.705158	1.692908	-0.005
171	26.11.2013	20	1.670169	1.705162	1.692901	-0.004
172	26.11.2013	20	1.670169	1.705198	1.692931	-0.012
173	26.11.2013	20	1.670208	1.704996	1.692766	0.033
174	26.11.2013	20	1.670137	1.705069	1.692750	-0.022
175	26.11.2013	20	1.670140	1.705063	1.692773	-0.003
176	26.11.2013	20	1.670153	1.705182	1.692899	-0.003
177	26.11.2013	20	1.670176	1.705123	1.692849	0.044
178	26.11.2013	20	1.670052	1.705402	1.693018	-0.033
179	26.11.2013	20	1.670039	1.705134	1.692745	-0.007
180	26.11.2013	20	1.670052	1.705346	1.692952	-0.004
181	26.11.2013	20	1.670077	1.705335	1.692995	0.001
182	26.11.2013	20	1.670101	1.705436	1.693078	0.007
183	26.11.2013	20	1.670100	1.705381	1.693046	-0.010
184	26.11.2013	20	1.670132	1.705347	1.693052	-
186	26.11.2013	10	1.670037	1.705352	1.692962	-
187	26.11.2013	10	1.670092	1.705334	1.692951	0.028
188	26.11.2013	10	1.670054	1.705329	1.692952	-0.028
189	26.11.2013	10	1.670108	1.705361	1.693014	0.021
190	26.11.2013	10	1.670091	1.705308	1.692979	0.030
191	26.11.2013	10	1.669973	1.705299	1.692836	-0.089
192	26.11.2013	10	1.670155	1.705347	1.693067	0.079
193	26.11.2013	10	1.670071	1.705321	1.692960	-0.058
194	26.11.2013	10	1.670181	1.705276	1.693039	0.080
195	26.11.2013	10	1.670022	1.705279	1.692847	-0.070
196	26.11.2013	10	1.670098	1.705300	1.692963	0.012
197	26.11.2013	10	1.670135	1.705277	1.692976	0.035
198	26.11.2013	10	1.670056	1.705323	1.692944	-0.056
199	26.11.2013	10	1.670165	1.705336	1.693070	0.041
200	26.11.2013	10	1.670136	1.705265	1.692978	0.024

Analysis no.	Date	[Re][1] (ppb)	$^{187}Re/^{185}Re$[2]	Raw $^{193}Ir/^{191}Ir$	Raw $^{187}Re/^{185}Re$	$\delta^{187}Re$[3]
201	26.11.2013	10	1.670028	1.705763	1.693363	0.006
202	26.11.2013	10	1.669900	1.705798	1.693300	-0.092
203	26.11.2013	10	1.670080	1.705671	1.693327	0.050
204	26.11.2013	10	1.670091	1.705601	1.693251	0.009
205	26.11.2013	10	1.670073	1.705820	1.693473	0.002
206	26.11.2013	10	1.670049	1.705764	1.693393	0.011
207	26.11.2013	10	1.669987	1.705674	1.693245	-0.032
208	26.11.2013	10	1.670032	1.705420	1.693055	0.004
209	26.11.2013	10	1.670066	1.705276	1.692898	0.021
210	26.11.2013	10	1.670031	1.705473	1.693062	-0.044
211	26.11.2013	10	1.670144	1.705374	1.693081	-
215	05.02.2014	15	1.669933	1.705611	1.693115	-
216	05.02.2014	15	1.669895	1.705602	1.693057	0.002
217	05.02.2014	15	1.669850	1.705615	1.693058	-0.016
218	05.02.2014	15	1.669860	1.705605	1.693041	-0.024
219	05.02.2014	15	1.669949	1.705609	1.693160	0.049
220	05.02.2014	15	1.669873	1.705643	1.693084	-0.037
221	05.02.2014	15	1.669922	1.705638	1.693136	0.012
222	05.02.2014	15	1.669930	1.705630	1.693124	0.010
223	05.02.2014	15	1.669902	1.705637	1.693120	-0.021
224	05.02.2014	15	1.669944	1.705605	1.693118	0.008
225	05.02.2014	15	1.669958	1.705628	1.693163	0.011
226	05.02.2014	15	1.669937	1.705664	1.693171	-0.008
227	05.02.2014	15	1.669942	1.705705	1.693212	0.011
228	05.02.2014	15	1.669911	1.705714	1.693221	-0.019
229	05.02.2014	15	1.669943	1.705744	1.693259	0.029
230	05.02.2014	15	1.669877	1.705752	1.693203	-0.033
231	05.02.2014	15	1.669920	1.705725	1.693212	0.016
232	05.02.2014	15	1.669909	1.705750	1.693232	0.003
233	05.02.2014	15	1.669889	1.705741	1.693192	-0.016
234	05.02.2014	15	1.669923	1.705738	1.693243	0.014
235	05.02.2014	15	1.669910	1.705736	1.693225	-0.010
236	05.02.2014	15	1.669930	1.705737	1.693237	0.028
237	05.02.2014	15	1.669855	1.705732	1.693167	-0.032
238	05.02.2014	15	1.669888	1.705718	1.693185	0.028
239	05.02.2014	15	1.669827	1.705723	1.693119	-0.028
240	05.02.2014	15	1.669858	1.705695	1.693129	0.008
241	05.02.2014	15	1.669862	1.705657	1.693092	-0.006
242	05.02.2014	15	1.669887	1.705657	1.693105	-0.015
243	05.02.2014	15	1.669963	1.705651	1.693175	0.052
244	05.02.2014	15	1.669864	1.705626	1.693060	-0.043
245	05.02.2014	15	1.669908	1.705665	1.693148	0.014
246	05.02.2014	15	1.669905	1.705676	1.693143	-0.001
247	05.02.2014	15	1.669907	1.705607	1.693099	0.022
248	05.02.2014	15	1.669834	1.705664	1.693102	-0.041
249	05.02.2014	15	1.669899	1.705622	1.693116	0.037
250	05.02.2014	15	1.669841	1.705978	1.693401	-0.025
251	05.02.2014	15	1.669868	1.705863	1.693314	0.019
252	05.02.2014	15	1.669833	1.705765	1.693163	-0.037

Analysis no.	Date	[Re][1] (ppb)	$^{187}Re/^{185}Re$[2]	Raw $^{193}Ir/^{191}Ir$	Raw $^{187}Re/^{185}Re$	$\delta^{187}Re$[3]
253	05.02.2014	15	1.669922	1.705435	1.692942	0.038
254	05.02.2014	15	1.669883	1.705408	1.692831	-
256	05.02.2014	9	1.669919	1.705284	1.692766	-
257	05.02.2014	9	1.669952	1.705301	1.692800	0.041
258	05.02.2014	9	1.669848	1.705191	1.692587	-0.042
259	05.02.2014	9	1.669886	1.705241	1.692677	0.001
260	05.02.2014	9	1.669921	1.705092	1.692584	0.024
261	05.02.2014	9	1.669875	1.705092	1.692490	-0.044
262	05.02.2014	9	1.669975	1.704962	1.692470	0.038
263	05.02.2014	9	1.669949	1.704948	1.692462	0.019
264	05.02.2014	9	1.669857	1.704925	1.692388	-0.037
265	05.02.2014	9	1.669890	1.704728	1.692190	-0.004
266	05.02.2014	9	1.669935	1.704807	1.692285	-0.009
267	05.02.2014	9	1.670012	1.704847	1.692397	0.040
268	05.02.2014	9	1.669956	1.704837	1.692355	-0.002
269	05.02.2014	9	1.669908	1.704671	1.692134	-0.020
270	05.02.2014	9	1.669928	1.704678	1.692109	0.009
271	05.02.2014	9	1.669917	1.704674	1.692131	-0.012
272	05.02.2014	9	1.669946	1.704627	1.692085	-0.008
273	05.02.2014	9	1.670002	1.704435	1.691970	0.028
274	05.02.2014	9	1.669966	1.704345	1.691845	-0.012
275	05.02.2014	9	1.669972	1.704597	1.692087	0.027
276	05.02.2014	9	1.669885	1.704595	1.691997	-0.048
277	05.02.2014	9	1.669960	1.704413	1.691906	0.000
278	05.02.2014	9	1.670034	1.704487	1.692042	0.030
279	05.02.2014	9	1.670006	1.704375	1.691900	0.009
280	05.02.2014	9	1.669950	1.704045	1.691475	-0.060
281	05.02.2014	9	1.670095	1.703437	1.691079	0.072
282	05.02.2014	9	1.669999	1.703755	1.691261	-
284	05.02.2014	8	1.669998	1.703234	1.690711	-
285	05.02.2014	8	1.670061	1.702984	1.690556	-0.001
286	05.02.2014	8	1.670126	1.702955	1.690540	-0.003
287	05.02.2014	8	1.670201	1.702806	1.690477	0.055
288	05.02.2014	8	1.670094	1.702667	1.690259	-0.052
289	05.02.2014	8	1.670160	1.702950	1.690572	0.010
290	05.02.2014	8	1.670191	1.702847	1.690564	0.022
291	05.02.2014	8	1.670148	1.702724	1.690437	-0.008
292	05.02.2014	8	1.670132	1.702569	1.690233	0.001
293	05.02.2014	8	1.670113	1.703027	1.690592	0.010
294	05.02.2014	8	1.670058	1.702881	1.690382	-0.064
295	05.02.2014	8	1.670218	1.702841	1.690543	0.050
296	05.02.2014	8	1.670209	1.702711	1.690373	0.018
297	05.02.2014	8	1.670141	1.702916	1.690563	-0.010
298	05.02.2014	8	1.670107	1.702722	1.690309	0.005
299	05.02.2014	8	1.670056	1.702880	1.690424	-0.052
300	05.02.2014	8	1.670180	1.703075	1.690760	0.071
301	05.02.2014	8	1.670069	1.703130	1.690693	-0.030
302	05.02.2014	8	1.670056	1.702710	1.690280	-
304	05.02.2014	5	1.670098	1.702800	1.690423	-

Analysis no.	Date	[Re][1] (ppb)	$^{187}Re/^{185}Re$[2]	Raw $^{193}Ir/^{191}Ir$	Raw $^{187}Re/^{185}Re$	$\delta^{187}Re$[3]
305	05.02.2014	5	1.670196	1.702563	1.690190	0.064
306	05.02.2014	5	1.670080	1.702593	1.690130	-0.040
307	05.02.2014	5	1.670099	1.702237	1.689852	-0.039
308	05.02.2014	5	1.670249	1.702109	1.689814	0.063
309	05.02.2014	5	1.670189	1.702338	1.689992	-0.052
310	05.02.2014	5	1.670302	1.702312	1.690059	0.130
311	05.02.2014	5	1.669981	1.702192	1.689652	-0.157
312	05.02.2014	5	1.670184	1.702141	1.689820	0.086
313	05.02.2014	5	1.670101	1.702256	1.689846	-0.046
314	05.02.2014	5	1.670172	1.701864	1.689508	-0.024
315	05.02.2014	5	1.670323	1.701929	1.689722	0.063
316	05.02.2014	5	1.670262	1.701837	1.689517	-0.010
317	05.02.2014	5	1.670234	1.701834	1.689529	-0.034
318	05.02.2014	5	1.670318	1.701323	1.689142	0.042
319	05.02.2014	5	1.670263	1.701512	1.689200	-0.008
320	05.02.2014	5	1.670236	1.701604	1.689314	-0.036
321	05.02.2014	5	1.670328	1.701579	1.689370	0.040
322	05.02.2014	5	1.670285	1.701674	1.689408	-0.052
323	05.02.2014	5	1.670417	1.701581	1.689467	-
		average	1.669963	1.705695	1.693212	**0.000**
		2SD	0.000297	0.003300	0.003169	
		2SD ‰	0.178	1.935	1.871	**0.084**

1 Re concentration in the standard (ppb)

[2]The ratio of $^{187}Re/^{185}Re$ which has been corrected for potential isobaric interference of osmium, and then corrected for instrumental mass bias using the $^{193}Ir/^{191}Ir$ ratio and the exponential law.

[3]Re isotope composition calculated by standard sample bracketing, using the standards analysed before and after each standard as bracketing standards.

Table A2: Table of Re isotope composition data for all analyses of the SRM3143 standard carried out with the Toarcian aged samples from the Yorkshire coast and presented in Chapter 6. For all standards analysed, Ir was added to make Ir concentration of 200 ppb.

Analysis no	Date	[Re][1] (ppb)	$^{187}Re/^{185}Re$[2]	Raw $^{193}Ir/^{191}Ir$	Raw $^{187}Re/^{185}Re$	$\delta^{187}Re$[3]
1	30.04.2013	20	1.669937	1.706290	1.693812	-
2	30.04.2013	20	1.669970	1.706146	1.693702	-0.018
3	30.04.2013	20	1.670065	1.705845	1.693477	0.045
4	30.04.2013	20	1.670007	1.705869	1.693458	-0.019
5	30.04.2013	20	1.670013	1.705860	1.693447	0.007
6	30.04.2013	20	1.669995	1.705704	1.693286	-0.026
7	30.04.2013	20	1.670062	1.705514	1.693169	0.044
8	30.04.2013	20	1.669982	1.705674	1.693271	-0.047
9	30.04.2013	20	1.670059	1.705246	1.692893	0.028
10	30.04.2013	20	1.670043	1.705382	1.692987	-0.010
11	30.04.2013	20	1.670060	1.705354	1.692981	-0.006
12	30.04.2013	20	1.670099	1.705362	1.693049	0.067
13	30.04.2013	20	1.669916	1.706396	1.693914	-0.089
14	30.04.2013	20	1.670030	1.705741	1.693344	0.070
15	30.04.2013	20	1.669910	1.706522	1.694028	-0.028
16	30.04.2013	20	1.669884	1.706584	1.694097	-0.010
17	30.04.2013	20	1.669891	1.706806	1.694270	-
38	30.04.2013	9	1.669929	1.706820	1.694362	-
39	30.04.2013	9	1.669831	1.706836	1.694264	-0.018
40	30.04.2013	9	1.669794	1.706797	1.694163	-0.006
41	30.04.2013	9	1.669776	1.707058	1.694407	-0.028
42	30.04.2013	9	1.669852	1.707007	1.694422	-
18	22.07.2013	10	1.669706	1.708848	1.696196	-
19	22.07.2013	10	1.669737	1.708913	1.696281	-0.034
20	22.07.2013	10	1.669882	1.708983	1.696487	0.077
21	22.07.2013	10	1.669769	1.708916	1.696340	-0.060
22	22.07.2013	10	1.669855	1.708975	1.696448	0.069
23	22.07.2013	10	1.669712	1.708985	1.696347	-0.068
24	22.07.2013	10	1.669794	1.708949	1.696354	0.048
25	22.07.2013	10	1.669718	1.708942	1.696326	0.002
26	22.07.2013	10	1.669634	1.708918	1.696170	-0.085
27	22.07.2013	10	1.669832	1.708856	1.696359	0.048
28	22.07.2013	10	1.669870	1.708784	1.696311	0.021
29	22.07.2013	10	1.669838	1.708815	1.696288	0.047
30	22.07.2013	10	1.669651	1.708417	1.695699	-0.121
31	22.07.2013	10	1.669868	1.708358	1.695895	-
32	23.07.2013	10	1.669590	1.708003	1.695218	-
33	23.07.2013	10	1.669700	1.708073	1.695382	0.021
34	23.07.2013	10	1.669741	1.708109	1.695498	0.054
35	23.07.2013	10	1.669602	1.708143	1.695306	-0.104
36	23.07.2013	10	1.669812	1.708121	1.695577	0.089
37	23.07.2013	10	1.669724	1.708100	1.695461	-0.016
38	23.07.2013	10	1.669691	1.708076	1.695327	0.004
39	23.07.2013	10	1.669643	1.708080	1.695363	-0.067
40	23.07.2013	10	1.669821	1.708123	1.695539	0.059
41	23.07.2013	10	1.669801	1.708166	1.695622	0.024

Analysis no	Date	[Re][1] (ppb)	$^{187}Re/^{185}Re$[2]	Raw $^{193}Ir/^{191}Ir$	Raw $^{187}Re/^{185}Re$	$\delta^{187}Re$[3]
42	23.07.2013	10	1.669700	1.708115	1.695439	0.010
43	23.07.2013	10	1.669567	1.708106	1.695299	-0.084
44	23.07.2013	10	1.669714	1.708035	1.695376	0.015
45	23.07.2013	10	1.669811	1.708023	1.695470	0.062
46	23.07.2013	10	1.669700	1.708031	1.695359	-0.034
47	23.07.2013	10	1.669701	1.708028	1.695346	-0.071
48	23.07.2013	10	1.669940	1.708028	1.695612	0.131
49	23.07.2013	10	1.669741	1.708128	1.695518	-0.032
50	23.07.2013	10	1.669649	1.708081	1.695354	-0.053
51	23.07.2013	10	1.669734	1.708084	1.695447	0.057
52	23.07.2013	10	1.669628	1.708163	1.695518	-0.063
53	23.07.2013	10	1.669734	1.708161	1.695523	0.022
54	23.07.2013	10	1.669766	1.708084	1.695497	0.047
55	23.07.2013	10	1.669640	1.708064	1.695332	-0.048
56	23.07.2013	10	1.669674	1.708064	1.695418	-0.001
57	23.07.2013	10	1.669712	1.708111	1.695470	-
58	12.09.2013	20	1.669957	1.706128	1.693685	-0.029
59	12.09.2013	20	1.669988	1.706112	1.693702	0.017
60	12.09.2013	20	1.669961	1.706078	1.693621	0.000
61	12.09.2013	20	1.669934	1.705934	1.693481	-0.012
62	12.09.2013	20	1.669948	1.706029	1.693580	-0.009
63	12.09.2013	20	1.669991	1.706021	1.693566	0.026
64	12.09.2013	20	1.669946	1.706043	1.693552	-0.029
65	12.09.2013	20	1.669998	1.705974	1.693535	0.036
66	12.09.2013	20	1.669929	1.705998	1.693521	-0.029
67	12.09.2013	20	1.669956	1.705981	1.693514	0.005
68	12.09.2013	20	1.669965	1.705968	1.693485	0.004
69	12.09.2013	20	1.669961	1.705982	1.693521	-0.014
70	12.09.2013	20	1.670005	1.705967	1.693505	-0.003
71	12.09.2013	20	1.670060	1.705967	1.693604	0.034
72	12.09.2013	20	1.670002	1.705972	1.693551	-0.036
73	12.09.2013	20	1.670063	1.705989	1.693621	0.041
74	12.09.2013	20	1.669986	1.705988	1.693563	-0.032
75	12.09.2013	20	1.670017	1.705977	1.693601	0.006
76	12.09.2013	20	1.670028	1.705991	1.693587	-
77	12.09.2013	20	1.670049	1.705955	1.693611	-
78	12.09.2013	20	1.669908	1.706082	1.693582	-0.044
79	12.09.2013	20	1.669912	1.706188	1.693720	-0.019
80	12.09.2013	20	1.669981	1.706337	1.693903	0.037
81	12.09.2013	20	1.669928	1.705887	1.693369	0.008
82	12.09.2013	15	1.669848	1.705911	1.693366	-0.039
83	12.09.2013	15	1.669901	1.705881	1.693358	-0.003
84	12.09.2013	15	1.669964	1.705902	1.693423	-0.007
85	12.09.2013	15	1.670052	1.705881	1.693546	0.088
86	12.09.2013	15	1.669847	1.705845	1.693267	-0.085
87	12.09.2013	15	1.669924	1.705876	1.693384	0.036
88	12.09.2013	15	1.669882	1.705848	1.693275	-0.008
89	12.09.2013	15	1.669866	1.705832	1.693268	-0.028
90	12.09.2013	15	1.669944	1.705841	1.693366	0.006
91	12.09.2013	15	1.670002	1.705808	1.693412	0.021

Analysis no	Date	[Re][1] (ppb)	$^{187}Re/^{185}Re$[2]	Raw $^{193}Ir/^{191}Ir$	Raw $^{187}Re/^{185}Re$	$\delta^{187}Re$[3]
92	12.09.2013	15	1.669991	1.705890	1.693498	0.023
93	12.09.2013	15	1.669902	1.705847	1.693307	-0.032
94	12.09.2013	15	1.669919	1.705902	1.693421	0.000
95	12.09.2013	15	1.669938	1.705882	1.693413	-0.021
96	12.09.2013	15	1.670026	1.706068	1.693671	0.058
97	12.09.2013	15	1.669922	1.706152	1.693638	-0.031
98	12.09.2013	15	1.669920	1.706119	1.693621	-0.020
99	12.09.2013	10	1.669986	1.706023	1.693606	0.060
100	12.09.2013	10	1.669852	1.705966	1.693406	-0.075
101	12.09.2013	10	1.669967	1.705953	1.693458	0.043
102	12.09.2013	10	1.669938	1.705938	1.693470	-0.015
103	12.09.2013	10	1.669958	1.705969	1.693506	0.010
104	12.09.2013	10	1.669945	1.705911	1.693452	-0.015
105	12.09.2013	10	1.669982	1.705911	1.693490	0.022
106	12.09.2013	10	1.669947	1.705938	1.693413	0.008
107	12.09.2013	10	1.669883	1.705922	1.693368	-0.043
108	12.09.2013	10	1.669963	1.706108	1.693699	0.019
109	12.09.2013	10	1.669979	1.706065	1.693662	0.028
110	12.09.2013	10	1.669903	1.706009	1.693479	-0.035
111	12.09.2013	10	1.669943	1.705925	1.693457	-0.012
112	12.09.2013	10	1.670025	1.706151	1.693765	0.035
113	12.09.2013	10	1.669989	1.705989	1.693561	-
114	5.02.2014	15	1.669933	1.705611	1.693115	-
115	5.02.2014	15	1.669895	1.705602	1.693057	0.002
116	5.02.2014	15	1.669850	1.705615	1.693058	-0.016
117	5.02.2014	15	1.669860	1.705605	1.693041	-0.024
118	5.02.2014	15	1.669949	1.705609	1.693160	0.049
119	5.02.2014	15	1.669873	1.705643	1.693084	-0.037
120	5.02.2014	15	1.669922	1.705638	1.693136	0.012
121	5.02.2014	15	1.669930	1.705630	1.693124	0.010
122	5.02.2014	15	1.669902	1.705637	1.693120	-0.021
123	5.02.2014	15	1.669944	1.705605	1.693118	0.008
124	5.02.2014	15	1.669958	1.705628	1.693163	0.011
125	5.02.2014	15	1.669937	1.705664	1.693171	-0.008
126	5.02.2014	15	1.669942	1.705705	1.693212	0.011
127	5.02.2014	15	1.669911	1.705714	1.693221	-0.019
128	5.02.2014	15	1.669943	1.705744	1.693259	0.029
129	5.02.2014	15	1.669877	1.705752	1.693203	-0.033
130	5.02.2014	15	1.669920	1.705725	1.693212	0.016
131	5.02.2014	15	1.669909	1.705750	1.693232	0.003
132	5.02.2014	15	1.669889	1.705741	1.693192	-0.016
133	5.02.2014	15	1.669923	1.705738	1.693243	0.014
134	5.02.2014	15	1.669910	1.705736	1.693225	-0.010
135	5.02.2014	15	1.669930	1.705737	1.693237	0.028
136	5.02.2014	15	1.669855	1.705732	1.693167	-0.032
137	5.02.2014	15	1.669888	1.705718	1.693185	0.028
138	5.02.2014	15	1.669827	1.705723	1.693119	-0.028
139	5.02.2014	15	1.669858	1.705695	1.693129	0.008
140	5.02.2014	15	1.669862	1.705657	1.693092	-0.006
141	5.02.2014	15	1.669887	1.705657	1.693105	-0.015

Analysis no	Date	[Re][1] (ppb)	$^{187}Re/^{185}Re$[2]	Raw $^{193}Ir/^{191}Ir$	Raw $^{187}Re/^{185}Re$	$\delta^{187}Re$[3]
142	5.02.2014	15	1.669963	1.705651	1.693175	0.052
143	5.02.2014	15	1.669864	1.705626	1.693060	-0.043
144	5.02.2014	15	1.669908	1.705665	1.693148	0.014
145	5.02.2014	15	1.669905	1.705676	1.693143	-0.001
146	5.02.2014	15	1.669907	1.705607	1.693099	0.022
147	5.02.2014	15	1.669834	1.705664	1.693102	-0.041
148	5.02.2014	15	1.669899	1.705622	1.693116	0.037
149	5.02.2014	15	1.669841	1.705978	1.693401	-0.025
150	5.02.2014	15	1.669868	1.705863	1.693314	0.019
151	5.02.2014	15	1.669833	1.705765	1.693163	-0.037
152	5.02.2014	15	1.669922	1.705435	1.692942	0.038
153	5.02.2014	15	1.669883	1.705408	1.692831	-
154	5.02.2014	9	1.669919	1.705284	1.692766	-
155	5.02.2014	9	1.669952	1.705301	1.692800	0.041
156	5.02.2014	9	1.669848	1.705191	1.692587	-0.042
157	5.02.2014	9	1.669886	1.705241	1.692677	0.001
158	5.02.2014	9	1.669921	1.705092	1.692584	0.024
159	5.02.2014	9	1.669875	1.705092	1.692490	-0.044
160	5.02.2014	9	1.669975	1.704962	1.692470	0.038
161	5.02.2014	9	1.669949	1.704948	1.692462	0.019
162	5.02.2014	9	1.669857	1.704925	1.692388	-0.037
163	5.02.2014	9	1.669890	1.704728	1.692190	-0.004
164	5.02.2014	9	1.669935	1.704807	1.692285	-0.009
165	5.02.2014	9	1.670012	1.704847	1.692397	0.040
166	5.02.2014	9	1.669956	1.704837	1.692355	-0.002
167	5.02.2014	9	1.669908	1.704671	1.692134	-0.020
168	5.02.2014	9	1.669928	1.704678	1.692109	0.009
169	5.02.2014	9	1.669917	1.704674	1.692131	-0.012
170	5.02.2014	9	1.669946	1.704627	1.692085	-0.008
171	5.02.2014	9	1.670002	1.704435	1.691970	0.028
172	5.02.2014	9	1.669966	1.704345	1.691845	-0.012
173	5.02.2014	9	1.669972	1.704597	1.692087	0.027
174	5.02.2014	9	1.669885	1.704595	1.691997	-0.048
175	5.02.2014	9	1.669960	1.704413	1.691906	0.000
176	5.02.2014	9	1.670034	1.704487	1.692042	0.030
177	5.02.2014	9	1.670006	1.704375	1.691900	0.009
178	5.02.2014	9	1.669950	1.704045	1.691475	-0.060
179	5.02.2014	9	1.670095	1.703437	1.691079	0.072
180	5.02.2014	9	1.669999	1.703755	1.691261	-
181	5.02.2014	8	1.669998	1.703234	1.690711	-
182	5.02.2014	8	1.670061	1.702984	1.690556	-0.001
183	5.02.2014	8	1.670126	1.702955	1.690540	-0.003
184	5.02.2014	8	1.670201	1.702806	1.690477	0.055
185	5.02.2014	8	1.670094	1.702667	1.690259	-0.052
186	5.02.2014	8	1.670160	1.702950	1.690572	0.010
187	5.02.2014	8	1.670191	1.702847	1.690564	0.022
188	5.02.2014	8	1.670148	1.702724	1.690437	-0.008
189	5.02.2014	8	1.670132	1.702569	1.690233	0.001
190	5.02.2014	8	1.670113	1.703027	1.690592	0.010
191	5.02.2014	8	1.670058	1.702881	1.690382	-0.064

Analysis no	Date	[Re][1] (ppb)	$^{187}Re/^{185}Re$[2]	Raw $^{193}Ir/^{191}Ir$	Raw $^{187}Re/^{185}Re$	$\delta^{187}Re$[3]
192	5.02.2014	8	1.670218	1.702841	1.690543	0.050
193	5.02.2014	8	1.670209	1.702711	1.690373	0.018
194	5.02.2014	8	1.670141	1.702916	1.690563	-0.010
195	5.02.2014	8	1.670107	1.702722	1.690309	0.005
196	5.02.2014	8	1.670056	1.702880	1.690424	-0.052
197	5.02.2014	8	1.670180	1.703075	1.690760	0.071
198	5.02.2014	8	1.670069	1.703130	1.690693	-0.030
199	5.02.2014	8	1.670056	1.702710	1.690280	-
200	5.02.2014	5	1.670098	1.702800	1.690423	-
201	5.02.2014	5	1.670196	1.702563	1.690190	0.064
202	5.02.2014	5	1.670080	1.702593	1.690130	-0.040
203	5.02.2014	5	1.670099	1.702237	1.689852	-0.039
204	5.02.2014	5	1.670249	1.702109	1.689814	0.063
205	5.02.2014	5	1.670189	1.702338	1.689992	-0.052
206	5.02.2014	5	1.670302	1.702312	1.690059	0.130
207	5.02.2014	5	1.669981	1.702192	1.689652	-0.157
208	5.02.2014	5	1.670184	1.702141	1.689820	0.086
209	5.02.2014	5	1.670101	1.702256	1.689846	-0.046
210	5.02.2014	5	1.670172	1.701864	1.689508	-0.024
211	5.02.2014	5	1.670323	1.701929	1.689722	0.063
212	5.02.2014	5	1.670262	1.701837	1.689517	-0.010
213	5.02.2014	5	1.670234	1.701834	1.689529	-0.034
214	5.02.2014	5	1.670318	1.701323	1.689142	0.042
215	5.02.2014	5	1.670263	1.701512	1.689200	-0.008
216	5.02.2014	5	1.670236	1.701604	1.689314	-0.036
217	5.02.2014	5	1.670328	1.701579	1.689370	0.040
218	5.02.2014	5	1.670285	1.701674	1.689408	-0.052
219	5.02.2014	5	1.670417	1.701581	1.689467	-
220	27.11.2014	15	1.670412	1.704118	1.692076	-
221	27.11.2014	15	1.670283	1.704680	1.692515	-0.042
222	27.11.2014	15	1.670294	1.704601	1.692437	-0.019
223	27.11.2014	15	1.670369	1.704356	1.692244	0.023
224	27.11.2014	15	1.670366	1.704279	1.692194	-0.022
225	27.11.2014	15	1.670435	1.704204	1.692211	0.028
226	27.11.2014	15	1.670412	1.703999	1.691959	-0.025
227	27.11.2014	15	1.670473	1.703737	1.691742	0.001
228	27.11.2014	15	1.670530	1.703651	1.691681	0.054
229	27.11.2014	15	1.670409	1.703637	1.691600	-0.078
230	27.11.2014	15	1.670549	1.702901	1.690996	0.072
231	27.11.2014	15	1.670447	1.702979	1.690979	-0.054
232	27.11.2014	15	1.670527	1.702994	1.691052	0.049
233	27.11.2014	15	1.670443	1.702997	1.690974	-0.037
234	27.11.2014	15	1.670482	1.702819	1.690836	-
235	27.11.2014	15	1.670499	1.702821	1.690828	-
236	27.11.2014	15	1.670407	1.702847	1.690820	-0.050
237	27.11.2014	15	1.670482	1.702955	1.690935	0.012
238	27.11.2014	15	1.670518	1.703005	1.691027	0.031
239	27.11.2014	15	1.670449	1.703085	1.691042	-0.015
240	27.11.2014	15	1.670433	1.703134	1.691103	-0.027
241	27.11.2014	15	1.670505	1.703123	1.691125	0.043

Analysis no	Date	[Re][1] (ppb)	$^{187}Re/^{185}Re$[2]	Raw $^{193}Ir/^{191}Ir$	Raw $^{187}Re/^{185}Re$	$\delta^{187}Re$[3]
242	27.11.2014	15	1.670432	1.703147	1.691087	-0.023
243	27.11.2014	15	1.670436	1.703174	1.691152	0.016
244	27.11.2014	15	1.670386	1.703204	1.691128	-
245	27.11.2014	15	1.670418	1.703269	1.691229	-
246	27.11.2014	15	1.670466	1.703315	1.691330	0.051
247	27.11.2014	15	1.670344	1.703412	1.691325	-0.052
248	27.11.2014	15	1.670395	1.703443	1.691342	0.001
249	27.11.2014	15	1.670442	1.703358	1.691303	-0.002
250	27.11.2014	15	1.670495	1.703410	1.691406	0.030
251	27.11.2014	15	1.670449	1.703417	1.691378	0.005
252	27.11.2014	15	1.670385	1.703474	1.691416	-0.061
253	27.11.2014	15	1.670527	1.703466	1.691492	0.061
254	27.11.2014	15	1.670465	1.703488	1.691496	-0.013
255	27.11.2014	15	1.670447	1.703459	1.691477	-0.016
256	27.11.2014	15	1.670482	1.703411	1.691430	0.008
257	27.11.2014	15	1.670490	1.703399	1.691443	0.017
258	27.11.2014	15	1.670441	1.703580	1.691531	0.023
259	27.11.2014	15	1.670316	1.703580	1.691481	-0.066
260	27.11.2014	15	1.670412	1.703623	1.691548	0.021
261	27.11.2014	15	1.670437	1.703516	1.691474	0.083
262	27.11.2014	15	1.670186	1.704718	1.692443	-0.057
263	27.11.2014	15	1.670125	1.704802	1.692481	-0.078
264	27.11.2014	15	1.670322	1.704552	1.692466	-
265	28.11.2014	15	1.670287	1.704676	1.692506	-
266	28.11.2014	15	1.670300	1.704110	1.691968	0.005
267	28.11.2014	15	1.670295	1.704264	1.692108	-0.005
268	28.11.2014	15	1.670307	1.703778	1.691634	0.006
269	28.11.2014	15	1.670301	1.703951	1.691785	0.016
270	28.11.2014	15	1.670241	1.703518	1.691346	-0.047
271	28.11.2014	15	1.670338	1.703622	1.691477	0.045
272	28.11.2014	15	1.670285	1.703736	1.691555	-0.043
273	28.11.2014	15	1.670375	1.702736	1.690624	0.047
274	28.11.2014	15	1.670308	1.703619	1.691458	-0.025
275	28.11.2014	15	1.670325	1.704073	1.691941	0.000
276	28.11.2014	15	1.670340	1.703927	1.691843	0.008
277	28.11.2014	15	1.670329	1.703843	1.691694	-0.030
278	28.11.2014	15	1.670417	1.703930	1.691896	0.043
279	28.11.2014	15	1.670360	1.703337	1.691190	-0.014
280	28.11.2014	15	1.670349	1.703835	1.691727	-0.017
281	28.11.2014	15	1.670395	1.703309	1.691193	0.030
282	28.11.2014	15	1.670341	1.703130	1.690954	-0.025
283	28.11.2014	15	1.670373	1.701563	1.689426	0.069
284	28.11.2014	15	1.670176	1.703034	1.690739	-0.077
285	28.11.2014	15	1.670235	1.703133	1.690880	0.024
286	28.11.2014	15	1.670212	1.702158	1.689801	-0.027
287	28.11.2014	15	1.670280	1.701900	1.689647	0.023
288	28.11.2014	15	1.670272	1.701372	1.689152	0.010
289	28.11.2014	15	1.670230	1.701172	1.688855	0.000
290	28.11.2014	15	1.670190	1.700969	1.688556	-0.011
291	28.11.2014	15	1.670187	1.701290	1.688975	-0.032

Analysis no	Date	[Re][1] (ppb)	$^{187}Re/^{185}Re$[2]	Raw $^{193}Ir/^{191}Ir$	Raw $^{187}Re/^{185}Re$	$\delta^{187}Re$[3]
292	28.11.2014	15	1.670291	1.700148	1.687870	0.047
293	28.11.2014	15	1.670237	1.699705	1.687316	-0.024
294	28.11.2014	15	1.670264	1.699992	1.687636	-0.052
295	28.11.2014	15	1.670466	1.698530	1.686391	0.111
296	28.11.2014	15	1.670297	1.700026	1.687758	-0.077
297	28.11.2014	15	1.670385	1.699081	1.686897	0.024
298	28.11.2014	15	1.670393	1.699559	1.687365	0.027
299	28.11.2014	15	1.670310	1.699483	1.687249	-0.057
300	28.11.2014	15	1.670419	1.699410	1.687216	0.090
301	28.11.2014	15	1.670227	1.699430	1.687019	-0.117
302	28.11.2014	15	1.670428	1.699026	1.686787	0.074
303	28.11.2014	15	1.670381	1.698704	1.686475	-
304	23.03.2015	20	1.670751	1.699499	1.687651	-
305	23.03.2015	20	1.670722	1.699273	1.687405	-0.018
306	23.03.2015	20	1.670755	1.699441	1.687612	0.018
307	23.03.2015	20	1.670727	1.699392	1.687546	-0.028
308	23.03.2015	20	1.670791	1.699664	1.687893	0.034
309	23.03.2015	20	1.670743	1.699515	1.687677	-0.026
310	23.03.2015	20	1.670781	1.699469	1.687645	0.015
311	23.03.2015	20	1.670769	1.699495	1.687667	-0.006
312	23.03.2015	20	1.670778	1.699460	1.687667	0.014
313	23.03.2015	20	1.670738	1.699467	1.687672	-0.021
314	23.03.2015	20	1.670770	1.699654	1.687868	0.011
315	23.03.2015	20	1.670765	1.699715	1.687884	-0.020
316	23.03.2015	20	1.670826	1.699708	1.687989	0.028
317	23.03.2015	20	1.670794	1.699812	1.688033	-0.011
318	23.03.2015	20	1.670799	1.699971	1.688195	-0.004
319	23.03.2015	20	1.670817	1.700004	1.688298	0.000
320	23.03.2015	20	1.670835	1.699727	1.687962	0.027
321	23.03.2015	20	1.670762	1.699769	1.687945	-0.047
322	23.03.2015	20	1.670844	1.699573	1.687861	0.055
323	23.03.2015	20	1.670741	1.699623	1.687793	-0.001
324	23.03.2015	20	1.670643	1.700715	1.688805	-0.018
325	23.03.2015	20	1.670606	1.700418	1.688444	-0.023
326	23.03.2015	20	1.670646	1.700350	1.688419	0.020
327	23.03.2015	20	1.670621	1.700657	1.688710	0.008
328	23.03.2015	20	1.670570	1.700889	1.688887	-0.001
329	23.03.2015	20	1.670522	1.700467	1.688420	-0.057
330	23.03.2015	20	1.670667	1.699767	1.687858	0.047
331	23.03.2015	20	1.670655	1.699745	1.687812	0.010
332	23.03.2015	20	1.670611	1.699756	1.687781	-
333	24.03.2015	15	1.670821	1.698595	1.686831	-
334	24.03.2015	15	1.670709	1.699258	1.687410	-0.043
335	24.03.2015	15	1.670741	1.698514	1.686718	0.014
336	24.03.2015	15	1.670727	1.698631	1.686749	0.004
337	24.03.2015	15	1.670699	1.698586	1.686724	-0.018
338	24.03.2015	15	1.670732	1.698867	1.686980	-0.005
339	24.03.2015	15	1.670783	1.698323	1.686474	0.035
340	24.03.2015	15	1.670716	1.698648	1.686681	-0.043
341	24.03.2015	15	1.670793	1.698462	1.686597	0.010

Analysis no	Date	[Re][1] (ppb)	$^{187}Re/^{185}Re$[2]	Raw $^{193}Ir/^{191}Ir$	Raw $^{187}Re/^{185}Re$	$\delta^{187}Re$[3]
342	24.03.2015	15	1.670839	1.699039	1.687296	-0.014
343	24.03.2015	15	1.670932	1.698160	1.686387	0.068
344	24.03.2015	15	1.670798	1.697948	1.686180	-0.065
345	24.03.2015	15	1.670881	1.697725	1.685967	0.035
346	24.03.2015	15	1.670847	1.697441	1.685642	0.004
347	24.03.2015	15	1.670801	1.697150	1.685337	-0.051
348	24.03.2015	15	1.670927	1.696730	1.684948	0.064
349	24.03.2015	15	1.670839	1.696493	1.684687	-0.042
350	24.03.2015	15	1.670890	1.695878	1.684041	0.000
351	24.03.2015	15	1.670940	1.695890	1.684132	0.035
352	24.03.2015	15	1.670872	1.695440	1.683569	-
353	24.03.2015	13	1.670760	1.693499	1.681466	-
354	24.03.2015	13	1.670866	1.694033	1.682232	0.036
355	24.03.2015	13	1.670852	1.694434	1.682613	-0.022
356	24.03.2015	13	1.670910	1.694480	1.682642	-0.037
357	24.03.2015	13	1.671093	1.694088	1.682443	0.096
358	24.03.2015	13	1.670956	1.694840	1.683091	-0.059
359	24.03.2015	13	1.671015	1.693867	1.682126	0.015
360	24.03.2015	13	1.671026	1.694068	1.682332	0.022
361	24.03.2015	13	1.670963	1.693867	1.682086	-0.048
362	24.03.2015	13	1.671060	1.693916	1.682250	0.028
363	24.03.2015	13	1.671063	1.693414	1.681852	0.013
364	24.03.2015	13	1.671024	1.693772	1.682116	-0.043
365	24.03.2015	13	1.671129	1.693611	1.681985	0.112
366	24.03.2015	13	1.670860	1.693813	1.682005	-0.118
367	24.03.2015	13	1.670986	1.693804	1.682029	0.077
368	24.03.2015	13	1.670854	1.693679	1.681808	-0.063
369	24.03.2015	13	1.670933	1.693089	1.681465	0.006
370	24.03.2015	13	1.670993	1.693978	1.682254	-
371	13.04.2015	15	1.670195	1.704492	1.692215	-
372	13.04.2015	15	1.670185	1.704520	1.692249	0.000
373	13.04.2015	15	1.670176	1.704646	1.692376	0.002
374	13.04.2015	15	1.670158	1.704663	1.692347	-0.003
375	13.04.2015	15	1.670151	1.704660	1.692370	-0.010
376	13.04.2015	15	1.670177	1.704690	1.692393	0.027
377	13.04.2015	15	1.670114	1.704745	1.692386	-0.026
378	13.04.2015	15	1.670137	1.704764	1.692454	-0.005
379	13.04.2015	15	1.670176	1.704617	1.692286	0.012
380	13.04.2015	15	1.670176	1.704647	1.692370	0.045
381	13.04.2015	15	1.670027	1.704887	1.692472	-0.074
382	13.04.2015	15	1.670126	1.704600	1.692268	0.042
383	13.04.2015	15	1.670085	1.704483	1.692090	-0.003
384	13.04.2015	15	1.670055	1.704208	1.691786	0.001
385	13.04.2015	15	1.670022	1.703718	1.691281	-0.037
386	13.04.2015	15	1.670113	1.702733	1.690351	0.023
387	13.04.2015	15	1.670127	1.702342	1.689913	0.029
388	13.04.2015	15	1.670043	1.702114	1.689688	-0.039
389	13.04.2015	15	1.670089	1.701328	1.688865	-
390	13.04.2015	15	1.670251	1.702302	1.690067	-
391	13.04.2015	15	1.670308	1.702192	1.689956	0.015

Analysis no	Date	[Re][1] (ppb)	$^{187}Re/^{185}Re$[2]	Raw $^{193}Ir/^{191}Ir$	Raw $^{187}Re/^{185}Re$	$\delta^{187}Re$[3]
392	13.04.2015	15	1.670315	1.702303	1.690110	0.014
393	13.04.2015	15	1.670275	1.702315	1.690067	-0.011
394	13.04.2015	15	1.670273	1.702298	1.690055	0.014
395	13.04.2015	15	1.670224	1.702405	1.690124	-0.014
396	13.04.2015	15	1.670223	1.702420	1.690104	0.019
397	13.04.2015	15	1.670160	1.702181	1.689866	-0.040
398	13.04.2015	15	1.670229	1.702182	1.689878	0.024
399	13.04.2015	15	1.670220	1.702098	1.689796	-0.012
400	13.04.2015	15	1.670252	1.702338	1.690064	0.064
401	13.04.2015	15	1.670068	1.701790	1.689316	-0.058
402	13.04.2015	15	1.670079	1.701748	1.689309	-0.016
403	13.04.2015	15	1.670144	1.701613	1.689227	0.011
404	13.04.2015	15	1.670174	1.701639	1.689296	0.056
405	13.04.2015	15	1.670015	1.701653	1.689117	-0.093
406	13.04.2015	15	1.670169	1.701473	1.689148	0.055
407	13.04.2015	15	1.670140	1.701173	1.688767	-0.037
408	13.04.2015	15	1.670236	1.701399	1.689085	0.059
409	13.04.2015	15	1.670136	1.700906	1.688486	-0.050
410	13.04.2015	15	1.670202	1.700737	1.688411	-0.031
411	13.04.2015	15	1.670372	1.698373	1.686125	-
412	13.04.2015	10	1.670413	1.699135	1.686945	-
413	13.04.2015	10	1.670397	1.698531	1.686303	-0.032
414	13.04.2015	10	1.670487	1.698198	1.686090	0.051
415	13.04.2015	10	1.670408	1.698478	1.686282	-0.010
416	13.04.2015	10	1.670362	1.698923	1.686657	-0.030
417	13.04.2015	10	1.670416	1.698362	1.686157	0.031
418	13.04.2015	10	1.670367	1.697849	1.685628	-0.032
419	13.04.2015	10	1.670425	1.698307	1.686099	0.016
420	13.04.2015	10	1.670428	1.698173	1.686021	0.041
421	13.04.2015	10	1.670294	1.698517	1.686204	-0.056
422	13.04.2015	10	1.670347	1.699129	1.686913	0.032
423	13.04.2015	10	1.670293	1.698800	1.686490	-0.040
424	13.04.2015	10	1.670373	1.699394	1.687147	0.044
425	13.04.2015	10	1.670306	1.699258	1.686983	-0.048
426	13.04.2015	10	1.670398	1.699183	1.686995	0.063
427	13.04.2015	10	1.670280	1.699528	1.687210	-0.029
428	13.04.2015	10	1.670259	1.699482	1.687174	-0.038
429	13.04.2015	10	1.670364	1.699028	1.686790	0.027
430	13.04.2015	10	1.670380	1.698572	1.686356	0.019
431	13.04.2015	10	1.670333	1.698652	1.686408	-0.023
432	13.04.2015	10	1.670362	1.698325	1.686076	-
433	27.04.2015	20	1.670328	1.702259	1.690106	-
434	27.04.2015	20	1.670264	1.702590	1.690340	0.004
435	27.04.2015	20	1.670184	1.702994	1.690672	-0.013
436	27.04.2015	20	1.670150	1.704310	1.691978	-0.005
437	27.04.2015	20	1.670133	1.704390	1.692052	-0.005
438	27.04.2015	20	1.670133	1.704390	1.692052	0.012
439	27.04.2015	20	1.670092	1.704357	1.691998	-0.018
440	27.04.2015	20	1.670111	1.704362	1.691992	-0.003
441	27.04.2015	20	1.670141	1.704397	1.692059	0.024

Analysis no	Date	[Re][1] (ppb)	$^{187}Re/^{185}Re$[2]	Raw $^{193}Ir/^{191}Ir$	Raw $^{187}Re/^{185}Re$	$\delta^{187}Re$[3]
442	27.04.2015	20	1.670091	1.704391	1.692031	-0.018
443	27.04.2015	20	1.670101	1.704304	1.691913	-0.009
444	27.04.2015	20	1.670143	1.704202	1.691873	0.013
445	27.04.2015	20	1.670141	1.704080	1.691743	0.030
446	27.04.2015	20	1.670040	1.704078	1.691657	-0.040
447	27.04.2015	20	1.670072	1.703930	1.691563	-0.010
448	27.04.2015	20	1.670137	1.703818	1.691481	0.013
449	27.04.2015	20	1.670158	1.703641	1.691336	0.031
450	27.04.2015	20	1.670075	1.703633	1.691227	-0.075
451	27.04.2015	20	1.670241	1.702636	1.690351	0.081
452	27.04.2015	20	1.670138	1.702971	1.690604	0.009
453	27.04.2015	20	1.670006	1.703221	1.690721	-0.070
454	27.04.2015	20	1.670106	1.702665	1.690256	0.049
455	27.04.2015	20	1.670044	1.702681	1.690240	-0.074
456	27.04.2015	20	1.670229	1.702020	1.689707	0.109
457	27.04.2015	20	1.670051	1.702335	1.689872	-
458	27.04.2015	15	1.670159	1.701991	1.689681	-
459	27.04.2015	15	1.670180	1.701663	1.689334	0.014
460	27.04.2015	15	1.670153	1.702174	1.689817	-0.047
461	27.04.2015	15	1.670283	1.702059	1.689819	0.070
462	27.04.2015	15	1.670181	1.701926	1.689624	-0.040
463	27.04.2015	15	1.670211	1.701978	1.689679	0.026
464	27.04.2015	15	1.670155	1.701726	1.689360	-0.022
465	27.04.2015	15	1.670173	1.701485	1.689130	-0.018
466	27.04.2015	15	1.670250	1.701932	1.689637	0.038
467	27.04.2015	15	1.670201	1.702106	1.689819	-0.004
468	27.04.2015	15	1.670165	1.702047	1.689679	-0.044
469	27.04.2015	15	1.670277	1.701925	1.689638	0.062
470	27.04.2015	15	1.670181	1.702037	1.689678	-0.032
471	27.04.2015	15	1.670193	1.702078	1.689735	-0.007
472	27.04.2015	15	1.670228	1.701830	1.689547	0.047
473	27.04.2015	15	1.670107	1.702360	1.689965	-0.058
474	27.04.2015	15	1.670179	1.702109	1.689772	0.048
475	27.04.2015	15	1.670092	1.702384	1.689984	-0.031
476	27.04.2015	15	1.670107	1.702270	1.689843	0.017
477	27.04.2015	15	1.670066	1.701943	1.689483	-
		average	1.684438	1.703207	1.690914	**0.000**
		2SD	0.000650	0.006661	0.006260	
		2SD ‰	0.386	3.911	3.702	**0.084**

1 Re concentration in the standard (ppb)

[2]The ratio of $^{187}Re/^{185}Re$ which has been corrected for potential isobaric interference of osmium, and then corrected for instrumental mass bias using the $^{193}Ir/^{191}Ir$ ratio and the exponential law.

[3]Re isotope composition calculated by standard sample bracketing, using the standards analysed before and after each standard as bracketing standards.

Table A3: Table of Re isotope composition data for all analyses of the standard SRM3143 carried out during measurement of the samples from the Baltic Sea and presented in Chapter 4. For all standards analysed, Ir was added to make Ir concentration of 200 ppb.

Analysis no	Date	[Re][1] (ppb)	$^{187}Re/^{185}Re$[2]	Raw $^{193}Ir/^{191}Ir$	Raw $^{187}Re/^{185}Re$	$\delta^{187}Re$[3]
1	27.04.2015	20	1.670328	1.702259	1.690106	-
2	27.04.2015	20	1.670264	1.702590	1.690340	0.004
3	27.04.2015	20	1.670184	1.702994	1.690672	-0.013
4	27.04.2015	20	1.670150	1.704310	1.691978	-0.005
5	27.04.2015	20	1.670133	1.704390	1.692052	-0.005
6	27.04.2015	20	1.670133	1.704390	1.692052	0.012
7	27.04.2015	20	1.670092	1.704357	1.691998	-0.018
8	27.04.2015	20	1.670111	1.704362	1.691992	-0.003
9	27.04.2015	20	1.670141	1.704397	1.692059	0.024
10	27.04.2015	20	1.670091	1.704391	1.692031	-0.018
11	27.04.2015	20	1.670101	1.704304	1.691913	-0.009
12	27.04.2015	20	1.670143	1.704202	1.691873	0.013
13	27.04.2015	20	1.670141	1.704080	1.691743	0.030
14	27.04.2015	20	1.670040	1.704078	1.691657	-0.040
15	27.04.2015	20	1.670072	1.703930	1.691563	-0.010
16	27.04.2015	20	1.670137	1.703818	1.691481	0.013
17	27.04.2015	20	1.670158	1.703641	1.691336	0.031
18	27.04.2015	20	1.670075	1.703633	1.691227	-0.075
19	27.04.2015	20	1.670241	1.702636	1.690351	0.081
20	27.04.2015	20	1.670138	1.702971	1.690604	0.009
21	27.04.2015	20	1.670006	1.703221	1.690721	-0.070
22	27.04.2015	20	1.670106	1.702665	1.690256	0.049
23	27.04.2015	20	1.670044	1.702681	1.690240	-0.074
24	27.04.2015	20	1.670229	1.702020	1.689707	0.109
25	27.04.2015	20	1.670051	1.702335	1.689872	-
27	27.04.2015	15	1.670159	1.701991	1.689681	-
28	27.04.2015	15	1.670180	1.701663	1.689334	0.014
29	27.04.2015	15	1.670153	1.702174	1.689817	-0.047
30	27.04.2015	15	1.670283	1.702059	1.689819	0.070
31	27.04.2015	15	1.670181	1.701926	1.689624	-0.040
32	27.04.2015	15	1.670211	1.701978	1.689679	0.026
33	27.04.2015	15	1.670155	1.701726	1.689360	-0.022
34	27.04.2015	15	1.670173	1.701485	1.689130	-0.018
35	27.04.2015	15	1.670250	1.701932	1.689637	0.038
36	27.04.2015	15	1.670201	1.702106	1.689819	-0.004
37	27.04.2015	15	1.670165	1.702047	1.689679	-0.044
38	27.04.2015	15	1.670277	1.701925	1.689638	0.062
39	27.04.2015	15	1.670181	1.702037	1.689678	-0.032
40	27.04.2015	15	1.670193	1.702078	1.689735	-0.007

Analysis no	Date	[Re][1] (ppb)	$^{187}Re/^{185}Re$[2]	Raw $^{193}Ir/^{191}Ir$	Raw $^{187}Re/^{185}Re$	$\delta^{187}Re$[3]
41	27.04.2015	15	1.670228	1.701830	1.689547	0.047
42	27.04.2015	15	1.670107	1.702360	1.689965	-0.058
43	27.04.2015	15	1.670179	1.702109	1.689772	0.048
44	27.04.2015	15	1.670092	1.702384	1.689984	-0.031
45	27.04.2015	15	1.670107	1.702270	1.689843	0.017
46	27.04.2015	15	1.670066	1.701943	1.689483	-
49	29.04.2015	10	1.670395	1.702449	1.690336	-
50	29.04.2015	10	1.670449	1.702245	1.690075	0.008
51	29.04.2015	10	1.670476	1.702359	1.690334	0.001
52	29.04.2015	10	1.670500	1.701726	1.689650	0.050
53	29.04.2015	10	1.670356	1.701720	1.689481	-0.039
54	29.04.2015	10	1.670342	1.702471	1.690319	-0.043
55	29.04.2015	10	1.670471	1.702049	1.690021	0.050
56	29.04.2015	10	1.670432	1.701931	1.689862	0.005
57	29.04.2015	10	1.670379	1.701992	1.689806	-0.058
58	29.04.2015	10	1.670518	1.701782	1.689789	0.078
59	29.04.2015	10	1.670395	1.702400	1.690253	-0.049
60	29.04.2015	10	1.670435	1.701867	1.689805	0.013
61	29.04.2015	10	1.670434	1.701878	1.689739	0.009
62	29.04.2015	10	1.670401	1.702138	1.689986	-0.003
63	29.04.2015	10	1.670377	1.702209	1.690083	-0.010
64	29.04.2015	10	1.670386	1.702099	1.690015	0.004
65	29.04.2015	10	1.670383	1.702016	1.689816	-0.006
66	29.04.2015	10	1.670400	1.702236	1.690094	0.016
67	29.04.2015	10	1.670362	1.702221	1.690077	-0.050
68	29.04.2015	10	1.670491	1.702178	1.690144	0.077
69	29.04.2015	10	1.670364	1.702784	1.690694	-0.058
70	29.04.2015	10	1.670429	1.702736	1.690692	0.026
71	29.04.2015	10	1.670408	1.702788	1.690729	-0.007
72	29.04.2015	10	1.670411	1.702840	1.690760	-0.001
73	29.04.2015	10	1.670415	1.702988	1.690924	0.005
74	29.04.2015	10	1.670403	1.703004	1.690914	0.010
75	29.04.2015	10	1.670359	1.703002	1.690881	-0.021
76	29.04.2015	10	1.670385	1.702959	1.690843	0.031
77	29.04.2015	10	1.670307	1.702886	1.690671	-0.038
78	29.04.2015	10	1.670357	1.702826	1.690694	0.081
79	29.04.2015	10	1.670137	1.703500	1.691166	-0.105
80	29.04.2015	10	1.670268	1.703529	1.691295	0.063
81	29.04.2015	10	1.670187	1.703015	1.690693	-0.040
82	29.04.2015	10	1.670240	1.703032	1.690782	0.017
83	29.04.2015	10	1.670235	1.702911	1.690623	-0.010
84	29.04.2015	10	1.670262	1.702195	1.689969	0.005

Analysis no	Date	[Re][1] (ppb)	$^{187}Re/^{185}Re$[2]	Raw $^{193}Ir/^{191}Ir$	Raw $^{187}Re/^{185}Re$	$\delta^{187}Re$[3]
85	29.04.2015	10	1.670274	1.702188	1.689892	-0.025
86	29.04.2015	10	1.670369	1.702122	1.689948	0.052
87	29.04.2015	10	1.670288	1.702037	1.689785	-0.036
88	29.04.2015	10	1.670330	1.702150	1.689955	-
91	16.11.2015	15	1.670710	1.701977	1.690168	-
92	16.11.2015	15	1.670602	1.702524	1.690575	-0.039
93	16.11.2015	15	1.670626	1.703044	1.691206	0.007
94	16.11.2015	15	1.670626	1.703044	1.691206	0.014
95	16.11.2015	15	1.670580	1.703210	1.691343	-0.005
96	16.11.2015	15	1.670551	1.703336	1.691399	-0.025
97	16.11.2015	15	1.670604	1.703470	1.691624	0.008
98	16.11.2015	15	1.670629	1.703490	1.691674	0.001
99	16.11.2015	15	1.670652	1.703874	1.692049	0.054
100	16.11.2015	15	1.670493	1.703707	1.691744	-0.080
101	16.11.2015	15	1.670602	1.703545	1.691668	0.040
102	16.11.2015	15	1.670577	1.703499	1.691574	-0.001
103	16.11.2015	15	1.670557	1.703434	1.691538	0.048
104	16.11.2015	15	1.670377	1.703897	1.691769	-0.057
105	16.11.2015	15	1.670388	1.703797	1.691729	-0.004
106	16.11.2015	15	1.670410	1.703568	1.691525	0.030
107	16.11.2015	15	1.670334	1.703927	1.691811	-
108	16.11.2015	7	1.670326	1.703643	1.691501	-
109	16.11.2015	7	1.670296	1.703690	1.691535	-0.044
110	16.11.2015	7	1.670415	1.703684	1.691590	0.068
111	16.11.2015	7	1.670306	1.703758	1.691563	-0.087
112	16.11.2015	7	1.670490	1.703687	1.691710	0.120
113	16.11.2015	7	1.670273	1.703813	1.691652	-0.102
114	16.11.2015	7	1.670397	1.703681	1.691615	0.063
115	16.11.2015	7	1.670312	1.703632	1.691504	-0.046
116	16.11.2015	7	1.670381	1.703676	1.691566	-0.003
117	16.11.2015	7	1.670459	1.703715	1.691662	0.060
118	16.11.2015	7	1.670336	1.703579	1.691440	-0.056
119	16.11.2015	7	1.670399	1.703642	1.691488	0.016
120	16.11.2015	7	1.670409	1.703509	1.691424	0.005
121	16.11.2015	7	1.670403	1.703163	1.690969	0.040
122	16.11.2015	7	1.670263	1.702738	1.690520	-0.061
123	16.11.2015	7	1.670326	1.703273	1.691141	-0.011
124	16.11.2015	7	1.670426	1.703176	1.691109	0.062
125	16.11.2015	7	1.670318	1.703604	1.691456	-0.060
126	16.11.2015	7	1.670411	1.703163	1.691066	0.032
127	16.11.2015	7	1.670395	1.703433	1.691326	-
		average	1.670314	1.702899	1.690714	**0.000**

Analysis no	Date	[Re][1] (ppb)	$^{187}Re/^{185}Re$[2]	Raw $^{193}Ir/^{191}Ir$	Raw $^{187}Re/^{185}Re$	$\delta^{187}Re$[3]
		2SD	0.000317	0.001607	0.001662	
		2SD ‰	0.190	0.944	0.983	**0.089**

1 Re concentration in the standard (ppb)

[2]The ratio of $^{187}Re/^{185}Re$ which has been corrected for potential isobaric interference of osmium, and then corrected for instrumental mass bias using the $^{193}Ir/^{191}Ir$ ratio and the exponential law.

[3]Re isotope composition calculated by standard sample bracketing, using the standards analysed before and after each standard as bracketing standards.